

## Supramolecular Coordination: Self-Assembly of Finite Two- and Three-Dimensional Ensembles

Rajesh Chakrabarty,<sup>\*,†</sup> Partha Sarathi Mukherjee,<sup>\*,‡</sup> and Peter J. Stang<sup>\*,†</sup>

<sup>†</sup>Department of Chemistry, University of Utah, 315 South 1400 East, Salt Lake City, Utah 84112, United States

<sup>‡</sup>Department of Inorganic and Physical Chemistry, Indian Institute of Science, Bangalore 560012, India

### CONTENTS

1. Introduction	6810	4.5.1. Host–Guest Chemistry	6881
2. Background and Design Principles	6811	4.5.2. Cavity Controlled Reactions	6887
2.1. Directional Bonding Approach	6812	4.5.3. Biological Applications	6892
2.2. Symmetry Interaction Approach	6812	5. Miscellaneous	6894
2.3. Paneling Approach	6813	5.1. Self-Selection and Self-Sorting in Coordination-Driven Self-Assembly	6894
2.4. Weak Link Approach	6814	5.2. Surface Confined Ensembles	6899
2.5. Dimetallic Building Block Approach	6815	5.3. Novel Characterization Methods	6902
3. Two-Dimensional Ensembles	6815	5.3.1. Mass Spectrometry	6902
3.1. Charged Systems	6815	5.3.2. Solution-Phase X-ray Measurement	6903
3.1.1. Molecular Rhomboids	6815	5.4. Photophysical Studies Using Laser Spectroscopy	6904
3.1.2. Molecular Triangles	6816	6. Conclusions and Prognostication	6905
3.1.3. Molecular Squares	6820	Author Information	6906
3.1.4. Triangle-Square Equilibrium	6822	Biographies	6906
3.1.5. Molecular Rectangles	6825	Acknowledgment	6907
3.1.6. Higher Polygons and Large Ring Systems	6827	References	6907
3.2. Neutral Systems	6830		
3.3. Chiral Systems	6835		
3.4. Functional Systems and their Properties	6839		
3.5. Applications and Uses of 2D Systems	6846		
3.5.1. Molecular Recognition	6846		
3.5.2. Chemosensing	6847		
3.5.3. Cavity Controlled Catalysis	6848		
3.5.4. Biological Applications	6850		
4. Three-Dimensional Nanoscopic Cages	6851		
4.1. Archimedean and Platonic Systems	6851		
4.1.1. Tetrahedra	6851		
4.1.2. Cubic Systems	6855		
4.1.3. Octahedra	6858		
4.1.4. Dodecahedra	6859		
4.1.5. Cuboctahedra	6859		
4.2. Other Coordination Cages	6860		
4.2.1. Trigonal Bipyramids and Double Squares	6860		
4.2.2. Adamantanoids	6861		
4.2.3. Trigonal Prisms	6862		
4.2.4. Tetragonal Prisms	6866		
4.2.5. Molecular Boxes	6868		
4.2.6. Molecular Spheres	6870		
4.3. Chiral Systems	6872		
4.4. Functionalized Systems	6875		
4.5. Applications and Uses of 3D Cages	6881		

### 1. INTRODUCTION

Fascination with supramolecular chemistry over the past few decades has led to the synthesis of an ever-increasing number of elegant and intricate functional structures with sizes that approach nanoscopic dimensions. Today, it has grown into a mature field of modern science whose interfaces with many disciplines have provided invaluable opportunities for crossing boundaries both inside and between the fields of chemistry, physics, and biology. This chemistry is of continuing interest for synthetic chemists, partly because of the fascinating physical and chemical properties and the complex and varied aesthetically pleasing structures that supramolecules possess. For scientists seeking to design novel molecular materials exhibiting unusual sensing, magnetic, optical, and catalytic properties, and for researchers investigating the structure and function of biomolecules, supramolecular chemistry provides limitless possibilities. Thus, it transcends the traditional divisional boundaries of science and represents a highly interdisciplinary field.

In the early 1960s, the discovery of “crown ethers”, “cryptands”, and “spherands” by Pedersen,<sup>1</sup> Lehn,<sup>2</sup> and Cram<sup>3</sup>, respectively, led to the realization that small, complementary molecules can be made to recognize each other through noncovalent interactions such as hydrogen bonding, charge–charge, donor–acceptor,

**Received:** March 12, 2011

**Published:** August 24, 2011

$\pi$ – $\pi$ , and van der Waals, etc. Such “programmed” molecules can thus be self-assembled by utilizing these interactions in a definite algorithm to form large supramolecules that have different physicochemical properties than those of the precursor building blocks. Typical systems are designed such that the self-assembly process is kinetically reversible; the individual building blocks gradually funnel toward an ensemble that represents the thermodynamic minimum of the system via numerous association and dissociation steps. By tuning various reaction parameters, the reaction equilibrium can be shifted toward the desired product. As such, self-assembly has a distinct advantage over traditional, stepwise synthetic approaches when accessing large molecules.

It is well-known that nature has the ability to assemble relatively simple molecular precursors into extremely complex biomolecules, which are vital for life processes. Nature’s building blocks possess specific functionalities in configurations that allow them to interact with one another in a deliberate manner. Protein folding, nucleic acid assembly and tertiary structure, phospholipid membranes, ribosomes, and microtubules, etc., are but a selective, representative example of self-assembly in nature that is of critical importance for living organisms. Nature makes use of a variety of weak, noncovalent interactions such as hydrogen bonding, charge–charge, donor–acceptor,  $\pi$ – $\pi$ , van der Waals, and hydrophilic and hydrophobic, etc., interactions to achieve these highly complex and often symmetrical architectures. In fact, the existence of life is heavily dependent on these phenomena. The aforementioned structures provide inspiration for chemists seeking to exploit the “weak interactions” described above to make scaffolds rivaling the complexity of natural systems.

The breadth of supramolecular chemistry has progressively increased with the synthesis of numerous unique supramolecules each year. On the basis of the interactions used in the assembly process, supramolecular chemistry can be broadly classified into three main branches: (i) those that utilize H-bonding motifs in the supramolecular architectures; (ii) processes that primarily use other noncovalent interactions such as ion–ion, ion–dipole,  $\pi$ – $\pi$  stacking, cation– $\pi$ , van der Waals, and hydrophobic interactions; and (iii) those that employ strong and directional metal–ligand bonds for the assembly process. However, as the scale and degree of complexity of desired molecules increase, the assembly of small molecular units into large, discrete supramolecules becomes an increasingly daunting task. This has been due in large part to the inability to completely control the directionality of the weak forces employed in the first two classifications above. Coordination-driven self-assembly, which defines the third approach, affords a greater control over the rational design of two- (2D) and three-dimensional (3D) architectures by capitalizing on the predictable nature of the metal–ligand coordination sphere and ligand lability to encode directionality. Thus, this third strategy represents an alternative route to better execute the “bottom-up” synthetic strategy for designing molecules of desired dimensions, ranging from a few cubic angstroms to over a cubic nanometer. For instance, a wide array of 2D systems (rhomboids, squares, rectangles, and triangles, etc.) and 3D systems (trigonal pyramids, trigonal prisms, cubes, cuboctahedra, double squares, adamantanoids, dodecahedra, and a variety of other cages) have been reported. As in nature, inherent preferences for particular geometries and binding motifs are “encoded” in certain molecules depending on the metals and functional groups present; these moieties help to control the way in which the building blocks assemble into well-defined, discrete supramolecules.<sup>4</sup>

Since the early pioneering work by Lehn<sup>5</sup> and Sauvage<sup>6</sup> on the feasibility and usefulness of coordination-driven self-assembly in the formation of infinite helicates, grids, ladders, racks, knots, rings, catenanes, rotaxanes, and related species,<sup>7</sup> several groups—those of Stang,<sup>8</sup> Raymond,<sup>9</sup> Fujita,<sup>10</sup> Mirkin,<sup>11</sup> Cotton,<sup>12</sup> and others<sup>13,14</sup>—have independently developed and exploited novel coordination-based paradigms for the self-assembly of discrete metallacycles and metallacages with well-defined shapes and sizes. In the past decade, the concepts and perspectives of coordination-driven self-assembly have been delineated and summarized in several insightful reviews covering various aspects of coordination-driven self-assembly.<sup>15</sup> In the past decade, the use of this synthetic strategy has led to metallacages dubbed as “molecular flasks” by Fujita et al.,<sup>16</sup> and Raymond et al.,<sup>17</sup> which due to their ability to encapsulate guest molecules, allowed for the observation of unique chemical phenomena and unusual reactions which cannot be achieved in the conventional gas, liquid, or solid phases. Furthermore, these assemblies found applications in supramolecular catalysis<sup>18,19</sup> and as nanomaterials as developed by Hupp et al.<sup>20</sup> and others.<sup>21,22</sup>

This review focuses on the journey of early coordination-driven self-assembly paradigms to more complex and discrete 2D and 3D supramolecular ensembles over the past decade. We begin with a discussion of various approaches that have been developed by different groups to assemble finite supramolecular architectures. The subsequent sections contain detailed discussions on the synthesis of discrete 2D and 3D systems and their functionalizations and applications.

## 2. BACKGROUND AND DESIGN PRINCIPLES

The assembly of supramolecular ensembles depends on the information coded within the complementary building blocks that form the rigid framework of the architectures. The highly directional and predictable nature of the metal–ligand coordination sphere is a critical feature of coordination-driven self-assembly. The energies of metal–ligand bonds (15–50 kcal/mol), which are intermediate between the energies of organic covalent bonds (ca. 60–120 kcal/mol) and the weak interactions (ca. 0.5–10 kcal/mol) that nature employs so elegantly to self-assemble biomolecules, help in modulating the coordination kinetics of the self-assembly process by introducing rigidity and reversibility. The kinetic reversibility between complementary building blocks, reaction intermediates, and self-assembled architectures provides a way for the system to self-correct (an “incorrectly” formed bond can dissociate and reassociate “correctly”), leading to a product that is thermodynamically more stable than the starting components and any kinetically formed intermediates. Transition metals, with their preferred coordination geometries, have served as acceptor units that can logically self-assemble with various rigid or flexible donors into predictable architectures. Although macrocyclization is a kinetically unfavorable process, thermodynamic conditions facilitate the formation of macrocycles at the expense of increased angle strain. This is due, among other factors, to the fact that entropy favors closed structures with a minimum number of components rather than polymeric structures, which involve a far larger number of components.

With a growing knowledge of the synthesis and characterization of large, complex molecules, the past few years have seen a tremendous proliferation of new supramolecules and strategies

to achieve complex topologies. Of the various strategies developed in recent years using metal–ligand coordination, *directional bonding*,<sup>8</sup> *symmetry interaction*,<sup>9</sup> *molecular paneling*,<sup>10</sup> *weak link*,<sup>11</sup> and *dimetallic building block*<sup>12</sup> approaches are the most extensively used and adopted. These synthetic strategies have led to a wide variety of 2D and 3D molecular architectures of different shapes and sizes, which can be modulated through the judicious choice of metals and ligands. The metal–ligand bond serves as the cornerstone in all of these design principles. Mechanistically, the first four approaches rely on thermodynamic control; the global minimum of the reaction coordinate is the desired product. The weak link approach utilizes both thermodynamic and kinetic control to access a variety of large, open, and flexible 2D and 3D structures.

### 2.1. Directional Bonding Approach

The directional bonding approach is a general, high-yielding synthetic strategy that gives access to a wide variety of 2D and 3D supramolecular ensembles.<sup>8</sup> Since the seminal studies on the rational synthesis of molecular squares in the early 1990s by Fujita<sup>23,24</sup> and Stang's<sup>25</sup> group a plethora of metalla-macrocycles and metallocages have been assembled using this design strategy. This rational design strategy allows for a combinatorial molecular library consisting of complementary building blocks that allows one to think retrosynthetically on how best to achieve the geometry of a particular discrete assembly.

There are two basic structural requirements for the construction of supramolecular architectures by this approach. First, the complementary precursor units must be structurally rigid with predefined bite angles; and second, the appropriate stoichiometric ratio of the precursors must be used. The donor building blocks are generally organic ligands having two or more binding sites possessing angular orientations ranging from 0 to 180° (Figure 1).

The acceptors are metal-containing subunits that are vital in this design approach because they possess available coordination sites, which are at a fixed angle relative to one another for binding incoming ligands. The symmetry and number of binding sites within each precursor unit guide the shape of the target assembly. While the design of monocyclic ensembles requires subunits having symmetry axes no higher than a 2-fold axis, polycyclic entities require one of the subunits to possess a symmetry axis higher than 2-fold. In this strategy, the shapes of the resulting monocyclic entities resemble convex polygons and those of polycyclic frameworks bear a resemblance to canonical polyhedra. For example, a molecular rectangle can be designed by the combination of two 0° acceptor units with 180° two donor units and vice versa. A molecular triangle can be prepared by the combination of three 60° donor units and three 180° acceptors. A molecular square can be accessed in different ways: the combination of four ditopic 90° angular units and four 180° linear units or the 2:2 assembly of two different 90° angular units. Three-dimensional polyhedral architectures can be designed using a combination of angular and linear subunits that have more than two binding sites (Figure 2). For example, a truncated tetrahedron can be designed by combining four tridentate subunits, where the angles between the binding sites are 120°, with six ditopic subunits having an angular disposition of 80–90°. A trigonal bipyramid can be formed in several ways, such as by combining two tritopic units, where the binding sites are orthogonal to each other, with three 80–90° ditopic units or by combining two tridentate 60° building blocks with three ditopic units which have 90° angles between the donor sites.

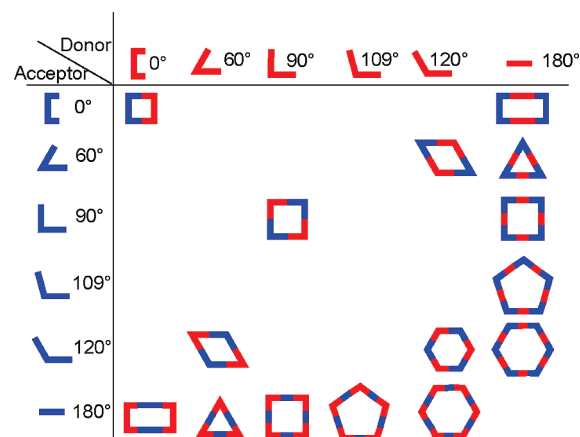


**Figure 1.** Combination of various building units for accessing convex polygons and canonical polyhedra.

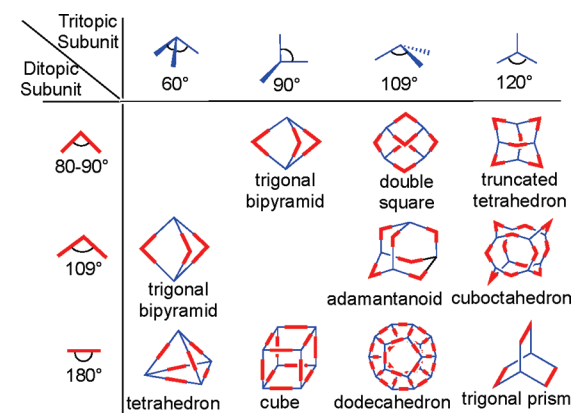


**Figure 2.** Three-dimensional architectures formed by the combination of ditopic and tritopic subunits by the directional bonding approach.

Similarly, eight tritopic subunits possessing 90° angles between their binding sites and 12 linear ditopic units lead to the formation of a cube. Although it is assumed that the angle subtended at the angular subunit does not change upon incorporation into the assembly, in practice the angles can distort up to several degrees. Nevertheless, due to the relatively weak nature of metal–ligand bonds compared to covalent ones, the final geometry of the supramolecular entity remains more or less intact.

### 2.2. Symmetry Interaction Approach

This design strategy has been developed as a rational synthetic approach for the synthesis of high-symmetry coordination clusters using metal–ligand bonds. It is based on the geometric relationship between the chelating ligands and the metals used. The strong binding affinity and coordination mode of chelating ligands, along with the inherent symmetry of the coordination sites available on the naked metal center, act as the driving force for the assembly process. In general, multibranched chelating ligands with rigid backbones are used in conjunction with transition metals or main group metals. The orientation of the multiple binding sites that are rigidly fixed is critical to the selectivity of a particular molecular geometry and helps to avoid the formation of oligomers and polymers. Similar to the directional bonding approach, it relies on the thermodynamic control and kinetic reversibility for error checking and self-correction.

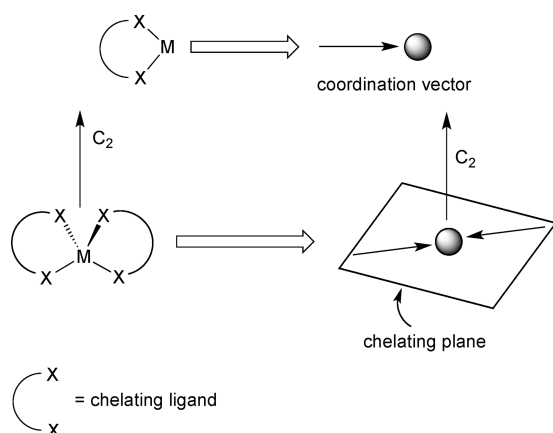


**Figure 3.** Coordinate vector and chelate plane for the symmetry interaction method.

Raymond and co-workers have defined the requisites of this design principle in terms of the geometric relationship between the ligand and the metal component using symmetry considerations.<sup>9</sup> A *coordinate vector* represents the interaction between a ligand and metal. For chelating ligands, the plane orthogonal to the major symmetry axis of a metal complex is the *chelate plane* (Figure 3), which in the case of bidentate chelators holds all chelate vectors. Thus, depending on the orientation of the chelate planes, the construction of high-symmetrical coordination clusters can be realized. Furthermore, the proper organization of the multiple binding sites with respect to one another is of paramount importance.

For example, to design a  $M_2L_3$  triple helicate having an idealized  $D_{3h}$  symmetry, it must be ensured that both the  $C_2$  and  $C_3$  axes are orthogonal and are preprogrammed into the chelating ligand and the metal center. Since the two pseudo-octahedral metal centers share the same  $C_3$  axis, the two chelating planes must be parallel to achieve the triple helicate (Figure 4).

A similar approach can be applied for the rational design of tetrahedral clusters. In a  $M_4L_6$  tetrahedron, the four metal atoms occupy the vertices and the six ligands are disposed on the edges of the tetrahedron. This requires that the  $C_2$  axes of the tetrahedron lie within the chelate plane at each of the metal centers. Furthermore, the chelate vectors within the ligand must maintain an angle of  $70.6^\circ$  (Figure 5a). A tetrahedron can also be generated by the combination of four metal atoms with four ligands ( $M_4L_4$ ). In this case, the four ligands occupy each of the four faces of the tetrahedron with four metal atoms at the vertices. Symmetry considerations thus require that both the ligands and metals possess  $C_3$  symmetry (Figure 5b).

### 2.3. Paneling Approach

This design strategy, pioneered by Fujita and co-workers, has led to the formation of various functional and aesthetically elegant 3D architectures that resemble platonic solids, including equilateral triangles, squares, and pentagons.<sup>10</sup> Thus, 3D molecular architectures can, in principle, be designed by reducing these polyhedra to molecular components. For example, a tetrahedron can be designed by stitching together four triangular panels, while an octahedron can be prepared by bringing together eight such triangular panels (Figure 6). Similarly, the paneling of squares results in the formation of cubes and prisms. In this paradigm, flat, panellike organic ligands having more than two linking sites are paneled together using appropriate structural corner units.

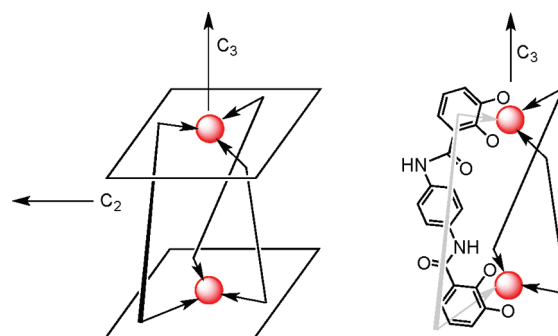


**Figure 4.** Design of a  $D_3$ -symmetrical triple helicate.

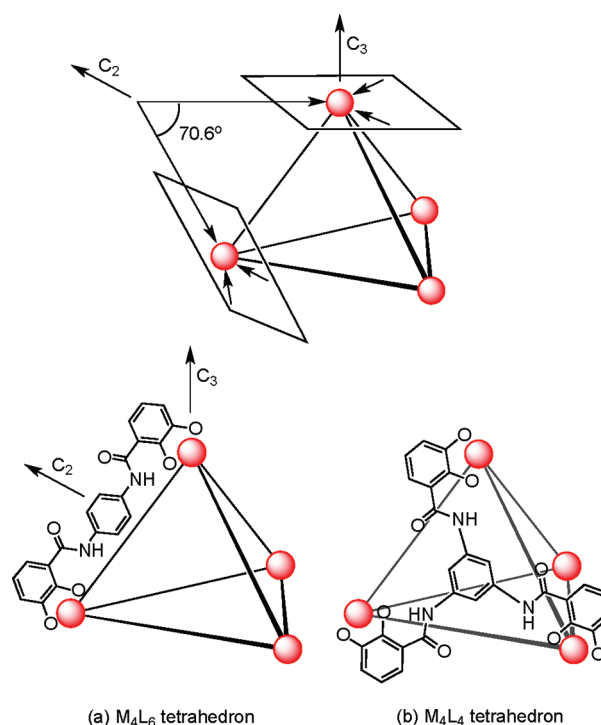


**Figure 5.** Design strategy for (a)  $M_4L_6$  and (b)  $M_4L_4$  tetrahedra by the symmetry interaction approach.

These 2D molecular panels span all or some of the faces of the resulting platonic architectures. The corner units employed are usually cis-protected square-planar Pt(II) or Pd(II) metal centers. In contrast to the naked metal centers used in the symmetry interaction approach, cis-protection makes the coordination geometry around the metal center convergent. This enables the efficient generation of discrete supramolecular arrays without the formation of oligomeric products.

The triangular molecular panels, in conjunction with the cis-blocked corner unit, lead to varied supramolecular architectures including the  $M_6L_4$  truncated tetrahedral cage, the  $M_6L_4$  square-pyramidal cone,  $M_8L_4$  tetrahedra and cones and  $M_{18}L_6$  hexahedra. Square and rectangular panels can be used to construct cubes, parallelepipeds, and prisms of various topologies—trigonal, square, pentagonal, and hexagonal, etc.—by the judicious introduction of multiple binding sites into the edges and/or corners of the panels. Placement of the donor binding sites in the panel is vital and guides the final geometry of the resulting



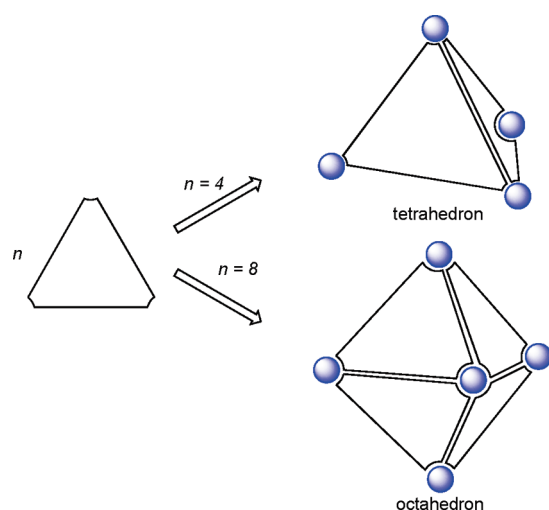


**Figure 6.** Representation for assembling a tetrahedron and an octahedron using triangular panels.

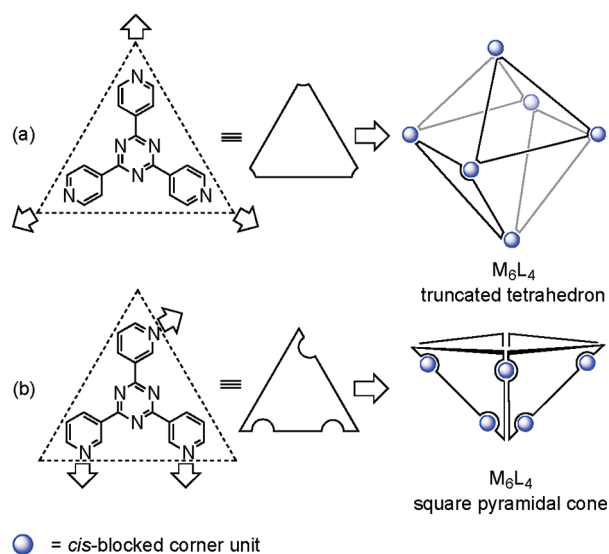


**Figure 7.** Representation for assembling: (a) a  $M_6L_4$  truncated tetrahedron and (b) an  $M_6L_4$  square-pyramidal cone using triangular panels.

architectures. For example, an  $M_6L_4$  octahedron can be designed by using triangular molecular panels having  $D_{3h}$  symmetry with three linking sites at the vertices of the triangle (Figure 7a).<sup>26</sup> The four triangular panels span alternate faces of the octahedron and are linked together at the vertices by cis-blocked corner units. A slightly different disposition of the donor sites in the triangular panel would result in the formation of a bowl-like  $M_6L_4$  square-pyramidal cone (Figure 7b).<sup>27</sup>

Similarly, tetratopic square panels having  $D_{4h}$  symmetry can lead to different topologies depending upon the positions of the donor sites on the panel (Figure 8). While panels having linking sites on the edges of the square form  $M_6L_3$  trigonal prisms,<sup>28</sup> donor sites on the four corners give access to  $M_{12}L_6$  hexagonal prisms.<sup>29</sup> One of the prime advantages of this strategy is that the ensembles formed through this approach have large accessible interior cavities, which have been exploited for reversible guest inclusion, molecular recognition, and cavity-driven catalysis.

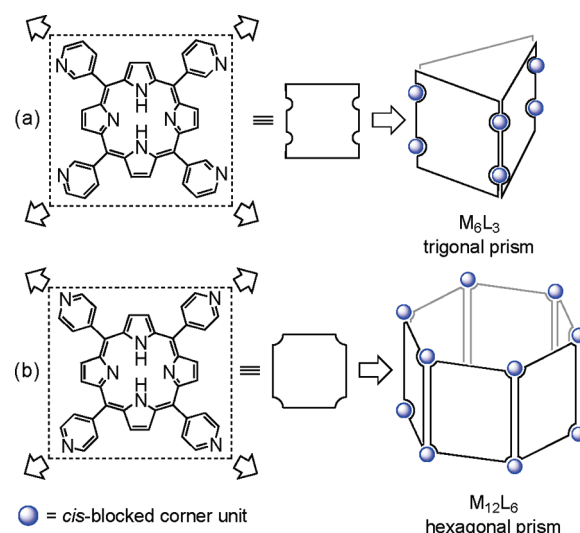
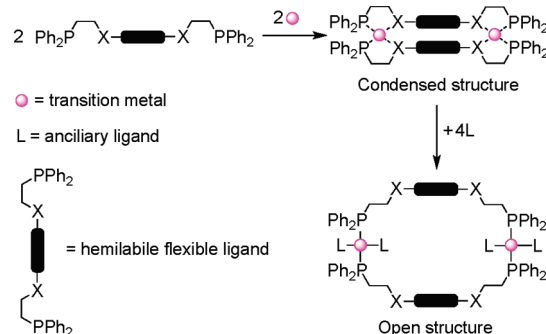


**Figure 8.** Representation for assembling: (a) a  $M_6L_3$  trigonal prism and (b) a  $M_{12}L_6$  hexagonal prism using tetratopic panels.

#### Scheme 1



However, to achieve some of the designed architectures, guest molecules need to be used as a template during the formation of the prisms.

#### 2.4. Weak Link Approach

In this design strategy, pioneered by Mirkin and co-workers, both 2D and 3D supramolecular assemblies are accessible using hemilabile ligands and transition metals.<sup>11</sup> The hemilabile, flexible ligands coordinate in a bidentate chelating mode to the metal center such that one of the metal–ligand bonds is weaker than the other. The formation of the kinetically controlled product is driven by the chelating effect of the bidentate ligands and the  $\pi$ – $\pi$  interaction between the two central bridging units (Scheme 1). The weak ligands of this condensed intermediate structure can be selectively displaced upon treatment with small molecules or ions that have stronger affinity for the metal center, thereby generating the thermodynamically controlled product. One important feature of this approach is the conformational flexibility of the ligand. The coordinative lability of the metal centers imparts flexibility to the supramolecular arrays, making this design strategy different from the other approaches in which the final products are rigid. The flexibility of the architectures also makes the ensembles potential candidates for applications that

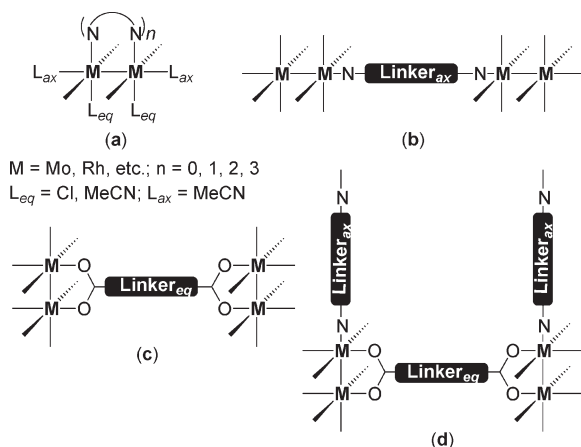


**Figure 9.** Modes of assembly of dinuclear units in dimetallic building block approach.

require conformational changes, such as in molecular sensing, catalysis, and host–guest chemistry. The fact that the metal centers are free for further coordination without the supramolecular assembly being destroyed makes this approach amenable for the construction of more complex topologies.

### 2.5. Dimetallic Building Block Approach

In Cotton's dimetallic building block approach<sup>12</sup> well-known paddlewheel or lantern frameworks form the basic structural units. Dimetallic units of  $\text{Mo}_2^{4+}$  and  $\text{Rh}_2^{4+}$  have been extensively used in conjunction with a variety of organic linkers to construct a wide array of neutral supramolecules. The cis-blocked dimetallic units have one or more of the edges blocked by nonlabile chelating N-donor ligands such as amidinate, while the other coordination sites are occupied by labile ligands such as acetonitrile or chloride ions (Figure 9). Polycarboxylate and polypyridyl ligands serve as the equatorial and axial ligands, respectively. Depending on the choice of the dimetallic unit (Figure 9a) and linkers, the units can be joined face-to-face with an axial linker (Figure 9b), end-to-end with an equatorial linker (Figure 9c), or by a combination of both linkers (Figure 9d).

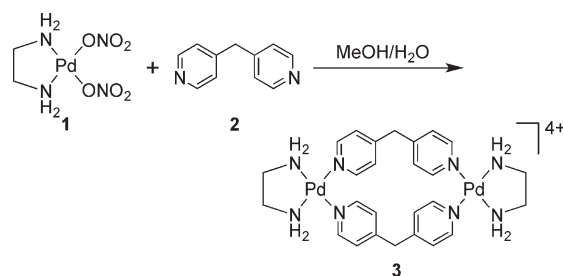
## 3. TWO-DIMENSIONAL ENSEMBLES

Since the synthesis of metal-cornered molecular squares by Fujita et al.<sup>23</sup> and Stang and Cao<sup>25</sup> in the early 1990s, a wide variety of metalla-macrocycles consisting of varied 2D geometries and sizes ranging from simple dinuclear rhomboids to endo- and exo-functionalized polynuclear hexagons have been prepared. Although most of these fascinating molecular ensembles were synthesized by employing the design principles described above (section 2), some have been obtained using different synthetic pathways, such as the transformation of mononuclear metal complexes or the metal-induced transformation of added reagents. Our main focus in this section will be on the synthetic and topological aspects of the self-assembled metallacycles using the design principles described above. The functional properties of these 2D architectures will be discussed in a separate subsection.

### 3.1. Charged Systems

In metal-mediated, self-assembled, supramolecular metallacycles, the reactivity and coordination geometry of the metal center plays a vital role in guiding the topologies of the final architectures. These ensembles have typically been prepared

**Scheme 2**



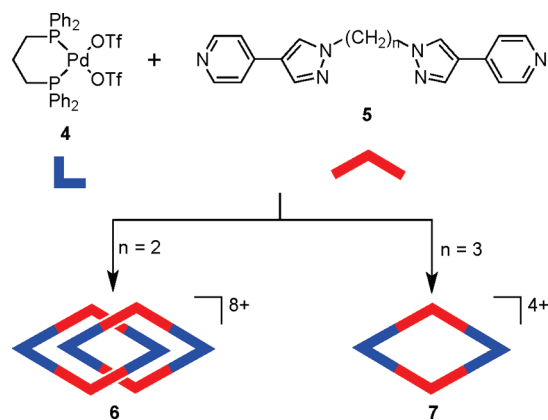
utilizing transition metals as directing units, due to their well-defined coordination preferences. In particular, electron-poor square-planar divalent  $\text{Pt}(\text{II})$  and  $\text{Pd}(\text{II})$  ions have been extensively used in conjunction with electron-rich nitrogen-containing moieties in the self-assembly process. In contrast, the use of main group metals as the directing units has found less favor with supramolecular chemists due to their rather unpredictable coordination preferences. Nevertheless, interest involving main group elements as structure-directing units has been growing in recent years.<sup>30</sup> The vast majority of these metallacycles are highly charged due to the use of neutral N-donor ligands with oxidized metal ions. This has a profound impact on both the solubilities of the complexes and their potential to act as hosts for anions/cations via electrostatic interactions.

**3.1.1. Molecular Rhomboids.** From a topological point of view, dinuclear molecular rhomboids are the simplest among the metallacycles. It has been observed that flexible bridging ligands generally favor the self-assembly of low-nuclearity macrocycles. Using the directional bonding approach, a molecular rhomboid can be assembled by a  $[2 + 2]$  combination of  $120^\circ$  donor and acceptor units. Fujita and co-workers reported some early examples of self-assembled dinuclear cationic molecular rhomboids.<sup>31–34</sup> In all of these assemblies, a high fidelity for the formation of the dinuclear macrocyclic cores was observed from a reaction of  $90^\circ$  cis-blocked  $[\text{Pd}(\text{en})(\text{NO}_3)_2]$  ( $\text{en}$  = ethylenediamine; 1) with bidentate bis(pyridine) based ligands having a wide range of angles between the donor sites. For example, the synthesis of rhomboid 3 involved the assembly of  $90^\circ$  cis-blocked 1 with bis(4-pyridyl)methane (2) in methanol–water medium (Scheme 2).

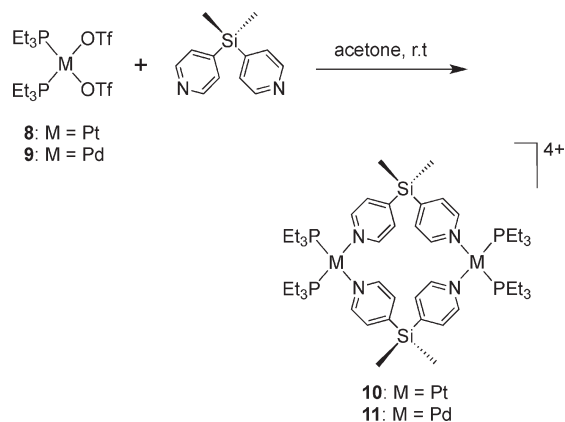
Introduction of flexible, nonlinear spacer  $1,4\text{-CH}_2(\text{C}_6\text{H}_4)\text{CH}_2$  in the bispyridyl bridging ligand led to the interesting observation of a dynamic equilibrium between a dinuclear rhomboid and an interpenetrating [2]catenane at ambient temperature.<sup>32,33</sup> The Pt analogue of 1 has led to the formation of a stable interpenetrating [2]catenane, due to the higher strength of the  $\text{Pt}-\text{N}$  bond.<sup>34</sup> Batten et al.<sup>35</sup> have demonstrated that the formation of a [2]catenane is also dependent on the length of the bridging ligand. The assembly of  $90^\circ$  cis-blocked  $[\text{Pd}(\text{dppp})(\text{OTf})_2]$  ( $\text{dppp}$  = 1,3-bis(diphenylphosphino)propane; 4) with ditopic ligands 5, containing two 4-(4-pyridyl)pyrazolyl arms that are connected by ethane and propane bridges, led to the formation of [2]catenane (6) and molecular rhomboid 7, respectively (Scheme 3). The face-to-face  $\pi$  interaction between the aromatic rings drives the formation of 6. Disruption of this array due to an increase in the length of the bridging ligand led to the formation of only a single noncatenated rhomboid (7).

Stang et al. have reported cationic dinuclear rhomboids of carbon- and silicon-based tectons using  $\text{cis-}[\text{Pt}(\text{PEt}_3)_2(\text{OTf})_2]$  (8)

Scheme 3



Scheme 4



and *cis*-[Pd(PEt<sub>3</sub>)<sub>2</sub>(OTf)<sub>2</sub>] (9) as the corner units.<sup>36</sup> For example, treatment of dimethylbis(4-pyridyl)silane with 90° corner units 8 and 9 in a 1:1 ratio led to the formation of silicon-containing rhomboids 10 and 11 (Scheme 4). An analogous rhomboid was also prepared from bispyridyl acetal using *cis*-[Pt(PEt<sub>3</sub>)<sub>2</sub>(OTf)<sub>2</sub>] as the corner unit. Multinuclear NMR, fast-atom bombardment–mass spectrometry (FAB–MS) and X-ray structural studies established the formation of the rhomboids. Due to the unexpected hydration of ketone, treatment of bis(4-pyridyl)-ketone with 8 gave a similar rhomboid instead of the less strained trimeric assembly. It was observed that entropy plays an important role in the formation of these macrocyclic systems, favoring the formation of the smallest macrocycle even though the hydration is thermodynamically disfavored. Similarly, using a bis(pyridyl) subunit possessing a tethered C<sub>60</sub> molecule in conjunction with 8 gave a supramolecular rhomboid containing two C<sub>60</sub> units.<sup>37</sup> Similarly, a series of molecular rhomboids have been prepared using flexible bispyridyl ligands to assemble molecular rhomboids.<sup>38</sup> The combination of a 60° bent bifunctional Pt(II)-based building block (12) with a structurally rigid 120° linker, 2,6-di(4,4'-dipyridyl)-9-thiabicyclo[3.3.1]nonane, resulted in an octacationic molecular rhomboid (13) having large cavity dimensions in excellent yields (Scheme 5).<sup>39</sup> Several other dinuclear endo and exo functionalized molecular rhomboids with large cavity spaces have been designed using the same 60° bent Pt(II) acceptor as the directing unit (*vide infra*).

Scheme 5

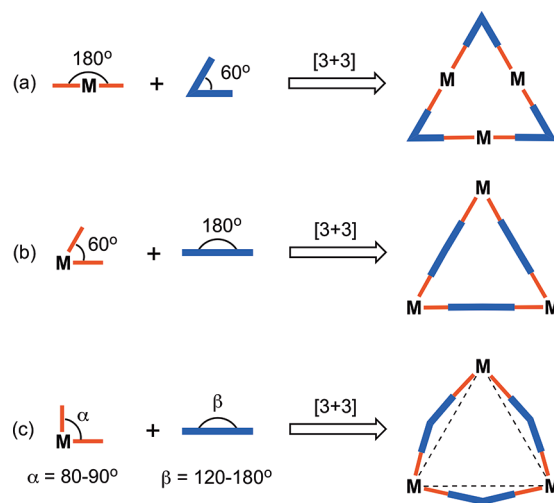
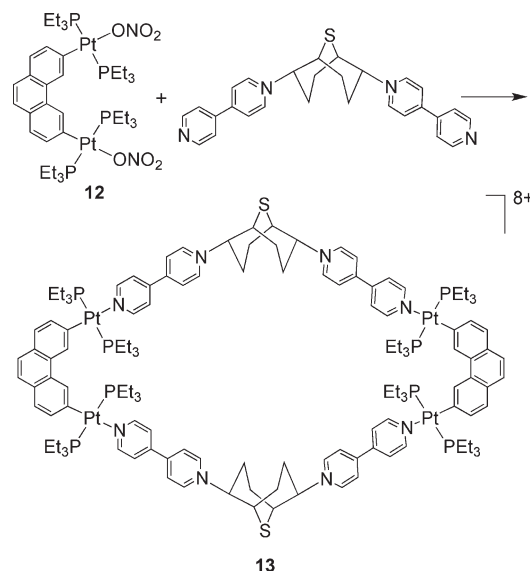


**Figure 10.** General design strategy for the synthesis of M<sub>3</sub>L<sub>3</sub> molecular triangles.

**3.1.2. Molecular Triangles.** A large number of molecular triangles designed by coordination-driven self-assembly have appeared in the literature in the past few decades and have been reviewed.<sup>40</sup> In principle, molecular triangles can be designed in three general ways (Figure 10). A strain-free molecular triangle can be obtained by the combination of 180° linear metal-containing acceptors with 60° angular donor moieties (Figure 10a). Though the complementary method should also lead to a triangle (Figure 10b), the lack of appropriate metalcorner acceptor units with 60° bite angles makes this assembly impractical. However, the combination of distorted metalcorner units with flexible linear donor units can also give rise to molecular triangles (Figure 10c).<sup>40</sup>

There exist a large number of strain-free molecular triangles wherein the 60° donor units occupy the vertices and linear metal-containing acceptors form the edges. A well-known family of triangles of this type are the [M(*μ*-pz)]<sub>3</sub> (14; M = Cu, Ag, Au)

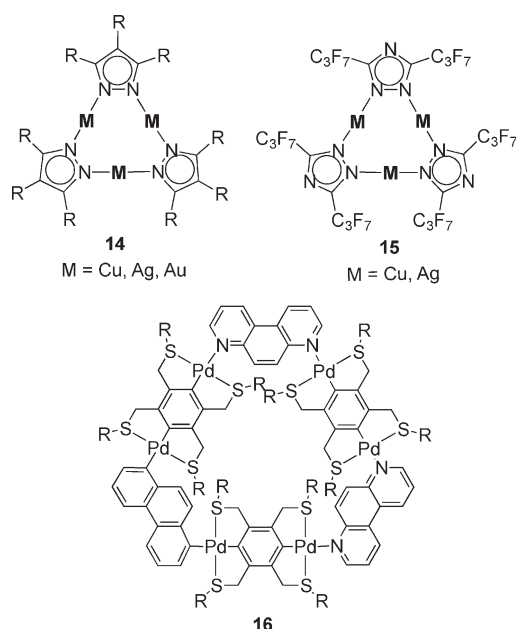


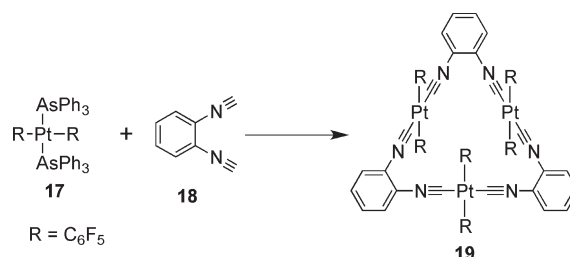
**Figure 11.** Few examples of molecular triangles of Cu(I), Ag(I), and Pd(II).

metallatriangles synthesized using pyrazole or substituted pyrazole and coinage metals (Figure 11).<sup>41,42</sup> Dias and co-workers have reported a number of such triangles containing fluorinated pyrazolate ligands and Cu(I), Ag(I), or Au(I).<sup>43</sup> These metallacycles have interesting photophysical properties with potential applications as molecular light-emitting devices.<sup>44</sup> Closely related Cu(I)<sup>45</sup> and Ag(I)<sup>46</sup> metallatriangles (**15**) of the fluorinated triazolate ligand have also been synthesized using the corresponding metal(I) oxides and the triazole. Other molecular triangles have also been reported, in which 4,7-phenanthroline acts as a rigid 60° donor occupying the corners, while the linear phenyl-bridged dipalladium fragment spans the sides of triangle **16**.<sup>47</sup>

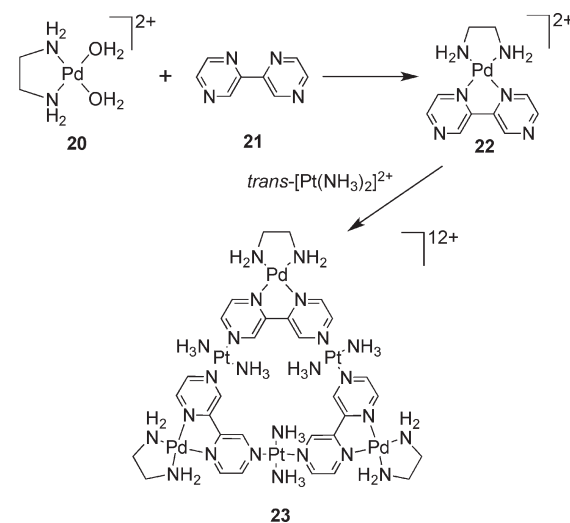
Espinete et al.<sup>48</sup> have reported the formation of a strain-free metallotriangle (**19**) via the 1:1 stoichiometric reaction of *trans*-[Pt(C<sub>6</sub>F<sub>5</sub>)<sub>2</sub>(AsPh<sub>3</sub>)<sub>2</sub>] (**17**) with 1,2-phenylene diisocyanide (**18**; Scheme 6). The solid-state structure showed that the phenylene diisocyanide moieties occupy the vertices while the *trans*-Pt(C<sub>6</sub>F<sub>5</sub>)<sub>2</sub> fragments act as the linear linkers comprising the sides. The C<sub>6</sub>F<sub>5</sub> rings dispose themselves perpendicular to the plane of the metallotriangle. Following this report, a heterometallic anionic Pt<sub>2</sub>Au triangle was synthesized in which *trans*-[Pt(PMe<sub>3</sub>)<sub>2</sub>]<sup>2+</sup> fragments spanned two of the edges with the other edge consisting of one Au(I) edge connected by an {*o*-C≡C-(C<sub>6</sub>Me<sub>4</sub>)C≡C}<sup>2-</sup> fragment.<sup>49</sup>

A novel approach for the formation of cationic metallotriangles of this type was demonstrated by Lippert's group where the vertices of the triangle are metal-containing 60° ligands.<sup>50</sup> The reaction between [Pd(en)(H<sub>2</sub>O)<sub>2</sub>]<sup>2+</sup> (**20**) and 2,2'-bipyrazine (2,2'-bpz; **21**) leads to the formation of a cis-blocked mononuclear complex [Pd(en)(2,2'-bpz)]<sup>2+</sup> (**22**) with two available N-donor sites with coordinate vectors oriented at 60°. The subsequent combination of **22** with *trans*-[Pt(NH<sub>3</sub>)<sub>2</sub>]<sup>2+</sup> in a 1:1 ratio forms the cationic metallotriangle **23** (Scheme 7).<sup>51,52</sup> Another strategy to achieve this class of metallotriangles involves the use of predesigned terpyridine-based angular linkers that possess a 60° angle between the two terpyridine binding sites.<sup>53</sup>

**Scheme 6**



**Scheme 7**

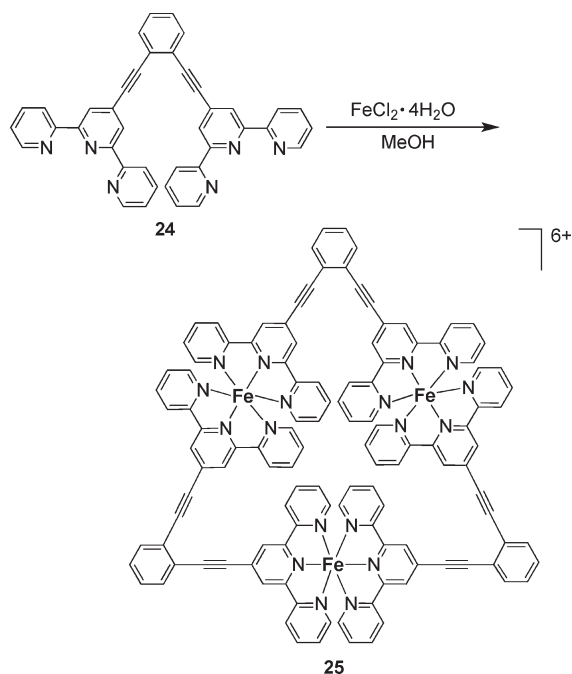


For example, the 1:1 stoichiometric reaction of terpyridine-based ligand **24** with FeCl<sub>2</sub>·4H<sub>2</sub>O or RuCl<sub>2</sub>·(DMSO)<sub>4</sub> in MeOH leads to the formation of cationic homonuclear molecular triangles [M<sub>3</sub>(**24**)<sub>3</sub>]<sup>4+</sup> [M = Fe<sup>2+</sup> (**25**), Ru<sup>3+</sup>] (Scheme 8).<sup>53</sup> NMR (<sup>1</sup>H, <sup>13</sup>C) and electrospray ionization–mass spectrometric (ESI-MS) studies established the formation of the molecular triangles. Heteronuclear triangles can also be accessed by a stepwise construction process by first preparing a [M<sub>2</sub>(**24**)<sub>2</sub>]<sup>4+</sup> species followed by treatment with a different metal ion. Similar predesigned terpyridine-based 60° ligand afforded a trinuclear Fe(II) molecular triangle and a tetranuclear molecular square.<sup>54</sup>

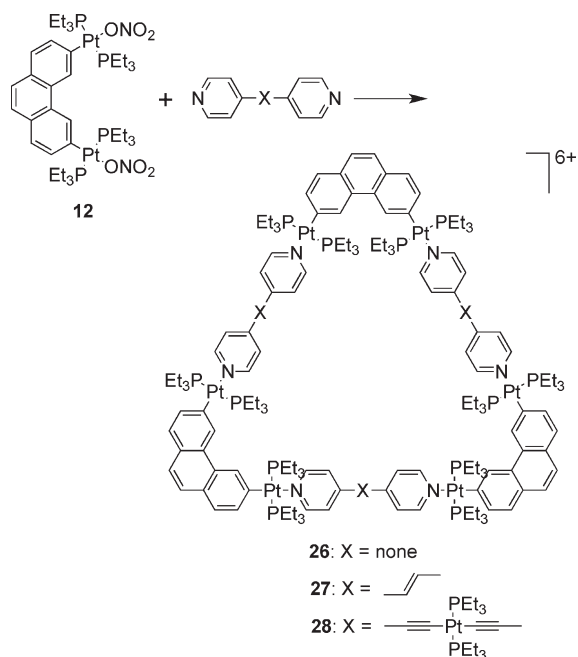
As mentioned above, the design of molecular triangles with 60° metal-containing corner units and linear donors as edges is impractical due to the unavailability of single-center acceptor units with 60° bond angles between the coordinated ligands. However, an elegant use of a 60° diplatinum(II) acceptor unit **12** has made it possible to realize such triangles through coordination-driven self-assembly.<sup>55</sup> The [3 + 3] assembly of **12** with different linear bridging bispyridyl ligands, 4,4'-bipyridine, *trans*-1,2-bis(4-pyridyl)-ethylene, and *trans*-[bis(4-pyridylthynyl)]bis(triethylphosphine)] platinum(II), allows for the formation of strain-free hexacationic supramolecular triangles (**26**–**28**; Scheme 9). The exclusive formations of the supramolecular triangles were confirmed by multinuclear NMR, elemental analysis, and ESI-MS, and in the case of **26**, by X-ray crystallography, which revealed a large, accessible cavity. Although the self-assembly of 90° metal corners with linear linkers should form molecular squares, the distortions from linearity of the linkers also permit the formation of



Scheme 8

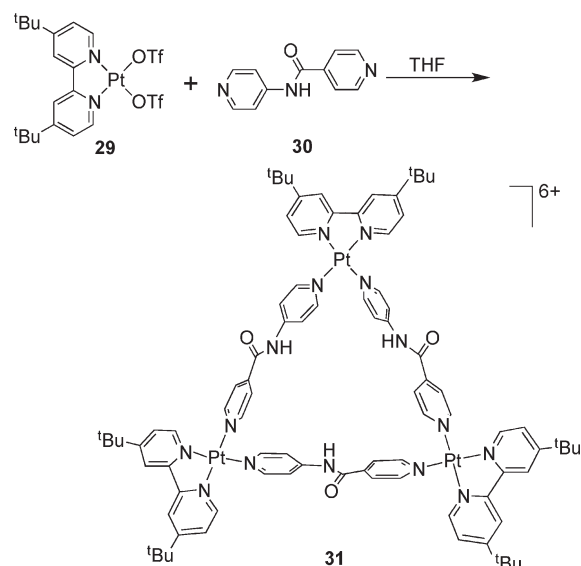


Scheme 9



triangular structures. A decrease in rigidity of the linkers (i.e., upon increasing the length) allows the coordination sphere to maintain near 90° angles; the strain of the trinuclear metallacycle is relieved by a bending of the ligands. A large number of molecular triangles reported in the past 2 decades belong to this class. The self-assembly of such triangular assemblies is often accompanied by the concomitant formation of molecular squares. Several research groups have extensively investigated the dynamic equilibria observed in such systems. A discussion of such systems is

Scheme 10

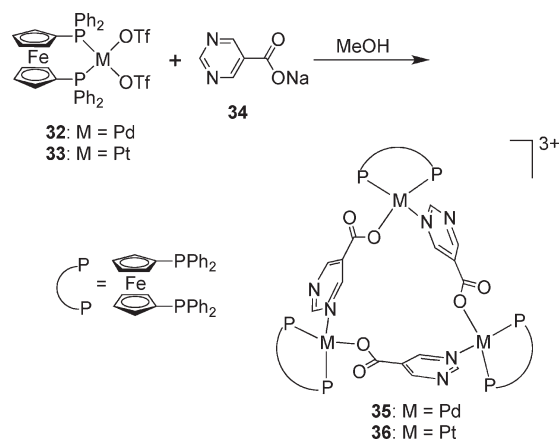


presented in section 3.1.4. There are, however, but a few examples where charged molecular triangles of this class were selectively obtained through coordination-driven self-assembly of cis-protected metal corner units with linear linkers.

Puddephat et al. have reported the synthesis of cationic molecular triangles by a combination of cis-blocked square-planar palladium(II) or platinum(II) units with linear unsymmetrical bis(pyridyl) ligands possessing bridging amides.<sup>56,57</sup> The [3 + 3] self-assembly of [Pt(bu<sub>2</sub>bpy)(OTf)<sub>2</sub>] (29; bu<sub>2</sub>bpy = 4,4'-di-*tert*-butyl-2,2'-bipyridine) with *N*-(4-pyridinyl)isonicotinamide (30) led to the formation of molecular triangle [Pt<sub>3</sub>(bu<sub>2</sub>bpy)<sub>3</sub>-(μ-*N*-(4-pyridinyl)isonicotinamide)<sub>3</sub>]<sup>6+</sup> (31), as shown in Scheme 10. The analogous Pd(II) acceptor unit [Pd(bu<sub>2</sub>bpy)(thf)<sub>2</sub>][BF<sub>4</sub>]<sub>2</sub> also forms a molecular triangle with 30. X-ray structural studies of 31 showed that the three platinum metals occupy the vertices of an approximately equilateral triangle. The unsymmetrical ligand 30 bridges the metal centers and is bowed slightly outward. Of the two possible isomers due to the relative orientation of the unsymmetrical linkers, only one of the lower symmetry isomers was isolated in the solid state.

Interestingly, the use of the ambidentate ligand 5-pyrimidine carboxylate with cis-blocked Pd(II) and Pt(II) metal corners led to the formation of the higher symmetry isomer out of two possible arrangements.<sup>58</sup> The [3 + 3] self-assembly of *cis*-[M(dppf)(OTf)<sub>2</sub>] (M = Pd (32), Pt (33); dppf = 1,1'-bis(diphenylphosphino)ferrocene) with sodium 5-pyrimidine carboxylate (5-pmc; 34) led to the formation of cationic triangles [(dppf)<sub>3</sub>Pd<sub>3</sub>(5-pmc)<sub>3</sub>](OTf)<sub>3</sub> (35) and [(dppf)<sub>3</sub>Pt<sub>3</sub>(5-pmc)<sub>3</sub>](OTf)<sub>3</sub> (36), as shown in Scheme 11. Multinuclear NMR, mass spectrometry, and X-ray structural studies established the formation of these complexes. The crystal structures show that both symmetrical heterometallic molecular triangles 35 and 36 consist of three partially distorted square-planar Pd(II) or Pt(II) centers present at the vertices, of an approximate triangle with three 5-pmc ligands bridging the metal centers in end-to-end fashion through the pyrimidyl-N on one end and the carboxylate-O on the other. The angle of ca. 100° between the two asymmetric donor sites in the 5-pyrimidine carboxylate ligand favors the exclusive formation of triangles over squares since it reduces the ring strain. A variable-temperature

Scheme 11



$^{31}\text{P}$  NMR study of complexes **35** and **36** established that the triangle is the only product in both cases. The steric bulkiness of the dppf ligand is also a driving force for the preferential formation of triangles. Similar self-selection for the symmetrical isomer was also observed in the self-assembly of the ambidentate isonicotinate ligand with  $90^\circ$  acceptor, *cis*-[Pd(dppf)(OTf)<sub>2</sub>] (**32**).<sup>59</sup> Hor et al. have used nicotinates (Nic) as ambidentate linkers for the exclusive assembly of molecular triangles using phosphine-based Pd(II) and Pt(II) metal complexes as corner building units.<sup>60</sup> The molecular triangles [(dppf)<sub>3</sub>Pt<sub>3</sub>(Nic)<sub>3</sub>](OTf)<sub>3</sub> and [(PPh<sub>3</sub>)<sub>6</sub>Pt<sub>3</sub>(Nic)<sub>3</sub>](OTf)<sub>3</sub> were synthesized by self-assembly. Use of the dimetallic gold containing unit [Au<sub>2</sub>(dppf)(MeCN)<sub>2</sub>](OTf)<sub>2</sub> in the self-assembly with isonicotinate as the linker led to the formation of hexametallic gold cornered metallotriangles.<sup>61</sup>

Extended and flexible ditopic bispyridyl ligands “beaded” with cucurbituril have been used to assemble interesting molecular necklaces by coordination-driven self-assembly.<sup>62</sup> To design the ditopic flexible ligand, terminal pyridyl groups were attached to 1,4-diaminobutane or 1,5-diaminopentane to form short “strings” that were then treated with cucurbituril “beads” to form stable pseudorotaxanes. The self-assembly of the ditopic ligands with  $90^\circ$  *cis*-blocked [Pt(en)(NO<sub>3</sub>)<sub>2</sub>] (**37**) led to the formation of cationic molecular triangles. X-ray structural studies on the 1,5-diaminopentane-derived ditopic ligand showed that Pt(II) metal units occupy the vertices of the triangle and are linked on the edges by the sigmoidal-shaped bispyridyl rotaxane (Figure 12). The nature of the pseudorotaxane linkers and reaction conditions significantly influences the final assembly. While refluxing conditions leads exclusively to triangular assemblies, reaction at lower temperature leads to a mixture of triangle and square.

Stang et al. have established the formation of an unusual molecular triangle [(PMe<sub>3</sub>)<sub>6</sub>Pt<sub>3</sub>(μ-pyz)<sub>3</sub>](OTf)<sub>6</sub> (**39**) upon treatment of *cis*-[Pt(PMe<sub>3</sub>)(OTf)<sub>2</sub>] (**38**) with pyrazine (Scheme 12).<sup>63</sup> Solid-state structural studies show that, despite the considerable strain present in **39**, the coordination geometry about the Pt atoms is not significantly distorted from ideal  $90^\circ$  angles to account for the triangular assembly. This result was believed to be due to a combination of entropic factors and the electronic effects of having two platinum centers per pyrazine unit. Two isostructural Pd(II)- and Pt(II)-based triangles have been synthesized and structurally characterized using short 4,5-dicyanoimidazolato ligands as the linkers and [M(bu<sub>2</sub>bpy)Cl<sub>2</sub>] (M = Pd, Pt) as the metal corners.<sup>64</sup>

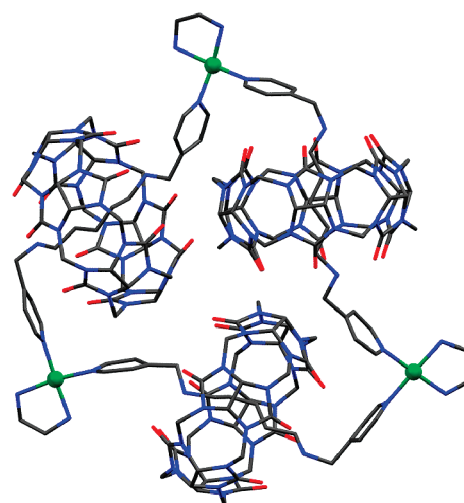
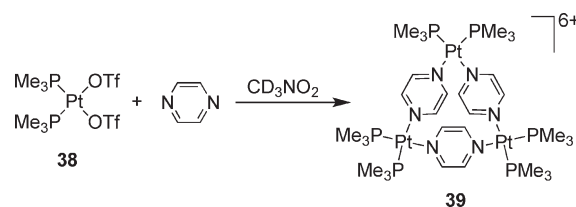


Figure 12. Structure of a triangular molecular necklace. Color code: green, Pt; red, O; blue, N; gray, C.

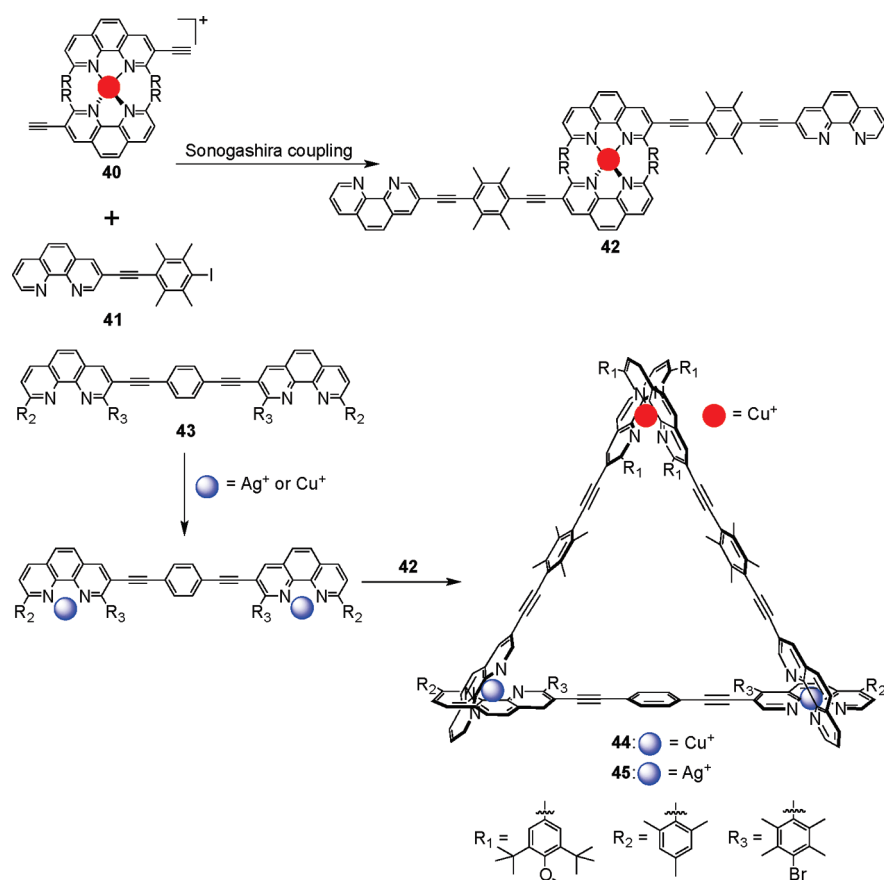
Scheme 12



A redox-active molecular triangle [(cyclen)<sub>3</sub>Ru<sub>3</sub>(bpy)<sub>3</sub>]Cl<sub>6</sub> (cyclen = 1,4,7,10-tetraazacyclododecane) was synthesized by the 1:1 stoichiometric self-assembly of [(cyclen)Ru(DMSO)-Cl]Cl and 4,4'-bpy in a 3:1 ethanol:water mixture.<sup>65</sup> X-ray structural studies revealed a strained equilateral triangle wherein the 4,4'-bpy bridges are bowed outward, forcing the pyridine rings in each linker to be coplanar and perpendicular to the Ru<sub>3</sub> triangle. Using [Ru<sup>II</sup>([9]aneS<sub>3</sub>)] ([9]aneS<sub>3</sub> = 1,4,7-trithiacyclononane) as corner unit, kinetically inert Ru<sub>3</sub> molecular triangles that display well-behaved reversible electrochemical behavior were also reported through self-assembly.<sup>66,67</sup> For example, a reaction of [(9]aneS<sub>3</sub>)Ru(DMSO)Cl<sub>2</sub>] and 9-methyladenine in the presence of a strong Brønsted base led to the formation of a mixed valent Ru<sub>3</sub> molecular triangle. <sup>1</sup>H NMR, FAB, and high-resolution mass spectra as well as elemental analysis established the formation of the tricationic Ru<sub>3</sub> molecular triangles. The triangular complexes were found to be kinetically inert in all oxidation states.

Schmittel and Mahata have designed several heterometallic and heteroleptic triangles through a novel multicomponent approach.<sup>68</sup> The metallacycles were assembled in a stepwise fashion. A kinetically locked copper(I) complex [Cu(phen)<sub>2</sub>]PF<sub>6</sub> (**40**) was constructed as a hinge to which free phenanthroline units **41** were attached through Sonogashira coupling, resulting in hinge **42** (Scheme 13). Treatment of precursor **42** with linear ligand **43**, containing two free phenanthroline units, in the presence of Cu(I) and Ag(I) ions resulted in the formation of trinuclear metallacycles [Cu<sub>3</sub>(**43**)(**42**)](PF<sub>6</sub>)<sub>3</sub> (**44**, homometallic and heteroleptic) and [CuAg<sub>2</sub>(**43**)(**42**)](PF<sub>6</sub>)<sub>3</sub> (**45**, heterometallic and heteroleptic). Using a similar strategy, it was possible to synthesize heterometallic isosceles molecular triangles.<sup>69</sup>

Scheme 13



**3.1.3. Molecular Squares.** Among the metal-mediated assembly of molecular polygons, molecular squares are the most extensively studied.<sup>70</sup> Interest in square metallacycles has been fueled by their ease of preparation, conformational stability, and the distinctive properties they exhibit. According to the directional bonding approach, a molecular square can be formed by the combination of a 90° corner unit with a linear bridging ligand. Thus, there are two complementary ways to design a molecular square: (a) by the combination of a 90° metal-containing acceptor having two accessible cis-coordination sites with linear donor units (Figure 13a) and (b) by using a 180° linear metal-containing acceptor and a ligand with 90° turn (Figure 13b). Almost any transition metal with a square-planar, trigonal-bipyramidal, or octahedral geometry can be used as a corner unit. However, transition metals with square-planar geometries are most widely used because cis-protected 90° metal corner units can be easily derived by blocking adjacent coordination sites with strong chelating ligands, leaving the other two sites accessible for ligand substitution.

Fujita et al. described the first molecular square (**46**) via coordination-driven self-assembly of 90° cis-protected palladium(II) with 4,4'-bipyridine as the linear linker, under ambient conditions (Scheme 14).<sup>23,24</sup> Since then, a vast number of molecular squares have been reported utilizing this strategy. Interestingly, the Pt(II) analogue of square **46** can be obtained only after heating the reaction mixture at 100 °C for 4 weeks. This is due to the kinetic inertness of the Pt–N bond relative to the Pd–N bond.

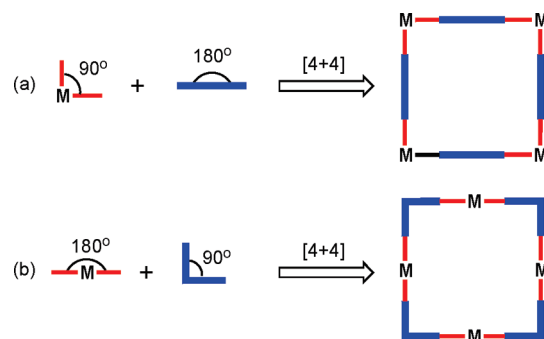
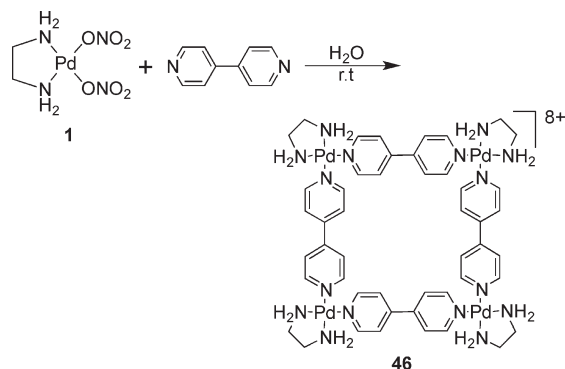


**Figure 13.** General design strategy for the synthesis of  $M_4L_4$  molecular squares.

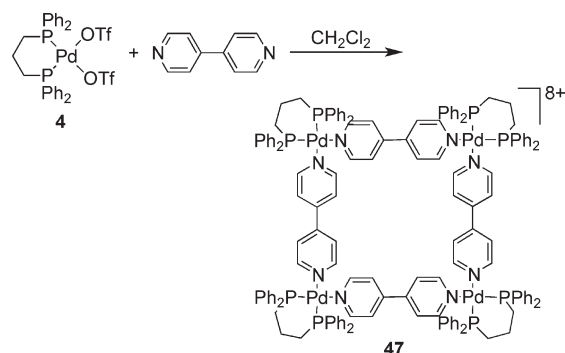
Consequently, Pt(II)-containing molecular squares are more stable than their palladium analogues. This exemplifies that kinetically stable macrocycles can be obtained under thermodynamic control.

Stang and co-workers have used diphosphine-blocked cis-blocked Pd(II) and Pt(II) complexes extensively as 90° metalcorner units to synthesize a large library of molecular squares of varied size and functionality.<sup>8</sup> For example, the phosphino-based counterpart (**47**) of Fujita's square can be assembled from a 1:1 stoichiometric mixture of 90° cis-blocked  $[\text{Pd}(\text{dppp})(\text{OTf})_2]$  (**4**) and 4,4'-bipyridine in  $\text{CH}_2\text{Cl}_2$  (Scheme 15).<sup>25</sup> The selection of phosphine complexes as corner units enables easy monitoring

Scheme 14



Scheme 15

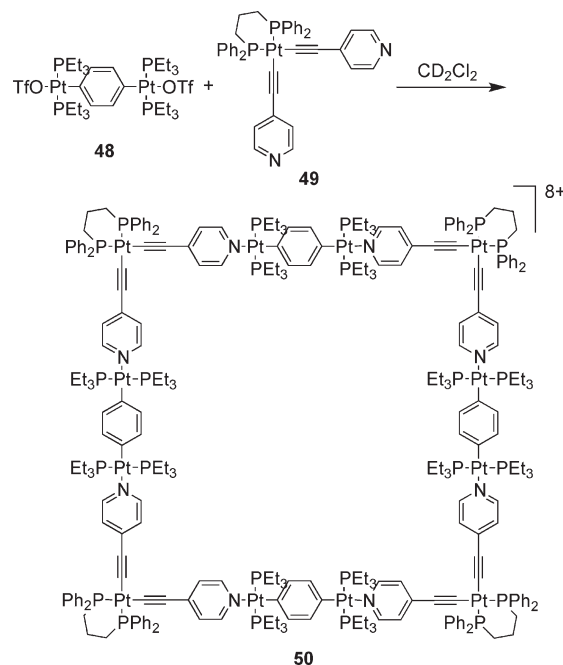


and reliable characterization of the self-assembled products through  $^{31}\text{P}$  NMR spectroscopy. However, the use of phosphine-based ligands makes the ensembles hydrophobic, in contrast to the ensembles derived from amine-based acceptor units.

A number of square assemblies containing various other rigid linking subunits, such as *p*-benzonitrile, 1,4-dicyanobenzene, 4,4'-dicyano-1,1'-biphenyl, diazapyrene, and diazaperylene, combined with both chelated and nonchelated bisphosphines have been reported by the same group.<sup>71,72</sup> The versatility of this self-assembly strategy allows for the synthesis of a series of molecular squares that contain crown ethers or calixarenes as angular units<sup>73</sup> or squares which contain porphyrins as linear linking components.<sup>74</sup> All of these molecular squares were isolated in high yields as robust, air-stable, microcrystalline solids and characterized by multinuclear NMR, mass spectrometry, and X-ray crystallographic studies.

Several platinum-based, large metallo-supramolecular squares with linear metal-containing acceptors on the edges and donor ligands with a  $90^\circ$  turn were also designed using a similar strategy.<sup>75,76</sup> For example, molecular square **50** was made by the self-assembly of linear diplatinum ditopic acceptor **48** with alkynylpyridine-containing donor ligand **49** in  $\text{CD}_2\text{Cl}_2$  at room temperature (Scheme 16). Use of bis(heteroarylodonium) salts as corner units have also led to similar molecular squares with large dimensions. These novel supramolecular species were formed in quantitative yields as assessed by NMR via spontaneous self-assembly and their tetrameric natures were established by electrospray ionization–Fourier transform–ion cyclotron resonance–mass spectrometry (ESI-FT-ICR-MS), multinuclear

Scheme 16



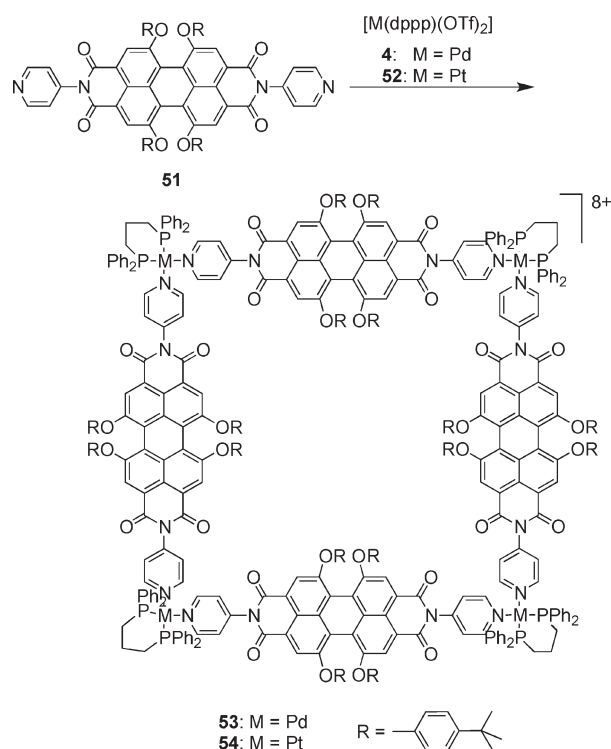
NMR, and physical data. Force field calculations and modeling established the size of these species as ranging from approximately 3.6 to 4.7 nm (diagonally) and from 2.6 to 3.4 nm (side). Likewise, a series of molecular squares were recently assembled from  $90^\circ$  Pt(II)-based alkynylpyridine-containing donor ligands via coordination-driven self-assembly.<sup>77</sup> Photophysical studies of these metallacycles revealed high room-temperature phosphorescence quantum yields and lifetimes attributed to the excited state becoming localized on the  $\pi$ -conjugated bridging ligands following intramolecular charge transfer sensitization.

A series of terpyridine-based, cationic, novel heterometallic squares  $\{(\text{dppf})\text{Pd}[(\text{pyterpy})_2\text{Ru}]\}_4(\text{PF}_6)_8(\text{OTf})_8$  and  $\{\text{fac-Br}(\text{CO})_3\text{Re}[(\text{pyterpy})_2\text{M}]\}_4(\text{PF}_6)_8$  ( $\text{M} = \text{Fe}, \text{Ru}, \text{or Os}$ ,  $\text{pyterpy} = 4'-(4'''\text{-pyridyl})-2,2':6',2''\text{-terpyridine}$ ), were prepared by a self-assembly between  $\text{Re}(\text{CO})_5\text{Br}$  or  $[\text{Pd}(\text{dppf})(\text{OTf})_2]$  (**32**) with  $(\text{pyterpy})_2\text{M}(\text{PF}_6)_2$ .<sup>78</sup> Würthner et al. have constructed molecular squares of nanometer dimensions via the self-assembly of ditopic perylene bisimide bridging ligands with Pt(II) and Pd(II) phosphine corner units.<sup>79</sup> Treatment of ditopic perylene ligand **51** with  $[\text{M}(\text{dppp})(\text{OTf})_2]$  ( $\text{M} = \text{Pd}$  (**4**),  $\text{Pt}$  (**52**)) in  $\text{CH}_2\text{Cl}_2$  leads to the exclusive formation of molecular squares **53** and **54** (Scheme 17). The squares were characterized by elemental analysis,  $^1\text{H}$  and  $^{31}\text{P}$  NMR spectroscopy, and mass spectrometry. The optical and electrical properties of the ligands are conserved in the final assemblies with platinum-based molecular square **54** showing a fluorescence quantum yield of almost unity and multiple, fully reversible redox couples. Ferrocenyl<sup>80</sup> and pyrene<sup>81</sup> functional moieties were also incorporated into the perylene bisimide bridging ligands. The assembly of these functionalized ligands with the Pt(II) phosphine corner unit gave functionalized molecular squares with interesting photophysical and electrochemical properties.

Several other molecular squares were also assembled using titanocene<sup>82,83</sup> and fluxional thiacycrown-based<sup>84</sup> ligands as the corner units. The reactions of the low-valent titanocene sources  $[\text{Cp}^*\text{Ti}(\eta^2\text{-C}_2(\text{SiMe}_3)_2)]$  and  $[\text{BuCp}^*\text{Ti}(\eta^2\text{-C}_2(\text{SiMe}_3)_2)]$



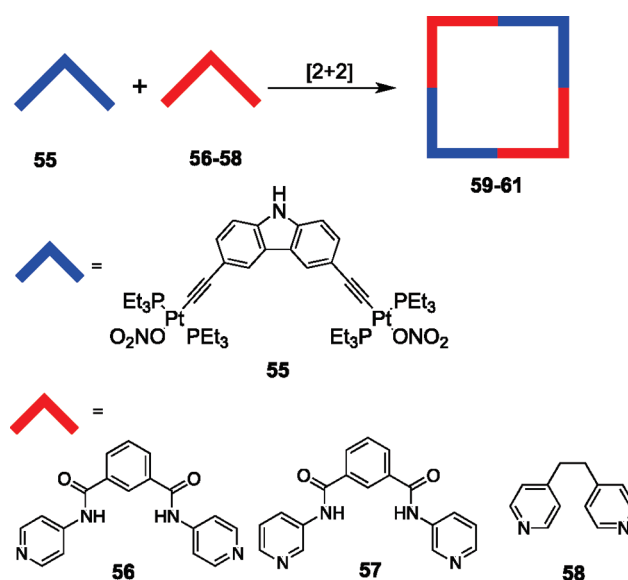
Scheme 17



with various ditopic bridging linkers such as pyrazine, tetrazine, 4,4'-bipyridine, and *trans*-4,4'-azobispyridine resulted in the formation of titanium-based supramolecular squares.<sup>82</sup> Similarly, treatment of a thiocrown-capped Pt(II) complex, [Pt([9]aneS<sub>3</sub>)Cl<sub>2</sub>] with 4,4'-bipyridine in the presence of silver triflate led to a platinum(II) molecular square incorporating four fluxional thiocrown ligands at the corners.<sup>84</sup> Hor et al. have described a cationic molecular square [(dppf)<sub>4</sub>Pt<sub>4</sub>(isonicotinate)<sub>4</sub>](OTf)<sub>4</sub> obtained through a ligand displacement reaction in which a dinuclear Pt<sub>2</sub>Br<sub>2</sub>(dppf)<sub>2</sub>(C<sub>8</sub>H<sub>4</sub>S<sub>2</sub>) species exchanges with isonicotinic acid to release free bithiophene, giving the molecular square.<sup>85</sup> Solid-state structural studies revealed that a highly symmetrical structure was formed with the four bridging isonicotinate ligands oriented in a head-to-tail fashion. In a separate study, the palladium analogue of the molecular square was crystallized from an equilibrating mixture of a triangle and square (*vide infra*).<sup>86</sup>

A series of [2 + 2] self-assembled molecular squares were recently reported utilizing a 90° platinum(II)-based carbazole ligand as the acceptor in conjunction with various flexible ditopic ligands as donors.<sup>87</sup> The treatment of 3,6-bis[*trans*-Pt(PEt<sub>3</sub>)<sub>2</sub>(NO<sub>3</sub>)(ethynyl)]carbazole (**55**) with pyridyl donor ligands 1,3-bis(4-pyridyl)isophthalamide (**56**); 1,3-bis(3-pyridyl)isophthalamide (**57**), and 1,2-di(4-pyridyl)ethane (**58**) led to the formation of molecular squares **59–61** in good yields (Scheme 18). Multinuclear NMR and ESI-MS studies established the formation of the squares. Fluorescence studies on the square **59** showed that it could selectively sense pyrophosphate anion. Enhancement of fluorescence intensity was observed upon titration with aqueous P<sub>2</sub>O<sub>7</sub><sup>4−</sup> in dimethylformamide (DMF) solution. Interestingly, no such perturbation in fluorescence intensity was observed when the titration was carried out with other anions (F<sup>−</sup>, ClO<sub>4</sub><sup>−</sup>, H<sub>2</sub>PO<sub>4</sub><sup>−</sup>). A novel redox-active [2 + 2] molecular square containing two

Scheme 18



vinyllogous tetrathiafulvalenes and two molybdenum tetracarbonyl fragments was also reported via coordination-driven self-assembly of complementary angular units.<sup>88</sup>

Mirkin et al. have designed a tetranuclear hetero-bimetallic square through the cooperative ligand binding properties of square-planar and tetrahedral metal centers.<sup>89</sup> The treatment of a flexible phosphinothioether-based hemilabile ligand with a mononuclear Rh(I) source in a 2:1 ratio, followed by the addition of 1 equiv of Zn(II) leads to the formation of heterobimetallic square **62** in high yield (Figure 14). X-ray structural studies have shown that the two square-planar Rh(I) centers and the two distorted tetrahedral Zn(II) centers are bound by four hemilabile ligands. It was observed that the *cis*-phosphine/*cis*-thioether arrangement of the ligands around the Rh center is crucial in enforcing the directionality of the ligand.<sup>89</sup> A homometallic Rh(I) tetranuclear metallacycle (**63**) was also isolated and structurally characterized (Figure 14).<sup>90</sup>

**3.1.4. Triangle-Square Equilibrium.** The composition of a self-assembly product depends upon the rapid chemical exchange between the complementary building blocks, reaction intermediates, and the final ensembles. This enables the system to self-correct, giving the most stable thermodynamically controlled product. However, thermodynamic control only affords the formation of a single product when there is a sufficient energetic advantage of one species over the other possible species. There are several metallo-supramolecular systems where two or more macrocyclic species exist in dynamic equilibrium in solution, due to the lack of a clear thermodynamic preference for one species over the other.

According to the directional bonding approach the self-assembly of 90° metal corners with linear and relatively rigid bridging ligands, in principle, should result in molecular squares. However, several such systems have afforded instead an equilibrium mixture of supramolecular squares and triangles. These equilibria can be rationalized from a thermodynamic point of view; a delicate balance between entropy and enthalpy determines the ratio of squares and triangles. While a molecular square is enthalpically favored due to a smaller conformational strain as

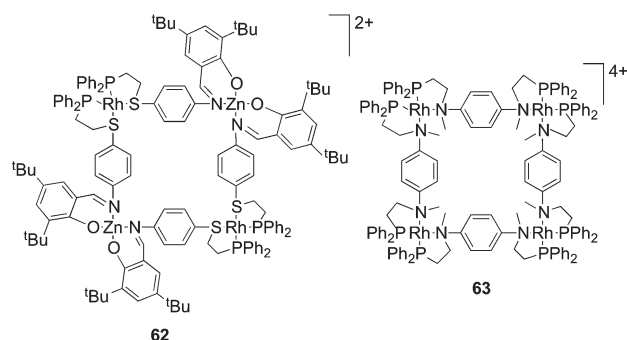


**Figure 14.** Rh(I) based squares through the cooperative ligand binding properties.

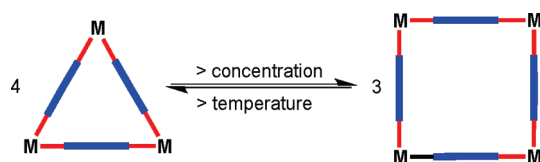


**Figure 15.** Equilibrium between a self-assembled molecular triangle and a square.

compared to triangles, entropy favors the formation of triangles since they are assembled from a smaller number of components. The equilibrium between triangle and square can be written as

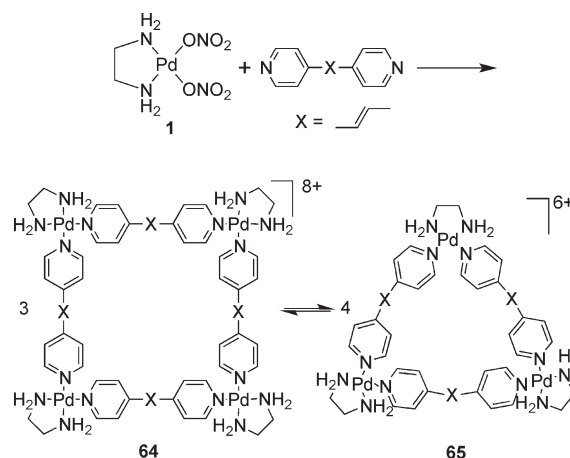


Thus, according to Le Chatelier's principle, an increase in the concentration of the components in the mixture shifts the equilibrium from triangles to squares, while an increase in temperature drives the equilibrium toward the triangles, since the transformation from squares to triangles is expected to be an endothermic process (Figure 15).

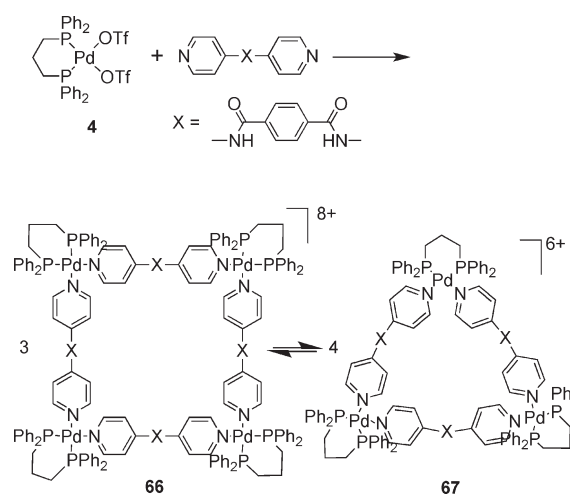
The nature of the linear ligands also plays a vital role in the triangle–square equilibrium. An increase in the flexibility of the ligands favors the formation of triangles by delocalizing strain through small deformations in the backbone. Sufficiently rigid linkers shift the equilibrium significantly in the direction of the molecular square since the enthalpic gain compensates for the entropic penalty of square formation. It was Fujita et al. who first observed that molecular triangles are favored over the corresponding squares when extended and constitutionally flexible bispyridyl linkers were employed.<sup>91</sup> For example, the assembly of  $[\text{Pd}(\text{en})(\text{NO}_3)_2]$  (**1**) with *trans*-1,2-bis(4-pyridyl)ethylene led to the formation of two different macrocycles: molecular square **64** and molecular triangle **65** (Scheme 19). The two macrocycles were in dynamic equilibrium with **64** being the major product. At higher concentration, the equilibrium shifted toward the square, producing three molecules of **64** from four molecules of **65**.

Schalley et al.<sup>92</sup> have employed a series of extended and flexible bispyridyl linkers with *cis*-blocked  $[\text{M}(\text{dppp})(\text{OTf})_2]$ , ( $\text{M} = \text{Pd}$  (**4**),  $\text{Pt}$  (**52**)) complexes as the corner building units to demonstrate the triangle–square equilibrium in solution. Scheme 20 shows the equilibrium for Pd(II) square **66** and triangle **67** in the reaction of  $[\text{Pd}(\text{dppp})(\text{OTf})_2]$  (**4**) and *N,N'*-di(4-pyridyl)terephthalamide. The complexes under study were characterized by a

**Scheme 19**



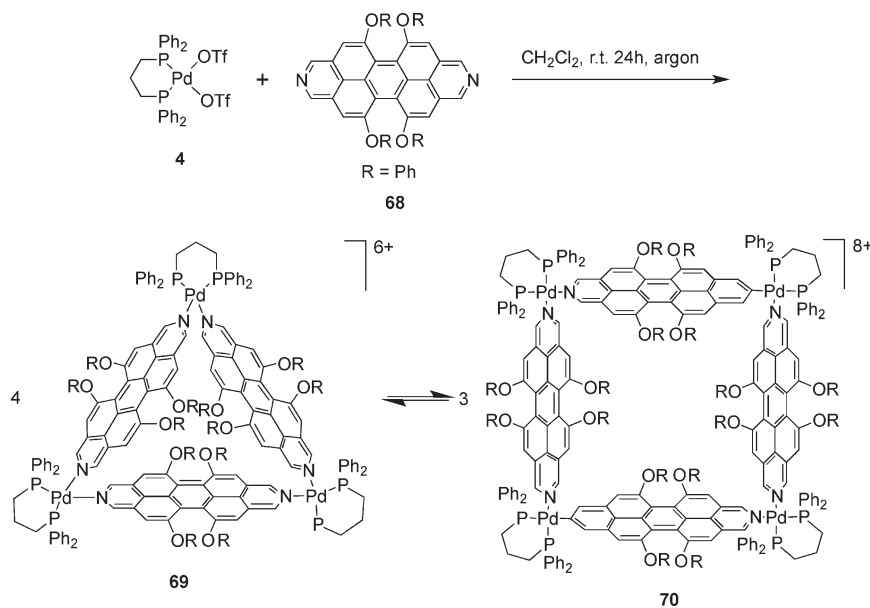
**Scheme 20**



combination of multinuclear NMR, ESI-FT-ICR-MS, and X-ray crystallography. Temperature, concentration, and solvent type significantly influenced the equilibrium. At higher temperature, the equilibration of the squares and triangles is significantly faster as determined from variable-temperature NMR spectroscopy. Due to the greater kinetic stability, the ligand exchange process in the Pt(II) complexes is slow compared to the Pd(II) complexes. Consequently, the triangle–square equilibration is significantly faster for Pd(II) complexes than their Pt(II) analogues. It was observed that the square:triangle ratio is influenced by the change in building block concentration. Increasing amounts of nonpolar solvents promotes the exchange processes, resulting in an increased preference for triangle formation.<sup>92</sup>

The triangle–square equilibria also depend on the nature of the ancillary ligands on the metal fragments. It has been shown that even the rigid linker 4,4'-bipyridine can lead to a mixture of the two macrocycles: square and triangle when 2,2'-bipyridine replaces the ethylenediamine capping ligand.<sup>91</sup> The effect on the equilibrium of the ancillary ligands on the metal fragments was suggested to be due to the steric repulsion between the 2,2'-bipyridine and 4,4'-bipyridine moieties present in the macrocycles, pushing the equilibrium to some extent toward the formation of

Scheme 21



the molecular triangle. A recent study on the influence of the steric properties of chelating diamines on the position of the trimeric–tetrameric equilibrium has also corroborated the above suggestion.<sup>93</sup> In the self-assembly of  $[\text{Pd}(\text{N}–\text{N})](\text{NO}_3)_2$  with 4,4′-bipyridine as the bridging ligand, the effects of several diamine ancillary ligands (N–N) such as *N,N,N′,N′*-tetramethylethylenediamine, *N,N,N′,N′*-tetraethylethylenediamine, 1,3-diaminopropane, *N,N′*-dimethylpiperazine, homopiperazine, and ethylenediamine on the final assembly were systematically investigated by <sup>1</sup>H and DOSY NMR spectroscopy and X-ray diffraction. All of the chelating diamine ligands exhibited dynamic triangle–square equilibria. Molecular triangles became the major components of the mixture when the diamine was bulky, while less bulky chelates favored molecular squares.

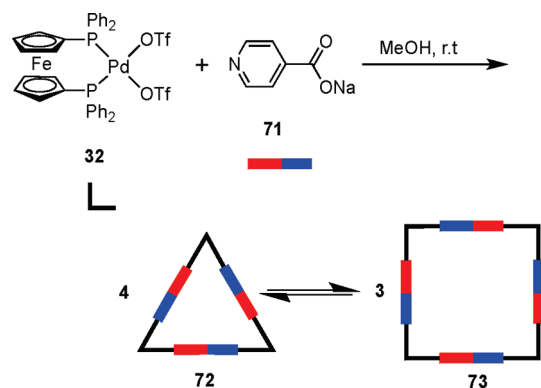
Ferrer and co-workers<sup>94</sup> have also extensively investigated the effect of the ancillary ligands on the equilibria between molecular triangles and squares with different diphosphine chelating ligands. The reaction of cis-blocked  $[\text{M}(\text{P}–\text{P})(\text{OTf})_2]$  precursors (M = Pt, Pd) obtained from different diphosphines—dppp, dpfp, and 1,2-bis(diethylphosphino)ethane (depe) with the rigid linker 1,4-bis(4-pyridyl)tetrafluorobenzene—led to the formation of a mixture of the corresponding molecular squares and triangles. The characterization of the dynamic triangle–square equilibria by multinuclear NMR in combination with mass spectrometry revealed a dependency of the square:triangle ratio on several factors, such as the nature of the metal corners, concentration, and solvent. The use of sterically demanding diamines 4,4′-*R*<sub>2</sub>bpy (R = H, Me, *t*-Bu) as ancillary ligands in the cis-protected palladium(II) and platinum(II) complexes  $[\text{M}(4,4′\text{-R}_2\text{bpy})(\text{OTf})_2]$  (M = Pd, Pt; R = H, Me, *t*-Bu) with the same 1,4-bis(4-pyridyl)tetrafluorobenzene ligand also showed a dynamic equilibrium between molecular triangle and square.<sup>95</sup> However, the analogous reactions where ethylenediamine was used as the ancillary ligand led to only molecular squares.<sup>94</sup> Interestingly, it has also been shown that mononuclear species may also participate in square–triangle equilibria when longer octafluoro-containing rigid linkers are

used in conjunction with *cis*- $[\text{Pd}(\text{tmen})(\text{NO}_3)_2]$  (tmen = tetramethylethylenediamine).<sup>96</sup>

The nature of the linear linkers also has a profound impact on triangle–square equilibria. In their study of the self-assembly of 90° cis-protected  $[\text{Pd}(\text{dppp})(\text{OTf})_2]$  (**4**) with phenoxy-substituted diazadibenzoperylene linear linker, **68**, Würthner and co-workers have observed a complex dynamic equilibria between molecular triangle **69** and square **70** (Scheme 21).<sup>97</sup> Linear linker **68** has a highly twisted and nonflexible aromatic backbone. Despite the possibility of  $\pi$ – $\pi$  interactions between the two phenyl groups of the dppp ligand and the  $\pi$ -surface of the diazadibenzoperylene ligands, which should stabilize the molecular square, the steric requirement of the phenoxo groups on **70** drives the equilibrium toward the triangle, as more space is available. The additional space makes the triangle energetically favorable, despite the distorted geometry at the metal centers. However, the use of a perylene bisimide ligand that is significantly longer and thus can reduce the steric crowding of the phenoxo substituents results in the exclusive formation of the molecular square.<sup>98,99</sup>

Unfortunately, selective isolation of both species involved in a square–triangle equilibrium is not always possible. In their investigation of the equilibrating mixture of a triangle and square obtained by the self-assembly of  $[\text{Pt}(\text{PMe}_3)_2(\text{OTf})_2]$  (**38**) with bispyridyl ethylene (bpe), Stang and co-workers accomplished the selective crystallization of either of the two species via the appropriate choice of solvents and nature of the anions present in the system.<sup>100</sup> While the cationic molecular square was crystallized as the triflate salt,  $[(\text{PMe}_3)_2\text{Pt}(\text{bpe})_4](\text{OTf})_8$ , the molecular triangle was crystallized as a mixed triflate/cobalticarbonyl salt,  $[(\text{PMe}_3)_2\text{Pt}(\text{bpe})_3](\text{OTf})_4(\text{CoB}_{18}\text{C}_4\text{H}_{22}^-)_2$ . Similar results were observed in a study<sup>86</sup> focused on the use of ambidentate linkers to construct supramolecular macrocycles with cis-blocked Pd(II) and Pt(II) complexes as corner pieces. The self-assembly reaction of 90° acceptor *cis*- $[\text{Pt}(\text{dpfp})(\text{OTf})_2]$  (**33**) with an equimolar amount of the ambidentate ligand sodium isonicotinate (**71**) allows for the formation of a

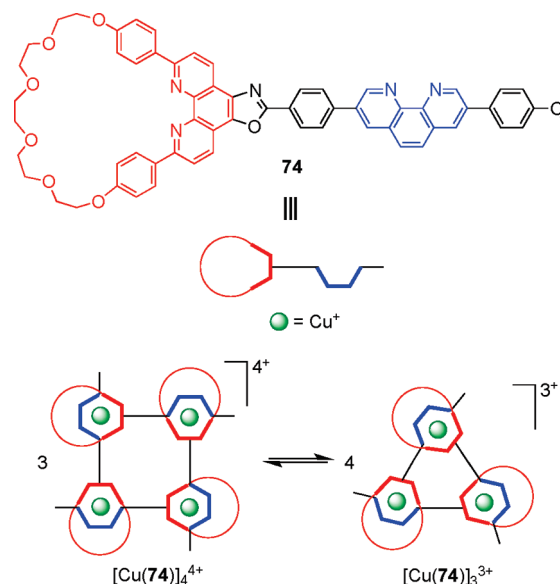
Scheme 22



mixture of symmetrical triangles (72) and squares (73) in solution (Scheme 22). Selective crystallization of a rhomboid was achieved from a dynamic equilibrium between a supramolecular dimeric rhomboid and trimeric hexagon.<sup>101</sup> However, the species isolated in the solid state might not be necessarily the predominant species in solution. An analogous reaction using *cis*-[Pd(tmen)(NO<sub>3</sub>)<sub>2</sub>] also produced a mixture of symmetrical triangles and squares in solution. The assemblies were characterized by <sup>1</sup>H, <sup>31</sup>P, and DOSY NMR spectroscopy and X-ray diffraction. Though only the molecular square crystallized in both cases, the solution composition was a mixture of square and triangle, with the latter as the major component in both cases. The square:triangle ratio depends on the temperature as well as the concentration of the building blocks.<sup>86</sup>

There are other systems where self-assembly reactions have led to the formation of a mixture of triangles and squares without any equilibrium between them. For example, Yu et al. have reported the synthesis of bispyrazole-based molecular triangles and squares using Pd(II)- and Pt(II)-based dimetal clips.<sup>102</sup> The self-assembly reaction of a series of tetramethyl-substituted bispyrazolato ligands—3,3',5,5'-tetramethyl-4,4'-bipyrazolyl, 1,4-bis-4'-(3',5'-dimethyl)-pyrazolylbenzene, and 1,4-bis-4'-(3',5'-dimethyl)-pyrazolylbiphenyl—of different lengths with dimetal clips [M(2,2'-bpy)(NO<sub>3</sub>)<sub>2</sub>]<sub>2</sub>(NO<sub>3</sub>)<sub>2</sub> (M = Pd or Pt) or [M(phen)(NO<sub>3</sub>)<sub>2</sub>]<sub>2</sub>(NO<sub>3</sub>)<sub>2</sub> (M = Pd or Pt, phen = 1,10-phenanthroline) allowed for the formation of molecular triangles and squares through spontaneous deprotonation of the pyrazolato ligands. As determined by NMR, the macrocycles were stable and no dynamic equilibrium between the corresponding triangles and squares was observed. The treatment of Pd(II) dimetal clips with the longer bispyrazolate linkers led to the formation of a non-equilibrating mixture of the corresponding molecular triangles and squares. The triangle:square ratio is dependent on the length of connecting linkers. With longer linkers, the ratio of triangle:square is nearly unity. However, with shorter ligands, the triangle:square ratio significantly shifts in favor of the square. Interestingly, with the shortest bispyrazole ligand (3,3',5,5'-tetramethyl-4,4'-bipyrazolyl), molecular triangles were obtained exclusively with both Pd(II) and Pt(II) dimetal clips. These tetrasubstituted bispyrazole linkers have interplanar angles of about 50–90° due to the steric repulsion of the four methyl groups, resulting in the formation of distorted metallo-macrocyclic assemblies. The synthesis of symmetrical triangular and square assemblies using an unsubstituted coplanar 4,4'-bipyrazolate ligand has also been reported.<sup>103</sup>

Scheme 23



Sauvage et al.<sup>104,105</sup> have observed the existence of a dynamic equilibrium between trinuclear and tetranuclear cyclic pseudorotaxanes. The Cu(I)-mediated assembly of trinuclear [Cu(74)]<sub>3</sub><sup>3+</sup> and tetranuclear [Cu(74)]<sub>4</sub><sup>4+</sup> pseudorotaxanes were attained by using a phenanthroline-containing macrocycle which is rigidly attached to a filament bearing a second phenanthroline unit, 74 (Scheme 23).<sup>105</sup> The coordination vectors of the two binding sites are orthogonal to each other, forcing the ligand to orient in an isofashion. A similar ditopic ligand having phenanthroline and terpyridine binding sites orthogonal to each other gave a non-equilibrating mixture of dinuclear and trinuclear macrocycles where the Cu(I) atom was pentacoordinated to a terpyridine unit and a phenanthroline unit from another ligand.<sup>106</sup>

**3.1.5. Molecular Rectangles.** The design and synthesis of molecular rectangles has motivated supramolecular chemists for some time, largely due to their interesting photophysical and molecular recognition properties.<sup>107</sup> However despite the relative topological simplicity, the syntheses of molecular rectangles are not straightforward. The combination of a 90° metal precursor with two rigid linear linkers of differing lengths in the absence of any driving bias should result in a molecular rectangle. However, two molecular squares of different sizes are generally obtained instead of a rectangle due to the strong enthalpic driving force in favor of square formation (Figure 16) and the lack of selective recognition by the two different linear linkers. Only in the case of Re(I) were a few rectangles obtained using a three-component assembly approach where two linear linkers of different lengths were utilized.<sup>108</sup>

As a result, various groups have developed several different approaches over the past few years for the preparation of supramolecular rectangles. Stang and co-workers have developed an approach wherein a pre-designed platinum-based molecular clip containing two parallel donor sites that are disposed in the same direction is treated with linear ditopic ligands to achieve self-assembled molecular rectangles.<sup>109</sup> The [2 + 2] self-assembly of diplatinum(II) molecular acceptor 1,8-bis[*trans*-Pt(PEt<sub>3</sub>)<sub>2</sub>(NO<sub>3</sub>)]anthracene (75) with rigid bispyridyl bridging ligands—4,4'-bipyridine, *trans*-1,2-bis(4-pyridyl)ethylene, 1,4-bis(4'-pyridylethynyl)benzene,



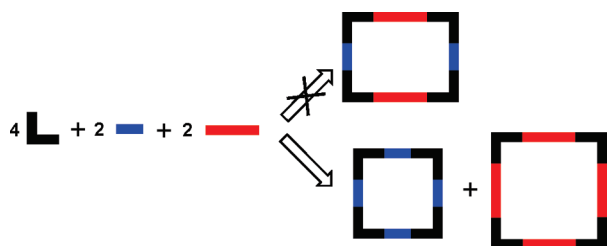


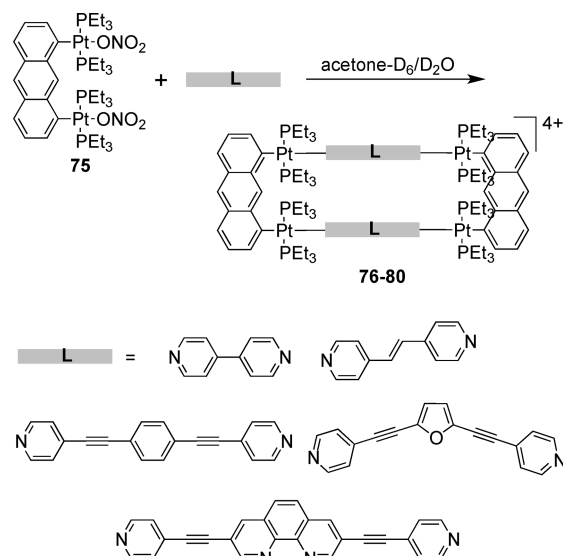
**Figure 16.** Formation of molecular squares of different sizes instead of a rectangle due to the strong enthalpic driving force.

2,5-bis(4'-pyridylethynyl)furan, and 3,8-bis-pyridin-4-yl-ethynyl-[1,10]-phenanthroline—led to the formation of cationic molecular rectangles **76–80** (Scheme 24). Characterization of the rectangles was accomplished with multinuclear NMR and UV–visible spectroscopy, FAB–MS, and X-ray crystallography. Spectroelectrochemical studies on **76** and **77** showed that the compounds could be reversibly reduced at the neutral bispyridyl acceptor ligands while oxidation occurs at the dianionic anthracene clips.<sup>110</sup> The phenanthroline functionalized molecular rectangle **80** has been shown to act as an optical sensor for Ni(II), Cd(II), and Cr(III) ions.<sup>111</sup>

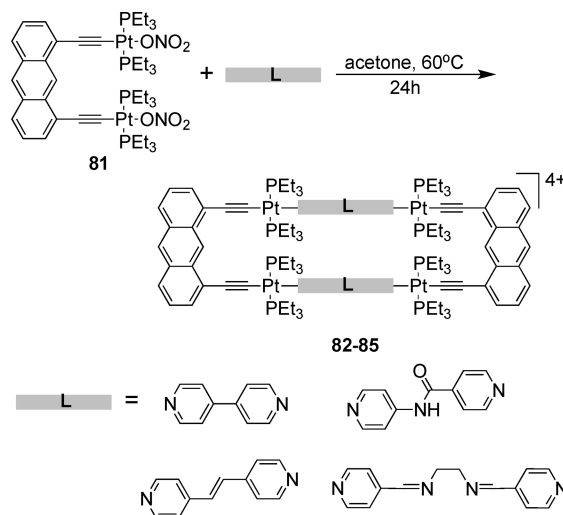
Similarly, the [2 + 2] self-assembly of a diplatinum(II) molecular clip (**75**) with a linear unsymmetrical bispyridyl ligand, *N*-(4-pyridinyl)isonicotinamide (**30**), led to the formation of a symmetrical rectangle.<sup>112</sup> Of the two possible linkage isomers, only the most symmetrical one was observed on the basis of multinuclear NMR, mass spectrometry, and X-ray structural studies. The solid-state structure of the rectangle shows that the bispyridyl ligands occupy the long edge of the rectangle. A functionalized bis(pyridyl)-substituted perylene diimide ligand was also incorporated by treatment with the anthracene-based clip (**75**) to form a functional molecular rectangle.<sup>113</sup> Extending the same strategy further, a series of discrete cationic rectangles (**82–85**) were synthesized using a di-Pt(II) molecular clip containing ethynyl functionality **81** with bispyridyl linear linkers such as 4,4'-bipyridine, *trans*-1,2-bis(4-pyridyl)ethylene, *N*-(4-pyridyl)-isonicotinamide, and *N,N'*-bis(4-pyridylidene)ethylenediamine (Scheme 25).<sup>114</sup> The assemblies were characterized by multinuclear NMR and mass spectrometry. Rectangle **85** was designed with the aim of introducing a N<sub>4</sub> pocket that could act as a receptor site for transition metal ions. The incorporation of ethynyl functionalities introduced fluorescent behavior into the discrete assemblies. Molecular rectangle **85** was fluorescent and showed quenching in solution upon the binding of hard transition metal ions (Fe<sup>3+</sup>, Cu<sup>2+</sup>, Ni<sup>2+</sup>, and Mn<sup>2+</sup>) into the N<sub>4</sub> pocket. Ko et al. have reported a series of Pt<sub>4</sub> rectangles from a diplatinum aromatic molecular clip bearing two symmetrically bound platinum moieties.<sup>115</sup>

Bosnich et al. reported the synthesis of a molecular clip bearing two symmetrically bound terpyridyl chelators separated by aromatic spacers.<sup>116</sup> Dipalladium(II) complexes of these spacer-chelators readily form large molecular rectangles with linear linkers such as 4,4'-bipyridine. Hupp and co-workers have designed rhenium-based molecular rectangles via a stepwise process (Scheme 26).<sup>117</sup> A stable bimetallic edge **86** was created first by treating *fac*-Re(CO)<sub>3</sub>Cl with a rigid 2,2-bipyrimidine ligand. Subsequent assembly of the edges with bispyridyl ditopic linker 4,4'-bipyridine and *trans*-1,2-bis(4-pyridyl)ethylene resulted in the formation of cationic molecular rectangles **87** and **88**.<sup>117</sup> Cationic molecular rectangles containing cofacial porphyrin edges were assembled from the reaction of

**Scheme 24**



**Scheme 25**

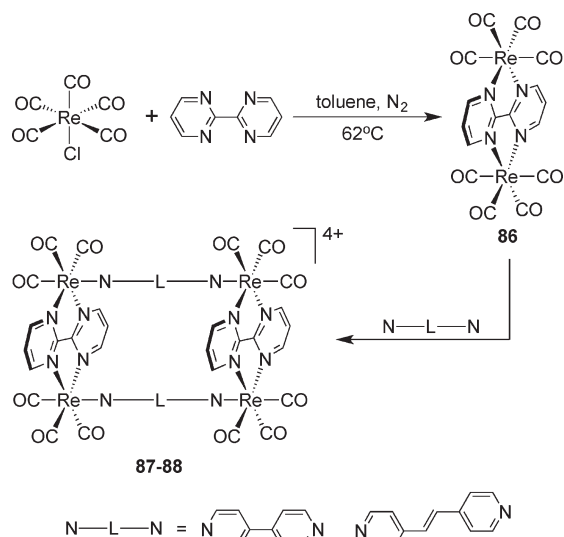


bis(4-ethynylpyridyl)porphyrin with bimetallic edge **86** in an equimolar ratio.<sup>118</sup>

Süss-Fink and co-workers<sup>119</sup> have prepared the cationic molecular rectangle [Ru<sub>4</sub>(*p*-cymene)<sub>4</sub>(μ-bpy)<sub>2</sub>(μ-C<sub>2</sub>O<sub>4</sub>)<sub>2</sub>]<sup>4+</sup> (**91**) by first creating a bimetallic edge **90**, formed from the treatment of dimeric ruthenium arene precursors **89** with oxalate, and then assembling it with the ditopic linear linker 4,4'-bipyridine in MeOH (Scheme 27). Alternately, reactions of [Cp<sup>\*</sup>MCl<sub>2</sub>]<sub>2</sub> (M = Rh, Ir) with bidentate ligand (L = pyrazine; L' = diisocyanide) gave the bimetallic edge [Cp<sup>\*</sup>MCl<sub>2</sub>(L or L')]<sub>2</sub>, which upon treatment with silver trifluoromethanesulfonate (AgOTf) led to tetranuclear cationic metallarectangular complexes [Cp<sup>\*</sup><sub>2</sub>M<sub>2</sub>Cl<sub>2</sub>-(L)(L')]<sub>2</sub>(OTf)<sub>4</sub> containing different ligands.<sup>120</sup>

Building upon the same strategy, Therrien's group<sup>121</sup> prepared a series of cationic arene ruthenium-based molecular rectangles having large cavities. For example, metallarectangles [Ru<sub>4</sub>(η<sup>6</sup>-*p*-cymene)<sub>4</sub>-(μ-N∩N)<sub>2</sub>(OO∩OO)<sub>2</sub>]<sup>4+</sup> were synthesized from the dinuclear

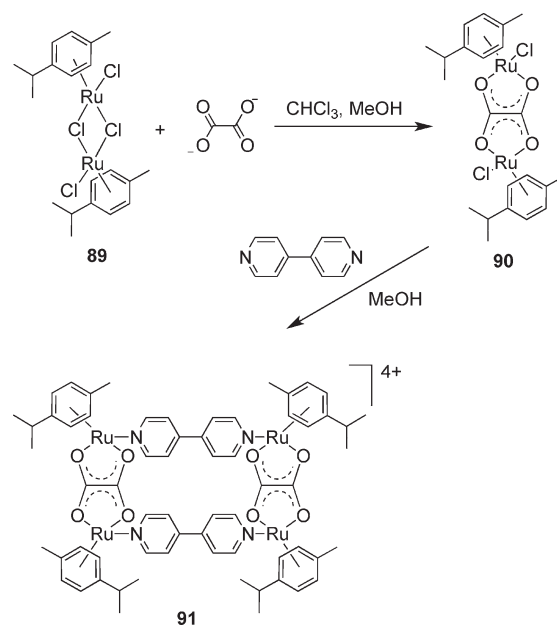
Scheme 26



arene ruthenium complexes  $[\text{Ru}_2(\eta^6\text{-}p\text{-cymene})_2(\mu\text{-OO} \cap \text{OO})_2\text{-Cl}_2]$  ( $\text{OO} \cap \text{OO} = 2,5\text{-dihydroxy-1,4-benzoquinonato (dhbq)},^{122}$   $2,5\text{-dichloro-3,6-dihydroxy-1,4-benzoquinonato (dchq)},^{122}$   $5,8\text{-dihydroxy-1,4-naphthoquinonato (dhnq)},^{123}$   $9,10\text{-dihydroxy-1,4-anthraquinonato (dhaq)},^{124}$  or  $6,11\text{-dihydroxy-naphthacene-5,12-dionato (dhtq)}^{124}$ ) by reaction with pyrazine, bipyridine, or 1,2-bis(4-pyridyl)ethylene linkers ( $\text{N} \cap \text{N} = \text{pyrazine, 4,4'-bipyridine, 1,2-bis(4-pyridyl)ethylene}$ ) in the presence of  $\text{AgOTf}$  in methanol. The complexes were characterized by spectroscopic methods, X-ray crystallography, and cyclic voltammetry. Host-guest studies using aromatics as the guest molecules in these metallarectangles suggested that metallarectangles incorporating 1,2-bis(4-pyridyl)ethylene as the linkers were able to host an anthracene, pyrene, perylene, or coronene molecule in their cavity while rectangles having 4,4'-bipyridine as the linker can only encapsulate anthracene. However, out-of-cavity interactions were observed between 4,4'-bipyridine-containing rectangles and pyrene, perylene, or coronene. In contrast, the small pyrazine-containing metallarectangles show no interaction in solution. Jin and co-workers have also synthesized similar metallarectangles by the combination of the unsaturated dinuclear arene ruthenium, iridium, and rhodium clips and various linear bidentate pyridyl connectors, pyrazine, 4,4'-bipyridine, 1,2-bis(4-pyridyl)ethylene, and 4-[5-(4-pyridyl)-1,3,4-oxadiazol-2-yl]pyridine to generate the corresponding metallarectangles.<sup>125,126</sup> The metallarectangles having 1,2-bis(4-pyridyl)ethylene as the connectors were also shown to undergo a  $[2 + 2]$  cycloaddition of the olefinic double bonds under UV radiation both in solution and in the solid state.<sup>127,128</sup> Recently, the same group reported the synthesis of half-sandwich iridium metallarectangles induced by C-H activation.<sup>129,130</sup> Bimetallic edges, formed from half-sandwich iridium arene precursors and pyrazine or bispyridyl linkers, were converted to tetranuclear metallarectangles upon treatment with dicarboxylic acids such as fumaric acid, 1,3-benzenedicarboxylic acid, 5-amino-1,3-benzenedicarboxylic acid, or azobenzene 4,4'-dicarboxylic acid. The  $\text{Cp}^*\text{Ir}^{\text{III}}$  fragment catalyzes the C-H activation of dicarboxylic acids to build the macrocyclic architectures.

Silver-based cationic molecular metallacycles were designed using 4-(2-pyridyl)pyrimidine (**92**) as the ligand.<sup>131</sup> Due to the presence of the two orthogonal metal binding sites, a head-to-tail

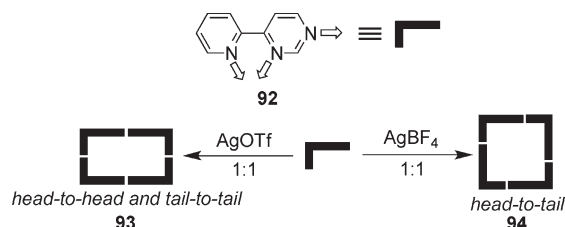
Scheme 27



aggregation would give a molecular square while the head-to-head or tail-to-tail aggregation would result in a rectangle. The reaction of **92** with  $\text{AgOTf}$  in a 1:1 stoichiometric ratio led to head-to-head and/or tail-to-tail aggregation, resulting in rectangular ensemble **93** (Scheme 28). However, the use of  $\text{AgBF}_4$  (instead of  $\text{AgOTf}$ ) led to the formation of square assembly **94** with a head-to-tail aggregation. Treatment of a N-methylated bis(amidopyridine) ligand with silver salts  $\text{AgNO}_3$ ,  $\text{AgO}_2\text{CCF}_3$ ,  $\text{AgO}_3\text{SCF}_3$ ,  $\text{AgBF}_4$ , and  $\text{AgPF}_6$  gave the corresponding cationic disilver(I) macrocycles.<sup>132</sup> Heteronuclear cationic molecular rectangles having two redox-active ferrocene subunits and a pair of transition metal atoms were reported by Lindner et al.<sup>133</sup> A redox-active Pd-based rectangle  $[(\eta^5\text{-C}_5\text{H}_4\text{C}_2\text{-3-py})_2\text{Fe}]_2\text{Pd}_2\text{Cl}_4$  was prepared from  $\text{PdCl}_2(\text{COD})$  and  $(\eta^5\text{-C}_5\text{H}_4\text{C}_2\text{-3-py})_2\text{Fe}$ . The same donor clip yielded a Ag(I)-based molecular rectangle upon treatment with  $\text{AgClO}_4$ . The  $\text{Ni}_2$  rectangle,  $[(\eta^5\text{-C}_5\text{H}_4\text{C}_2\text{-4-py})_2\text{Fe}]_2\text{Ni}_2(\text{NO}_3)_4$ , was obtained by treatment of  $[\text{Ni}(\text{H}_2\text{O})_6](\text{NO}_3)_2$  with  $(\eta^5\text{-C}_5\text{H}_4\text{C}_2\text{-4-py})_2\text{Fe}$ .

**3.1.6. Higher Polygons and Large Ring Systems.** Several other higher order 2D polygons have been reported by using specifically designed organic acceptors with directional metal acceptors. Using the directional bonding approach, hexagonal assemblies can be realized in two complementary ways (a) by the combination of six  $120^\circ$  units with six complementary linear units or (b) by the combination of three  $120^\circ$  units with three complementary  $120^\circ$  units. Similarly, discrete pentagonal ensembles can be assembled by the incorporation of five  $108^\circ$  building units with five complementary linear units. For example, Scheme 29 illustrates the assembly of a molecular hexagon via the combination of nitrogen-containing corner units having  $120^\circ$  bond angles with complementary linear organometallic linking units. As the covalent angle of an  $\text{sp}^2$  hybrid carbon is  $120^\circ$ , in the case of bis-(4-pyridyl)ketone (**95**), treatment with **96** in dichloromethane at room temperature afforded the desired hexamer, **97**.<sup>134</sup> In a complementary approach, the  $120^\circ$  diplatinum(II) acceptor forms the corner unit with 4,4'-bipyridine as the linear linker to also afford a  $[6 + 6]$  molecular hexagon. A  $[3 + 3]$  molecular

Scheme 28



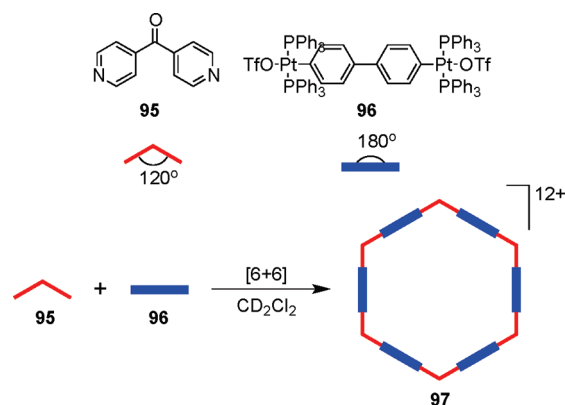
hexagon was assembled from a 1:1 reaction of **95** with complementary  $120^\circ$  di-Pt(II) acceptor.<sup>135</sup>

However, an equilibrium mixture of hexagonal and pentagonal metallacycles was often observed in such an assembly due to the small,  $12^\circ$  difference between the  $120^\circ$  internal turning angles needed for the hexagonal assembly and the  $108^\circ$  angle in analogous pentagonal assemblies. The relatively large size of the assemblies and the flexibility of the building units allow the distortion needed for shifting the equilibrium from one to the other. The use of two metal–carbonyl coordinated dipyrindyl donors, **98** and **99**, with linear diplatinum(II) acceptor **100** led to the interesting observation that the steric bulk of the metal carbonyl corners controls the hexagonal–pentagonal equilibrium (Scheme 30).<sup>136</sup> The use of a sterically less-imposing ligand (**98**) resulted in a mixture of a  $[5+5]$  pentagon (**101**) and a  $[6+6]$  hexagon (**102**), while the exclusive formation of a  $[5+5]$  pentagon (**103**) was achieved by the use of bulkier molybdenum donor ligand **99** with linear organoplatinum(II) acceptor **100**. Multinuclear NMR and electrospray ionization–time-of-flight–mass spectrometry (ESI-TOF-MS) established the formation of these assemblies.

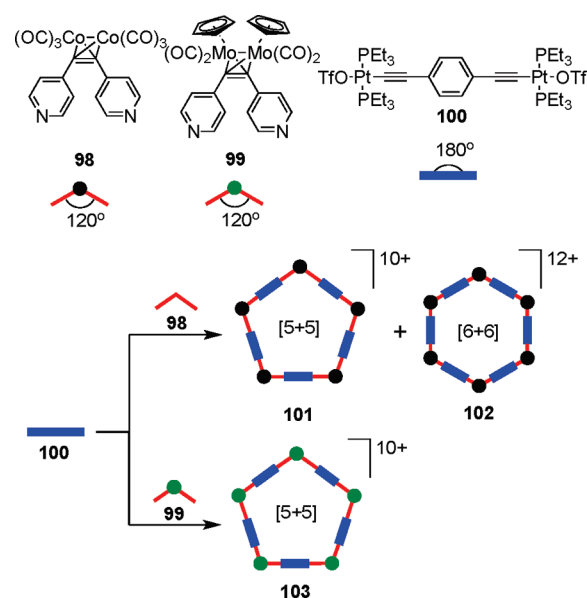
Using a different approach developed by Lehn and co-workers, naked metal ions were utilized as the effectors to trigger the spontaneous ordering of individual components into higher order stereospecific circular helicates.<sup>137</sup> Iron-containing metallacyclic pentagons and hexagons were assembled by using a trisbipyridyl ligand, tris(2,2'-bipyridine). When the ligand was treated with  $\text{FeCl}_2$  in ethylene glycol at  $170^\circ\text{C}$ , the formation of a pentanuclear assembly was observed, while replacement of  $\text{FeCl}_2$  with  $\text{FeSO}_4$  led to the generation of hexanuclear circular helicates. In the pentanuclear assembly, the chloride ion occupied the cavity of the macrocycle and is perhaps responsible for the preferred formation of the molecular pentagon in the first reaction. However, increasing the flexibility of the trisbipyridyl ligand by introducing ether linkages led only to molecular squares with different  $\text{Fe(II)}$  salts.<sup>138</sup> These reactions demonstrate the remarkable influence of the ion-templating effect on the formation of polynuclear assemblies.

Dunbar et al. extensively investigated the role of anions in anion-templated self-assembly reactions between first-row transition metal ions and a divergent bis-bipyridine ligand.<sup>139,140</sup> Anions can direct the course of an assembly process via non-covalent interactions due to their wide range of coordination geometries, pH sensitivity, and high free energy of solvation. In the reaction of 3,6-bis(2-pyridyl)-1,2,4,5-tetrazine (bptz) with  $\text{Ni}^{2+}$  ions, the larger anion  $[\text{SbF}_6]^-$  favored the formation of molecular pentagon  $[\{\text{Ni}_5(\text{bptz})_5(\text{CH}_3\text{CN})_{10}\}\text{C}[\text{SbF}_6]^{9+}]$ , while relatively smaller anions –  $\text{ClO}_4^-$  and  $\text{BF}_4^-$  yielded molecular squares  $[\{\text{M}_4(\text{bptz})_4(\text{CH}_3\text{CN})_8\}\text{C}[\text{X}]^{7+}]$  ( $\text{M} = \text{Ni(II)}, \text{Zn(II)}$ ;  $\text{X} = \text{ClO}_4^-$  and  $\text{BF}_4^-$ ). The molecular pentagon can easily be converted to the square in the presence of an excess of  $\text{BF}_4^-$ ,

Scheme 29



Scheme 30



$\text{ClO}_4^-$ , or  $\text{I}^-$  anions. However, the  $\text{Ni(II)}$  square can be partially converted to the less stable pentagon only under more forcing conditions in the presence of excess  $[\text{SbF}_6]^-$  ions. Thus, by proper choice of counterions, the assembly process can be tuned to the desired macrocyclic assembly. These circular helicates can have helical (interwoven) and parallel (grid-type) arrangements of the ligands, depending on the transoid or cisoid orientations of the coordinating sites in the ligand. This is in contrast to the assemblies generated through the directional paradigm, where all the ligands and the metal centers lie on the same plane. von Zelewsky and co-workers synthesized an interwoven molecular hexagon by employing a pinene-2,2'-bipyridine ligand.<sup>141</sup> Treatment of the  $\alpha,\alpha'$ -bis(pinene-2,2'-bipyridyl)-*p*-xylene linker with  $\text{AgPF}_6$  in a mixture of acetonitrile and chloroform spontaneously led to the formation of circular single-stranded helicates, as observed from X-ray structural studies. NMR and circular dichroism (CD) spectroscopies in solution, along with ESI-MS results, indicated that the assembly was stable in solution. An equilibrating mixture of a  $[2 \times 2]$  grid-type tetranuclear assembly and a hexanuclear assembly was obtained when a ligand designed with a rigid 4,

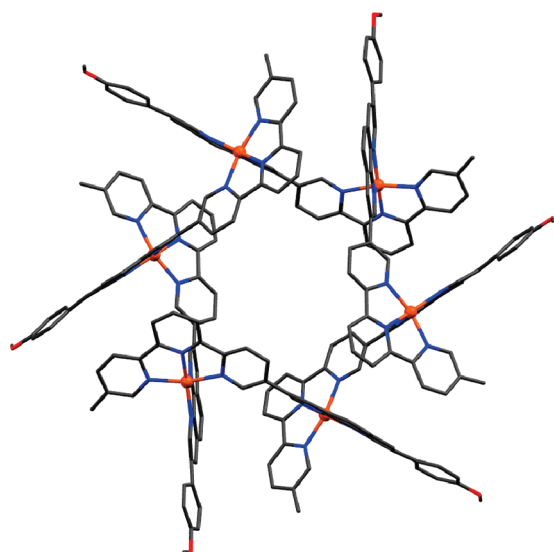
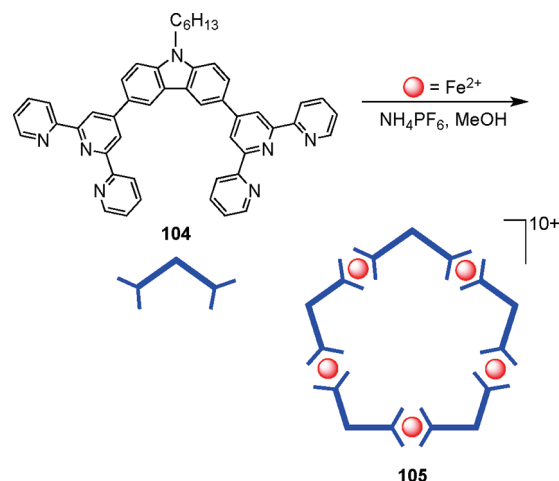


**Figure 17.** Molecular structure of  $[\text{Cu}_6(\text{terpy-phen})_6(\text{PF}_6)_6]^{6+}$ . Weakly coordinating  $\text{PF}_6^-$  were omitted for clarity. Color code: golden, Cu; red, O; blue, N; gray, C.

7-phenanthroline unit between the two binding sites was treated with copper(II) cations in a 1:1 ratio in acetonitrile.<sup>142</sup> Interestingly, a solvent-dependent reversible switching between tetramer and hexamer was observed. While acetonitrile favored the formation of hexamer, nitromethane afforded the formation of the tetranuclear assembly only. Coronado et al. have reported the synthesis of a metallo-supramolecular hexagon from the self-assembly of a mixture of Cu(II) ions and a rigid heteroditopic ligand containing phenanthroline and terpyridine binding units.<sup>143</sup> The 1:1 reaction of a ditopic ligand containing a terpyridine tridentate ligand and a 1,10-phenanthroline bidentate moiety directly connected to one another (terpy-phen) with  $\text{Cu}(\text{OAc})_2$  in methanol yielded the hexameric cation  $[\text{Cu}_6(\text{terpy-phen})_6(\text{PF}_6)_6]^{6+}$  (Figure 17). Each copper ion is bound to two ligands through the phenanthroline and terpyridine binding sites and a weakly coordinated  $\text{PF}_6^-$  anion. As expected for grid-type assemblies, the coordinating ligands are disposed in a cisoid fashion above and below the mean plane of the hexamer.

A number of higher ordered 2D multinuclear supramolecular assemblies were constructed using specifically designed mono- and bis-terpyridine ligands with various transition metals.<sup>144</sup> Newkome and co-workers assembled both homonuclear<sup>145</sup> and heteronuclear<sup>146,147</sup> hexametallc macrocycles using a bis-(terpyridyl) monomer possessing a  $120^\circ$  angle with respect to the two ligating moieties. The reaction of the bis(terpyridyl) monomer with 2 equiv of  $\text{RuCl}_3 \cdot n\text{H}_2\text{O}$  or  $\text{FeCl}_2 \cdot 4\text{H}_2\text{O}$  produced the corresponding bis-metallic adducts which, on further treatment with 1 equiv of bis(terpyridyl) ligands under reducing conditions, yields the self-assembled diamagnetic hexameric ruthenium and iron-based macrocycle of benzenoid architecture. More recently, sterically congested, hexameric Pd(II)- and Cd(II)-tetrakispyridinyl-based macrocycles were reported using both mono- and tridentate coordination sites.<sup>148</sup> In addition to  $^1\text{H}$  and  $^{13}\text{C}$  NMR and 2D COSY NMR studies, the formation of these hexagonal macrocycles was established using traveling wave ion mobility mass spectrometry (TWIM-MS) which allowed for the deconvolution of the isotope patterns of different charge states, thus avoiding the isomer superposition prevalent in

**Scheme 31**



regular ESI-MS and FT-MS. The same group also reported a novel family of metallocyclic pentagons constructed by the facile self-assembly of a bis(terpyridine)carbazole (**104**) utilizing terpyridine–metal coordination as the driving force for the assembly process.<sup>149</sup> The treatment of **104** with 1 equiv of  $\text{M}^{2+}$  ion [ $\text{M} = \text{Fe}$  (**105**), Ru, Zn] in MeOH allowed for the formation of pentameric cationic macrocycles (Scheme 31). Multinuclear NMR, UV–visible, and mass spectrometry established the structures of these pentagonal architectures. The photophysical studies on these pentagonal assemblies showed interesting light harvesting properties.

Recently, a series of anion-templated hexanuclear macrocycles has been reported, formed by treating half-sandwich Rh(III) metal corners with deprotonated 2,4-diacetyl-5-hydroxy-5-methyl-3-(3-pyridinyl)cyclohexanone (dhmpc).<sup>150</sup> The size of the counteranion significantly affects the nuclearity of the final self-assembled macrocycles. While larger counteranions  $\text{OTf}^-$ ,  $\text{PF}_6^-$ , and  $\text{SbF}_6^-$  favor the formation of hexanuclear metalla-macrocycles,  $\text{BF}_4^-$  favors the formation of a tetranuclear metalla-macrocycle. Single-crystal X-ray structural analysis for the macrocycles reveals that the two counteranions are encapsulated within the cavities of each of the host hexanuclear metalla-macrocycles. Figure 18 shows the molecular structure of  $[\text{Cp}^*\text{Rh}(\text{dhmpc})_6]^{6+}$ .  $^1\text{H}$  NMR studies also indicated the retention of the counterions within the molecular cavities in solution. Interestingly, the tetranuclear macrocycle can be converted to hexanuclear macrocyclic assemblies by the addition of the appropriate anion as its  $[\text{NBu}_4]^+$  salt with preferred selectivity for larger anions in the order of  $\text{SbF}_6^- > \text{PF}_6^- > \text{OTf}^- > \text{BF}_4^- > \text{Cl}^-$ .

The weak link approach (WLA), a strikingly different design strategy, developed by Mirkin and co-workers has led to the realization of a vast plethora of flexible 2D homo- and heterodimetallic macrocyclic rings.<sup>11</sup> These large ring systems have been prepared from specifically designed hemilabile ligands containing phosphanyl alkyl ether, thioether, and amine groups. The phosphorus group serves as the strong binding site for the late transition metals while ether, thioether, and amine groups serve as the weak binding sites. These ligands also provide a way to control the reactivity of the condensed structures and incorporate functionalities, such as fluorescent, redox-active, or catalytic moieties, into the final supramolecular architecture. In one early demonstration of this strategy, a Rh(I)-containing



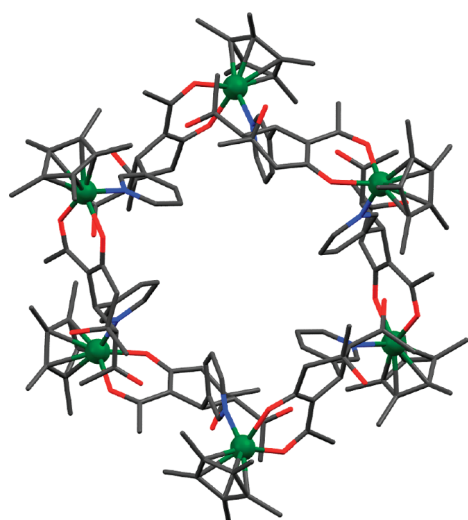
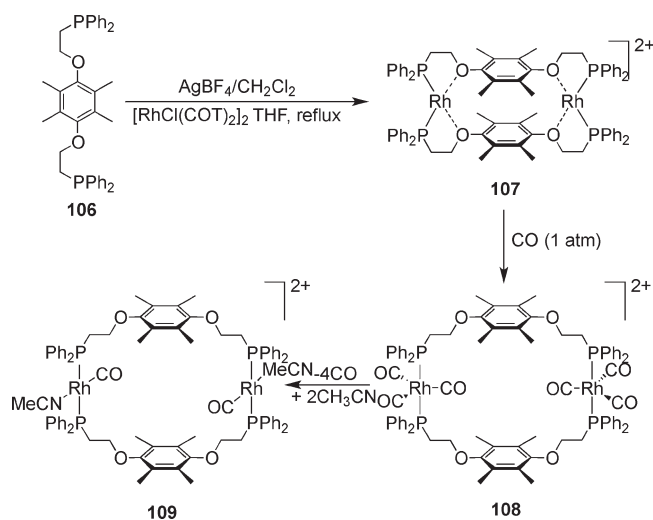


**Figure 18.** Molecular structure of  $[\text{Cp}^*\text{Rh}(\text{dhmpc})_6]^{6+}$ . Color code: green, Rh; red, O; blue, N; gray, C.

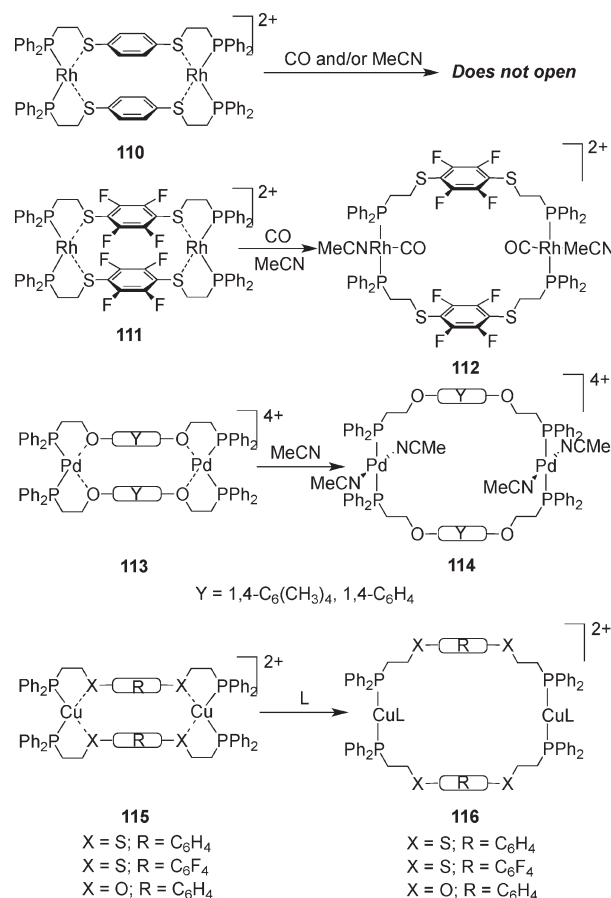
### Scheme 32



homodimetallic cationic macrocycle was synthesized from phosphinoether-based hemilabile ligand 1,4-bis[2-(diphenylphosphanyl)ethoxy]-2,3,5,6-tetramethylbenzene (**106**).<sup>151</sup> A 1:1 stoichiometric reaction of **106** with a Rh(I) precursor formed by the reaction between  $[\text{RhCl}(\text{COT})_2]_2$  (COT = cyclooctene) and  $\text{AgBF}_4$  in  $\text{CH}_2\text{Cl}_2$  resulted in a condensed macrocycle **107**. The addition of strongly coordinating CO (1 atm) in  $\text{CH}_2\text{Cl}_2$  resulted in displacement of the labile  $\text{Rh}^{\text{I}}-\text{O}$  bond leading to the formation of a large cationic macrocycle (**108**) in quantitative yield. Removal of CO from **108** and dissolution in MeCN resulted in the MeCN adduct of **109** (Scheme 32).

Subsequently, reports of the use of other weak linkers, such as thioether and amines, to synthesize a number of bimetallic Rh(I) cationic macrocycles have emerged.<sup>152</sup> For example, treatment of a Rh(I) source with the thioether-containing hemilabile ligand 1,4-bis[2-(diphenylphosphino)ethylthio]benzene led to the formation of a cationic fused macrocycle (**110**).<sup>153</sup> Interestingly, due to the greater inertness of the metal–thioether bond, the  $\text{Rh}^{\text{I}}-\text{S}$  bonds of **110** are inert under conditions that result in the

### Scheme 33

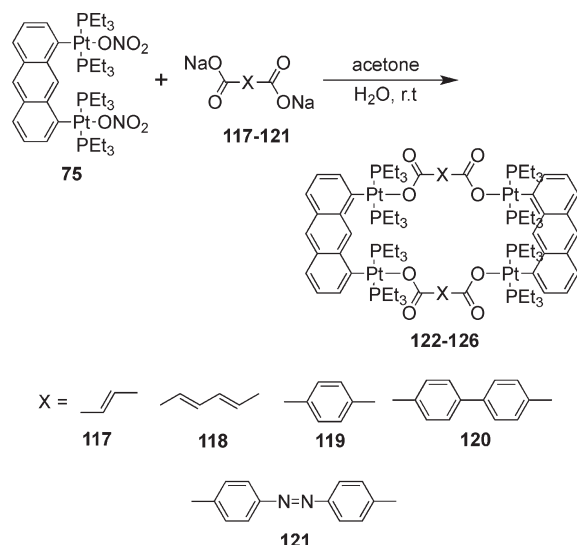


displacement of the ether moieties in complex **107** upon addition of CO,  $\text{CH}_3\text{CN}$ , or both. However, altering the electronics of the aromatic core in the thioether-containing ligand allows the opening up of the condensed structure by ancillary ligands.<sup>154</sup> Introduction of fluoride substituents on the aromatic core of the phosphinothioether-based ligand allows for the synthesis of condensed macrocycles **111** that reacts similarly to the ether-based macrocycles to give expanded macrocycle **112** (Scheme 33). Also reported were several other Pd(II)-, Ir(I)-, Ru(II)-, and Cu(I)-based cationic macrocycles. Treating a Pd(II) source with phosphinoalkyl ether-containing hemilabile ligands gave access to condensed cationic complexes (**113**) which could be opened up into larger metallacycles (**114**) by treatment with MeCN (Scheme 33).<sup>155</sup> Similarly, the cationic bimetallic Cu(I) macrocycles, **116**, have been synthesized by addition of small ancillary ligands such as acetonitrile, isonitriles, diimines, or pyridine to the condensed structures, **115** (Scheme 33).<sup>156</sup> Hetero-bimetallic macrocycles can also be synthesized by using dissymmetric hemilabile ligands that incorporate both ether and thioether weak links. Due to the differences in the labilities of metal–ether and metal–thioether bonds, different metals can be selectively placed on the macrocycles by changing the reaction conditions.<sup>157</sup>

### 3.2. Neutral Systems

As described above, the majority of synthetic strategies for metalla-macrocycles involve the use of neutral polypyridyl

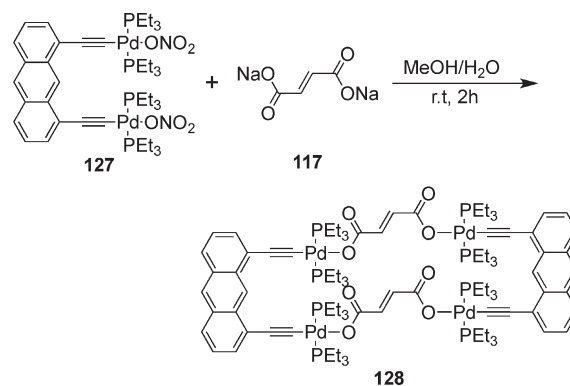
Scheme 34



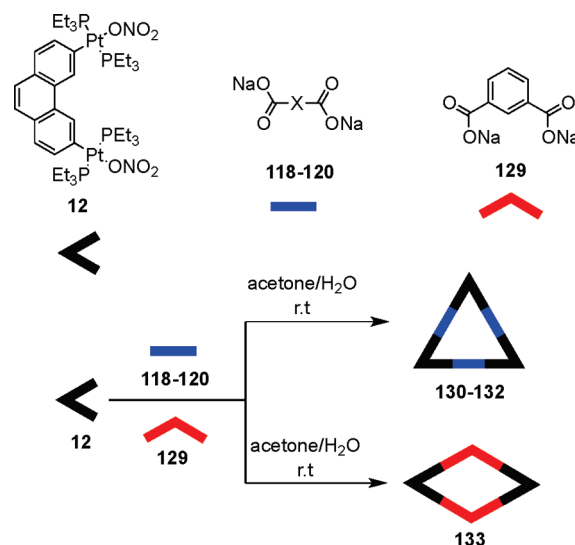
ligands with multivalent metal ions that result in charged assemblies. In these charged species, counterions often block the cavities that are formed; however, in contrast, neutral assemblies can provide a cavity devoid of counterions that may serve as a host for the encapsulation of neutral organic guests. Neutral assemblies can be designed by (1) directly using anionic bridging ligands that can compensate for the cationic metal charge or (2) synthesizing a neutral precursor acceptor followed by treatment with a neutral donor.

Square-planar divalent platinum and palladium complexes, in which two or three coordinating sites are occupied by strong M–P or M–C bonds and the remaining site(s) are coordinated by labile, weakly coordinating anion(s) such as nitrate and triflate, have been used as the acceptor units with dianionic bridging ligands as the donor linkers. The spontaneous self-assembly of neutral nanoscopic molecular rectangles **122–126** was achieved by a 1:1 stoichiometric combination of an acetone solution of a pre-designed platinum-based molecular clip, 1,8-bis[*trans*-Pt(PEt<sub>3</sub>)<sub>2</sub>(NO<sub>3</sub>)]anthracene (**75**), with an aqueous solution of linear dicarboxylates **117–121** (Scheme 34).<sup>158,159</sup> Multinuclear NMR, mass spectrometry, and single-crystal X-ray structural analysis established the formation of the macrocycles. The utilization of the Pt–O bonding interaction as the driving force for designing the discrete assemblies is an interesting feature of these macrocycles, as large supramolecules incorporating a Pt–O bond were believed to be unstable due to the unfavorable hard–soft combination. Platinum-based macrocycles incorporating cyclic oxocarbon-dianions, squarate and croconate, and their acyclic analogue, oxalate, have also been synthesized in excellent yield via self-assembly. The combination of diplatinum molecular clip **75** with all three dianions afforded molecular rectangles.<sup>160</sup> In all cases, multinuclear NMR spectra were consistent with the formation of single, highly symmetrical species. Single-crystal X-ray structural studies of these rectangles revealed that all of the ligands coordinate to the molecular clip in bis-monodentate mode. An analogous neutral Pd<sub>2</sub> rectangle, **128**, was reported which used a pre-designed ethynyl-containing Pd(II)-based molecular clip (**127**) in conjunction with disodium fumarate as the donor linker (Scheme 35).<sup>161</sup> Rectangle **128** represents an example of a neutral Pd(II) macrocycle obtained

Scheme 35



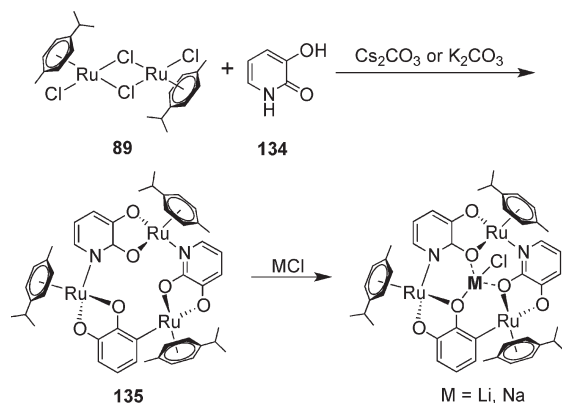
Scheme 36



using Pd–O coordination bonding as the driving force. While oxygen-based hard donors are expected to be unsuitable for the soft acid Pd(II), the electrostatic interaction between the anionic fumarate and Pd(II) plays an important role in obtaining this neutral molecular rectangle.

Building upon a similar strategy, neutral molecular rhomboids and triangles were assembled using dicarboxylate anions as the donor linkers.<sup>158,159</sup> Both kinds of macrocycles use 60° Pt(II)-based building block **12** as an acceptor unit and ditopic linear **118–120** (in the case of triangles **130–132**) or angular **129** (in the case of rhomboid **133**) dicarboxylate bridging ligands (Scheme 36). The formations of the macrocycles were unambiguously confirmed by single-crystal X-ray structural analyses and NMR spectroscopy. The crystallographic studies revealed the presence of different types of channels within the crystal lattices that were occupied by solvent molecules. The diplatinum 60° acceptor unit **12** also produced a supramolecular rhomboid with croconate (C<sub>5</sub>O<sub>5</sub><sup>2–</sup>) ion and a molecular triangle with squarate ion.<sup>160</sup> Multinuclear NMR, single-crystal X-ray crystallography, and FAB–MS established the formation of the assemblies. Heterobimetallic Pt<sub>4</sub>Fe<sub>2</sub> neutral macrocycles were assembled using a flexible bridging 1,1'-ferrocenedicarboxylate as the donor linker.<sup>162</sup> While the combination of the 1,1'-ferrocenedicarboxylate

Scheme 37



with 0° Pt-based molecular clip **75** as the acceptor unit leads to a neutral molecular rectangle, the use of 60° Pt-based molecular clip **12** leads to a neutral rhomboid. Spectroelectrochemical analysis of the molecular rectangle reveals a reversible two-electron transfer due to the ferrocenyl moieties.

Severin and co-workers have demonstrated the formation of a series of neutral metallacycles from half-sandwich Ru(II), Rh(III), and Ir(III) metal corners and tridentate linkers.<sup>163</sup> For example, treatment of  $[(p\text{-cymene})\text{RuCl}_2]_2$  (**89**) with 3-hydroxy-2-pyridone **134** in the presence of base ( $\text{Cs}_2\text{CO}_3$  or  $\text{K}_2\text{CO}_3$ ) allowed the formation of trinuclear metallacycle **135** in a diastereoselective manner in almost quantitative yield (Scheme 37).<sup>164</sup> The macrocycle **135** showed high affinity and selectivity for  $\text{Li}^+$  and  $\text{Na}^+$  ions at its central receptor site. The formation of the macrocycle **135** was confirmed by mass spectrometric and single-crystal X-ray analysis. The dianion of 3-hydroxy-2-pyridone acts as a bridging, tridentate ligand with the half-sandwich ruthenium centers occupying the vertices of the triangle. A prerequisite for the formation of such trinuclear macrocycles is that the ligands must be relatively rigid and the two coordinate vectors must be orthogonal. Other di-, tri-, and tetranuclear metallacycles of Ru(II) and Rh(III) were also obtained using deprotonated heterocyclic compounds such as 2-hydroxynicotinic acid, 2-aminonicotinic acid, imidazole-4-carboxylic acid, 2,3-dihydroxyquinoline, 2,3-dihydroxyquinoxaline, or 6-methyl-2,3-phenazinediol as linkers.<sup>165</sup> Using the same strategy, hexanuclear coordination cages of the formula  $[(\text{C}_5\text{Me}_4\text{R})\text{M}(\text{C}_7\text{H}_3\text{NO}_4)]_6$  ( $\text{M} = \text{Rh}, \text{Ir}; \text{R} = \text{Me}, \text{H}$ ) were obtained by the stepwise treatment of  $[(\text{C}_5\text{Me}_4\text{R})\text{MCl}_2]_2$  with  $\text{AgOAc}$  followed by pyridine-3,5-dicarboxylic acid.<sup>166</sup>

The same group has also demonstrated the formation of neutral macrocycles that contain four or 10 palladium metal centers using 2,3-dihydroxypyridine and its derivative as the dianionic bridging ligands.<sup>167</sup> The reaction of chloro-bridged palladium-based acceptor unit  $[(\text{PEt}_3)_2\text{PdCl}_2]_2$  (**136**) with 2,3-dihydroxypyridine **137** in methanol, using  $\text{Cs}_2\text{CO}_3$  as the base, led to the formation of a neutral tetranuclear molecular square (**138**; Scheme 38). The use of 5-chloro-2,3-dihydroxypyridine under similar condition gave a decameric complex. Similar to 2,3-dihydroxypyridine, the use of 2-hydroxynicotinate also resulted in the formation of a tetranuclear molecular square. However, a potential drawback of these assembly reactions is that they do not give a single product and often need additional crystallization for purification.

Scheme 38

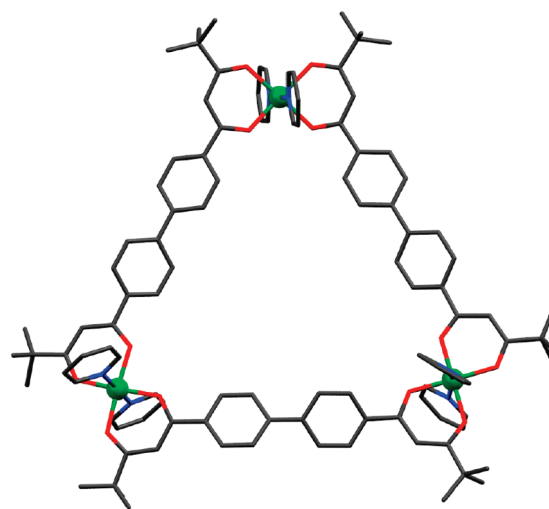
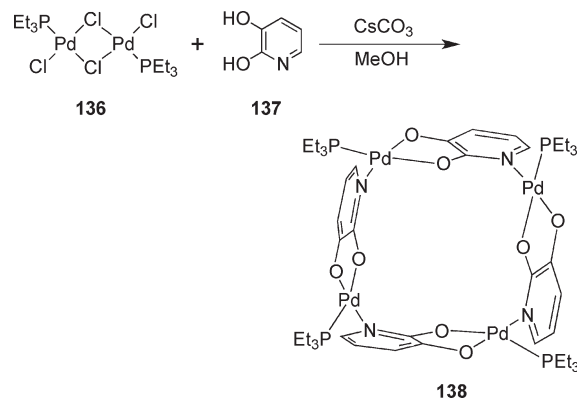
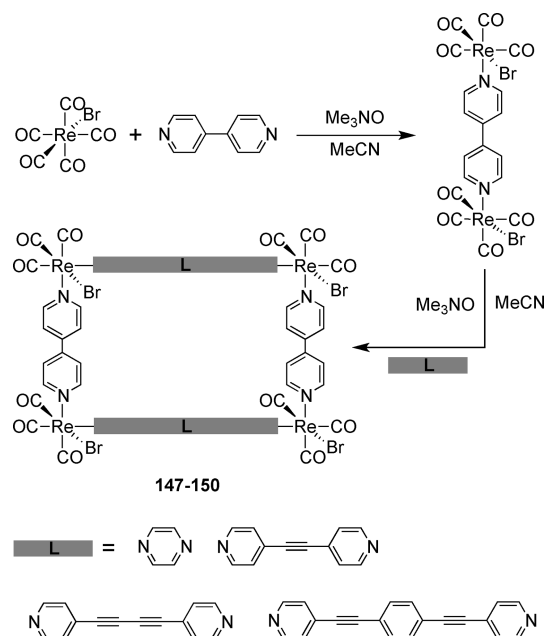


**Figure 19.** Molecular structure of  $\text{Co}_3\text{L}_3(\text{pyridine})_6$  [ $\text{H}_2\text{L} = 1,1'-(4,4'\text{-biphenylene})\text{bis-}3,3\text{-dimethylpentane-}1,3\text{-dione}$ ]. Color code: green, Co; red, O; blue, N; gray, C.

Lindoy and co-workers utilized a range of aryl-linked bis- $\beta$ -diketonato ligands incorporating both parallel and 60° orientated coordination vectors to form a variety of neutral supramolecular architectures with appropriate transition metal ions.<sup>168</sup> While 1,3-phenylene-linked bis- $\beta$ -diketonato ligands led to the formation of dinuclear metallacycles,<sup>169,170</sup> 1,4-phenylene-linked bis- $\beta$ -diketonato ligands gave trinuclear assemblies.<sup>171,172</sup> These planar “platformlike” macrocycles, upon interaction with ditopic heterocyclic bases, led to the formation of both sandwichlike discrete and extended 3D supramolecular architectures.<sup>173,174</sup> Recently, the same group reported one of the largest neutral triangular supramolecular assemblies.<sup>175</sup> A biphenyl-spaced  $\beta$ -diketonate ligand with its donor sets oriented at 60° was used to form the trinuclear metallacycle,  $\text{Co}_3\text{L}_3(\text{pyridine})_6$  [ $\text{H}_2\text{L} = 1,1'-(4,4'\text{-biphenylene})\text{bis-}3,3\text{-dimethylpentane-}1,3\text{-dione}$ ]. The single-crystal X-ray structural analysis (Figure 19) showed the formation of a discrete triangular architecture in which three  $\beta$ -diketonate ligands bridge three Co(III) ions such that each ligand forms the side of a neutral, essentially equilateral triangle. Each Co(III) center is in a pseudooctahedral geometry wherein the axial coordination sites are occupied by pyridine ligands. The metallacycle contains a considerable triangular void area

Scheme 40

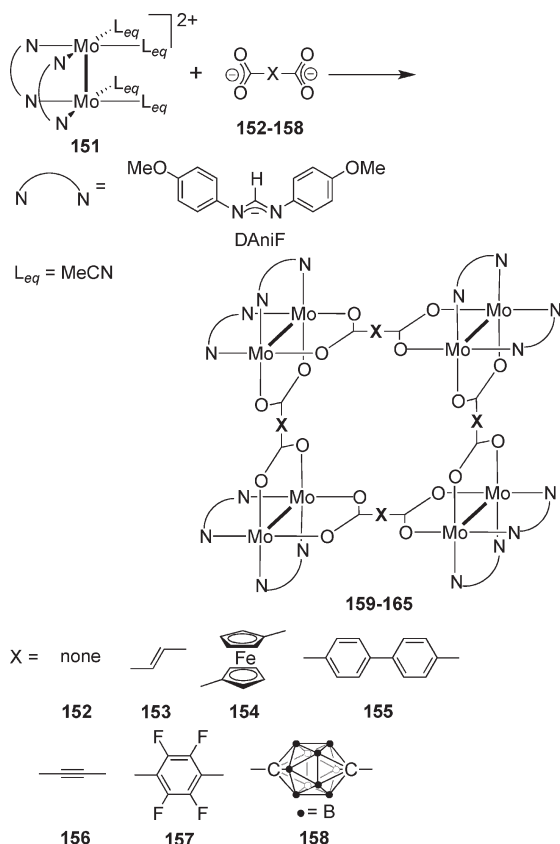


A series of neutral luminescent molecular rectangles [ $\{\text{Re}(\text{CO})_3(\mu\text{-bpy})\text{Br}\}\{\text{Re}(\text{CO})_3(\mu\text{-L})\text{Br}\}\}_2$  [**147**, L = pz; **148**, L = 4,4'-dipyridylacetylene (dpa); **149**, L = dipyridylbutadiyne (dpb); and **150**, L = 1,4-bis(4'-pyridylethynyl)-benzene (bpeb)] having *fac*- $\text{Re}(\text{CO})_3\text{Br}$  as corners and bpy as the bridging ligand on one side and bipyridyl ligands of varying

Through the dimetallic building block approach, Cotton and co-workers have described a large number of neutral metalla-macrocycles such as loops, triangles, and squares using dimetallic paddle-wheel units as the corner pieces to link divalent anions, such as dicarboxylates.<sup>12</sup> Because of the idealized orthogonality between the planes defined by the metal atoms and replaceable equatorial ligands, these dimetallic units, upon treatment with equatorial linkers, form square arrays. The first series of neutral molecular squares (**159**–**165**) derived from quadruply bonded dimolybdenum subunits were synthesized via the reaction of  $[\text{Mo}_2(\text{cis-DAniF})_2(\text{CH}_3\text{CN})_4]^{2+}$  (**151**; DAniF = *N,N'*-di-*p*-anisylformamidinate) and  $(\text{Bu}^n_4\text{N})_2(\text{Carb}^{2-})$  [ $\text{Carb}^{2-}$  = oxalate (**152**), fumarate (**153**), acetylenedicarboxylate (**154**), tetrafluoroterephthalate (**155**), ferrocene dicarboxylate (**156**), 4,4'-biphenyldicarboxylate (**157**), and carborane dicarboxylate (**158**)] as shown in Scheme 41.<sup>185,186</sup> The X-ray structural characterization of molecular squares **159**–**162** showed that each corner consisted of a quadruply bonded dimolybdenum unit, with two cisoid formamidinate paddles and two carboxylate paddles from the dicarboxylate linkers. The conformation of each dicarboxylate anion is such that both carboxylate groups are equatorially disposed.



Scheme 41



The dimensions of the squares, defined by the four  $\text{Mo}_2$  corners in each molecule, are  $7 \times 7$ ,  $9 \times 9$ ,  $10 \times 10$ , and  $15 \times 15 \text{ \AA}^2$  for **159–162**, respectively. Thus, tuning the shape and size of the linkers can modulate the dimensions of the channels created by the squares.  $^1\text{H}$  NMR studies on the squares showed that they are fairly stable in solution and are highly symmetrical. These compounds also display rich electrochemical behaviors that are affected by the nature of the carboxylate linkers. Extending this strategy to other metals, similar neutral molecular squares having  $\text{Rh}_2^{4+}$  units were reported by treating  $[\text{Rh}_2(\text{cis-DAniF})_2(\text{CH}_3\text{CN}_{eq})_4(\text{CH}_3\text{CN}_{ax})_2](\text{BF}_4)_2$  with  $(\text{Et}_4\text{N}^+)_2(\text{Carb}^{2-})$  where  $\text{Carb}^{2-}$  represents the dicarboxylate anions bicyclo[1.1.1]pentane-1,3-dicarboxylate, tetrafluoroterephthalate, 1,4-cubanedicarboxylate, terephthalate, fumarate, and *trans*-1,4-cyclohexanedicarboxylate.<sup>187</sup> Neutral molecular squares having ruthenium corner pieces,  $\text{Ru}_2^{5+}$ , using oxalate and terephthalate as the linkers were also reported by the same group.<sup>188</sup> The groups of Bonar-Law<sup>189,190</sup> and Schiavo<sup>191</sup> have also reported a few other dirhodium neutral squares based on  $\text{Rh}_2^{4+}$  corner units and dicarboxylate anions as the linkers.

Several neutral molecular triangles were also synthesized using the dimetallic corner units such as  $[\text{Mo}_2^{4+}]$ ,<sup>192</sup>  $[\text{Rh}_2^{4+}]$ ,<sup>193,194</sup> and  $[\text{Re}_2^{5+}]$ <sup>195</sup> by varying the reaction conditions and length and flexibility of the dianionic linkers. Several neutral triangles designed using this strategy were obtained by treating dimolybdenum  $[\text{Mo}_2^{4+}]$  subunits,  $[\text{Mo}_2(\text{cis-DAniF})_2(\text{CH}_3\text{CN})_4]^{2+}$  with flexible 1,4-cyclohexanedicarboxylate linkers.<sup>192</sup> The molecular triangle  $[\{\text{cis-Mo}_2(\text{DAniF})_2(1,4\text{-O}_2\text{C}-\text{C}_6\text{H}_{10}-\text{CO}_2)\}_3]$ , as observed from crystal structure analysis, has  $\text{Mo}_2(\text{DAniF})_2$  units occupying the three vertices of the triangle while both

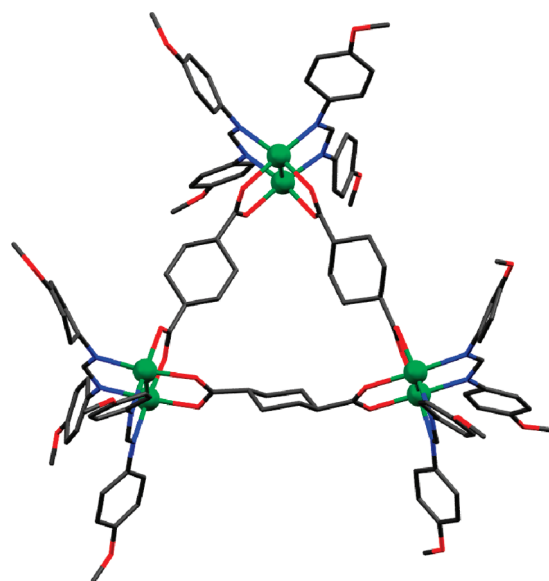
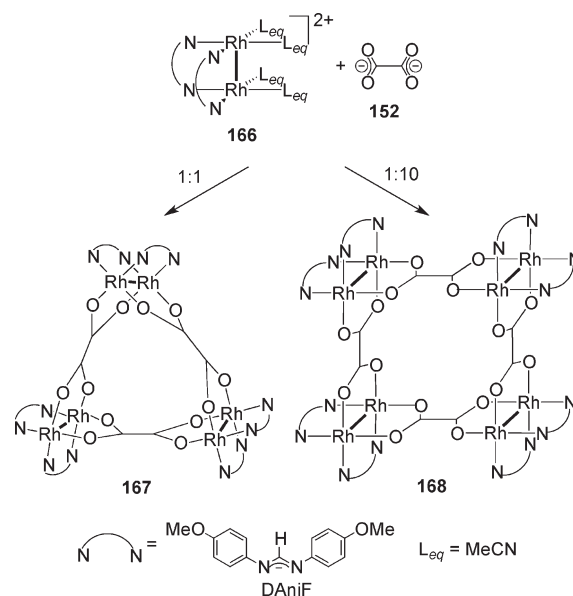


Figure 20. Single-crystal X-ray structure of  $[\text{cis-Mo}_2(\text{DAniF})_2(1,4\text{-O}_2\text{C}-\text{C}_6\text{H}_{10}-\text{CO}_2)]_3$ . Color code: green, Mo; red, O; blue, N; gray, C.

Scheme 42



carboxylate groups of the 1,4-cyclohexanedicarboxylate linker orient themselves in an equatorial (eq,eq) fashion. Figure 20 shows the molecular structure of the triangle.

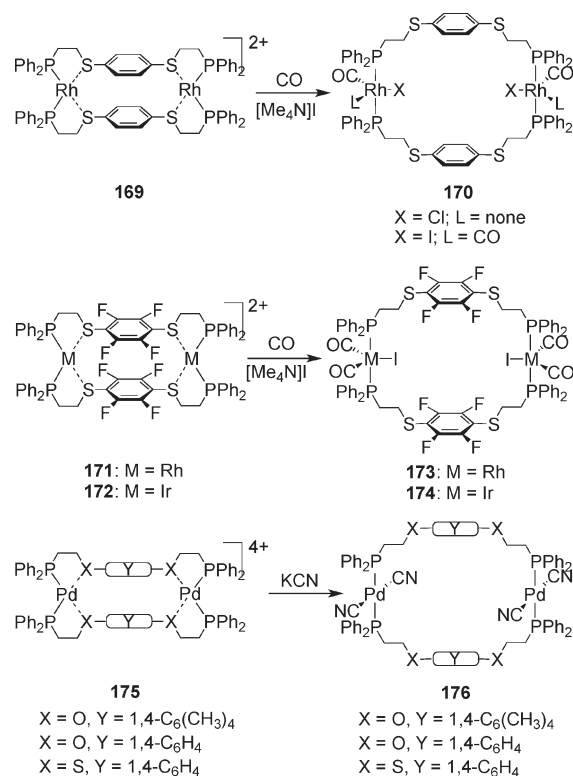
An analogous  $[\text{Rh}_2(\text{DAniF})_2]^{2+}$  dimetallic corner unit also led to the formation of a neutral molecular triangle  $[\text{Rh}_2(\text{DAniF})_2(\mu_4\text{-C}_2\text{O}_4)]_3$  (**167**) from a 1:1 equimolar mixture of  $[\text{Rh}_2(\text{cis-DAniF})_2(\text{CH}_3\text{CN})_4]^{2+}$  (**166**) and  $(\text{C}_2\text{O}_4^{2-})$  (**152**), in near quantitative yield. Interestingly, using a 10-fold excess of oxalate linker, under the same reaction conditions, selectively gave the corresponding molecular square  $[\text{Rh}_2(\text{DAniF})_2(\mu_4\text{-C}_2\text{O}_4)]_4$  (**168**; Scheme 42).<sup>193,194</sup> In solution, a dynamic equilibrium between the triangle **167** and square **168** was found to exist. The dirhodium complex *cis*- $\text{Re}_2(\mu\text{-O}_2\text{CCH}_3)_2\text{Cl}_2(\mu\text{-dppm})_2$  ( $\text{dppm} = \text{Ph}_2\text{PCH}_2\text{PPh}_2$ ), which contains two substitutionally labile acetate

ligands, afforded the molecular triangle  $[cis-Re_2Cl_2(\mu-dppm)_2-(\mu-O_2CC_6H_4CO_2)]_3$  upon treatment with an excess of terephthalic acid in refluxing ethanol.<sup>195</sup> By employing  $[cis-Mo_2(DAniF)_2]^{2+}$  as the vertex building block and terephthaloyldiamidate as the linker, dimolybdenum-containing neutral metallacycles of general formula  $[cis-Mo_2(DAniF)_2((ArNOC)_2-C_6H_4)_2]_n$  were synthesized and structurally characterized.<sup>196</sup> The geometries of the products are guided by the identities of the aromatic groups present in the linkers. When the aromatic group is phenyl, a molecular triangle is the exclusive product; changing the aromatic substituents to *p*-trifluoromethylphenyl or *m*-trifluoromethylphenyl affords a molecular square selectively.

Cotton and Murillo have also investigated the dynamic equilibrium between a neutral molecular square,  $[cis-Mo_2(DAniF)_2]_4-(O_2CC_6F_4CO_2)_4$  (**164**), and its corresponding triangle,  $[cis-Mo_2(DAniF)_2]_3-(O_2CC_6F_4CO_2)_3$ , in  $CDCl_3$  solution from a reaction mixture of  $[cis-Mo_2(DAniF)_2]^{2+}$  and the perfluoroterephthalate anion.<sup>197</sup> The compounds were characterized by X-ray structural studies and solution NMR spectroscopy. Since the perfluoroterephthalate linkers are linear and relatively rigid, the formation of a molecular square was expected. However, multinuclear NMR studies show that a dynamic equilibrium exists between the square and triangle. As determined from NMR studies, the conversion of squares to triangles is entropically favored but enthalpically disfavored with an equilibrium constant of  $1.98(7) \times 10^{-4}$  at 23.7 °C. However, a recent study showed that use of substoichiometric amounts of oxalate gave a molecular triangle as the major product with no observable equilibrium with its molecular square counterpart.<sup>198</sup>

Mirkin and co-workers synthesized a number of neutral metallamacrocycles using a wide range of transition metal precursors with a variety of flexible hemilabile ligands by the weak link approach. In one of the early examples of this strategy, they reported the formation of a Rh(I)-containing, neutral macrocycle via the halide induced ring opening of a cationic condensed intermediate by breaking a weak  $Rh^I-S$  bond.<sup>153</sup> A 1:1 equimolar mixture of  $[RhCl(COT)_2]_2$  and the phosphinothioether-based hemilabile ligand 1,4-bis[2-(diphenylphosphino)ethylthio]benzene combined to form a cationic condensed intermediate (**169**; Scheme 43). The addition of  $[Me_4N]Cl$  in the presence of CO (1 atm) resulted in the displacement of the labile  $Rh^I-S$  bonds leading to the formation of neutral macrocycle **170** in quantitative yield. Condensed macrocycles containing ether instead of thioether linkages can also be opened up by  $CO/Cl^-$  to give neutral macrocycles. Using a bis(phosphinoalkyl-thioether)arene ligand with a fluorinated aryl group,  $[1,4-(Ph_2PCH_2CH_2S)_2-C_6F_4]$ , instead of benzene-based phosphinothioether-based hemilabile ligands, Rh(I)- and Ir(I)-containing neutral macrocycles were reported.<sup>154</sup> Treatment of  $[Rh(NBD)Cl]_2$  (NBD = norbornadiene) or  $[IrCl(COT)_2]_2$  with  $[1,4-(Ph_2PCH_2CH_2S)_2-C_6F_4]$  generated condensed structures **171** and **172**, respectively. Addition of  $CO/I^-$  cleaved the  $Rh-S$  and  $Ir-S$  bonds to yield **173** and **174**, respectively (Scheme 43). Expanding the paradigm to other  $d^8$  square-planar transition metals, the same group reported Pd(II)-based neutral macrocycles by treating  $[Pd(MeCN)_4][BF_4]_2$  with phosphinoalkyl ether or a thioether-containing hemilabile ligand to give condensed cationic complexes **175**, which can be opened up into neutral metallocycles **176** by introducing  $CN^-$  ions (Scheme 43).<sup>155</sup> Similarly, the  $d^8$  octahedral transition metal Ru(II) was used to synthesize neutral condensed and open macrocycles by addition of CO, pyridine, and alkyl diamines.<sup>199</sup>

Scheme 43



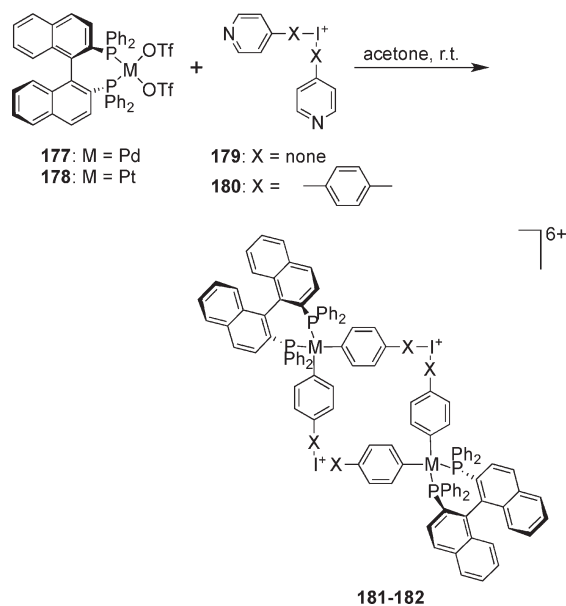
### 3.3. Chiral Systems

Due to their ability to mimic complex biological systems, chiral supramolecular assemblies have been extensively studied over the past 2 decades.<sup>200</sup> The biological implications of chirality demand that we improve our ability to access chiral molecules as pure entities.<sup>201</sup> Through properly designed and preprogrammed building units, supramolecular self-assembly can provide relatively easy, simple access to chiral supramolecules with controlled stereochemistry that may help in our understanding of nature's intricate biochemical processes. Furthermore, these systems may also provide ways to study newer approaches to enantioselective molecular recognition, chiral sensing, and asymmetric catalysis.

Chiral 2D metallacycles are among the most extensively studied due to their relative ease of preparation and their potential applications in enantioselective recognition, sensing, and catalysis.<sup>200</sup> The rational design of these discrete chiral ensembles by the directional bonding approach can be achieved by using (1) chiral metal auxiliaries as corner units with achiral multidentate ligands as the connectors, (2) achiral metal corner units with chiral multidentate ligands as the connectors, (3) inherently chiral metal centers having specific coordination geometries with achiral multidentate linkers, or (4) combinations of the above.

In the first strategy, appropriate metal corner units with optically active chiral auxiliaries<sup>202</sup> are combined with achiral bridging ligands, resulting in chiral metallacycles. An early example of this strategy was provided by Stang et al. wherein optically active  $[M(R-BINAP)(OTf)_2]$  ( $M = Pd$  (**177**) or  $Pt$  (**178**), BINAP = 2,2'-bis(diphenylphosphino)-1,1'-binaphthalene) were used as shape-defining corner units due to their high reactivity toward the coordination of nitrogen-containing ligands, as well as the significant degree of conformational rigidity of BINAP.<sup>203,204</sup> When treated with 90° diaza ligands, bis(3-pyridyl)iodonium

Scheme 44



triflate (**179**) or bis(4-(4-pyridyl)phenyl)iodonium triflate (**180**), chiral supramolecular squares **181** and **182** were obtained (Scheme 44).<sup>203</sup> The macrocyclic nature of these complexes was established by multinuclear NMR and confirmed by mass spectrometric analysis. Reactions of anthracene-based  $C_{2h}$  symmetrical diaza ligands 2,6-diazaanthracene and 2,6-diazaanthracene-9,10-dione with  $[\text{M}(\text{R-BINAP})(\text{OTf})_2]$  ( $\text{M} = \text{Pd}$  (**177**) or  $\text{Pt}$  (**178**)) have also led to the formation of similar chiral molecular squares.<sup>203</sup> Interestingly, as determined from  $^{31}\text{P}$  NMR studies, the use of 2,6-diazaanthracene in acetone at ambient temperature as the linker led to only a single diastereomer out of a possible six. However, the use of 2,6-diazaanthracene-9,10-dione under similar conditions led to a mixture of diastereomers. Chiral macrocyclic assemblies containing two or four porphyrin units were also readily synthesized by employing  $[\text{cis-Pd}(\text{R-BINAP})(\text{OTf})_2]$  (**177**) as the chiral metal auxiliary with di- and tetra-pyridyl-substituted porphyrins.<sup>205</sup> The chiral macrocycles have a chirality-induced puckered geometry of  $D_2$  symmetry at ambient temperature. The high solubility and ease of synthesis of these self-assembled chiral porphyrin macrocycles provides excellent examples for the study of porphyrin exciton coupling interactions and induced circular dichroism.

A homochiral molecular triangle was reported by Mirkin et al., in which a chiral enantiopure (*S*)-binaphthyl diamine derivative was used as the corner linker.<sup>206</sup> Each corner linker encloses a  $\text{Cu}(\text{II})$  ion chelated by the  $\text{N}, \text{N}, \text{O}^-, \text{O}^-$  set of donor atoms which further connect to a  $[\text{Cu}(\text{py})_3(\text{H}_2\text{O})]$  fragment through the carboxylate groups present on the periphery of the salen precursors to form a molecular triangle (Figure 21). It is the inherent chirality of the  $\text{Cu}(\text{II})$ -enclosed corner unit that imparts the chirality to the molecular triangle. Interestingly, an unusual solvent-induced, spontaneous and reversible transformation of the triangular macrocyclic complex into a homochiral helical polymer was also observed.

In the second approach, chiral metallacycles were assembled by interacting chiral organic multidentate ligands with achiral

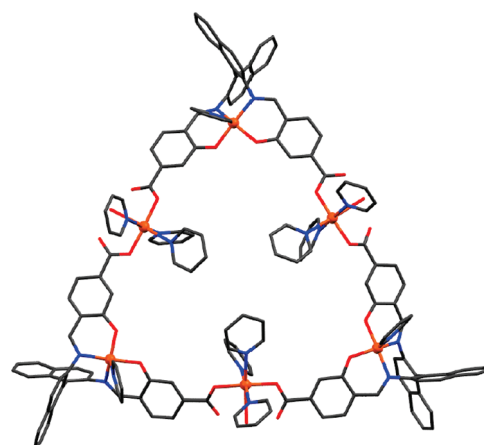
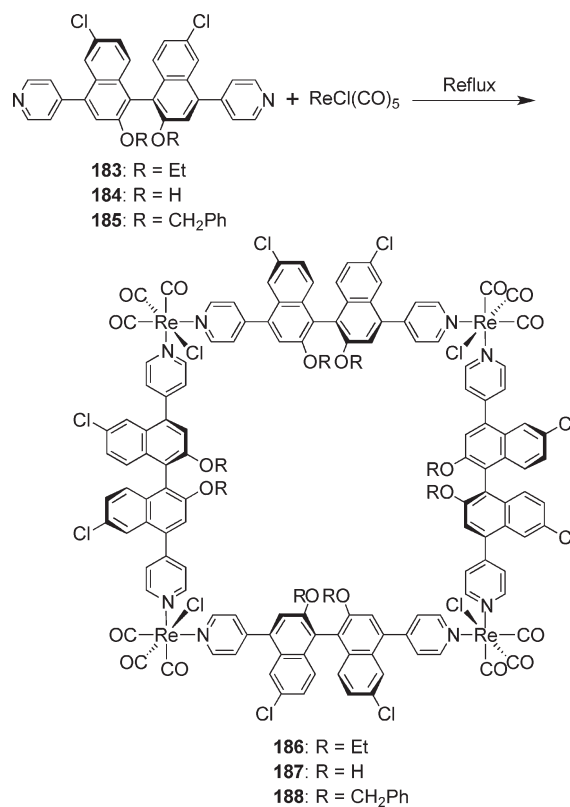


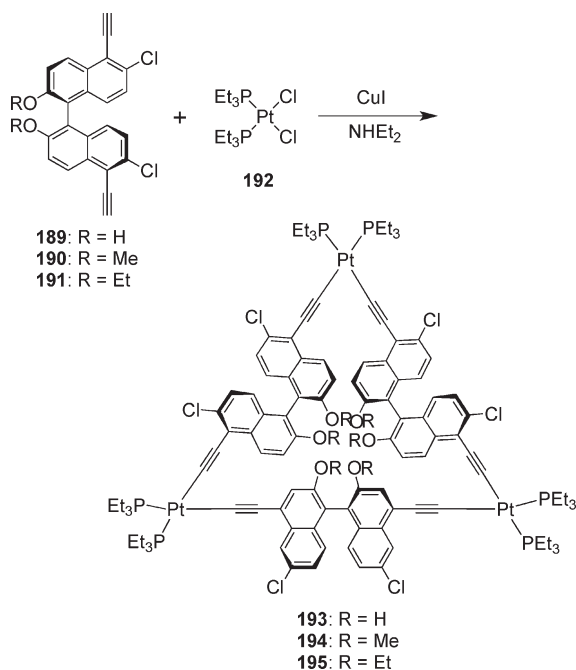
Figure 21. X-ray crystal structure of the homochiral molecular triangle. Color code: golden, Cu; red, O; blue, N; gray, C.

Scheme 45



metal auxiliary units. An example of this approach was provided by Lin and co-workers wherein they used pyridyl functionalized-1,1'-binaphthyl ligands (**183–185**) derived from enantiopure 1,1'-binaphthyl-2,2'-diol (BINOL) with achiral *fac*- $[\text{ReCl}(\text{CO})_5]$  metal corners to assemble a family of chiral molecular squares (**186–188**; Scheme 45).<sup>207</sup> The formations of the chiral metallacycles were confirmed by NMR, mass spectrometry, UV–visible, and CD spectroscopic techniques. Using angular bipyridine bridging ligands derived from enantiopure 1,1'-binaphthyl-2,2'-diol (BINOL) and  $[\text{M}(\text{dppe})]^{2+}$  ( $\text{M} = \text{Pd}$  or  $\text{Pt}$  and  $\text{dppe} = \text{bis}(\text{diphenylphosphino})\text{ethane}$ ) metallocorners, a

Scheme 46



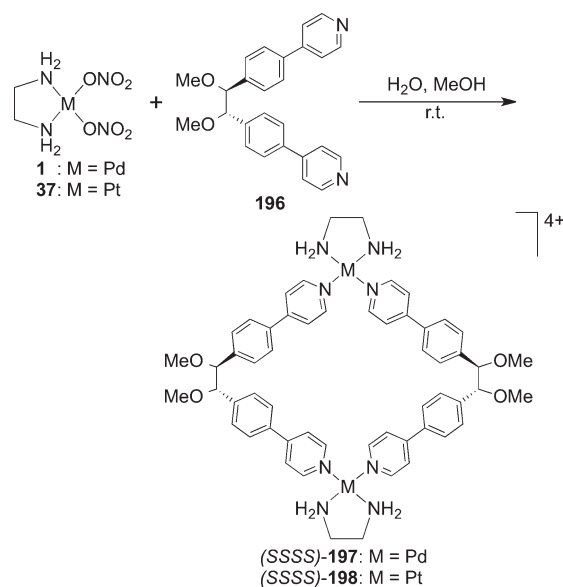
series of chiral molecular squares were readily assembled by the same group.<sup>208</sup> The macrocycles were characterized by a variety of techniques including infrared, UV–visible, CD, multinuclear NMR spectroscopies and ESI-MS. All of these chiral molecular squares were highly luminescent in solution at room temperature with good quantum efficiency.

A series of chiral molecular triangles, **193–195**, was afforded by the equimolar treatment of bis(alkynyl) derivatives of BINOL ligands **189–191** with the cis-protected Pt(II) metalcorner, *cis*-[PtCl<sub>2</sub>(PEt<sub>3</sub>)<sub>2</sub>] (**192**), utilizing the facile insertion of Pt(II) into alkyne C–H bonds (Scheme 46).<sup>209</sup> Although, from a geometric consideration, molecular squares were expected, the kinetic preference for smaller metallacycles drives the assembly toward the exclusive formation of molecular triangles. Interestingly, replacement of cis-blocked ligand **159** with *cis*-[Pt(4,4'-d<sup>4</sup>BuPy)Cl<sub>2</sub>] leads to both a molecular triangle and a square in 29 and 22% yields, respectively.<sup>210</sup> However, using the same ligand systems, molecular squares can be exclusively formed via stepwise directed-assembly reactions in modest yields.<sup>211</sup>

A mixture of chiral organometallic molecular polygons, ranging from triangles to octagons, resulted when 1 equiv of *trans*-[PtCl<sub>2</sub>(PEt<sub>3</sub>)<sub>2</sub>] was treated with the atropisomeric bridging ligand 2,2'-diacetyl-1,1'-binaphthyl-6,6'-bis(ethyne).<sup>212</sup> The analytically pure molecular polygons were isolated by silica gel column chromatography and characterized by ESI-MS, multinuclear NMR, and CD spectroscopy. By adopting a similar methodology, the robustness of the Pt–alkynyl bond was utilized to assemble chiral dinuclear metallocyclophanes with *exo*<sup>213</sup> and *endo*<sup>214</sup> functionalization. Jiang and Lin<sup>215</sup> also reported a series of chiral mesoscopic metallacycles having as many as 47 metal centers using a stepwise assembly method. These molecular polygons were built from a similar binaphthyl-based ligand and *trans*-Pt(PEt<sub>3</sub>)<sub>2</sub> as the metalcorner.

Another category of ditopic chiral linkers has side chains connected by an ethylene bridge with a rigid gauche conformation.

Scheme 47

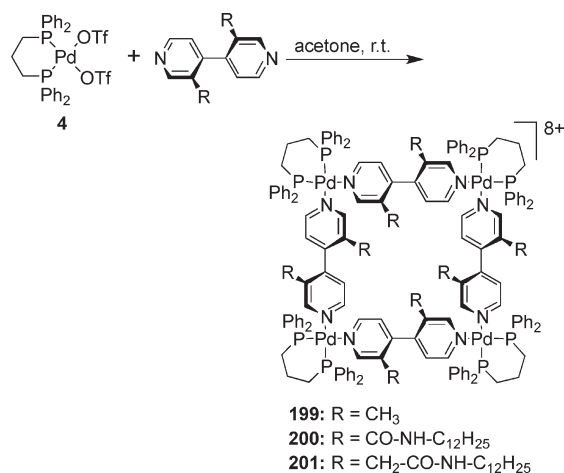


Chiral, enantiopure metallocsupramolecular rhomboids have been self-assembled in solution through the coordination of bis-pyridyl-substituted chiral ditopic ligands with *cis*-blocked Pd(II) and Pd(II) acceptors.<sup>216</sup> For example, treatment of chiral ditopic ligand **196** with [M(en)(NO<sub>3</sub>)<sub>2</sub>] [M = Pd (**1**), Pd (**37**)] led to the assembly of enantiopure SSSS rhomboids, **197–198** (Scheme 47). The R-enantiomer also forms under the same conditions as the all-S enantiomer. The assemblies were characterized in detail by NMR and CD spectroscopies in solution and by ESI-FT-ICR-MS in the gas phase and could be adsorbed and imaged at surfaces in an electrochemical environment. The chirality of these assemblies manifests itself on surfaces at both local and global levels.<sup>216</sup> Jeong et al. have used a very similar carboxylate functionalized bis-pyridyl-substituted chiral ditopic ligand with Cu(II) ions in DMF to self-assemble a chiral triangular metallacycle.<sup>217</sup> A chiral C<sub>3</sub>-symmetric hexanuclear triangular-prismatic copper(II) cluster was also assembled from an enantiomeric dipeptidic N,N'-terephthaloyl-bis(S-aminocarboxylato) ligand.<sup>218</sup>

Schalley and co-workers have also established the diastereoselective self-assembly of metallo-supramolecular squares utilizing axially chiral 4,4'-bipyridine bridging ligands. Chiral molecular squares **199–201** were synthesized by the treatment of enantiopure chiral 4,4'-bipyridine ligands with *cis*-blocked Pd(II) building block [Pd(dppp)(OTf)<sub>2</sub>] (**4**) as the corner units in a 1:1 molar ratio (Scheme 48).<sup>219</sup> Corresponding Pt(II)-based chiral molecular squares were also prepared. Amino acids such as (S)-alanine incorporated into the axially chiral 4,4'-bipyridine ligands afforded amino acid functionalized chiral metallo-supramolecular squares.<sup>220</sup> As established from multinuclear NMR and X-ray structural studies, only one diastereomer was formed in which the side chains were positioned outward and the pairwise, opposite bipyridines had the same axial chirality. Although the chiral centers of the alanines favor one of the axially chiral biaryl configurations in the free ligand, the ratio of both diastereomers is strictly 1:1 in the squares. This diastereoselectivity is governed by the stereoelectronic effects of the dppp ligand, which lead to the exclusive formation of heterochiral assemblies.



Scheme 48

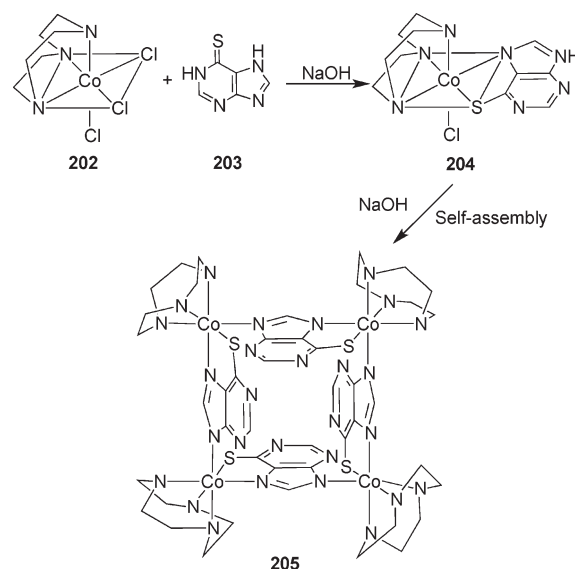


The synthesis of enantiopure molecular rectangles was achieved using the platinum-based molecular clip, 1,8-bis[*trans*-Pt(PEt<sub>3</sub>)<sub>2</sub>(NO<sub>3</sub>)]anthracene (**75**) with (2*R*,3*R*)-(+)-tartarate and (2*S*,3*S*)-(–)-tartarate.<sup>221</sup> These enantiopure rectangles showed the phenomenon of induced circular dichroism (ICD). Although (2*R*,3*R*)-(+)-tartaric acid is CD-inactive in the long wavelength and shows only one negative Cotton effect at 214 nm, the corresponding molecular rectangle showed bands which corresponded to anthracene moiety above 350 nm. This indicated the presence of ICD in the anthracene moiety and, as such, in the chiral supramolecule upon association with chiral inducers, (2*R*,3*R*)-(+)-tartarate dianions.

In an interesting study, Yeh and Raymond observed supramolecular chiral induction in dinuclear triple-stranded helicates composed entirely of achiral components.<sup>222</sup> The anionic helicates show strong intermolecular asymmetric induction in the presence of chiral organic cationic molecules such as *N*-methyl-s-nicotinium (*s*-nic), *N*-methyl cinchoninium (*cinc*), and *N*-methylquininium (*quin*). These chiral cations can transmit chirality to the metal centers of the helicates (by associating in the cleft between the ligand planes) leading to the determination of the chirality of the entire helicate. The van der Waals contact and cation– $\pi$  interaction plays an important role in communicating chirality to these metallohelicates. In fact, due to the precise nature of these interactions, minor variations in the structures of the chiral cation as well as the central ligand scaffold of the helicate significantly affect the level of intermolecular chiral induction.<sup>222</sup>

In the third strategy, inherently chiral octahedral (tris-chelated) metal complexes were used to assemble chiral metallacycles with achiral multidentate ligands as the building blocks. Chiral molecular triangles and squares of Co(III) were reported by Yamanari et al.<sup>223</sup> through the self-assembly of inherently chiral mononuclear octahedral complexes based on the multidentate bridging ability of the achiral ligands. The treatment of *fac*-[CoCl<sub>3</sub>(tacn)] (**202**; tacn = 1,4,7-triazacyclononane) with purine-6-thiones (**203**) in the presence of an equimolar amount of NaOH initially produced a chiral species, **204**. Subsequent deprotonation resulted in the formation of chiral molecular square **205** via self-assembly of the mononuclear complex, **204** (Scheme 49). Along the same line, reaction of octahedral Co(II) ions with multidentate achiral ligands which have a  $\sim 90^\circ$  twist (*D*<sub>2h</sub> symmetry), such as the

Scheme 49



tetraacetylene dianion, facilitated the formation of chiral molecular squares.<sup>224</sup> The reaction between [Mo(CO)<sub>6</sub>] and 3,6-di-*tert*-butyl-1,2-benzoquinone in the presence of trace quantities of dioxygen led to the initial formation of molybdenum complexes of 3,6-di-*tert*-butylcatechol. Condensation of this monomer through bridging oxo ligands gives cyclic, chiral [Mo-( $\mu$ -O)(3,6-DBCat)<sub>2</sub>]<sub>4</sub> square with four Mo centers of the same chirality.<sup>225</sup>

Using the dimetallic building block approach, Cotton and co-workers described a series of chiral molecular triangles containing Rh<sub>2</sub><sup>4+</sup> dimetallic corner units.<sup>226</sup> The reaction of *cis*-Rh<sub>2</sub>(C<sub>6</sub>H<sub>4</sub>PPh<sub>2</sub>)<sub>2</sub><sup>2+</sup> units with the tetraethylammonium salts of the linear dicarboxylates, in organic solvents, produced racemic crystals of the corresponding chiral molecular triangles [Rh<sub>2</sub>(C<sub>6</sub>H<sub>4</sub>PPh<sub>2</sub>)<sub>2</sub>]<sub>3</sub>( $\mu$ -L)<sub>3</sub>X<sub>3</sub> (L = oxalate, terephthalate, and 4,4'-biphenyldicarboxylate; X = DMF, py).<sup>227</sup> Due to the head-to-tail arrangement of the two orthometalated bridging ligands, the *cis*-Rh<sub>2</sub>(C<sub>6</sub>H<sub>4</sub>PPh<sub>2</sub>)<sub>2</sub><sup>2+</sup> unit is inherently chiral, and the molecular triangles based on this unit are thus chiral. However, the chirality induced by the conformational arrangement of the ligands in these supramolecules is only secondary when compared to the chirality (*R* or *S*) that arises from the configurational arrangement of the molecules. Interestingly, as determined from single-crystal structural analysis, multinuclear NMR, mass spectrometry, and electrochemical studies, molecular triangles were exclusively formed both in solution and in the solid state. The reason for this well-defined preference was due to the preferred twist (ca. 23°) of the *cis*-Rh<sub>2</sub>(C<sub>6</sub>H<sub>4</sub>PPh<sub>2</sub>)<sub>2</sub> corners which induces very little strain on the triangular structures as compared to the corresponding square structures. Thus, the entropic preference for the smaller ring becomes the controlling thermodynamic factor. A resolved enantiomer of the same starting dimetallic corner unit *cis*-Rh<sub>2</sub>(C<sub>6</sub>H<sub>4</sub>PPh<sub>2</sub>)<sub>2</sub><sup>2+</sup> resulted in enantiopure molecular triangles (RRR and SSS).<sup>228</sup> As ascertained from the crystal structural analysis, the enantiomers are isostructural. Figure 22 shows the single-crystal X-ray structure of the SSS-[*cis*-Rh<sub>2</sub>(C<sub>6</sub>H<sub>4</sub>PPh<sub>2</sub>)<sub>2</sub>(O<sub>2</sub>CC<sub>6</sub>H<sub>4</sub>CO<sub>2</sub>)(py)<sub>3</sub>(MeOH)<sub>3</sub>]<sub>3</sub>. Cotton et al. have also reported enantiopure chiral molecular loops RR-[*cis*-Rh<sub>2</sub>(C<sub>6</sub>H<sub>4</sub>PPh<sub>2</sub>)<sub>2</sub>(py)<sub>2</sub>(O<sub>2</sub>C(CF<sub>2</sub>)<sub>n</sub>CO<sub>2</sub>)<sub>2</sub>] (*n* = 2, 3)

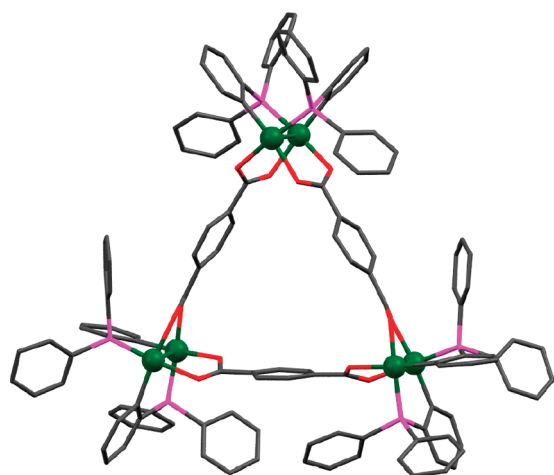


**Figure 22.** Single-crystal X-ray structure of  $\text{SSS-[cis-Rh}_2(\text{C}_6\text{H}_4\text{PPh}_2)_2\text{-(O}_2\text{CC}_6\text{H}_4\text{CO}_2\text{)(py)}_2\text{]}_3$ . Axial py and MeOH ligands were omitted for clarity. Color code: green, Rh; pink, P; red, O; gray, C.

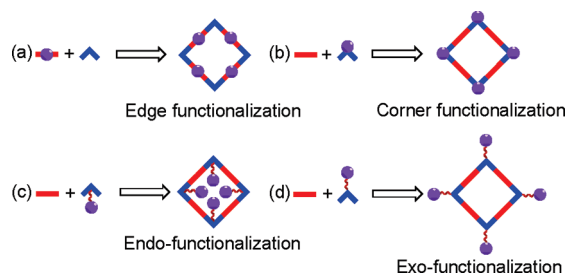


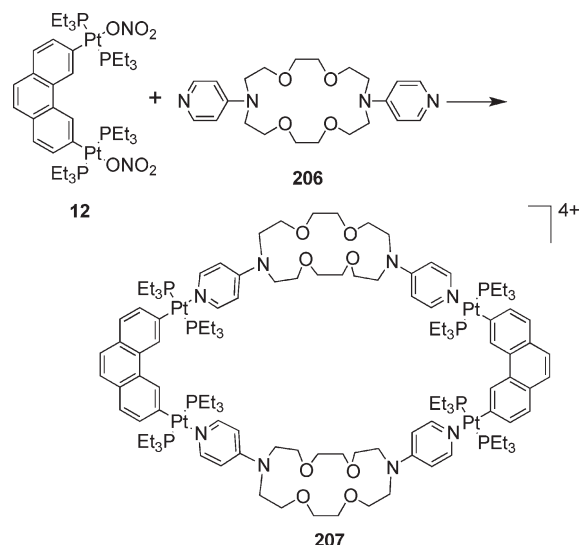
**Figure 23.** Incorporation of functional moieties into assemblies through the use of functionalized edge or corner building blocks or covalent attachment of functional groups endo or exo to the metallacycles.

using the same  $\text{Rh}_2^{4+}$  dimetallic unit  $\text{cis-Rh}_2(\text{C}_6\text{H}_4\text{PPh}_2)_2^{2+}$  in organic solvents.<sup>229</sup>

### 3.4. Functional Systems and their Properties

The rational design and synthesis of functionalized metallo-supramolecular architectures through coordination-driven self-assembly has generated a great deal of interest in recent times and has been extensively reviewed.<sup>230</sup> Several of these functional assemblies can be employed as precursors of electronic, catalytic, and photophysical materials and used for molecular recognition and encapsulation. Assemblies containing transition metals are generally more sensitive and responsive to electro- and photochemical stimuli as compared to metal-free organic structures. The rigid architecture of the supramolecular ensembles offers well-defined scaffolds for the incorporation of functional moieties where the stoichiometry and position of the individual functional groups can be precisely controlled. Moreover, upon formation, these functional moieties can interact further to give rise to a higher level of functionality. The directional bonding approach, due to its highly modular nature, allows the incorporation of various functionalities into the edge and corner of a building block. Likewise, tethering of functional moieties through a covalent attachment to the building blocks allows the positioning of the functionality into the cavity or on the periphery of a resulting assembly (Figure 23).

**Scheme 50**



A variety of functional moieties such as crown ethers, carboranes, cavitands, dendrimers, ferrocenyl units, and lipophilic and lipophobic groups onto the edges and corners and on the periphery of a number of discrete supramolecular assemblies.<sup>231</sup> The combination of functionalized diaza crown ethers with a 0, 60, or 90° di-Pt(II) acceptors led to the facile formation of a series of geometrically distinct edge and corner functionalized supramolecules. Incorporation of a flexible pyridine functionalized 18-member diaza crown ring was achieved by treatment with varying Pt(II) acceptors, for example, the [2 + 2] self-assembly of 60° di-Pt(II) acceptor **12** with a diaza crown ring, **206**, led to the formation of cationic metallacycle **207** (Scheme 50).<sup>232</sup> Neutral, Pt-based discrete assemblies containing flexible 32-member dibenzo crown ether were also synthesized and characterized by NMR and X-ray structural studies.<sup>233</sup>

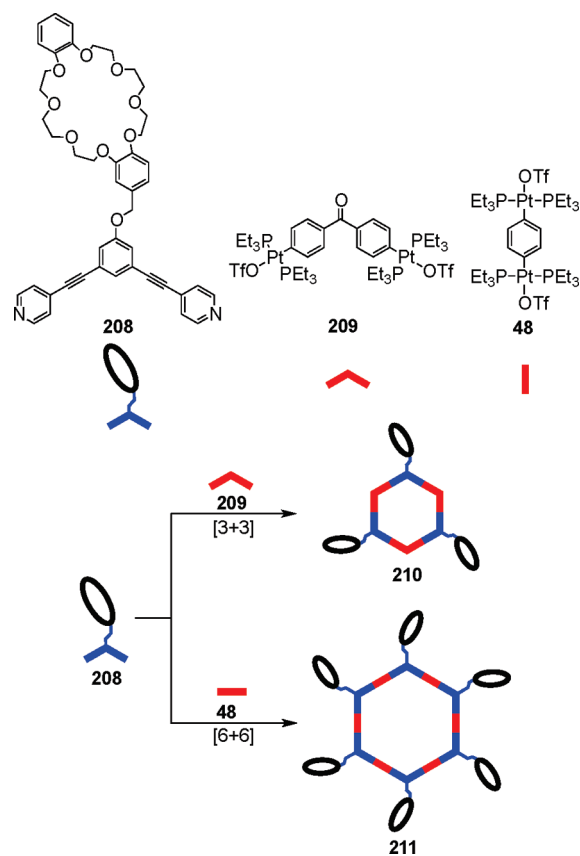
If properly functionalized, cavitands can be utilized as building units for supramolecular ensembles to give unique structures. The introduction of diametrically opposed pyridyl donor groups at the bridging positions on the rim of a cavitand bowl can lead to the formation of corner functionalized metallacycles.<sup>234</sup> For example, the tethering of two tolyl pyridyl moieties as bridging ligands on a cavitand bowl and subsequent self-assembly with *fac*-[Re(CO)<sub>5</sub>Br] in chloroform gave a self-assembled rhombic metallacycle after 24 h, which is neutral and kinetically stable at room temperature.<sup>235</sup> <sup>1</sup>H NMR and ESI-MS studies established the formation of the metallacycle. Similarly, diametrically opposed pyridyl groups substituted on the rim of a cavitand bowl, which, projecting outward at an angle of 60° relative to one another, generated corner functionalized metallo-supramolecular assemblies when assembled with linear ditopic Pt(II) acceptors.<sup>236</sup> The [2 + 2] and [3 + 3] self-assembly of a pyridyl-containing cavitand corner donor units with 60 and 180° diplatinum acceptors led to cavitand functionalized rhombic and triangular supramolecular assemblies, respectively. The assemblies and building blocks were characterized with multinuclear NMR spectroscopy, ESI-MS, and elemental analysis. Similarly, a number of metallacycles were assembled by incorporating carborane functionalized linear donors as well as linear and 120° carborane functionalized di-Pt(II) acceptors.<sup>237,238</sup>

Treating the linear carborane-containing bis-pyridyl donor with 0, 60, and 90° Pt(II) acceptors led to the formation of [2 + 2] rectangular, [3 + 3] triangular, and [4 + 4] square metallacycles, respectively.<sup>237</sup> Likewise, the treatment of an edge functionalized carborane-containing linear diplatinum(II) acceptor units, upon combination with a 90° bis-pyridyl donor unit, generated a large metallocupramolecular square. The assemblies and building blocks were characterized with multinuclear NMR spectroscopy, ESI-MS, and elemental analysis. In addition to these examples, neutral molecular rectangles and rhomboids were designed using platinum–oxygen bonds as the driving force for assembly.<sup>238</sup> The combination of *m*- and *p*-carborane dicarboxylate units with a 0° diplatinum acceptor yielded a neutral molecular rectangle and a rhomboid, respectively. Multinuclear NMR and X-ray structural studies established the formations of the assemblies.

Edge functionalized hydrophobic and hydrophilic self-assembled supramolecular rectangles were synthesized from functionalized 180° 1,4-bis(4-ethynylpyridyl)-2,3-substituted benzenes with 0° diplatinum(II) acceptors via coordination-driven self-assembly to give supramolecular rectangles.<sup>239</sup> The hydrophobic rectangles were functionalized with C<sub>6</sub>H<sub>13</sub>, C<sub>12</sub>H<sub>25</sub>, and C<sub>18</sub>H<sub>37</sub> alkyl chains while the hydrophilic rectangles were decorated with methyl terminated di-, tetra-, and hexaethylene glycol units. Multinuclear NMR (<sup>1</sup>H and <sup>31</sup>P) and ESI-MS were used to characterize the assemblies. Molecular force-field modeling suggested that the hydrophobic and hydrophilic chains of each exohedrally functionalized rectangle prefer to wrap around and aggregate in solution. Similar edge functionalized alkoxy-bridged Re(I) supramolecular rectangles decorated with long alkyl chains (C<sub>4</sub>H<sub>9</sub>, C<sub>8</sub>H<sub>17</sub>, and C<sub>12</sub>H<sub>25</sub>) have also been reported.<sup>240</sup> In the presence of increasing water concentrations these Re(I) rectangles aggregated in solution. Such self-aggregation led to an enhanced luminescence efficiency presumably from the restriction of torsional molecular motion in the aggregates. Furthermore, intermolecular quenching experiments of Re(I) aggregates with various amines and quinones showed aggregation-facilitated electron transfer between the rectangles and electron donors and acceptors via both static and dynamic quenching processes.

Considerable research effort has been expended on the functionalization of metallo-supramolecular squares by employing functional ligands or/and metal corners in the assembly processes. Upon square formation, these functions may interact, leading to a higher level of functionality. Moreover, the cavities of the molecular square may accommodate guest molecules. Notably, Würthner et al. have designed light harvesting metallo-supramolecular squares having of perylene bisimide walls and fluorescent antenna dyes.<sup>241</sup> The fluorescent dye 4-dimethylamino-1,8-naphthalimide was incorporated at the bay area of *N*, *N'*-bispyridyl perylene bisimide ligand. Subsequent assembly of this ditopic ligand with [Pd(dppp)(OTf)<sub>2</sub>] gave a self-assembled molecular square. Optical studies of the macrocycle by UV–visible and steady-state and time-resolved fluorescence spectroscopy revealed that the light captured by the dye antennas gets transported to the perylene-bisimide core by a fluorescence resonance mechanism with high quantum efficiency. Thus, this multichromophore square assembly with aminonaphthalimide antenna dyes is an artificial model for the cyclic light harvesting complexes in purple bacteria. Earlier a molecular square having 16 pyrene chromophores attached to four ditopic bay functionalized perylene bisimide chromophores exhibited extremely fast electron-transfer processes that are normally only observed in solid materials.<sup>81</sup>

Scheme 51



Multiple crown ethers were incorporated into the metallo-supramolecular assemblies by exofunctionalization of the building blocks with crown ethers to yield 2D macrocycles with well-defined cavities with varied geometries.<sup>242,243</sup> Dibenzo[24]crown-8 was appended to both the 120° donor and the 120° acceptor units through covalent attachment. The combination of the predesigned 120° bispyridyl donor unit, 208, containing dibenzo[24]crown-8 pendent with the complementary 120° di-Pt(II) acceptor, 209, in a 1:1 stoichiometric ratio allowed the formation of a [3 + 3] hexagonal metalocyclic assembly, 210. A [6 + 6] hexagonal assembly, 211, was afforded when 208 was treated with the 180° di-Pt(II) acceptor, 48 (Scheme 51).

Likewise, by using a similarly designed dibenzo[24]crown-8 pendent containing a 120° diplatinum(II) acceptor unit, different types of [3 + 3] and [6 + 6] hexagonal assemblies can be generated through combination with di-2-pyridyl ketone (60° donor) and 4,4'-bipyridine (180° donor), respectively. Rhomboidal assemblies containing multicrown ethers can also be synthesized via the [2 + 2] self-assembly of 120° di-Pt(II) acceptor and 120° bis-pyridyl donor unit (208) with their complementary 60° building blocks. These multicrown architectures have been investigated as the hosts for the multivalent self-assembly of poly[2]pseudorotaxanes. Dialkylammonium ions can form a 1:1 host–guest complex with dibenzo[24]crown-8 ether in nonprotic solvents held together by H-bonding,  $\pi$ – $\pi$  stacking interactions, and electrostatic forces. Hence, dibenzylammonium ions were used to form a new class of poly[2]pseudorotaxanes from the above discrete molecular rhomboids and hexagons having pendant multicrown ether moieties in



their periphery.<sup>242,243</sup> As determined by multinuclear 1D and 2D NMR as well as mass spectrometry, the hexagonal assemblies such as **210** and **211** can complex three and six dibenzylammonium ions, respectively. The rhomboidal assemblies can complex two such ions. In all cases, the underlying rigid nature of the 2D polygonal cavity is retained while the flexibility of each crown ether is reduced as a result of host–guest complexation. The orthogonal, noninteracting nature of the coordination-driven self-assembly of the underlying polygons allows for rhomboidal and hexagonal poly[2]pseudorotaxanes to be prepared.

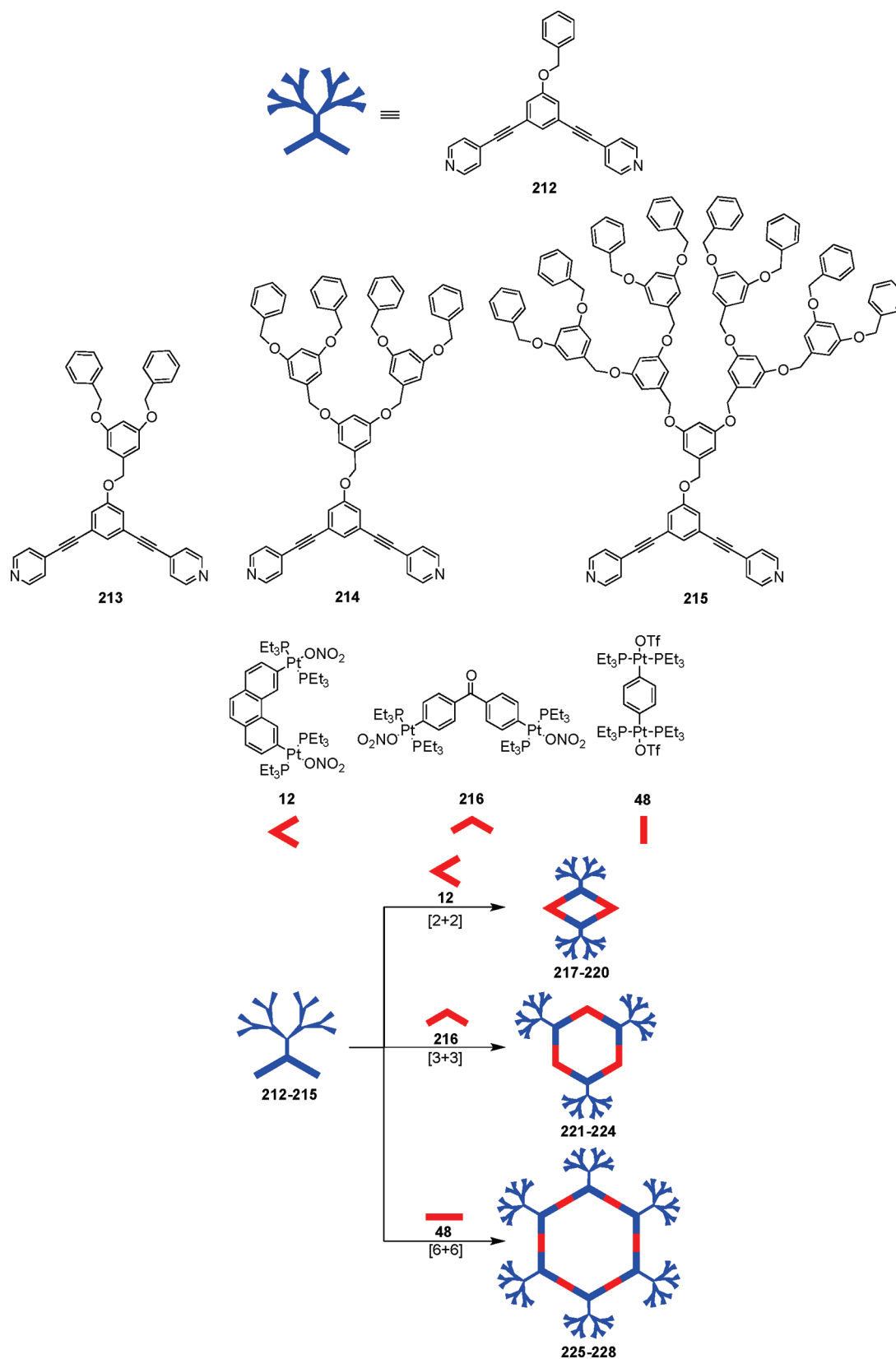
Dendritic moieties were also incorporated into metallo-supramolecular assemblies via the directional bonding approach by functionalizing the building blocks with predesigned dendrons. Dendrimers are highly branched, monodisperse macromolecules emanating from a central core. Incorporation of these dendritic moieties as functional units in supramolecular assemblies is of interest due their potential application in biology,<sup>244</sup> catalysis,<sup>245</sup> and photo- and electrochemistry.<sup>246</sup> A number of metallodendrimers of varying size and shape were assembled by the combination of predesigned bis-pyridyl donor building blocks **212**–**215** on which Fréchet-type dendrons were tethered through covalent attachment. The self-assembly of rhomboidal metallodendrimers, **217**–**220**, was achieved by the combination of 120° Fréchet-type dendritic donor units **212**–**215** and 60° di-Pt(II) acceptor unit **12** in a 1:1 stoichiometric ratio (Scheme 52).<sup>247,248</sup> Single-crystal X-ray structural studies of rhomboidal metallodendrimers **217** and **218** showed well-defined rhombic structure with approximately  $2.3 \times 1.3$  nm<sup>2</sup> cavities. Treatment of 120° donors **212**–**215** with 120° diplatinum(II) acceptor units **216** and 180° diplatinum(II) acceptor **48** units led to the formation of [3 + 3] hexagons **221**–**224** and [6 + 6] hexagons **225**–**228**, respectively (Scheme 52). In a complementary approach, [3 + 3] coordination-driven self-assembly between 120° diplatinum acceptor subunits containing tethered dendrons with the bis-pyridyl donor building blocks afforded six-component hexagonal metallodendrimers.<sup>249</sup> Likewise, neutral dendritic metallacycles were achieved through the platinum–oxygen coordination bonds. The combination of rigid 120° dicarboxylate donor linkers functionalized with Fréchet-type dendrons with complementary 60 and 120° di-Pt(II) acceptor subunits **12** and **216** yielded neutral rhomboidal metallodendrimers and hexagonal metallodendrimers, respectively.<sup>250</sup> All of these assemblies were characterized with multinuclear NMR, mass spectrometry, and elemental analysis. Molecular modeling studies revealed that these exo functionalized cavity-cored metallacycles have well-defined cavities and may thus function as transport vehicles for small, biologically active molecules. Similar Fréchet-type dendrons were also incorporated on the edges of Pd(II)- and Pt(II)-based metallo-supramolecular squares.<sup>251</sup> Functionalization of 4,4'-bipyridines in their 3,3'-positions with different generations of Fréchet-type dendrons and subsequent self-assembly with [M(dppp)(OTf)<sub>2</sub>] (M = Pd, Pt) led to nanometer-sized metallo-supramolecular squares. ESI-FT-ICR-MS and NMR experiments established the formation of these dendritic molecular squares, which showed interesting dynamic behavior. Variable-temperature NMR studies revealed the coexistence of different conformers in solution, which interconvert slowly due to high barriers for both ligand rotation, caused by the dppp phenyl groups and for the racemization of the bipyridine ligands. The ligand exchange process was much slower for the Pt(II) squares as compared to their Pd(II) analogues.

The design and synthesis of macromolecules that contain multiple redox centers is of interest due to their potential application in electro- and photochemical devices.<sup>246</sup> However, traditional covalent synthetic strategies to prepare functionalized dendritic and polymeric architectures have often led to relatively unsatisfactory yields and demand considerable synthetic effort. Exo functionalization of the building blocks at the vertices with ferrocene moieties and their subsequent self-assembly with complementary subunits provides an efficient synthetic pathway with precise control over the location and number of the ferrocenyl moieties introduced into the system. Following a synthetic strategy similar to that above, the combination of a 1:1 stoichiometric ratio of ferrocene appended bispyridyl 120° donor unit **229** with 60, 120, and 180° diplatinum acceptors **12**, **209**, and **48** allows the self-assembly of [2 + 2] rhomboidal **230**, [3 + 3] hexagonal **231**, and [6 + 6] hexagonal **232** metallacycles, respectively (Scheme 53).<sup>252</sup> In a complementary approach, ferrocenyl tethered 120° di-Pt(II) acceptor units were assembled into a [6 + 6] hexagon by treatment with the linker 4,4'-bipyridine.<sup>253</sup> A [3 + 3] self-assembly between the ferrocenyl appended bispyridyl 120° donor unit **229** with complementary ferrocenyl tethered 120° di-Pt(II) acceptor units yields a hexagonal metallacycle with six ferrocenyl units. Multinuclear NMR and mass spectrometric analysis confirmed the formation of these assemblies. Electrochemical investigations on the multi-ferrocenyl assemblies **230**–**232** revealed that the redox sites are well-isolated from each other electrochemically and are active. The sizes of the assemblies have an effect on the observed diffusion coefficients and half-wave potentials. Larger hexagonal assemblies led to a decrease in diffusion coefficient and an increase in half-wave potential. Heterofunctional hexagons containing orthogonal functionalities, redox-active ferrocenyl—host—guest crown ether,<sup>254</sup> ferrocenyl—Fréchet-type dendrons,<sup>255</sup> and host—guest crown ether—Fréchet-type dendrons,<sup>256</sup> were also assembled through a coordination-driven self-assembly approach. The precise positioning of the functional groups present at the vertex of the hexagons leads to supramolecules that are capable of carrying out a variety of functions both simultaneously and independently. Recently, Newkome et al.<sup>257</sup> reported the formation of pentameric and hexameric metallamacrocycles functionalized with sugar moieties at the corners from the Fe(II) mediated complexation of 120° 3,5-bis(terpyridinyl)-arene ligands. Treatment of 120° 3,5-bis(terpyridinyl)arene donors with FeCl<sub>2</sub>·4H<sub>2</sub>O in MeOH for 24 h gave a mixture of pentameric (4.3%) and hexameric (11.9%) metalla-macrocycles which were separated by gradient column chromatography. Although the hexamer was the expected product, the formation of pentamer was a result of an initially formed kinetic product. <sup>1</sup>H NMR, <sup>13</sup>C NMR, UV–visible spectroscopy, cyclic voltammetry, and mass spectrometry established the structures of the macrocycles. These macrocycles generated nanofibers having diameters ranging from 10 to 80 nm.

Endo functionalized two-dimensional supramolecular architectures have also been designed via coordination-driven self-assembly.<sup>258</sup> The construction of endo functionalized metallacycles including two [2 + 2] rhomboids (**235** and **236**) and a [3 + 3] hexagon (**237**) were achieved by the self-assembly of a 120° dipyridyl donor ligand (**233**) with three different di-Pt(II) acceptors **12**, **234**, and **209**, respectively (Scheme 54). The metallacycles, containing several nitrobenzyl moieties at their interior surfaces, were characterized by multinuclear NMR (<sup>31</sup>P and <sup>1</sup>H) and ESI-MS. Significant C–H···O hydrogen bonding between the nitrobenzyl acceptor and the edge molecules of the



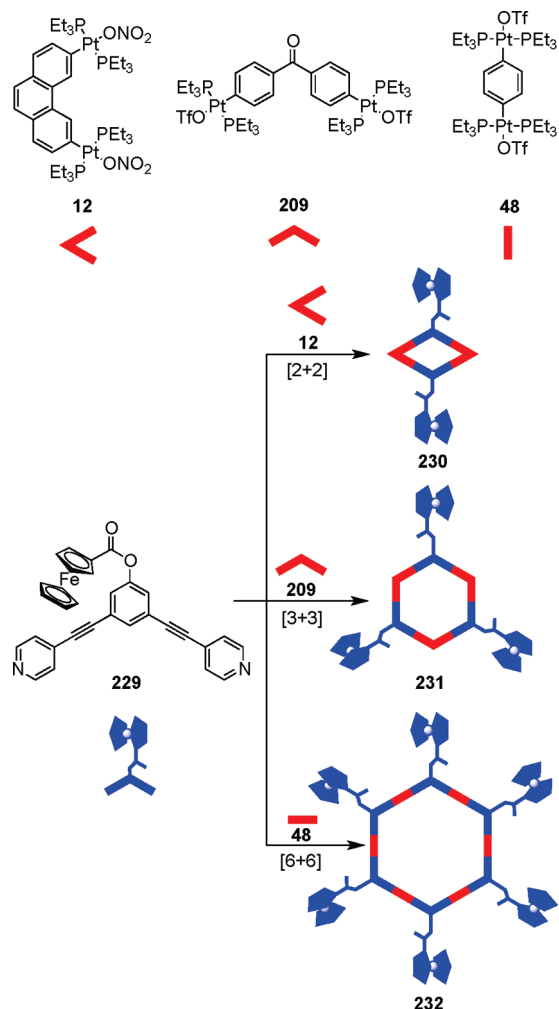
Scheme 52



supramolecular architecture was observed in the [2 + 2] rhomboid **235**, and this interaction gradually decreased upon the

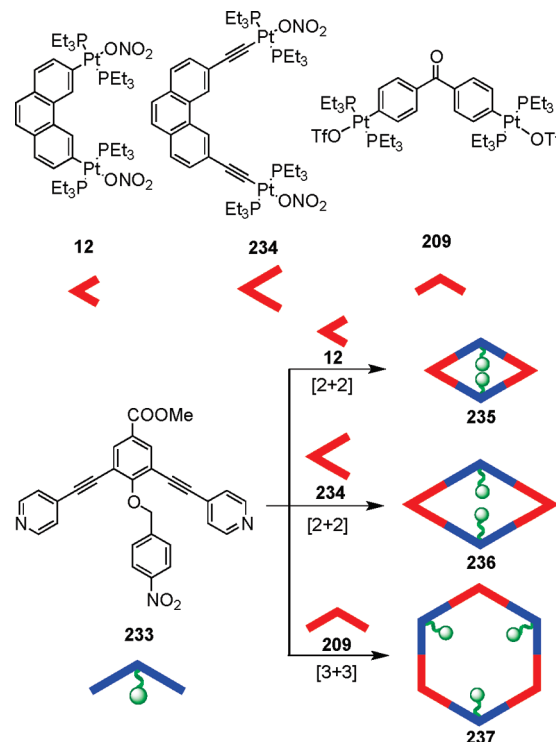
enlargement of the resulting polygonal structures from **235**, through a rhomboid **236**, to a hexagon **237**.

Scheme 53

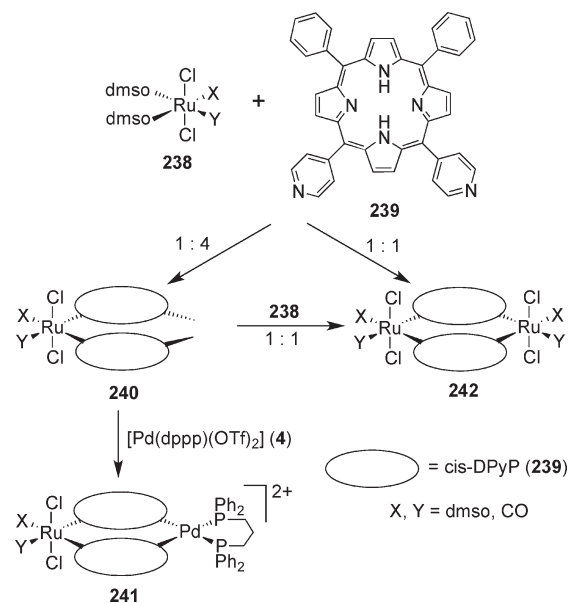


The incorporation of porphyrin moieties into supramolecular assemblies has generated much interest in recent years due to their potential application in varied fields such as photodriven molecular switches, artificial photosynthetic systems, fluorescence-based chemical sensors, photonic wires, reaction catalysis, and anticancer pharmaceutical behavior.<sup>259</sup> Ligands derived from porphyrin units have the ability to serve as either linear or angular building units depending on the position of the donor functional groups, leading to both edge and corner functionalized supramolecular metallacycles. One of the earliest examples where porphyrin units were used to assemble metallacycles was provided by the work of Drain and Lehn in 1994.<sup>260</sup> The formation of edge functionalized neutral molecular squares was achieved by treating 5,15-(4-pyridyl)-10,20-phenylporphyrin (4'-*trans*-DPyP) or its Zn complex with 1 equiv of *cis*-Pt(NCPh)<sub>2</sub>Cl<sub>2</sub>. Similar treatment of 5,10-derivatized isomers (4'-*cis*-DPyP or its Zn complex) with *trans*-Pt(NCPh)<sub>2</sub>Cl<sub>2</sub> gave corner functionalized assemblies. Studies performed by Stang et al.<sup>205</sup> also involved the use of derivatized porphyrin units not only as the corners but also as the edges of self-assembled metallacyclic squares using bisphosphine coordinated Pd(II) and Pt(II) angular and linear modules as the metallic precursor. Hetero-bimetallic [2 + 2] metallacycles of porphyrins have been assembled through a

Scheme 54

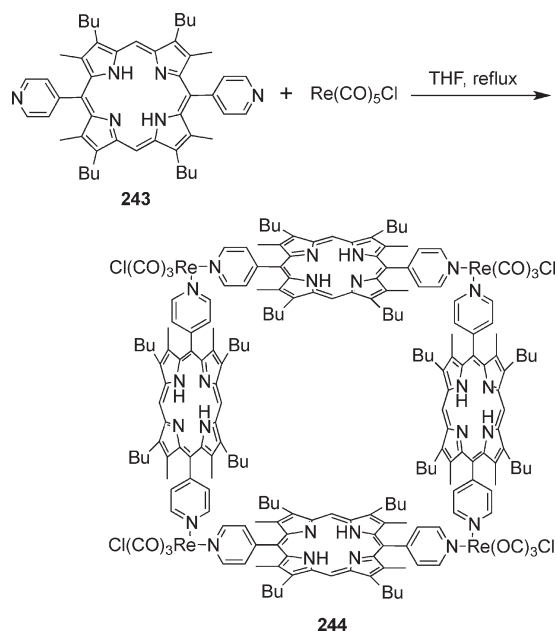


Scheme 55



two-step modular approach using octahedral Ru(II) units as the building blocks.<sup>261</sup> Treatment of [*trans,cis,cis*-RuCl<sub>2</sub>(DMSO)<sub>2</sub>(CO)<sub>2</sub>] (**238**) with 5,10-(4-pyridyl)-10,20-phenylporphyrin (4'-*cis*-DPyP; **239**) in a 1:4 molar ratio allowed for the formation of bis-porphyrin ruthenium intermediate **240** which can be quantitatively assembled by reaction with [Pd(dppp)(OTf)<sub>2</sub>] (**4**) into a [2 + 2] rhomboidal metallacycle, **241** (Scheme 55). X-ray structural studies revealed a butterfly

Scheme 56



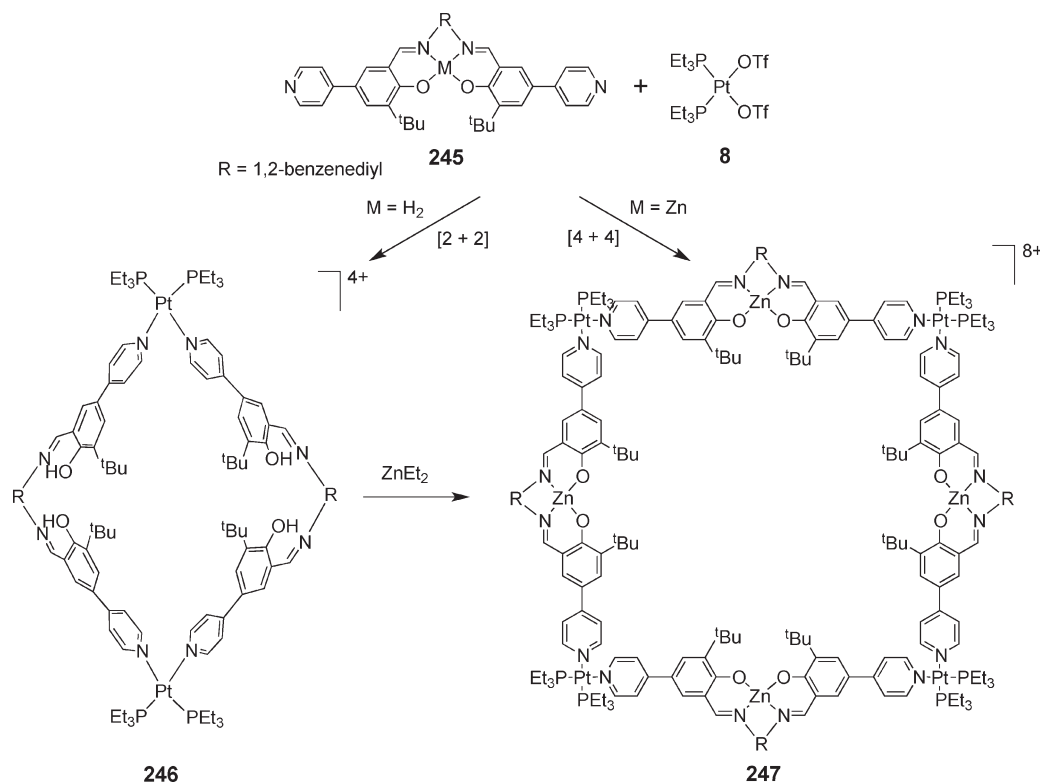
geometry due to stacking interactions between a phenyl ring of the dppp and the pyridyl ring of the porphyrin. The structural features compare well with the palladium [2 + 2] metallacycle  $[\text{Pd}(\text{dppp})(\text{cis-DPyP})_2](\text{OTf})_4$  reported earlier by Stang et al.<sup>36</sup> Homometallic neutral metallacycles of porphyrins  $[\text{RuCl}_2(\text{DMSO-S})_2(\text{cis-DPyP})]_2$  (**242**) can be obtained by treatment of the bis-porphyrin ruthenium intermediate, **240**, with 1 equiv of **238** (Scheme 55).<sup>262</sup> Interestingly, treatment of **238** with 5,10-(3-pyridyl)-10,20-phenylporphyrin (3'-*cis*-DPyP) rather than of 4'-*cis*-DPyP yielded the corresponding [2 + 2] metallacycle with a staggered geometry in which two porphyrin units were held in a slipped cofacial arrangement by the ruthenium metal corners.<sup>263</sup> This staggered geometry, as determined by X-ray structural studies, is reminiscent of those of the special pair of bacteriophylls in the reaction centers and of adjacent B850 units in the LH2 light harvesting antenna systems of photosynthetic bacteria.<sup>264</sup> Metalation of **242** with zinc acetate led to incorporation of Zn in to the porphyrin cavities. These Zn metalated metallacycles can further be assembled through axial coordination with linear bridging ligands to form molecular sandwiches and wires. As determined from NMR studies, the titration of Zn metalated macrocycles with 1 equiv of 4,4'-bipyridine leads rapidly to the quantitative assembling of sandwich-like 2:2 supramolecular adducts where the porphyrin moieties adopt cofacial geometry, as evidenced by X-ray crystallographic studies.<sup>262</sup>

Hupp et al. have studied in some detail the synthetic and functional chemistry of molecular squares having porphyrins as edges and  $\text{Re}(\text{CO})_5\text{Cl}$  as corners.<sup>265</sup> The nanoscale cavities of these porphyrin assemblies were chemically tailored for incorporation of receptor groups with high affinities for specific ions or molecules.<sup>266,267</sup> For example, the edge functionalized supramolecular square,<sup>268</sup> **244**, derived from 2,8,12,18-tetrabutyl-3,7,13,17-tetramethyl-5,15-bis(4-pyridyl)porphyrin (**243**) and  $\text{Re}(\text{CO})_5\text{Cl}$  (Scheme 56) renders lattices of **244** responsive to aqueous Zn(II) ions upon cavity functionalization with tris(2-aminoethyl)-amine, whereas functionalization with 1,6-hexanedithiol enhanced the lattice response to molecular iodine by a mechanism involving

formation of a charge-transfer complex.<sup>266,267</sup> Fabrication of these porphyrinic squares as thin membrane films led to size-selective transport, and thus they act as nanofilters for various probe molecules.<sup>269</sup> Photoelectrochemical cells based on these cavity-containing porphyrinic molecular squares were able to sensitize flat indium–tin oxide (ITO) electrodes to photocurrent production with visible light.<sup>270,271</sup> Recently, it has been demonstrated that large porphyrinic squares derived from *meso*-triazolyl-appended zinc(II) porphyrins can show efficient energy transfer between the *meso*–*meso*-linked zinc(II) porphyrin units, thus having interesting implications toward development of artificial light harvesting apparatus.<sup>272</sup> Covalently linked cyclic porphyrin arrays have been synthesized to mimic natural light harvesting systems and to investigate the highly efficient energy migration processes occurring in these systems for future applications in molecular photonics.<sup>273,274</sup> Molecular rectangles containing cofacial porphyrin edges were synthesized by the same group through the reaction of bis(4-ethynylpyridyl)porphyrin with  $[\text{Re}_2(\text{CO})_6\text{Cl}_2(\mu\text{-bipyrimidine})]$  or a  $[\text{Re}_2(\text{CO})_6(\mu\text{-bis}(\text{benzimidazolates}))]$  in an equimolar ratio.<sup>118</sup> The collapsed structure of the macrocycles brings the two porphyrin faces in close proximity, thereby substantially reducing the cavity for the incorporation of guest molecules. However, the distortion of the nominally rigid ethynylpyridyl linkages in the porphyrin ligand edges imparts significant charge-transfer characteristics to these rectangles. A series of neutral rhenium-based symmetric porphyrin dimers synthesized by the reaction of the methoxyphenyl derivatives of 4'-*cis*-DPyP with octahedral  $\text{Re}(\text{CO})_5\text{Cl}$  in tetrahydrofuran (THF) display efficient intramolecular porphyrin–porphyrin energy transfer.<sup>275</sup> A cyclic self-assembled tetramer of an asymmetric *meso*-ethynylpyridyl functionalized zinc(II) porphyrin was also structurally characterized.<sup>276</sup> Femtosecond transient absorption and anisotropy spectroscopies have established fast energy transfer within a self-assembled cyclic porphyrin tetramer between porphyrin subunits.

Metallosalen complexes have long been known for their ubiquitous use in a variety of catalytic transformations.<sup>277</sup> Salen scaffolds have been incorporated into metallo-supramolecular assemblies via the coordination-driven directional bonding approach.<sup>278</sup> The availability of a large and diverse library of salen scaffolds and the relative ease with which salen moieties can be derivatized make them ideal building blocks for the construction of functional, supramolecular assemblies for their potential application in various areas of research such as catalysis,<sup>277</sup> materials,<sup>279</sup> and biology.<sup>280</sup> Hupp et al.<sup>281</sup> have assembled a series of metallacycles having salen scaffolds at the edges. For example, the reaction of bis(4-pyridyl) functionalized salen ligand **245** with **8** gave access to a [2 + 2] molecular loop **246** and a [4 + 4] molecular square **247** (Scheme 57). When free base semiflexible ligand **245** was used, preferential formation of a molecular loop was observed in nearly quantitative yield. The curvature that allows for loop closure, as determined from X-ray structural studies, was achieved via backbone distortion of the bridging salen ligand and likely entropic effects predominate in the assembly process. Alternatively, molecular square **247** was obtained directly by combination of **8** with Zn(II)-**245** ligand. Using a similar approach, the same group has introduced pyridyl-containing salen scaffolds into molecular squares using  $\text{Re}(\text{CO})_5\text{Cl}$  as corner units. The use of the bimetallic edge  $[(\text{CO})_4\text{Re}]_2\text{-BisBzIm}$  **86** instead of  $\text{Re}(\text{CO})_5\text{Cl}$  resulted in the formation of molecular rectangles.<sup>282</sup> Interestingly, postmetalation of the salen cavities of the molecular loop **246** with  $\text{ZnEt}_2$ , which

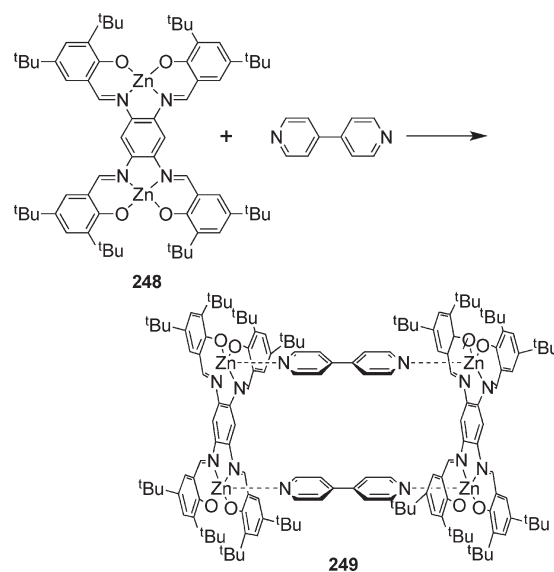
Scheme 57



reduces the flexibility of the salen segments, leads to quantitative supramolecule-to-supramolecule transformation to the analogous molecular square **247**.<sup>281</sup> Similar structural conversion from tetranuclear to dinuclear squares induced by light was also observed earlier.<sup>283</sup> Introduction of donor and acceptor centers in the same molecule can induce self-complementarity, leading to self-coordination and formation of supramolecular structures without participation of other ligands.

The templated approach to higher order supramolecular assemblies using bis-Zn(II)-salen building blocks and various ditopic bipyridine donors through coordinative Zn(II)– $\text{N}_{\text{py}}$  interactions have been demonstrated.<sup>284</sup> The use of bipyridine ligands of various sizes such as 4,4'-bipyridine, 1,4-di(4-pyridyl)benzene, and 1,2-di(4-pyridyl)ethane enabled the modulation of the dimensions of the resulting assemblies. For example,  $[2 + 2]$  assembly of bis-Zn(II)-(salphen) **248** with 4,4'-bipyridine generated dimeric assembly **249** (Scheme 58). Binding and NMR studies showed that macrocyclic assemblies were formed under dilute conditions. The solid-state structure of the bipyridine congener shows the presence of porous channels that could be potentially exploited to make porous materials and in the construction of supramolecular transition metal catalysts. Similarly, a  $[2 + 2]$  assembly of bis-Zn(II)-(salphen) with a bispyridyl Ni(salphen) derivative led to the formation of a rectangular metallacycle through Zn(II)–N coordination.<sup>285</sup> Salen-based molecular scaffold that contains both pyridyl donor and Lewis acidic Zn(II) acceptor sites in the same molecule have been designed and as a consequence, the molecular scaffolds assemble into a tetrameric vase structure through self-coordination.<sup>286</sup> Although the building block was achiral, the tetrameric assembly was chiral and both enantiomeric forms were present in the

Scheme 58



solid-state structure. A metal-templated approach recently afforded a tetra-Zn(salphen) supramolecular assembly from the combination of a diimine based on 3,3'-diaminobenzidine scaffold and a dialdehyde precursor, 4,6-dihydroxy-1,3-benzenedicarboxaldehyde, in the presence of  $\text{Zn}(\text{OAc})_2 \cdot 2\text{H}_2\text{O}$  as a templating agent.<sup>287</sup> The macrocycle showed strong cooperative self-assembly mediated by the formation of Zn(salphen) dimer units held together via  $\mu_2$ -phenoxo interactions.



### 3.5. Applications and Uses of 2D Systems

Over the past few decades, metallosupramolecular architectures have found applications in various fields such as molecular recognition, photo- and electrochemical sensing, cavity controlled catalysis, and molecular biology. These applications exploit the presence of the cavity in the assemblies.

**3.5.1. Molecular Recognition.** The design of discrete molecular entities that can selectively recognize molecules and signal the presence of a specific analyte is one of the main achievements of supramolecular chemistry.<sup>230</sup> The use of supramolecular assemblies as hosts for molecular recognition is governed by various noncovalent interactions such as electrostatic, hydrogen bonding, and van der Waals interactions. Metallo-supramolecules have generated a great deal of interest due to the relative ease with which they can be designed from simple complementary metal precursors and organic ligands. The necessary components to detect analytes and generate analytically useful and observable signals can be incorporated into the ensembles, and the stoichiometry and position of the individual functional groups can be precisely controlled. From a biological point of view, studies on molecular recognition using supramolecular ensembles allow for the development and design of small discrete molecules that can interact with biological systems for therapeutic use, e.g., as anticancer drugs. One of the early examples of the application of metallo-supramolecular assembly toward molecular recognition was provided by the investigations carried out by Maverick et al. in 1986,<sup>288,289</sup> in which they studied the binding properties of various guest molecules such as pyridine, quinuclidine, pyrazine, and diazabicyclo[2,2,2]octane (DABCO) in chloroform solutions by a cofacial copper(II) dinuclear metallacycle. X-ray crystallographic and solution studies have shown that DABCO preferentially binds at the cavity with a binding constant of 220 L/mol.

Molecular squares, with their tunable and easily accessible cavities, can lead to the selective inclusion of a wide range of organic molecules. Some of the early pioneering work of Fujita and Stang has shown that molecular squares can selectively recognize a wide variety of aromatic guests through various noncovalent interactions. For example, the first molecular square,  $[\{Pd(en)(4,4'-bipyridine)\}_4]^{8+}$  **46** synthesized by Fujita and his co-workers<sup>23,24</sup> showed the ability to recognize neutral aromatic guests such as benzene, naphthalene, and so on, through charge-transfer interactions as well as hydrophobic interactions between the electron-deficient pyridine nuclei and the electron-rich aromatic guests. While the binding of small molecules such as dimethoxybenzenes showed small binding constants,<sup>290</sup> the larger 1,3,5-trimethoxybenzene formed 1:1 host–guest complexes in D<sub>2</sub>O (Figure 24). However, incorporation of a highly electron-deficient perfluorinated phenylene moiety in molecular rhomboid **250** led to high size and shape-specific molecular recognition of various polymethoxybenzenes such as 1,3,5-trimethoxybenzene, *p*-dimethoxybenzene, *m*-dimethoxybenzene, and *o*-dimethoxybenzene with association constants  $K_a = 2500, 2680, 1560$ , and  $1300\text{ M}^{-1}$ , respectively.<sup>291</sup> Other large substrates were poorly or hardly recognized.

Stang et al. successfully encapsulated dihydroxynaphthalenes in a related molecular square  $[\{Pd(dppp)(4,4'-bipyridine)\}_4]^{8+}$  (**47**) in CD<sub>3</sub>OD.<sup>292</sup> Later, they were able to introduce Lewis base recognition sites into the squares by encapsulating AgOTf molecules through interactions with the ethynyl bonds.<sup>293</sup> This host–guest precursor, **251**, that contains silver atoms coordinated via the “ $\pi$ -tweezer effect” between each respective set of

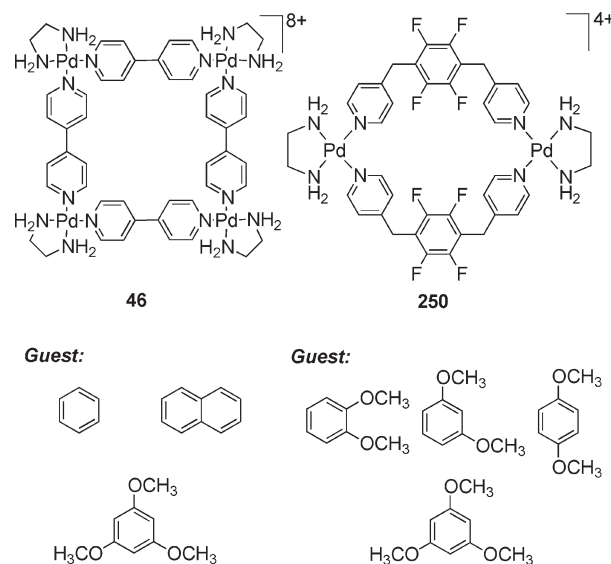


**Figure 24.** Molecular square,  $[\{Pd(en)(4,4'-dipyridyl)\}_4]^{8+}$  (**46**), and molecular rhomboid **250** for selective binding of aromatic guest molecules.

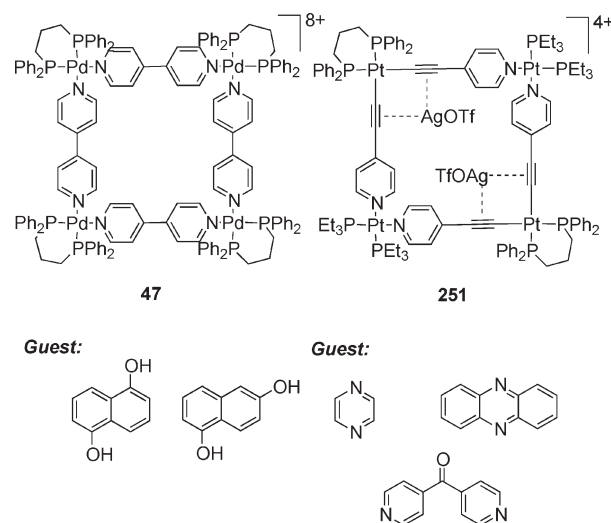


**Figure 25.** Molecular square,  $[\{Pd(dppp)(4,4'-dipyridyl)\}_4]^{8+}$  (**47**), and AgOTf encapsulated host–guest precursor **251** for dihydroxynaphthalenes and Lewis bases, respectively.

acetylene moieties, serves as the receptor for bidentate coordinating Lewis bases such as pyridine, pyrazine, phenazine, or 4,4'-dipyridyl ketone (Figure 25).<sup>292</sup> Single-crystal X-ray structure determination of the phenazine encapsulated molecular square revealed a 1:1 stoichiometry of the Lewis acid–base receptor host–guest complex. The overall geometry of the perimeter for this complex is almost planar with the guest phenazine oriented nearly orthogonal to the Pt–Pt<sup>2+</sup>–Pt plane.

Jeong et al.<sup>294</sup> reported a palladium-based metallomacrocyclic **252** with two topologically discrete binding subcavities that showed homotropic cooperative binding behavior toward *N,N,N',N'*-tetramethylterephthalamide through hydrogen bonding (Figure 26). It was proposed that the binding of the guest molecule in one subcavity allosterically activates the other subcavity to form stronger hydrogen bonds with the second

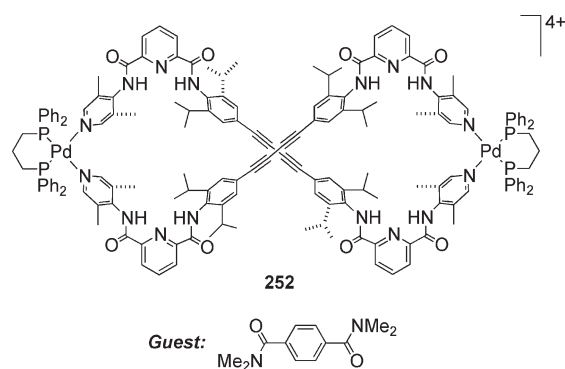


**Figure 26.** Metallomacrocycle **252** containing two topologically discrete binding subcavities for homotropic cooperative binding of guest molecules.

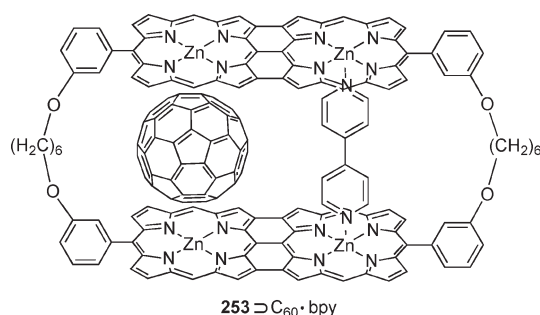


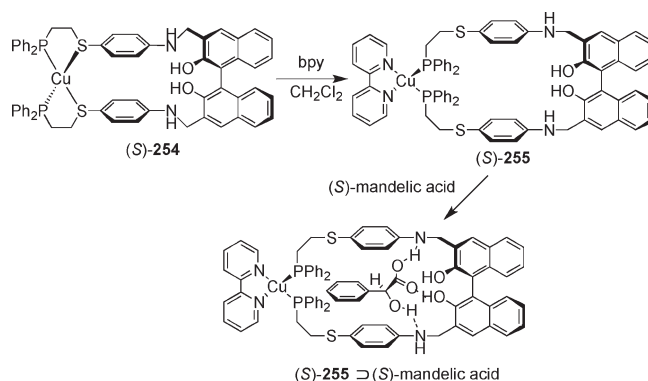
**Figure 27.** Heterotropic cooperative binding in macrocycle **253** having cofacial, fused zinc porphyrin arrays.

guest molecule. The same group also designed and explored a series of osmium(IV) molecular squares and rectangles for the molecular recognition of various diamide guests.<sup>295</sup> While the osmium-based molecular square selectively binds adipamide and terephthalamide, osmium(IV) rectangle was found to preferentially bind a larger amide guest, such as biphenyldicarboxamide. The strong binding of the diamides was due to the presence of hydrogen-bonding pockets of the hosts. Hydrogen-bonding sites have also been utilized for the size-selective molecular recognition of a number of mono- and disaccharides in neutral platinum(II)-based metallacycles.<sup>296</sup> Fluorescence and  $^1\text{H}$  NMR studies established a 1:1 binding stoichiometry in chloroform through intermolecular hydrogen-bonding interactions.

Heterotropic cooperative binding of fullerene and a diamine (4,4'-bipyridine or  $N,N,N',N'$ -tetramethylhexane-1,6-diamine) was achieved in a macrocycle having cofacial, fused zinc porphyrin arrays (Figure 27).<sup>297</sup> The guest molecules, with complementary electronic effects on the binding properties of **253**, communicate with one another through the  $\pi$ -electronic conjugation. The binding of diamine increases the electron density in the porphyrin ring, which disfavors the binding of a second diamine molecule but favors the binding of an electron acceptor such as fullerene. Similarly, binding of fullerene into the host activates the subsequent binding of the diamine into the other cavity.

**3.5.2. Chemosensing.** The essential components of a fluorescent chemosensor are a molecular recognition unit for selective interaction with an analyte and a signaling unit, generally a chromophore or a fluorophore. These are designed in such a way that the binding unit and the event reporter (chromophore

**Scheme 59**



or fluorophore) are structurally integrated so as to maximize the communication between the units. Since luminescence is very sensitive to subtle changes in geometry upon binding of a guest, fluorescent chemosensors are attractive for sensing of various analytes. Recently, electron-rich and photoluminescent heterometallic self-assembled molecular squares were shown to exhibit high quenching selectivities and sensitivities toward multicarboxylate anions and nitroaromatics, particularly picric acid.<sup>298</sup> No significant quenching was noticed with electron-rich molecules such as benzene, xylene, and 2,4,6-TMP, even at relatively higher quencher concentrations. A similar quenching pattern was observed with polar aromatics such as benzoic acid and phloroglucinol. The highly selective quenching effect with electron-poor molecules was ascribed to the induced  $\pi$ - $\pi$  interactions between the  $\pi$  electron system of the metallic donor of the molecular square and the analyte.

Chiral, luminescence molecular squares have been shown to exhibit interesting enantioselective fluorescence quenching behavior by chiral amino alcohols in THF.<sup>207</sup> The emission was assigned to both ligand-centered and MLCT excited states. The luminescence signal of the enantiopure molecular square can be quenched by both enantiomers of 2-amino-1-propanol but at significantly different rates. The quenching of the luminescence is proposed to be due to the inclusion of the chiral amino alcohols in the cavity of the squares through hydrogen-bonding interactions. Enantioselective molecular sensing of chiral mandelic acid was investigated by using specifically designed tweezer complexes.<sup>299</sup> The enantiometrically pure monomeric four-coordinate Cu(I) metallacycle **(S)-254** upon chelation of 2,2'-bipyridine (bpy) to the Cu(I) center breaks the weak Cu-S links and opens up the condensed structure, **(S)-254**, into a 27-membered macrocycle **(S)-255** which can recognize mandelic acid (Scheme 59). Thus, the binding of the (*R*)- or (*S*)-mandelic acid was pseudoallosterically regulated by binding of the ancillary ligand bpy, resulting in an increased cavity size. The condensed structure **(S)-254** shows no binding of the guest molecules due to the inaccessibility of the binding pocket, as determined from fluorescence intensities.

Severin and co-workers have designed a number of half-sandwich complexes of Ru(II), Rh(III), and Ir(III) with arene or cyclopentadienyl ligands as sensors for small cations and anions.<sup>163</sup> Many of these metallacycles were found to act as highly selective receptors for lithium and sodium ions, the binding constants being dependent upon the nature of the half-sandwich complex, the ligand, and the pH.<sup>300,301</sup> While the trinuclear

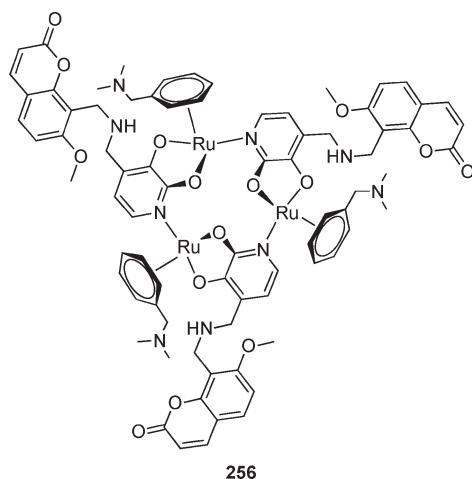


**Figure 28.** Trinuclear Ru(II) metallomacrocycles (**256**) for high affinity and selective binding of  $\text{Li}^+$  and  $\text{Na}^+$  ion.

Ru(II) metallo-macrocycles (**256**, Figure 28) showed high affinity and selectivity for  $\text{Li}^+$  and  $\text{Na}^+$  ion,<sup>164,302</sup> the Ir(III) macrocycles act as a fluoride ion receptor in which a precoordinated lithium ion serves as the binding site.<sup>303</sup> The quantification of the host–guest complexes were done by NMR, electrochemical, and colorimetric methods. Extending the same strategy further, they have also designed and synthesized a Ru-based metallomacrocycle for the selective detection of lithium ions in water and in serum by fluorescence spectroscopy.<sup>304</sup> An interesting feature of these macrocycles is the incorporation of different pendent fluorophores—pyrene, dansyl, and methoxycoumarin—into the trinuclear metallacycles. The cavities in the assemblies serve as a  $\text{Li}^+$  ion recognition unit. Addition of LiCl to an aqueous solution of metallomacrocycle led to an increase in the fluorescence signal intensity due to a “turn on” response of the receptor upon binding of  $\text{Li}^+$ . Fluorescent titration with NaCl instead of LiCl showed a negligible response, indicating its highly specific and selective nature. The application of methoxycoumarin-appended sensor **256** in a complex matrix such as human serum also revealed its high specificity and selectivity toward biologically important lithium ion.

Puddephatt and co-workers<sup>305</sup> have synthesized several Pd(II)-based molecular triangles using a 4(3*H*)-pyrimidone ligand which act as efficient anion sensors. Binding of the anions was determined by X-ray structural and NMR studies in solution. The  $^1\text{H}$  NMR titration data demonstrated that the molecular triangles are an effective host for planar nitrate and tetrahedral oxoanions. X-ray structures determined for triangles showed that binding of  $\text{BF}_4^-$ ,  $\text{ClO}_4^-$ , and  $\text{CF}_3\text{SO}_3^-$  follow the 1:1 binding model. The oxoanions, including  $\text{ClO}_4^-$ ,  $\text{NO}_3^-$ ,  $\text{HSO}_4^-$ , and  $\text{CF}_3\text{SO}_3^-$ , are bound more strongly than  $\text{BF}_4^-$  while  $\text{PF}_6^-$  is bound more weakly. A series of dinuclear cationic Ag(I) macrocycles synthesized from N-methylated bis(amidopyridine) ligands showed easy anion exchange properties.<sup>132</sup> As determined from structural studies, the counterions occupy the cavity of the macrocycles. Anion exchange studies carried out with ESI-MS demonstrated that these counterions could be replaced by other anions of a similar nature. Similarly, Pd(II) “lantern complexes” synthesized from bispyridyl amide ligands were shown to act as hosts for either cations or anions by adjusting the conformation of the amide substituents to accommodate the guests.<sup>306,307</sup>

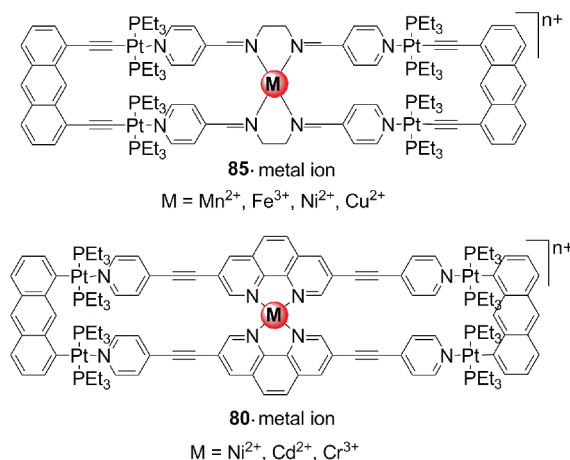


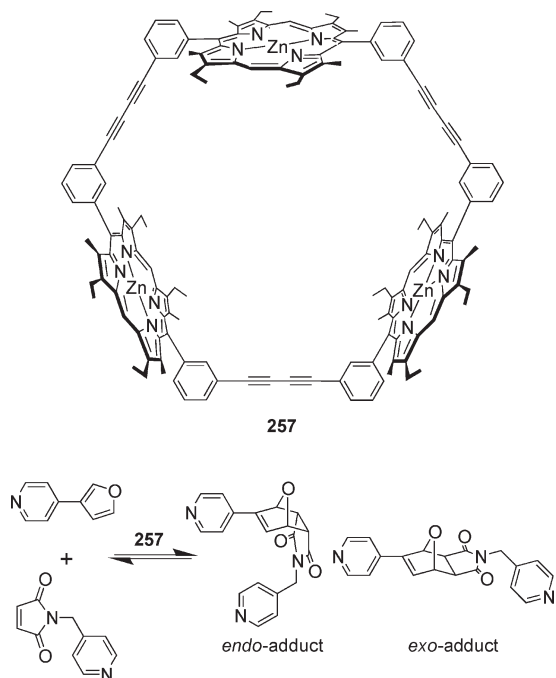
**Figure 29.** Molecular rectangles having  $\text{N}_4$  pockets for selective chemosensing of 3d transition metal ions.

A molecular rectangle **85** that can selectively sense 3d transition metal ions has also been designed and synthesized.<sup>114</sup> The anthracene-based clip acts as the fluorophore, while the edge functionalized imine-based donor that contains a  $\text{N}_4$  pocket for binding moderately hard transition metal ions acts as a molecular recognition site (Figure 29). Due to the presence of a metal ion receptor site, the solution fluorescence intensity was quenched efficiently upon titration with 3d transition metal ions such as  $\text{Mn}^{2+}$ ,  $\text{Fe}^{3+}$ ,  $\text{Ni}^{2+}$ , and  $\text{Cu}^{2+}$ . Interestingly, no such quenching was observed when the titration was performed with soft metal ions ( $\text{Zn}^{2+}$  or  $\text{Cd}^{2+}$ ) with a  $d^{10}$  electronic configuration. The metal-containing design of these rectangles and the presence of a specific binding core for metal ions make them suitable as fluorescent sensors for transition metal ions. Stang et al. have also designed a molecular rectangle (**80**) containing the phenanthroline moiety on the longer edge and have shown that it is an efficient chemosensor for  $\text{Ni}^{2+}$ ,  $\text{Cd}^{2+}$ , and  $\text{Cr}^{3+}$  up to a 1:1 host–guest ratio (Figure 29).<sup>111</sup> Binding of the metal ions in the  $\text{N}_4$  pocket was determined by UV–visible spectroscopy.

Lu et al. have assembled two gondola-shaped tetrarhenium metallocyclophanes, which were capable of selectively recognizing metal ions and planar aromatic molecules.<sup>308</sup> The metallocycles were formed via a reaction of  $\text{Re}(\text{CO})_3$ , a ditopic heterocyclic clip, and a bischelating bridging unit using an orthogonal bonding approach. These highly luminescent cyclophanes selectively bind mercury cations and anthracene molecules. With  $\text{Hg}^{2+}$  ions, quenching of the emission was observed with formation of a 1:1 host–guest complex, as determined by binding studies. With other metal ions such as  $\text{Li}^+$ ,  $\text{Sr}^{2+}$ ,  $\text{Co}^{2+}$ ,  $\text{Ni}^{2+}$ ,  $\text{Cu}^{2+}$ ,  $\text{Zn}^{2+}$ ,  $\text{Pb}^{2+}$ , and  $\text{Ag}^+$  these metallocyclophanes showed no significant fluorescent quenching activity.

**3.5.3. Cavity Controlled Catalysis.** One of the major applications of supramolecular chemistry is the design and understanding of catalysts and catalytic processes. Supramolecular architectures provide a unique opportunity for the study of noncovalent interactions that govern the binding of the reactants into conformations suitable for lowering the energy of the transition state of a given transformation. The cavity of an assembly can also stabilize reactive species or lead to enhanced reactivity and selectivity by isolating encapsulated guests from the bulk environment and can catalyze reactions effectively due to guest discrimination.<sup>17</sup> Supramolecular catalysts can also

Scheme 60

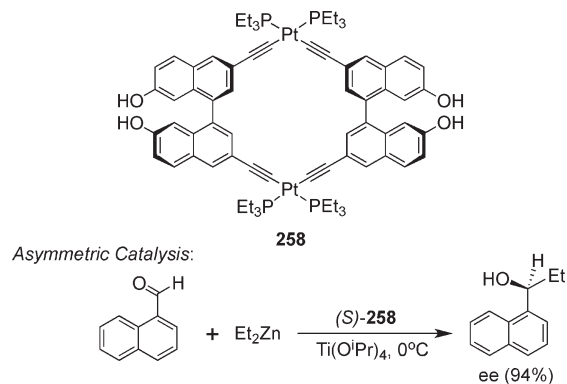


activate otherwise unreactive substrates without the use of distinct covalent interactions between the catalyst and substrate, promoting reactions which cannot occur under normal conditions. With the vast number of metallo-supramolecular assemblies known and the ease with which new molecules of predictable geometries can be generated, the study of their catalytic activity is an attractive proposition for supramolecular chemists.

One of the earliest examples of the application of metallo-supramolecular architecture in a catalytic organic transformation was provided by Sanders and co-workers where they used a covalently bound trimeric porphyrin (**257**) as a host for the acceleration of the intramolecular Diels–Alder reaction of a furan-based diene and a maleimide-based dienophile (Scheme 60).<sup>309</sup> In the absence of any catalyst, both endo- and exo-adduct were observed. However, with 1 equiv of **257**, the reaction rate was enhanced 200-fold with the exo-adduct as the sole product observed. The metallo-supramolecular assembly was also found to be an active catalyst for the acyl-transfer reaction. The reaction proceeded through a tightly bound intermediate, in which both the pyridyl ring and the imidazole group were coordinated to two of the Zn(II) centers within **257**, bringing the reactive sites into close proximity.<sup>310</sup>

Lin et al.<sup>213</sup> investigated enantioselective catalysis using chiral metallo-supramolecular cyclophane **258** derived from the enatiopure BINOL ligand and *cis*-[Pt(PEt<sub>3</sub>)<sub>2</sub>Cl<sub>2</sub>]. A combination of **258** with Ti(O<sup>*i*</sup>Pr)<sub>4</sub> forms an active catalyst for the enantioselective diethylzinc additions to aromatic aldehydes to afford the corresponding chiral secondary alcohols (Scheme 61). With 1-naphthaldehyde as the substrate, a 95% conversion with 94% enantiomeric excess (ee) was observed. Interestingly, enantioselectivity drops when smaller aromatic aldehydes were used as substrates and was postulated to be due to the rigid architecture of the metallo-cyclophane **258**. However, the disposition of chiral dihydroxy groups in an endo fashion renders the catalyst

Scheme 61



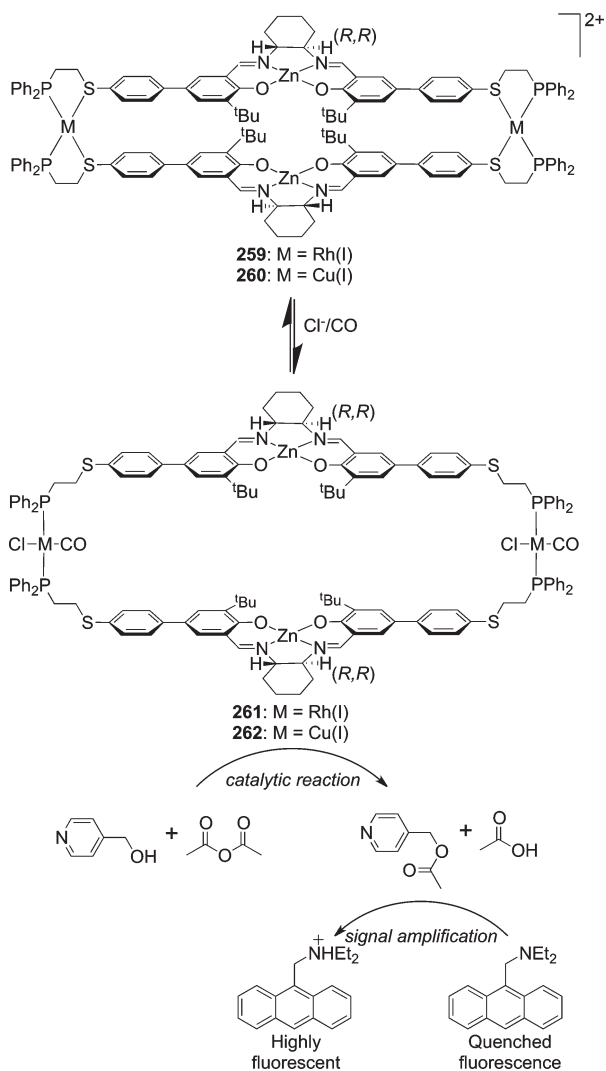
less enantioselective due to the steric congestion preventing the reaction with Ti(O<sup>*i*</sup>Pr)<sub>4</sub> to form an active catalyst.<sup>214</sup> The Ti(IV) complex of metallo-supramolecular triangle **193** was also found to efficiently catalyze the enantioselective (ee up to 92%) additions of diethylzinc to aromatic aldehydes.<sup>209</sup>

Hupp et al.<sup>311</sup> have used a zinc porphyrin lined metallacyclic square to encapsulate a simple manganese porphyrin unit, a known catalyst for epoxidation reactions. Manganese porphyrin catalysts suffer deactivation under aerobic conditions. The protective encapsulation provided by the supramolecular square to the dipyrindyl and tetrapyrindyl form of the manganese porphyrin catalyst units prevents this deactivation and affords a 10- to 100-fold increase in turnover number and a substantial increase in the lifetime of the Mn catalyst. With the dipyrindyl catalyst, the square also induced substrate size selectivity by preventing access to the active site by large substrate molecules.<sup>311</sup>

Allosteric regulation is a ubiquitous form of control for biological molecules to regulate substrate binding but is a rarity for synthetic catalysts.<sup>312,313</sup> Mirkin et al. have developed metallo-supramolecular architectures containing two structural domains that can mimic an abiotic assay similar to the enzyme-linked immunosorbent assay (ELISA).<sup>314</sup> An important design feature of these allosteric catalysts is the structural Rh(I) and Cu(I) metal centers which act as allosteric regulators while the chiral Zn(II)-salen moieties act as the catalytic active sites. The reversible binding of CO and Cl<sup>−</sup> at the metal (M) centers in **259** (M = Rh(I)) and **260** (M = Cu(I)) results in the opening up of the structure to **261** and **262**, respectively (Scheme 62). This opening up allowed substrate molecules to enter so that they could undergo a fast intramolecular reaction. The investigations of the acyl-transfer reaction between acetic anhydride and pyridyl carbinol showed that the reaction rate increased significantly upon binding of CO and Cl<sup>−</sup> at the M centers, which opened up the structure.<sup>315</sup> Since metallocalens can catalyze the reaction in a bimetallic fashion, the substrate molecules can access the cavity and can undergo a faster intramolecular reaction. Coupling of the catalytic amplification step to a pH-sensitive fluorophore (diethylaminomethylantracene) that interacts with the reaction byproduct, acetic acid, provides a straightforward method for visually and spectrophotometrically monitoring the reaction. Recently, the same group has developed a supramolecular triple-layer allosteric catalyst for the ring-opening polymerization of  $\epsilon$ -caprolactone.<sup>316</sup> The allosteric supramolecular structure contains a monometallic catalytic site buried in the middle layer of a triple layer of the complex, which can reversibly open and



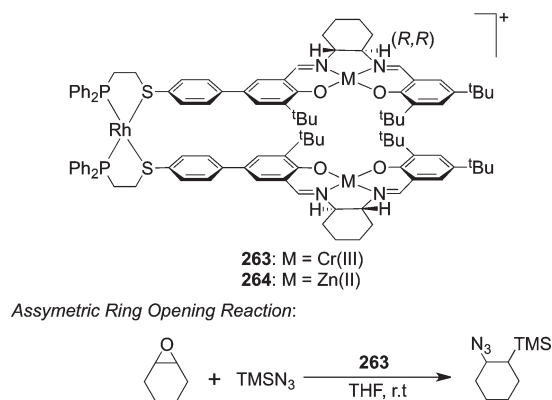
Scheme 62



close upon addition of small molecules and elemental anions, thus reversibly exposing and concealing the catalytic center. The ring-opening polymerization of  $\epsilon$ -caprolactone can be turned on by the in situ opening of the triple-layer complex and then completely turned off by re-forming it through the abstraction of Cl<sup>-</sup>, the allosteric effector agent, without appreciable loss of catalytic activity.

Supramolecular allosteric cofacial porphyrin assemblies can also function as catalysts for acyl-transfer reactions.<sup>317,318</sup> The cavities of these macrocycles are tunable via introduction of simple ancillary ligands that bond to the structure control domains. This enables the cofacial porphyrin structures to act as allosteric catalysts capable of discriminating different substrate combinations and selectively transforming them into the desired products. The change in cavity size that occurs allows the acyl-transfer reaction between pyridylcarbinol and 1-acetylimidazole. A tetrametallic macrocycle having two Zn catalytic centers assembled via the weak link approach was shown to be an efficient allosteric catalyst for the hydrolysis of 2-(hydroxypropyl)-*p*-nitrophenyl phosphate (HPNP), a model substrate for RNA.<sup>319</sup> The binding of CO and Cl<sup>-</sup> induces a transition of the catalytically inactive condensed structure to the highly active open structure. Of the Cr(III)- and

Scheme 63

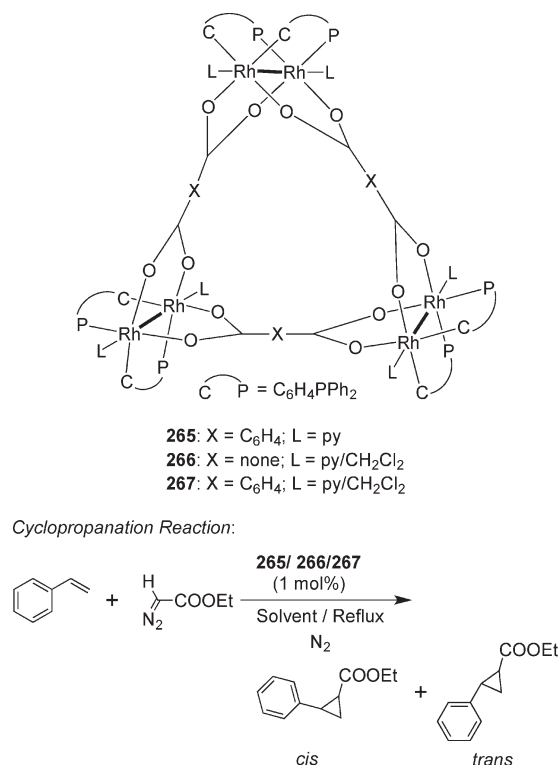


Zn(II)-containing molecular tweezer complexes **263** and **264**, Cr(III)-containing tweezer, **263**, was found to be an active enantioselective catalyst for the asymmetric ring-opening reaction of cyclohexane oxide by azidotrimethylsilane (TMSN<sub>3</sub>; Scheme 63).<sup>320</sup>

Cotton et al.<sup>228</sup> investigated a metal carbene transformation using the model intermolecular cyclopropanation of styrene with thyl diazoacetate in both homogeneous and heterogeneous phases by using enantiopure chiral molecular triangles SSS-[*cis*-Rh<sub>2</sub>-(C<sub>6</sub>H<sub>4</sub>PPh<sub>2</sub>)<sub>2</sub>(C<sub>8</sub>H<sub>4</sub>O<sub>4</sub>)(py)<sub>2</sub>]<sub>3</sub> (**265**), SSS-[*cis*-Rh<sub>6</sub>(C<sub>6</sub>H<sub>4</sub>PPh<sub>2</sub>)<sub>6</sub>(C<sub>2</sub>O<sub>4</sub>)<sub>3</sub>(py)<sub>5</sub>(CH<sub>2</sub>Cl<sub>2</sub>)<sub>2</sub>] (**266**), and SSS-[*cis*-Rh<sub>6</sub>(C<sub>6</sub>H<sub>4</sub>PPh<sub>2</sub>)<sub>6</sub>(C<sub>14</sub>H<sub>8</sub>O<sub>4</sub>)<sub>3</sub>(py)<sub>4</sub>(CH<sub>2</sub>Cl<sub>2</sub>)<sub>2</sub>] (**267**) obtained from the dimetallic corner unit *cis*-Rh<sub>2</sub>(C<sub>6</sub>H<sub>4</sub>PPh<sub>2</sub>)<sub>2</sub> (Scheme 64). These studies showed that the metallo-supramolecular ensembles were very active and had remarkable enantioselectivity.<sup>228</sup> The enantio-control achieved was superior to that of known dirhodium(II) catalysts with chiral carboxamide ligands.<sup>321</sup>

**3.5.4. Biological Applications.** Recently, 2D metallo-supramolecular assemblies have been investigated as potential candidates for selective antitumor therapies. G-quadruplexes are the most recent secondary DNA structures that are being considered as targets for anticancer drug design.<sup>322</sup> Guanine-rich stretches of DNA can self-assemble into a cyclic arrangement of four guanines (G-quartet) held together by eight Hoogsteen hydrogen bonds. Further association of these G-quartets leads to the stacking of tetramers on top of each other to form four-stranded structures called a G-quadruplex. These G-quadruplexes appear at the ends of chromosomes in the telomeric and transcriptional regulatory regions in several important oncogenes. Because telomere maintenance mechanisms and the transcriptional regulation of oncogene expression are important targets for drug design, G-quadruplexes represent potentially important targets in drug development. Sleiman et al.<sup>323</sup> have shown that Fujita's platinum-based metallo-supramolecular square<sup>23</sup> [{Pt(en)(4,4'-bipyridine)}<sub>4</sub>]<sup>8+</sup> could efficiently bind to G-quadruplex DNA and effectively inhibit telomerase activity. Thermal denaturation studies with duplex and quadruplex FRET probes and enzymatic assays demonstrated that [{Pt(en)(4,4'-bipyridine)}<sub>4</sub>]<sup>8+</sup> strongly binds to G-quadruplexes and can act as an inhibitor of telomerase. The highly electropositive nature of this square, as well as hydrogen-bonding interactions between the ethylenediamine ligands and phosphates of the DNA backbone, contributed to the observed strong binding affinity to the G-quadruplex. The interaction of DNA with supramolecular squares [{Pt(en)(4,4'-bipyridine)}<sub>4</sub>]<sup>8+</sup> and [{Pt(en)(1,4-bis-(4-pyridyl)tetrafluorobenzene)}<sub>4</sub>]<sup>8+</sup> showed modification of

Scheme 64



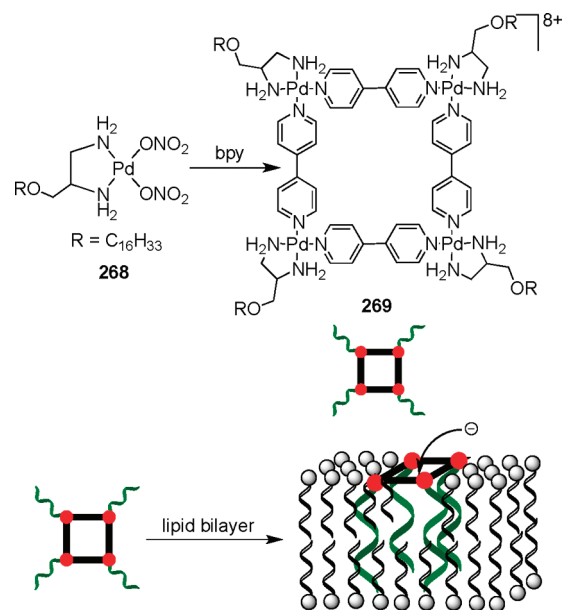
the secondary and tertiary structure of DNA due to intercalation between base pairs.<sup>324</sup> Assays against HL-60 tumor cell lines displayed discrete antiproliferative behavior for both molecular squares as compared to cisplatin. Appending a long lipophilic chain on one of the carbon atoms of the ethylenediamine moiety of **268**, followed by self-assembly with 4,4'-bipyridine, formed molecular square **269** and led to the interesting observation of channel formation in planar bilayer lipid membranes (Scheme 65).<sup>325</sup> It was hypothesized that the membrane-bound lipophilic metallo-supramolecular square led to the formation of long-lived and highly conducting ion channels due to extended aggregation of the complexes and lipids surrounding a toroidal pore in the membrane.

Therrien et al. have investigated a series of cationic arene ruthenium-<sup>122</sup> and osmium-based<sup>326</sup> tetranuclear molecular rectangles for their anticancer activity against ovarian A2780 cancer cells lines. The large rectangles incorporating 1,2-bis(4-pyridyl)ethylene linkers are more cytotoxic than the 4,4'-bipyridine-containing smaller cationic rectangles. However, the observed cytotoxicity may also arise due to fragmentation of the rectangles within the cell, leading to cytotoxic mononuclear complexes. Similar ruthenium-based molecular rectangles having dipyridyl amides as linkers also showed potent anticancer activity against various human cancer cell lines.<sup>327</sup> Dyson et al., in their study on the cytotoxic activity of a series of trinuclear *p*-cymene ruthenium metallacycles on human cancer and fibroblast cells, observed the interconversion between trimeric metallacycles and monomeric complexes as a function of pH.<sup>328</sup>

## 4. THREE-DIMENSIONAL NANOSCOPIC CAGES

Self-assembly processes to form complex three-dimensional (3D) structures, such as the icosahedral or dodecahedral shapes of the viral capsids, are abundant in nature. However, abiological

Scheme 65



preparation of such complex structures has proved challenging. Thus, not surprisingly, many of the first examples of complex 3D topologies were the result of serendipity rather than design. However, the development of different design principles over the past couple of decades (section 2) for the preparation of high-symmetry coordination cages via self-assembly has led to an incredible variety of structures ranging from simple “platonic” solids (tetrahedron, octahedron, cube, dodecahedron, and icosahedron), which have faces consisting of only single regular polygons, to more complex “Archimedean” solids, which have faces consisting of two or more regular polygons, with precise control over the geometry. Coordination-driven self-assembly provides synthetic control on a supramolecular scale to carefully design and understand the geometric requirements of a particular ligand vis-à-vis the stereoelectronic preferences of a specific metal center. In this section, we will discuss the synthetic and topological aspects of the self-assembled coordination cages, their functional properties, and various applications and uses.

### 4.1. Archimedean and Platonic Systems

**4.1.1. Tetrahedra.** A tetrahedron, the simplest of the platonic solids, can be assembled utilizing a few different metal–ligand stoichiometries: (a) M<sub>4</sub>L<sub>6</sub> tetrahedra, where the four metal ions occupy the vertices and the six ligands act as the edges, (b) M<sub>4</sub>L<sub>4</sub> tetrahedra, where the metal ions act as the four vertices, and the four faces of the tetrahedra are covered by ligands with 3-fold symmetry, and (c) M<sub>6</sub>L<sub>4</sub> tetrahedra, or truncated tetrahedra, where the ligands occupying each of the four faces of the tetrahedron are connected by metal centers on the middle of the edges (Figure 30).

In 1988, Saalfrank and co-workers serendipitously stumbled upon the first coordination-driven tetrahedral assembly.<sup>329</sup> In their pursuit of tetradonor-substituted allenes, the double deprotonation of malonic ester with methyl Grignard to generate its dianion led to the in situ formation of a ditopic, bisbidentate ligand (L) via C–C coupling of two dialkyl malonate monoanions with oxalyl chloride and spontaneous deprotonation of

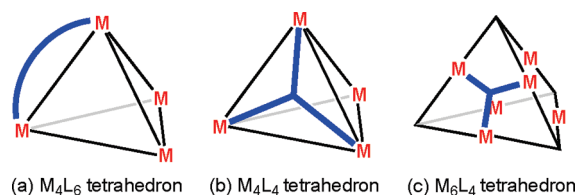
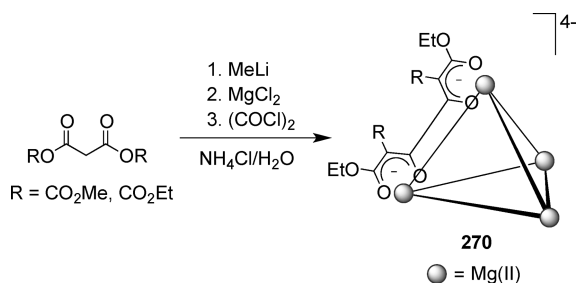


**Figure 30.** Schematic representation of the different ways of assembling a tetrahedral topology. Only one of the ligands is shown for clarity.

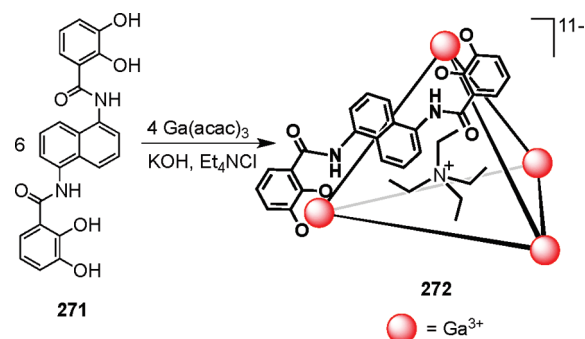
#### Scheme 66



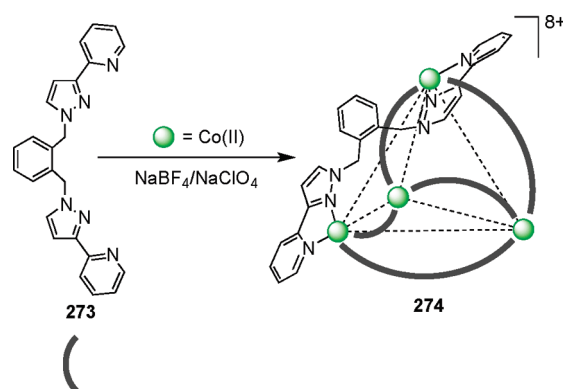
the bis(enol) intermediates (Scheme 66). The tetraanionic assembly  $[(\text{NH}_4)_4\{\text{Mg}_4(\text{L})_6\}]$  (**270**) consists of a distorted tetrahedron composed of four magnesium(II) ions occupying the apexes, which are linked along each of the six edges by the bisdentate ligands such that each of the four magnesium(II) ions are octahedrally coordinated. The ammonium counterions are hydrogen bonded to the oxygen donors at the triangular faces of the tetrahedron.<sup>330</sup> Temperature-dependent  $^1\text{H}$  NMR studies showed the presence of homochiral, racemic complexes that were kinetically stable on the NMR time scale. Replacement of magnesium(II) by divalent transition metals allowed the syntheses of the corresponding tetranuclear complexes  $[(\text{NH}_4)_4\{\text{M}_4(\text{L})_6\}]$  ( $\text{M} = \text{Mn}(\text{II}), \text{Co}(\text{II}), \text{Ni}(\text{II}), \text{Zn}(\text{II})$ ).<sup>331</sup> Homovalent and mixed-valent tetranuclear iron complexes  $[\text{M}\{\text{Fe}^{\text{II}}_n\text{Fe}^{\text{III}}_{4-n}(\text{L})_6\}]^{n\pm}$  ( $\text{M} = \text{NH}_4^+, \text{Na}^+, \text{K}^+, \text{Cs}^+, \text{H}_2\text{O}$ ) can also be accessed by using  $\text{FeCl}_2$  or  $\text{FeCl}_3$ .<sup>332</sup> The use of 4,4'-phenylene and 4,4'-biphenylene as spacers in the bisdentate ligands led to tetrahedra with enlarged cavities. For instance, deprotonation of the stable tetramethyl 2,2'-terephthaloyldimalonate compound with sodium hydride yielded a negatively charged ditopic tetradentate ligand, which reacted with iron(III) chloride to form a tetrahedral tetrairon core bridged by six chelate ligands with a much larger cavity.<sup>333</sup>

Raymond and co-workers assembled early examples of anionic  $M_4L_6$  and  $M_4L_4$  tetrahedral clusters with trivalent and tetravalent metal ions such as  $\text{Ga}(\text{III})$ ,  $\text{Al}(\text{III})$ ,  $\text{In}(\text{III})$ ,  $\text{Fe}(\text{III})$ ,  $\text{Ti}(\text{IV})$ , and  $\text{Sn}(\text{IV})$  using the symmetry interaction approach and delineated the design principles in order to predict and construct the formation of self-assembled systems, as discussed in section 2.2.<sup>9</sup> Though composed of achiral building units, many of these tetrahedral assemblies are intrinsically chiral (vide infra, section 4.3). The use of bis-hydroxamate<sup>334,335</sup> and bis-catecholate-based<sup>336</sup> ligands having  $C_2$  symmetry and octahedral metal ions have led to the assembly of a vast number of tetrahedral clusters of varying sizes. For example, deprotonation of 6 equiv of **271** with  $\text{KOH}$ , followed by the addition of  $\text{Et}_4\text{NCl}$  and 4 equiv of  $\text{Ga}(\text{acac})_3$  led to the isolation tetrahedral assemblies  $[\text{NEt}_4\{\text{Ga}_4(\text{271})_6\}]^{11-}$

#### Scheme 67



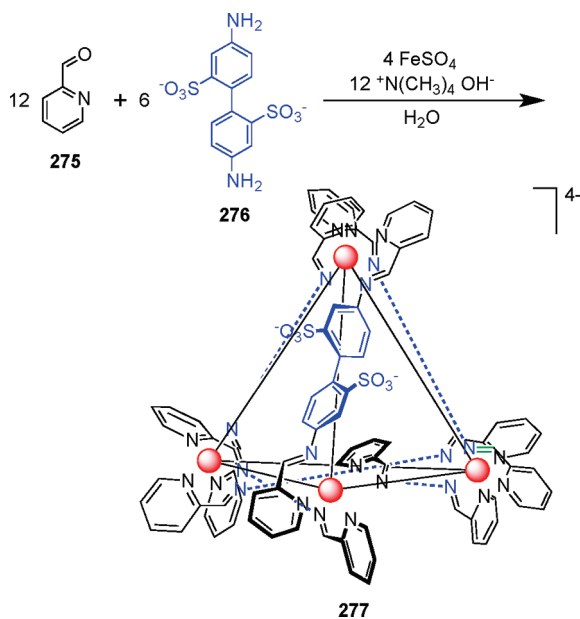
#### Scheme 68



(**272**; Scheme 67).<sup>336</sup> The naphthalene spacer between the two pyrocatechol units provides rigidity and predisposes the ligand for interaction with the trivalent metals to exclusively form tetrahedral assemblies over the entropically more favorable  $M_2L_3$  helicates.<sup>336</sup> These anionic, tetrahedral assemblies can selectively encapsulate a variety of monocationic guests (vide infra, section 4.5.1)<sup>337</sup> and can form without thermodynamically templating cationic guest molecules. However, the formation of  $M_4L_6$  tetrahedra with larger cavities, using anthracene in the ligand backbone, can only be achieved in the presence of suitable cationic guest molecules. In the absence of such a guest, entropically favored  $M_2L_3$  triple helicates are formed. Although the use of a bulkier spacer such as pyrene<sup>338</sup> prevents the formation of helicates, tetrahedra are formed only in the presence of a guest molecule. Larger  $M_4L_6$  cages with 1,1'-binaphthyl as the spacer have also been designed with an aim to accommodate larger guest molecules.<sup>339</sup>

McCleverty, Ward, and co-workers have reported a number of cationic  $M_4L_6$  tetrahedra utilizing symmetry interaction approach.<sup>340</sup> These tetrahedra were assembled from flexible bispyrazolylpyridine ligands with 1,2-phenyl,<sup>341,342</sup> 2,3-naphthyl,<sup>343,344</sup> 9,10-anthracenyl,<sup>344</sup> and biphenyl<sup>345,346</sup> spacers between the binding sites. Treatment of bispyrazolylpyridine ligands having a 1,2-phenyl central spacer (**273**) with a divalent metal  $\text{Co}(\text{II})$  as their fluoroborate or perchlorate salt afforded racemic tetrahedral cages  $[\text{Co}_4(\text{273})_6\text{X}]\text{X}_7$  [ $\text{X} = \text{BF}_4^-, \text{ClO}_4^-$ ] (**274**; Scheme 68).<sup>341,342</sup> X-ray structural studies showed that the ligands in **274** bridge along each of the six edges, spanning two

Scheme 69



metal ions. Each pseudo-octahedral metal ion is coordinated by a bidentate unit from each of three different ligands with one of the tetrahedral counterions trapped in the cage cavity. In fact, the formation of these intrinsically chiral assemblies was templated by the trapped anions. The encapsulated  $\text{BF}_4^-$  anion is complementary in both charge and shape to the cavity with respect to the  $\text{Co}_4$  tetrahedron. Each fluorine atom of the trapped anion is directed toward the center of a triangular face of the  $\text{Co}_4$  tetrahedron. Interestingly, variable-temperature  $^{11}\text{B}$  and  $^{19}\text{F}$  NMR studies revealed that the  $\text{BF}_4^-$  anion is effectively trapped within the cavity and does not exchange with the seven outer-sphere  $\text{BF}_4^-$  counterions.<sup>342</sup> Similar flexible bispyrazolylpyridine ligands having 1,8-naphthyl spacers led to a  $\text{M}_{12}\text{L}_{18}$  assembly having a topology consistent with a truncated tetrahedron with  $T$  symmetry upon reaction with  $\text{Co(II)}$  or  $\text{Zn(II)}$  in the presence of  $\text{NaBF}_4$  or  $\text{NaClO}_4$ .<sup>347</sup> However, in a study using a related tetrahedral  $[\text{Fe}_4\text{L}_6]^{8+}$  ( $\text{L} = \text{5},\text{5}'''\text{-dimethyl-2},\text{2}':\text{5}',\text{5}''':\text{2}'',\text{2}'''\text{-quaterpyridine}$ ) complex it has been shown that templating by polyatomic anions is not always necessary for the assembly of cage structures as demonstrated by the isolation of the anion-free cage.<sup>348</sup>

In an elegant approach, Nitschke and co-workers<sup>349</sup> designed  $\text{M}_4\text{L}_6$  tetrahedral cages utilizing dynamic covalent and coordinative bonds in tandem from multicomponent systems. The synthesis of the tetrahedral cage, 277, was achieved by treatment of 2-formylpyridine (275) and 4,4'-diaminobiphenyl-2,2'-disulfonic acid (276) subcomponents with iron(II) and base in aqueous media (Scheme 69). The single-crystal X-ray structure analysis of the tetramethylammonium salt of 277 revealed that the dynamic covalent bonds formed in situ between a 4,4'-diaminobiphenyl-2,2'-disulfonic acid and two 2-formylpyridine moieties give rise to a bis-bidentate ligand which cheleates the  $\text{Fe(II)}$  atoms occupying the vertices of the tetrahedron in a hexamine ligand environment. Strong binding interactions between the  $\text{Fe(II)}$  and imine ligands confer structural stability to cage 277. The sulfonate groups of 4,4'-diaminobiphenyl-2,2'-disulfonic acid are symmetrically exposed to the exterior of the cage thereby contributing toward its solubility in aqueous solutions.

Tetrahedral cage 277 was also assembled from a multicomponent system via a sequential self-assembly approach.<sup>350</sup> Each of the imine ligands formed from three different amines have flexible, bent, and linear rigid motifs, respectively. When treated with 2-formylpyridine, they form entropically favored, self-assembled architectures through a self-sorting process. The cage has an internal void volume of 141 Å.

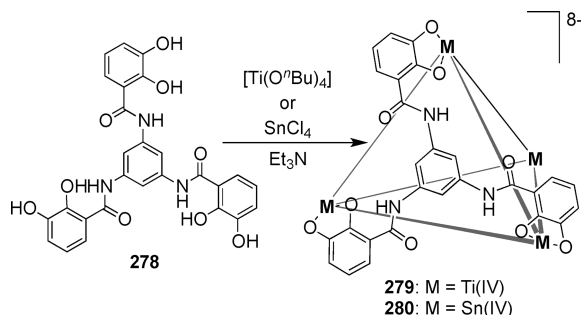
Recently, the same group reported a new class of  $\text{M}_4\text{L}_6$  tetrahedral cages, which have reconfigurable exteriors in solution.<sup>351</sup> The  $\text{Fe(II)}$ -templated reaction of 3,3'-bipyridine-6,6'-dicarboxaldehyde with para-substituted anilines led to the formation of these  $\text{M}_4\text{L}_6$  tetrahedral cages decorated with externally directed amine residues. For example, treatment of 3,3'-bipyridine-6,6'-dicarboxaldehyde with *p*-chloroaniline in the presence of an appropriate  $\text{Fe(II)}$  salt gave a homochiral tetrahedral cage having 12 *p*-chloroaniline residues on the periphery. The  $\text{C}_2$ -symmetric bis-bidentate pyridylimine ligands define the edges of the tetrahedron, bridging the four  $\text{Fe(II)}$  ions at the vertex. Addition of *p*-toluidine or *p*-methoxyaniline to a solution of a *p*-chloroaniline-containing cage resulted in the quantitative displacement of *p*-chloroaniline residues to form *p*-toluidine-containing and *p*-methoxyaniline-containing cages, respectively. Electronic effects drive these subcomponent substitutions wherein electron-rich anilines effectively substitute for the electron-poor aniline residue. Each of these cages encapsulates an anion within their cavities. The peripheral substitution does not impact the anion binding preferences in these cages and follows the order of  $\text{BF}_4^- < \text{OTf}^- < \text{PF}_6^-$ . Interestingly, a large library of 91 distinct heteroleptic  $\text{M}_4\text{L}_6$  cages, assembled from a reaction of 3,3'-bipyridine-6,6'-dicarboxaldehyde with *p*-chloroaniline, *p*-bromoaniline, and *p*-iodoaniline in the presence of  $\text{Fe(II)}$  ions, collapsed into a single homoleptic *p*-methoxyaniline-containing  $\text{M}_4\text{L}_6$  cage upon addition of more electron-rich *p*-methoxyaniline to the mixture.

Lindoy and co-workers assembled neutral  $\text{M}_4\text{L}_6$  tetrahedral cages by utilizing a  $\beta$ -diketonate ligand having phenylene spacers with its donor sets oriented at  $60^\circ$ . Treatment of iron(III) chloride with 1,4-phenylene-bridged bis- $\beta$ -diketonato ligands in THF in a 2:3 molar ratio led to the formation of a series of  $\text{M}_4\text{L}_6$  tetrahedral cages of the type  $[\text{Fe}_4\text{L}_6] \cdot (\text{solvent})_n$ .<sup>171</sup> Single-crystal X-ray structural studies of these cages revealed a tetrahedral topology with four iron(III) ions situated at the vertices of the tetrahedron and the six bis- $\beta$ -diketonato ligands defining the edges. Increasing the size of the bis- $\beta$ -diketonato ligand by extending the bridge between the coordination domains from phenylene to biphenylene led to the assembly of a large neutral  $\text{M}_4\text{L}_6$  tetrahedral cage.<sup>352</sup> Treatment of biphenylene-spaced bis- $\beta$ -diketonate ligand, 1,1'-(4,4'-biphenylene)bis-3,3-dimethylpentane-1,3-dione, with iron(III) chloride led to the formation of the cage with four encapsulated tetrahydrofuran guest molecules. A corresponding tetrahedral cage was assembled from a phenylene-spaced bis- $\beta$ -diketonate ligand, 1,1'-(1,4-phenylene)bis-hexane-1,3-dione, and could encapsulate only one tetrahydrofuran molecule as a guest.

A  $\text{M}_4\text{L}_4$  tetrahedron can be assembled by utilizing ligands that have three bidentate metal binding sites with a  $\text{C}_3$ -axis of symmetry in their idealized structure in conjugation with metal ions that prefer octahedral coordination geometries.<sup>9,353</sup> Raymond et al.<sup>354</sup> assembled  $\text{Ti(IV)}$ - and  $\text{Sn(IV)}$ -containing  $\text{M}_4\text{L}_4$  tetrahedrons, 279 and 280, using a catecholamide trigonal trisbidentate ligand (278) under basic conditions (Scheme 70).  $^1\text{H}$  NMR and mass spectrometric studies indicated the formation of  $\text{M}_4\text{L}_4$  clusters. The X-ray structural analysis of  $(\text{Et}_3\text{NH})_8[\text{Ti}_4(\text{278})_4]$  (279)



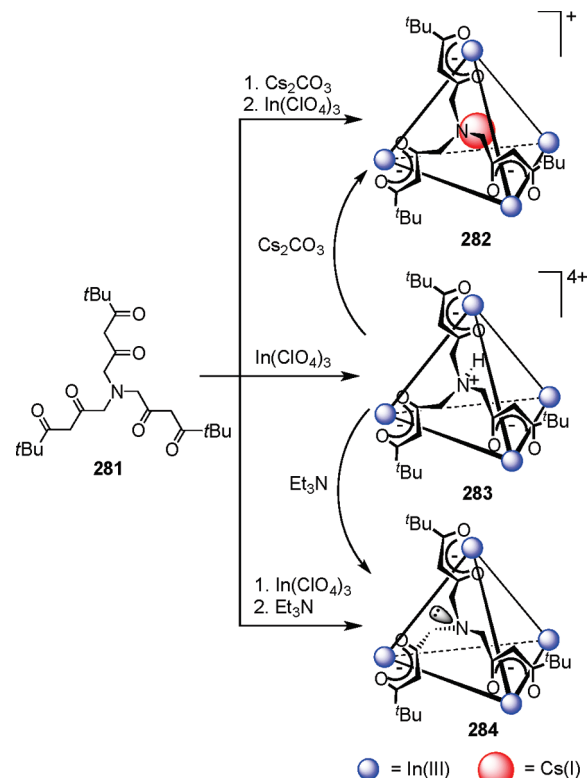
Scheme 70



revealed that the cluster lies on a crystallographic 3-fold axis but has the molecular symmetry of the rotation group  $T$ , such that all the metal ions have the same chirality (all D or L). Similarly, tetranuclear Fe(III) cages generated in a one-pot reaction from benzene-1,3,5-tricarboxylic acid trichloride, bis(*tert*-butyl malonate), methyl lithium, and iron(II) dichloride under aerobic conditions,<sup>355</sup> and tris-pyrazolyl borate based  $M_4L_4$  tetrahedral assemblies were also reported.<sup>356,357</sup> The internal cavities of these tetrahedral cages are too small to encapsulate guest molecules. Utilizing the same design strategy, Raymond et al. designed larger  $M_4L_4$  tetrahedra based on a  $C_3$ -symmetric ligand, 1,3,5-tris(4'-(2'',3''-dihydroxybenzamido)phenyl)benzene.<sup>358</sup> Tetrahedral assemblies with Al(III), Ga(III), In(III), and Ti(IV) as the pseudooctahedral metal centers were synthesized with cavity sizes of around 450 Å<sup>3</sup>. In contrast to tetrahedral clusters **279** and **280**, where no evidence of guest encapsulation was observed in the small cavity, these cages were able to encapsulate charge-, size-, and shape-selective guest molecules within their cavities. Along the same line, the assembly of triscatechol imine ligands with titanium(IV) ions in the presence of alkali metal carbonate as a base (Li, Na, K) in DMF led to the formation of metallo-supramolecular tetrahedra with huge internal cavities.<sup>359,360</sup> The X-ray crystal structure of the Ti(IV) catecholate octaanionic cluster showed the presence of an internal cavity with four potassium cations bound to the internal catecholate oxygen atoms. Additionally, three DMF molecules were bound to each of the potassium ions.

N-centered tripodal heptadentate ligands have been used to assemble  $M_4L_4$  tetranuclear clusters.<sup>361</sup> Treatment of **281** with  $Cs_2CO_3$  followed by the addition of  $In(ClO_4)_3$  in methanol resulted in a tetrahedral cluster  $[Cs\{In_4(281)_4\}]ClO_4$  (**282**) with a cesium ion as the encapsulated guest molecule (Scheme 71). The same reaction in the absence of base gave N-protonated tetranuclear In(III) complex  $[In_4(H-281)_4](ClO_4)_4$  (**283**) without the cesium guest molecule. Furthermore, treatment of  $In(ClO_4)_3$  with **281** and subsequent addition of triethylamine afforded the neutral tetranuclear complex  $[In_4(281)_4]$  (**284**). The tetrahedral cluster, **282**, was also accessible from **283** by deprotonation with  $Cs_2CO_3$ . Cluster **284** can be formed by the deprotonation of **283** with triethylamine (Scheme 71). All of these complexes were characterized by <sup>1</sup>H NMR spectroscopy, mass spectrometry, and single-crystal X-ray structural studies. While **282** and **283** crystallize as racemic mixtures of homochiral tetrahedra with  $\Delta\Delta\Delta\Delta$  or  $\Lambda\Lambda\Lambda\Lambda$ -*fac* stereoisomers with  $T$  molecular symmetry, complex **284** crystallizes in an idealized  $S_4$  symmetry with a  $\Delta\Delta\Delta\Delta$  configuration due to the loss of  $C_3$  symmetry of ligand **281** during deprotonation.

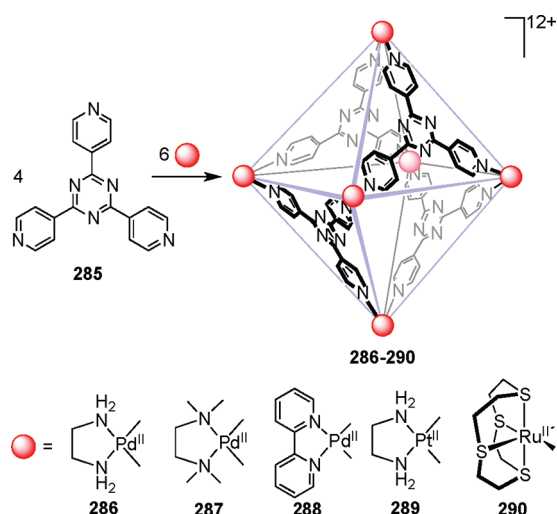
Scheme 71



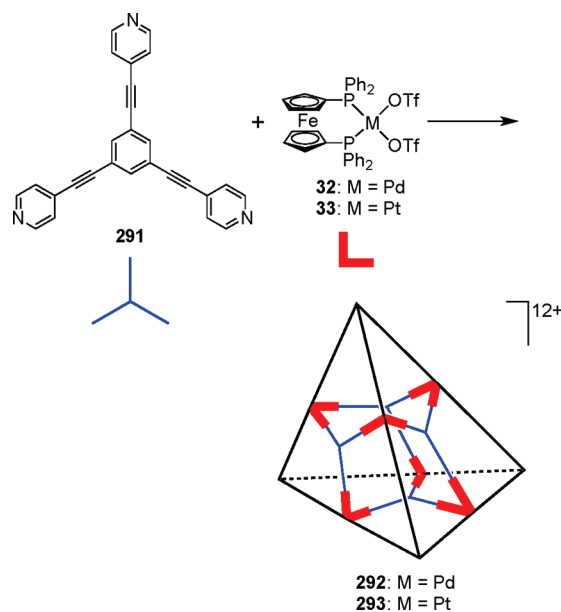
$M_6L_4$  tetrahedra or truncated tetrahedra contain tripodal ligands at each of their four faces connected by metal centers at the middle of the edges. They can also be envisioned as being derived from a tetrahedron whose corners have been capped. In 1995, Fujita et al.<sup>26</sup> reported the first synthesis of truncated tetrahedra (Fujita and co-workers refer to them as octahedral cages, depicting them as octahedral molecules with missing faces) using the molecular paneling approach.  $M_6L_4$  tetrahedral cages **286**–**290** were quantitatively assembled by the treatment of *cis*-capped metal ion hinges with 2,4,6-tri(4-pyridyl)-1,3,5-triazine **285** (Scheme 72). Each panel spans a face of the tetrahedron and is linked to another at the edges by six metal ions. For example, (en)Pd<sup>II</sup> cornered cage **286** was readily prepared by treating  $[Pd(en)(NO_3)_2]$  (**1**) with **285** in a 6:4 ratio in aqueous medium. Replacement of the end-capping ligand with (*N,N,N',N'*-tetramethylethylenediamine)Pd<sup>II</sup>, (2,2'-bipyridine)Pd<sup>II</sup>, or (en)Pt<sup>II</sup> resulted in cages **287**, **288**, and **289**, respectively, with altered bulk properties.<sup>362</sup> Use of  $[Ru([12]-aneS_4)(H_2O)(DMSO)](NO_3)_2$  under similar reaction conditions led to the formation of Ru(II)-cornered coordination cage **290** having interesting sensing properties.<sup>363</sup> NMR, cold-spray ionization mass spectrometry (CSI-MS), and X-ray crystal structural analysis established the formation of these assemblies.

Using the directional bonding approach, Stang et al. have designed truncated tetrahedra via the face-directed self-assembly of planar tritopic 120° subunits with angular ditopic 90° corner units. The ratio of faces to corners must be 2:3 with a total number of 10 subunits to obtain a closed structure. The  $[6 + 4]$  self-assembly reaction of 1,3,5-tris(4-pyridylethynyl)benzene (**291**) with *cis*- $[M(dppf)(OTf)_2]$  ( $M = Pd$  (**32**),  $Pt$  (**33**)) resulted in the formation of cationic  $M_6L_4$  truncated tetrahedra **292** and **293**

Scheme 72



Scheme 73



(Scheme 73).<sup>364</sup> The use of optically active, chiral 90° angular units,  $[M(R\text{-BINAP})(\text{OTf})_2]$ <sup>365</sup> ( $M = \text{Pd}$  (177) or  $\text{Pt}$  (178)) or  $cis\text{-}[\text{Pt}(\text{PMe}_3)(\text{OTf})_2]$ <sup>366</sup> (38) in conjugation with 291 has led to the formation of similar truncated tetrahedra. The structures of these tetrahedra were established by multinuclear (<sup>31</sup>P and <sup>1</sup>H) NMR spectroscopy, ESI-MS, and X-ray crystallography. Recently, the same group reported the coordination-driven self-assembly of a truncated tetrahedron (Figure 31) using 90° platinum acceptors and a hexapyridyl ligand with 6-fold symmetry, under mild conditions.<sup>367</sup> The tetrahedron was characterized by multinuclear (<sup>31</sup>P and <sup>1</sup>H) NMR spectroscopy, ESI-MS, X-ray crystallography, and pulsed-field-gradient spin-echo (PGSE) NMR, along with computational simulations. X-ray diffraction studies showed that the highly symmetrical hexapyridyl ligand acts as the faces and the 90° platinum acceptors are connectors at the edges. These truncated tetrahedra show a unique 3D nanoscale

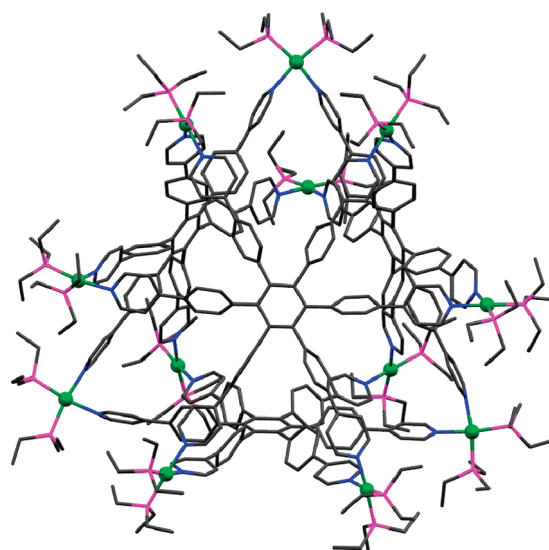


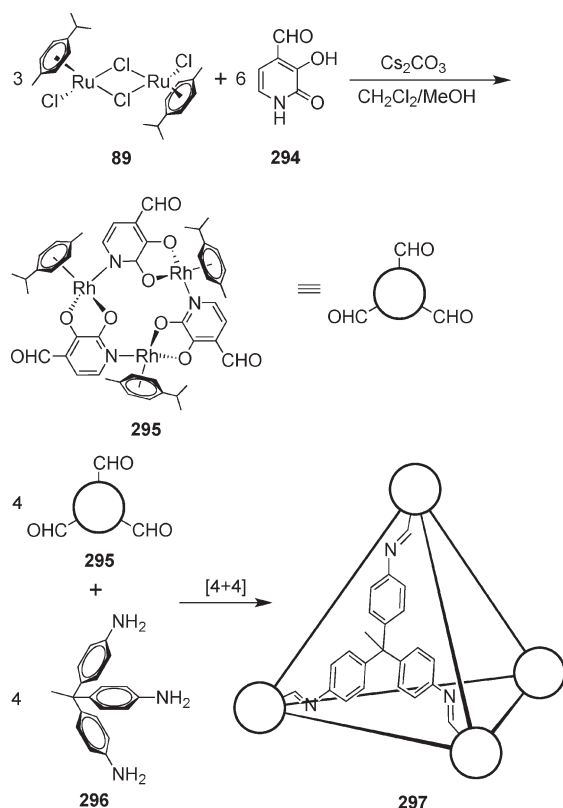
**Figure 31.** Single-crystal X-ray structure of a truncated tetrahedron formed using a hexapyridyl ligand. Solvents and  $\text{PF}_6^-$  are omitted for clarity. Color code: green, Pt; pink, P; blue, N; gray, C.

pore suitable for encapsulation of guest molecules and preliminary studies indicated that the nanocavity is able to encapsulate up to three molecules of 1,3,5-triphenylbenzene.

In an elegant approach, Severin and co-workers have recently assembled molecular cages with tetrahedral geometries by combining metalla-supramolecular chemistry with dynamic covalent chemistry in an orthogonal fashion.<sup>368,369</sup> Polycondensation of triamines with metalla-macroscopic building blocks, containing pendent aldehyde groups, has enabled the facile synthesis of these nanoscopic cages. Reactions of  $[(\text{arene})\text{RuCl}_2]_2$  [arene = *p*-cymene, 1,3,5- $\text{C}_6\text{H}_3\text{Me}_3$ , 1,3,5- $\text{C}_6\text{H}_3(i\text{-Pr})_3$ ] with formyl-substituted 3-hydroxy-2-pyridone ligands gave trinuclear metalla-macrocycles with pendant aldehyde groups. Subsequent condensation with  $\text{C}_3$ -symmetric triamines led to the formation of tetrahedral cages. For example, treatment of  $[(p\text{-cymene})\text{RuCl}_2]_2$  (89) with 4-formyl-3-hydroxy-2(1*H*)-pyridone (294) in the presence of  $\text{Cs}_2\text{CO}_3$  provided trinuclear metalla-macrocycle 295 (Scheme 74).<sup>369</sup> As observed from X-ray crystallographic studies, three pendent aldehyde groups in the metalla-macroscopic trimer were oriented toward the same face of the macrocyclic framework. A subsequent  $[4 + 4]$  condensation reaction of the macrocyclic trialdehyde, 295, with  $\text{C}_3$ -symmetrical triamine 1,1,1-tris(4-aminophenyl)ethane (296) in a mixture of  $\text{CH}_2\text{Cl}_2$  and MeOH led to the formation of tetrahedral cage 297 after several days. The formation of the molecular cage was supported by NMR and mass spectrometric studies. The X-ray crystal structure of the supramolecular tetrahedron 297 revealed that the trinuclear metalla-macrocycles occupy four vertices of a tetrahedron, while the triphenylamine units span each of the four faces. This paradigm can also be used to design even larger cages. Indeed, the use of an expanded triamine with the trialdehydic metalla-macrocycles gave  $[4 + 4]$  condensation products with larger dimensions.

**4.1.2. Cubic Systems.** Supramolecular cubic systems can be achieved by employing two distinct, yet related, design paradigms: (a) edge- and (b) face-directed self-assembly. In the edge-directed self-assembly method, the precursor subunits define the edges of the cube. Thus, an edge-directed cube can be assembled

Scheme 74



via the reaction of 8 tritopic  $90^\circ$  corner units with 12 ditopic linear linkers (Figure 32a). In the face-directed self-assembly paradigm, some or all of the faces of the target assemblies are spanned by the linkers themselves, which hold together the overall architecture. Thus, in this paradigm, a supramolecular cube results from the combination of 6 tetratopic, planar,  $90^\circ$  faces with 12 ditopic,  $90^\circ$  subunits (Figure 32b,c). Here, the corners of the cube are missing, while the surfaces are covered.

Thomas et al.<sup>370</sup> have reported an edge-directed  $M_8L_{12}$  supramolecular cube from 8 tritopic  $90^\circ$  corner units and 12 linear linkers following the directional bonding approach. The treatment of  $[(9\text{-}aneS_3)Ru(DMSO)Cl_2]$  (**298**) with 4,4'-bipyridine in a 8:12 molar ratio in the presence of silver triflate in nitromethane resulted in the cationic supramolecular cube, **299**, over a period of 4 weeks (Scheme 75). NMR and ESI-MS confirmed the structure of the cage compound. The kinetic stability of cube **299** in coordinating solvents such as acetonitrile also indicated the formation of an unstrained cubic structure. Electrochemical studies on **299** showed three irreversible oxidation processes.

Fujita and co-workers<sup>371</sup> have assembled a face-directed  $M_6L_{12}$  supramolecular cube by combining  $90^\circ$  ditopic linkers with palladium ions, which act as tetratopic acceptors. The reaction of ditopic ligand **300** with  $Pd(NO_3)_2$  in  $DMSO-d_6$  led to the quantitative self-assembly of a face-directed supramolecular cube (**301**; Scheme 76). In the molecular cube,  $Pd(II)$  ions are located in each face and ligand **300** acts as corner pieces.  $^1H$  NMR spectroscopy was in agreement with the formation of a single, highly symmetric product. After anion exchange from  $NO_3^-$  to  $OTf^-$  ions, CSI-MS studies confirmed the formation of a  $M_6L_{12}$  cube. Single-crystal X-ray structural studies revealed the

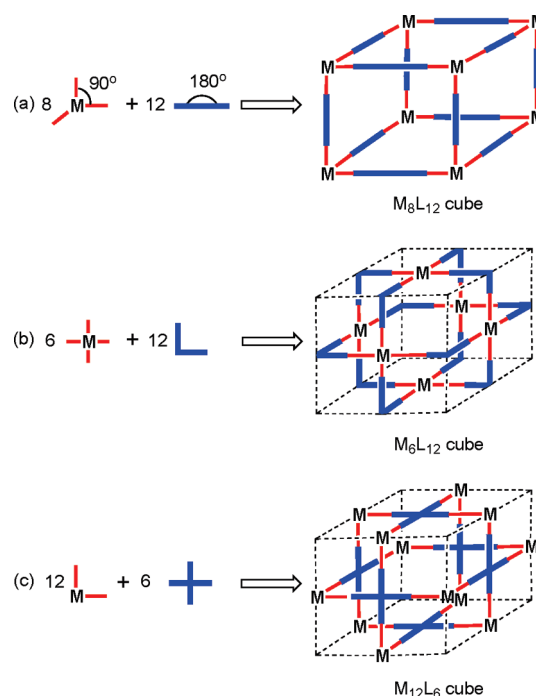
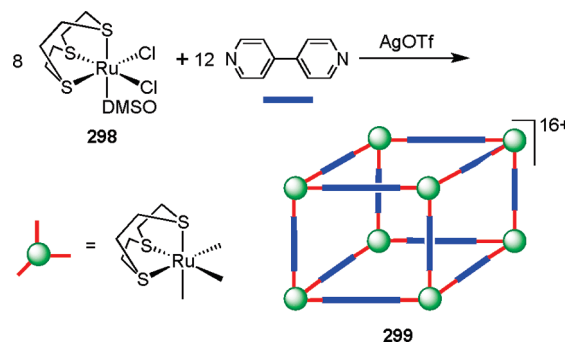


**Figure 32.** General design strategy for the synthesis of (a)  $M_8L_{12}$ , (b)  $M_6L_{12}$ , and (c)  $M_{12}L_6$  molecular cubes.

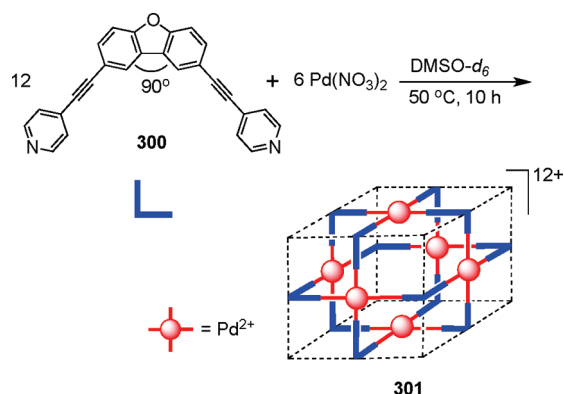
Scheme 75



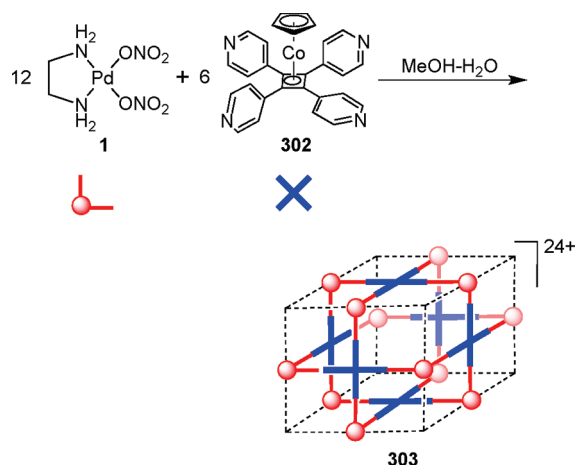
dimensions of nanoscale cube **301** to be approximately  $3 \times 3 \times 3 \text{ nm}^3$  ( $27 \text{ nm}^3$ ). Similar  $M_6L_{12}$  cubes were also realized using a bimesityl-based tetrapyrrolic ligand.<sup>372</sup> Slow evaporation of a solution of a 1:1 mol equiv of  $Cu(OAc)_2 \cdot H_2O$  or  $Ni(NO_3)_2 \cdot 6H_2O$  and the tetrapyrrolic ligand in MeOH over a period of 7–10 days yielded the molecular cubes. Although NMR and mass spectrometric studies were inconclusive, the single-crystal X-ray studies showed the compounds to be supramolecular cubes with  $O_h$  symmetry. The nature of the counterions plays a vital role in the assembly of these cages.

Brisbois et al.<sup>373</sup> designed a  $M_{12}L_6$  supramolecular cube by assembling 12 ditopic  $90^\circ$  metal corner units and 6 tritopic linkers through the directional bonding paradigm. The treatment of 12 equiv of **1** with 6 equiv of tetrapyrrolic ligand scaffold **302** in a methanol–water mixture led to the quantitative assembly of metallo-supramolecular cube **303** (Scheme 77). NMR and mass spectrometric studies confirmed the formation of the cube. The tetrapyrrolic ligand, **302**, spanned the faces of the cube while the (en) $Pd^{II}$  hinges clipped the edges.

Scheme 76



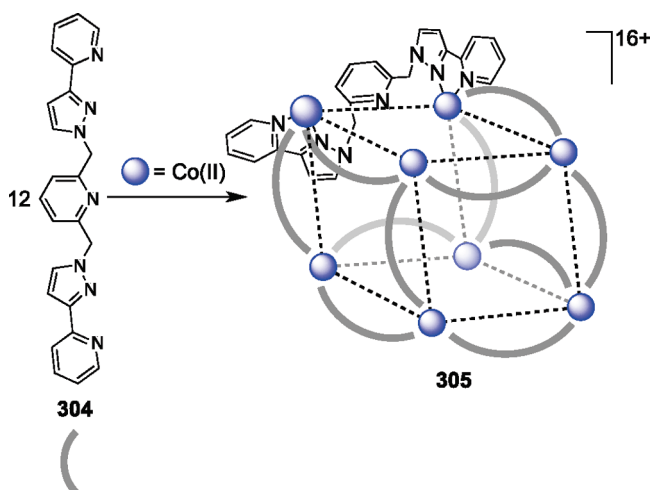
Scheme 77



In other strategies, cyanides have been utilized as effective ditopic linkers in a design approach wherein dimerization of two molecular squares in a complementary orientation result in a molecular cube. Rauchfuss and co-workers<sup>374</sup> successfully applied this approach to design novel organometallic cubes where metal centers occupy all eight corners. For example, in the first step in this synthesis, the tricyanometalate  $\text{Et}_4\text{N}[\text{Cp}^*\text{Rh}(\text{CN})_3]$  ( $\text{Cp}^* = \text{C}_5\text{Me}_5$ ) was employed to prepare a  $\text{Rh}_4$  molecular square by treatment with the dimeric rhodium chloride complex  $[\text{Cp}^*\text{RhCl}_2]_2$ . The synthesis of the final molecular cube was achieved by removing the chloride ligand from the  $\text{Rh}_4$  molecular square with  $\text{AgPF}_6$  in acetonitrile. The same group also reported the formation of molecular cubes  $\{\text{M}[\text{Cp}^*\text{Rh}(\text{CN})_3]_4[\text{Mo}(\text{CO})_3]_4\}^{2-}$  ( $\text{M} = \text{K}^+, \text{Cs}^+$ ) isolated from reactions of  $[\text{Cp}^*\text{Rh}(\text{CN})_3]^-$  with equimolar  $[(\eta^6\text{-C}_6\text{H}_3)\text{Mo}(\text{CO})_3]$  in the presence of  $\text{K}^+$  or  $\text{Cs}^+$ .<sup>375</sup> The alkali metal ions act as templates in the formation of the organometallic cubes. X-ray crystallographic studies on the complexes revealed boxlike  $\text{M}_8(\mu\text{-CN})_{12}$  cages containing alkali metal cations at the center of the cages. The cages feature 12 external CO and 4 external  $\text{C}_5\text{Me}_5$  ligands. The directionality of the metal–cyanide bond was also used to assemble a supramolecular cube,  $[(\text{Cp}^*\text{WS}_3\text{Cu}_3)_8\text{Cl}_8(\text{CN})_{12}\text{Li}_4]$  from a precursor, the incomplete cubane-like compound  $[\text{PPh}_4][\text{Cp}^*\text{WS}_3(\text{CuCN})_3]$ .<sup>376</sup>

Long et al. prepared several molecular cubic clusters having analogous structures inherent to Prussian blue by utilizing ditopic

Scheme 78



cyanides as linkers. Reactions between  $[\text{M}(\text{H}_2\text{O})_3(\text{tacn})]^{3+}$  ( $\text{M} = \text{Cr}, \text{Co}$ ) and  $[\text{Co}(\text{CN})_3(\text{tacn})]^{12+}$  gave molecular box clusters  $[\text{Cr}_4\text{Co}_4(\text{CN})_{12}(\text{tacn})_8]^{12+}$  and  $[\text{Co}_8(\text{CN})_{12}(\text{tacn})_8]^{12+}$  with core structures consisting of single cubic units.<sup>377</sup> As determined from single-crystal X-ray crystallography, the structure of the latter species is shown to consist of a cube of eight  $\text{Co}^{\text{III}}$  ions occupying the corners capped by tacn ligands with each edge spanned by a linear cyanide bridge. The same group was also able to generate larger cubic metal–cyanide clusters by using a blocking ligand on one of the mononuclear reaction components.<sup>378</sup> This design paradigm was demonstrated by the synthesis of a 14 metal  $[(\text{Me}_3\text{tacn})_8\text{Cr}_8\text{Ni}_6(\text{CN})_{24}]^{12+}$  cluster. The geometry of this cluster consists of a cube of eight  $\text{Me}_3\text{tacn}$ -ligated  $\text{Cr}(\text{III})$  ions connected via bridging cyanide ligands to six square-planar  $\text{Ni}(\text{II})$  ions situated just above the center of each cube face. A still larger tetracapped edge-bridged cubic  $[(\text{Me}_3\text{tacn})_{12}\text{Cr}_{12}\text{Ni}_{12}(\text{CN})_{48}]^{12+}$  cluster was synthesized from the direct assembly reaction between  $[(\text{Me}_3\text{tacn})\text{Cr}(\text{CN})_3]$ ,  $\text{NiL}_2$ , and KCN in aqueous solution.<sup>379</sup> The structure of this cluster features a cube of eight  $\text{Cr}(\text{III})$  centers linked along the edges by 12 trans-coordinated  $[\text{Ni}(\text{CN})_4]^{2-}$  units and capped on four faces by  $[(\text{Me}_3\text{tacn})\text{Cr}]^{3+}$  moieties.

Ward and co-workers have reported a number of supramolecular  $\text{M}_8\text{L}_{12}$  cubes using flexible bispyrazolylpyridine ligands and octahedral metal ions via the symmetry interaction approach.<sup>340</sup> For example, the bispyrazolylpyridine ligand, **304**, having a pyridyl spacer, reacts with  $\text{Co}(\text{II})$  salts to afford  $[\text{Co}_8(\text{304})_{12}]^{16+}$  cubic cage **305** (Scheme 78).<sup>380</sup> The metal ions occupy each vertex of the cube, and the ligands coordinate in a bis-bidentate bridging manner via the two bidentate pyrazolyl–pyridine units spanning each edge. Although ligand **304** is potentially pentadentate, the central pyridyl unit does not participate in the coordination and thus behaves like a bidentate bridging ligand having a *m*-phenylene spacer.<sup>381</sup> In contrast to the  $\text{M}_4\text{L}_6$  tetrahedral clusters synthesized using the same flexible bispyrazolylpyridine ligands, these assemblies are achiral due to the fact that the tris-chelate metal centers in these “cubes” do not have the same optical configuration and possess crystallographic inversion centers. There is a  $\text{C}_3$  axis in each case along the long diagonal, with the two  $\text{M}(\text{II})$  centers on this axis having a facial tris-chelate coordination, and the other six all having a meridional geometry.



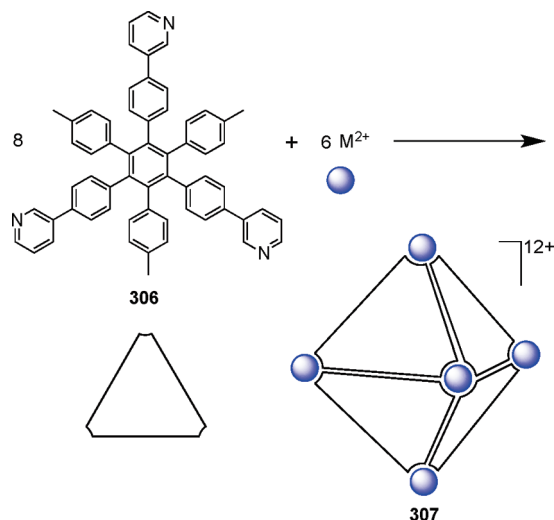
The combination of a  $C_3$  axis and an inversion center means that these cages actually have noncrystallographic  $S_6$  symmetry. There is extensive  $\pi$ – $\pi$  stacking between the overlapping portions of the ligand moieties. Similar octanuclear cubic assemblies with 1,5-naphthyl ( $L_{\text{naph}}$ ), 9,10-anthracenyl ( $L_{\text{anth}}$ ), 1,4-phenyl ( $L_{\text{ph}}$ ), 2,5-furan ( $L_{\text{fur}}$ ), and 2,5-thiophene ( $L_{\text{th}}$ ) spacers afforded  $[M_8L_{12}]^{16+}$  cages ( $M = \text{Cu, Zn, Co, Ni, and Cd}$ ).<sup>382</sup> While the cages based on  $L_{\text{naph}}$  have  $S_6$  symmetry, with diagonally opposite pairs of corners having *facial* tris-chelate configuration and the other six being *meridional*, all metal centers in these cages based on  $L_{\text{anth}}$  have meridional tris-chelate configurations. The cubic cages based on  $L_{\text{naph}}$  show extensive interligand aromatic  $\pi$ -stacking interactions at their peripheries. In contrast, cubes containing  $L_{\text{anth}}$  do not show significant interligand aromatic stacking interactions.

Recently, Nitschke and co-workers self-assembled a  $M_4L_6$  cubic cage utilizing dynamic covalent and coordinative bonds in tandem via a reaction between tetrakis(4-aminophenyl)porphyrin, 2-formylpyridine, and iron(II) triflate in DMF as evidenced by  $^1\text{H}$  NMR and ESI-MS studies.<sup>383</sup> Replacing tetrakis(4-aminophenyl)porphyrin with nickel(II)- or zinc(II)-tetrakis(4-aminophenyl)porphyrin under identical conditions yielded the nickel-containing and zinc-containing congeners. Single-crystal X-ray structure determined for the nickel-containing  $M_4L_6$  cubic cage showed that each face of the cube was spanned by the porphyrin ligands with each corner of the cube defined by a six-coordinate low-spin Fe(II) ion. All of the Fe(II) centers within each cage adopted the same  $\Delta$  or  $\Lambda$  configuration. In the crystal lattice, both enantiomers were present. The cubic cage has a large internal void volume ( $>1300 \text{ \AA}^3$ ), which enabled it to selectively encapsulate higher fullerenes from fullerene soot.

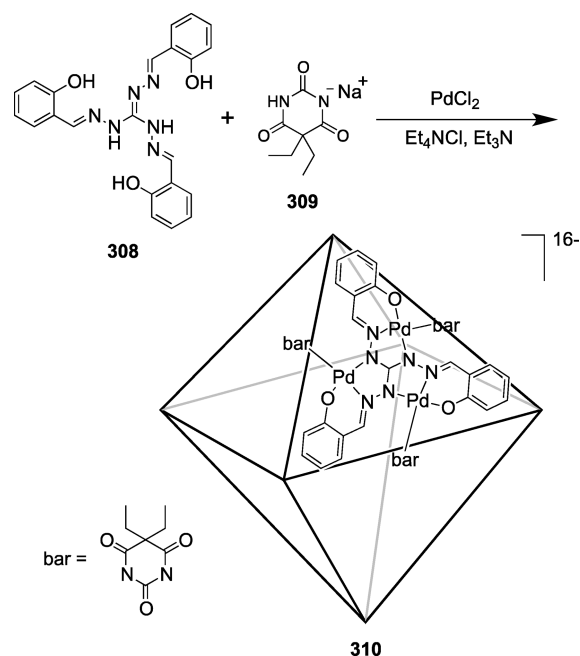
**4.1.3. Octahedra.** Formation of supramolecular octahedral architectures using a coordination-driven self-assembly is quite rare in the literature. Similar to cubic systems, supramolecular octahedral assemblies have been achieved through edge- and face-directed self-assembly paradigms. Shionoya et al. have reported the construction of  $M_6L_8$  octahedral metallo-supramolecular assemblies using a series of divalent  $d^5$ – $d^{10}$  transition metal ions  $M^{2+}$  ( $M = \text{Mn, Fe, Co, Ni, Pd, Pt, Cu, Zn, Cd, and Hg}$ ) and tritopic pyridyl ligand **306**.<sup>384</sup> A  $[6 + 8]$  assembly led to the formation of cationic  $[M_6(\mathbf{306})_8]^{12+}$  (**307**) octahedral-shaped cages in which six metal ions occupy the vertices and the eight faces of the octahedron are spanned by eight ligands (Scheme 79). Single-crystal X-ray structural studies on  $[\text{Hg}_6(\mathbf{306})_8]^{12+}$  revealed a 3 nm sized octahedron-shaped capsule with sides of 1.8 nm. It was also demonstrated that the  $[\text{Hg}_6(\mathbf{306})_8]^{12+}$  capsule is reversibly interconvertible with a  $[\text{Hg}_6(\mathbf{306})_4]^{12+}$  cage by changing the ratio of ligand to metal.<sup>385</sup> The structural interconversion between the two distinct complexes was accompanied by reversible changes in the coordination mode of the  $\text{Hg}^{2+}$  ion between octahedral and linear coordination geometries. A similar  $[\text{Pd}_6L_8]^{12+}$  cage has been reported with the cyclotrivenyl-type ligand—tris(isonicotinoyl)cyclotriguaiacylene—and a naked palladium ion.<sup>386</sup> Lah et al. assembled a similar face-directed molecular octahedron from a combination of 3,3',3''-[1,3,5-benzene-triyltris(carbonylimino)]trisbenzoate as a  $C_3$ -symmetric tritopic ligand and a paddlewheel  $\text{Cu}_2(\text{COO})_4$  moiety as a corner unit.<sup>387</sup> Here, eight ligand molecules span the faces of the octahedron connected by six  $\text{Cu}_2(\text{COO})_4$  paddlewheel units at the corners.

Müller et al. utilized a 3-fold chelating ligand, tris(2-hydroxybenzylidene)triaminoguanidinium chloride  $[\text{H}_6\text{L}]\text{Cl}$  (**308**), to form the triangular faces of an octahedral metallo-supramolecular

Scheme 79



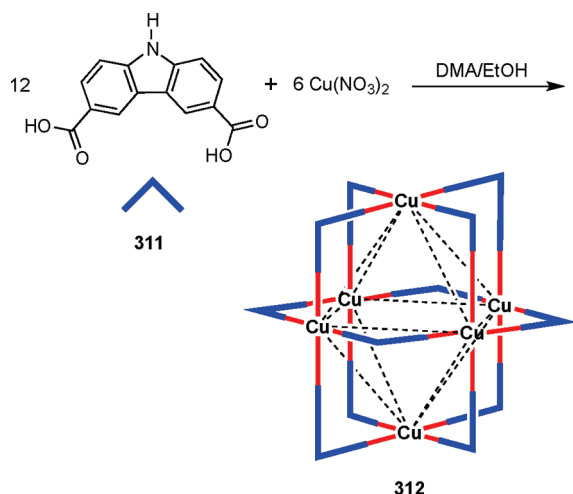
Scheme 80



assembly.<sup>388</sup> The one-pot reaction of  $\text{PdCl}_2$ ,  $\text{Et}_4\text{NCl}$ ,  $[\text{H}_6\text{L}]\text{Cl}$  (**308**), sodium 5,5-diethylbarbiturate ( $\text{NaHbar}$ , **309**), and  $\text{Et}_3\text{N}$  in acetonitrile at room temperature leads to the formation of an anionic octahedral molecular assembly  $[\{\text{Pd}_3\text{L}\}_8\{\mu\text{-(bar)}\}_{12}]^{16-}$  (**310**; Scheme 80). Octahedral complex **310** was characterized by  $^{13}\text{C}$  MAS NMR spectroscopy and X-ray crystallography. The solid-state structure showed that ligand **308** forms triangular molecular panels through N, N, O chelation with palladium, leaving a free coordination site for the bridging ligand. The ditopic sodium 5,5-diethylbarbiturate ( $\text{NaHbar}$ , **309**) ligands connect the faces of the octahedron through the middle of the edges.

Zhou and co-workers<sup>389</sup> have assembled an edge-directed supramolecular octahedron from an angular ( $90^\circ$ ) dicarboxylate

Scheme 81

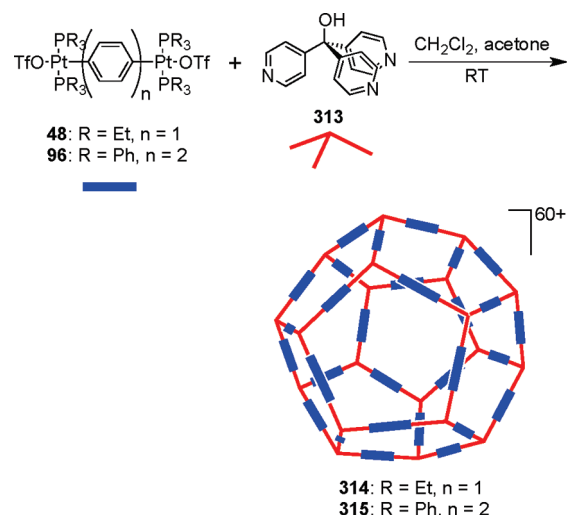


ligand and a paddlewheel  $\text{Cu}_2(\text{COO})_4$  cluster. A solvothermal reaction between 9H-carbazole-3,6-dicarboxylic acid ( $\text{H}_2\text{CDC}$ ; **311**) and  $\text{Cu}(\text{NO}_3)_2 \cdot 2.5\text{H}_2\text{O}$  in a 1:1 DMA:EtOH solution (DMA = *N,N*-dimethylacetamide) afforded molecular octahedron  $[\text{Cu}_2(\text{CDC})_2(\text{DMA})(\text{EtOH})]_6 \cdot x\text{S}$  (S = noncoordinated solvent molecule; **312**; Scheme 81). Single-crystal X-ray structural studies showed that the molecular octahedron is composed of six axially coordinated  $\text{Cu}_2(\text{COO})_4$  paddlewheel clusters occupying the vertices joined by 12 CDC linkage units along the edges. Interestingly, molecular octahedron **312** can be reversibly assembled into a three-dimensional metal organic framework by interlinking the octahedra through ditopic 4,4'-bipyridine ligands.

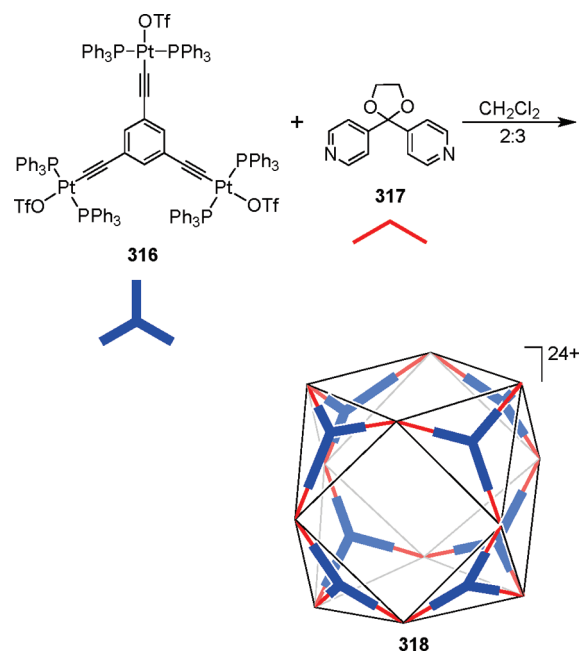
**4.1.4. Dodecahedra.** In principle, the most complicated member of the five Platonic polyhedra is a dodecahedron. It contains 12 fused five-membered rings that comprise the highest symmetry group  $I_h$ . The 12 pentagonal faces are formed from 20 vertexes and 30 edges. Hence, a dodecahedron can be prepared via edge-directed assembly of 20 tripodal subunits with approximately  $108^\circ$  directing angles in combination with 30 bidentate linear subunits. Only a few examples of Pt(II)-based molecular dodecahedra are known, where diplatinum-based linear linkers (**48**, **96**) were assembled with tripodal ligand tri-4-pyridylmethanol **313** to obtain dodecahedra **314** and **315** of nanodimensions (Scheme 82).<sup>390,391</sup> Though no direct structural evidence was provided for their exact shape, NMR along with mass spectrometric results and TEM images demonstrated the formation of the expected dodecahedra. These dodecahedra are significantly larger than the hydrocarbon  $\text{C}_{20}\text{H}_{20}$  of the same symmetry, synthesized by classical covalent synthesis in 23 steps.<sup>392,393</sup> The cavities of the self-assembled dodecahedra **314** and **315** are expected to be capable of encapsulating large globular oligomers and molecules with solvation shells.

**4.1.5. Cuboctahedra.** The cuboctahedron is a rare archimedean semiregular polyhedron that combines square and triangular faces. Overall it has 12 vertices, 24 edges, and a dihedral angle of  $125^\circ$  between the triangular and the square surfaces. Using the directional bonding approach, a cuboctahedron can be constructed by combining planar tridentate faces with  $108^\circ$  turning angles via bidentate angular components. Since a  $109.5^\circ$  angle is close to  $108^\circ$ , the bidentate angular linking subunit may have a

Scheme 82

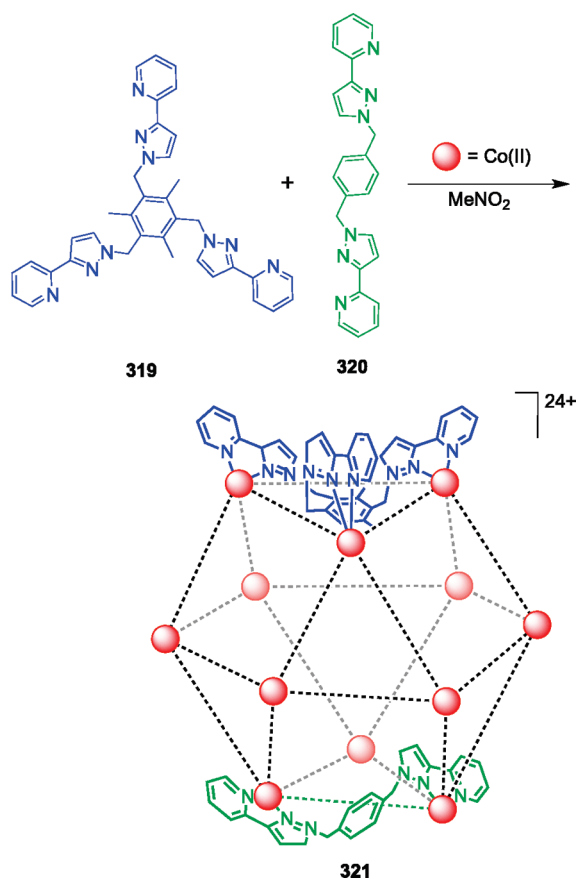


Scheme 83



tetrahedral atom connected to a rigid linear donor or acceptor site. Stang and co-workers have reported the formation of nanoscopic molecular cuboctahedra from the combination of 12 tritopic planar units and eight ditopic angular units.<sup>394</sup> The tridentate  $\text{Pt}_3$  acceptor, **316**, was treated with bidentate 4,4'-bipyridylacetate **317** in 2:3 molar ratio to obtain the first Pt-based molecular cuboctahedron **318** (Scheme 83). Despite its large molecular mass (26592 Da) and high charge (24+), cuboctahedron **318** is remarkably soluble in organic solvents, such as dichloromethane or acetone. In a complementary approach, 1,3,5-tris(4-pyridylethynyl)benzene **291** was assembled with bis(4-[*trans*-Pt( $\text{PPh}_3$ )<sub>3</sub>OTf]phenyl)ketone to yield similar cuboctahedra.<sup>394</sup> The self-diffusion coefficient at 25 °C was  $1.92 \times 10^{-2} \text{ cm}^2 \text{ s}^{-1}$ , which gave an experimental hydrodynamic

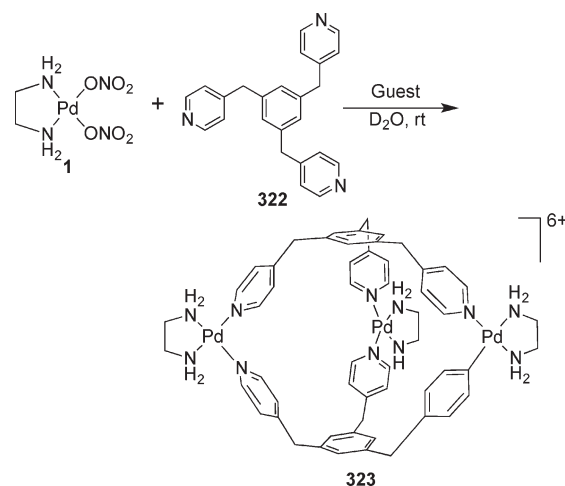
Scheme 84



diameter of 5.0 nm, was in good agreement with predictions based on force-field simulations as well as the size of the component building units. Finally, ESI-MS was used to establish the exact composition.

Ward and co-workers have also reported the formation of cuboctahedral cages from the combination of ligands having different binding modes with octahedral metal ions.<sup>395,396</sup> A 3:1:3 reaction of tris-bidentate ligand **319**, which can cap one triangular face of a metal polyhedron; a bis-bidentate ligand **320**, which can span one edge of a metal polyhedron; and a range of  $M^{2+}$  ions results in the assembly of mixed-ligand cuboctahedral cages  $[M_{12}(\mu_3\text{-}\mathbf{319})_4(\mu_2\text{-}\mathbf{320})_{12}]^{24+}$  [ $M = \text{Co}$  (**321**), Cu, Cd] in MeNO<sub>2</sub> (Scheme 84). Single-crystal X-ray structural studies of  $[M_{12}(\mu_3\text{-}\mathbf{319})_4(\mu_2\text{-}\mathbf{320})_{12}]^{24+}$  ( $M = \text{Cu}$ , Cd) show that they are isostructural, having a dodecanuclear cuboctahedral metal framework containing eight triangular and six square faces. Four of the eight triangular faces were capped by tripoly bridging ligands **319**. Twelve doubly bridging ligands **320** span the remaining edges. Counterions and solvent molecules occupy the central cavity. A cooperative interaction between the two types of ligand renders the formation of the mixed ligand cuboctahedral cage more favorable than the homoleptic cages. The ESI-MS on solutions of re-dissolved crystals showed a clear sequence of peaks corresponding to the intact mixed-ligand cage with no peaks for the homoleptic cages. All 12 tris-chelate metal centers have meridional geometry, and again, all have the same chirality, indicating that the same chiral configuration at each metal center is necessary for the closed cage to form.

Scheme 85



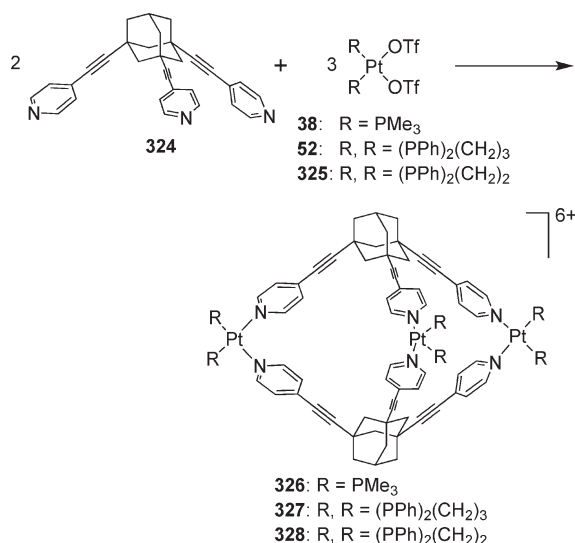
## 4.2. Other Coordination Cages

**4.2.1. Trigonal Bipyramids and Double Squares.** A large number of molecular trigonal bipyramids synthesized via coordination-driven self-assembly have been reported in the literature. In principle, a  $M_3L_2$  trigonal bipyramid can be designed by assembling two tritopic, tetrahedral donors with three ditopic 90° subunits through the edge-directed self-assembly. Fujita and co-workers prepared one of the earliest trigonal-bipyramidal cages in 1995.<sup>397</sup> Treatment of 2 equiv of the tritopic ligand 1,3,5-tris(4-pyridylmethyl)benzene, **322**, with 3 equiv of ditopic 90° **1**, in the presence of sodium 4-methoxyphenylacetate led to the exclusive formation of trigonal-bipyramidal cage **323** (Scheme 85). However, in the absence of a specific guest, self-assembly resulted in the formation of oligomeric products. Monocarboxylate guests with bulky hydrophobic moieties induce the assembly of **323** more effectively as compared to less hydrophobic substrates.

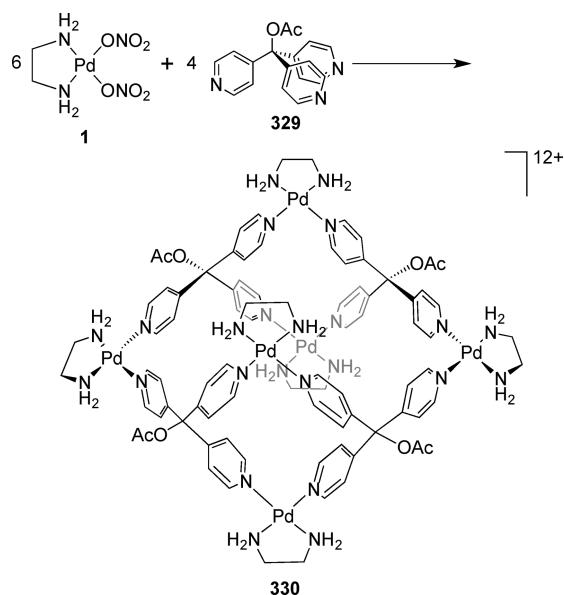
Stang et al. reported the synthesis of a number of  $M_3L_2$  trigonal-bipyramidal cages using tritopic 109° linkers.<sup>398,399</sup> A  $[2 + 3]$  self-assembly reaction between ~109° tripodal angular unit **324** and generic 90° angular units such as *cis*-[Pt(PMe<sub>3</sub>)<sub>2</sub>-(OTf)<sub>2</sub>] (**38**), *cis*-[Pt(dppp)(OTf)<sub>2</sub>] (**52**), and *cis*-[Pt(dppe)-(OTf)<sub>2</sub>] (**325**) resulted in trigonal-bipyramidal cages **326–328** (Scheme 86).<sup>398</sup> Multinuclear NMR studies and mass spectrometric analysis confirmed the formations of these cages. Similarly, the use of flexible tritopic tectons containing amide<sup>399</sup> and ester<sup>400</sup> functionalities resulted in the exclusive formation of trigonal-bipyramidal cages. Such a reaction, however, with less flexible ligands resulted in the formation of double square architectures.<sup>401,402</sup> For instance, treatment of **1** with the tripyridylmethane acetate (**329**) resulted in self-assembly of a double square cage (**330**) in which four ligand molecules are held together by six metal ions (Scheme 87).<sup>401</sup> Similarly use of preorganized tripodal metalloligand incorporating octahedral metal centers, aluminum or gallium, in which the orientation of the pyridyl coordination sites for self-assembly were controlled by the metal's octahedral coordination environment, afforded novel heterometallic trigonal-bipyramidal cages when assembled with appropriately angled (60 or 90°) platinum acceptors.<sup>403</sup>

The reaction of a rigid tripodal ligand having ester functionalities with a 90° Pt(II) acceptor also gave an assembly of similar

Scheme 86

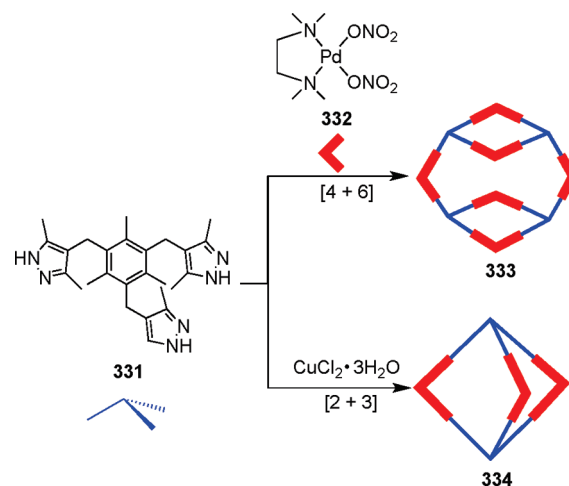


Scheme 87

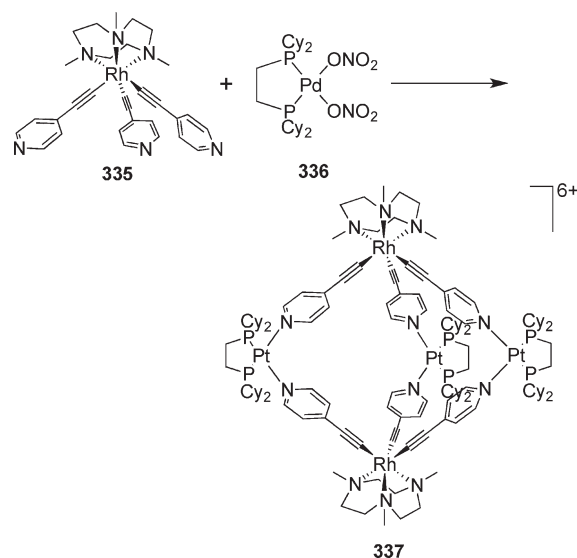


architecture.<sup>402</sup> Thus, if enough flexibility was incorporated into the tritopic units, the thermodynamics of the reaction would favor the formation of trigonal bipyramids over the double square architectures. The double square represents a balance between entropy, where the smallest structure is favored, and enthalpy, where the structure with the least strain is prevalent. A flexible tripodal ligand, **331**, containing pyrazolyl functionality led to a 2:3 self-assembled double square cage **333** upon treatment with *cis*-[Pd(tmen)(NO<sub>3</sub>)<sub>2</sub>] (**332**) in a 2:3 molar ratio (Scheme 88).<sup>404</sup> A similar reaction using CuCl<sub>2</sub>·3H<sub>2</sub>O instead of the *cis* 90° acceptor, **332**, yielded a Cu<sub>3</sub> trigonal-bipyramidal cage (**334**). For the M<sub>3</sub>L<sub>2</sub> trigonal-bipyramidal cage, **334**, the tripodal ligand adopts a symmetrical *cis,cis,cis*-conformation while in the double square cage **333** the ligand adopts a nonsymmetrical *cis,trans,trans*-conformation.

Scheme 88



Scheme 89

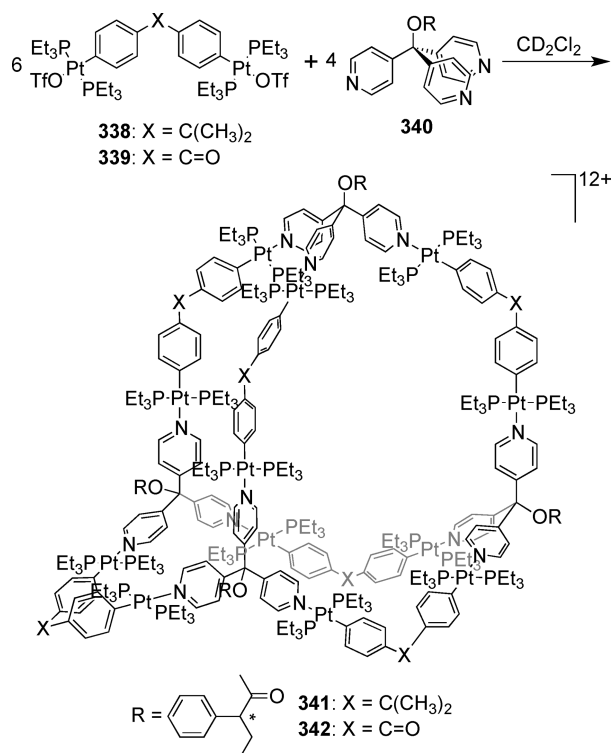


Youngs et al.<sup>405</sup> reported the synthesis of a trigonal-bipyramidal supramolecular cage based upon rhodium and platinum metal centers in a stepwise process. The treatment of 4-ethynylpyridine with *tert*-butyllithium, followed by its addition to (Me<sub>3</sub>tacn)-RhCl<sub>3</sub> afforded the formation of facial octahedral complex (Me<sub>3</sub>tacn)Rh(CCPy)<sub>3</sub> **335**. Subsequent assembly of the tritopic linker with the square-planar complex *cis*-[Pt(dcpe)(NO<sub>3</sub>)<sub>2</sub>] **336** [dcpe = 1,2-bis(dicyclohexylphosphino)ethane] resulted in a self-assembled hexacationic trigonal-bipyramidal cage (**337**; Scheme 89) with Rh(III) and Pt(II) atoms occupying the vertices. Multinuclear NMR and crystal structural studies were used to characterize the assembly.

**4.2.2. Adamantanoids.** Adamantanoids have a shape similar to a tetrahedron that has its edges kinked into 109.5° angles at their points of bisection. While these distortions cause the sides and angles to deviate from those of a tetrahedron, adamantane retains its overall symmetry, that of a point group *T<sub>d</sub>*. Supramolecular adamantanoids can be designed according to the directional



Scheme 90



bonding approach by adopting an edge-directed strategy. The shape itself consists of four fused, chair-conformed cyclohexane-like rings, which requires that all of the pertinent angles should be 109.5°, matching the ideal tetrahedral geometry of sp<sup>3</sup>-hybridized carbon atoms. Thus, a combination of six 120° ditopic units with four 109.5° tritopic units can lead to a self-assembled molecular adamantanoid. For example, a [6 + 4] self-assembly reaction between ditopic units (338 or 339) with tritopic units (340) in CD<sub>2</sub>Cl<sub>2</sub> led to the formation of adamantanoids **341** and **342** in quantitative yields (Scheme 90).<sup>406</sup> <sup>1</sup>H and <sup>31</sup>P NMR as well as ESI-MS studies confirmed the formation of these assemblies. As a result of the stereogenic centers present in the backbone of the ester moiety of ligand **340**, the resulting assemblies were chiral in nature. Fréchet-type dendron-decorated adamantanoids, assembled utilizing similar building units, have also been reported recently.<sup>407</sup>

Lin et al.<sup>408</sup> reported chiral M<sub>4</sub>L<sub>6</sub> adamantanoids from lanthanide salts and C<sub>2</sub> symmetric racemic mixtures of binaphthalene-based ligands. The treatment of lanthanide nitrate or perchlorate with 2,2-hydroxy-1,1-bis(naphthalene-6,6-dicarboxylate) (bda) forms distereoselective porous molecular adamantanoids [Ln<sub>4</sub>(bda)<sub>6</sub>(H<sub>2</sub>O)<sub>12</sub>] · 12DMF (Ln = Gd(III), La(III)). Single crystal X-ray structural studies on [Gd<sub>4</sub>(bda)<sub>6</sub>(H<sub>2</sub>O)<sub>12</sub>] · 12DMF (Figure 33) revealed the formation of a porous nanosized assembly having an internal cavity with a volume of ca. 1700 Å<sup>3</sup>. Within the adamantanoid, Gd atoms reside on the crystallographic 3-fold axis, adopting idealized tricapped trigonal-prismatic coordination geometries by ligating three chelating carboxylate groups from three different bda ligands and three water molecules. In the solid-state, six DMF molecules occupy the internal cavity.

**4.2.3. Trigonal Prisms.** The simplest way of designing a trigonal prism is the combination of an end-capped acceptor, a tritopic planar donor, and a bidentate linear donor in a 6:2:3 molar ratio.

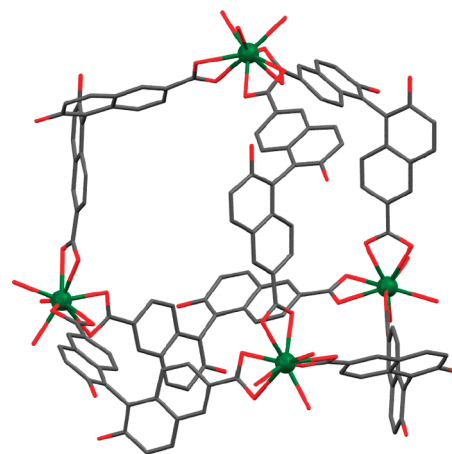
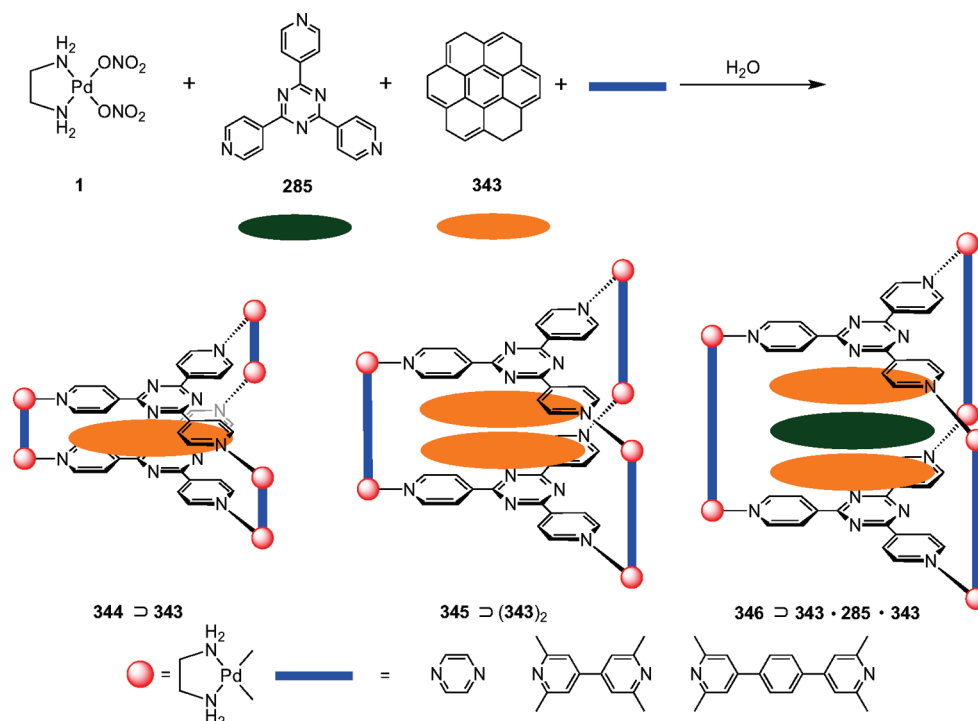


**Figure 33.** X-ray crystal structure of [Gd<sub>4</sub>(bda)<sub>6</sub>(H<sub>2</sub>O)<sub>12</sub>] · 12DMF. Color code: green, Gd; red, O; gray, C.

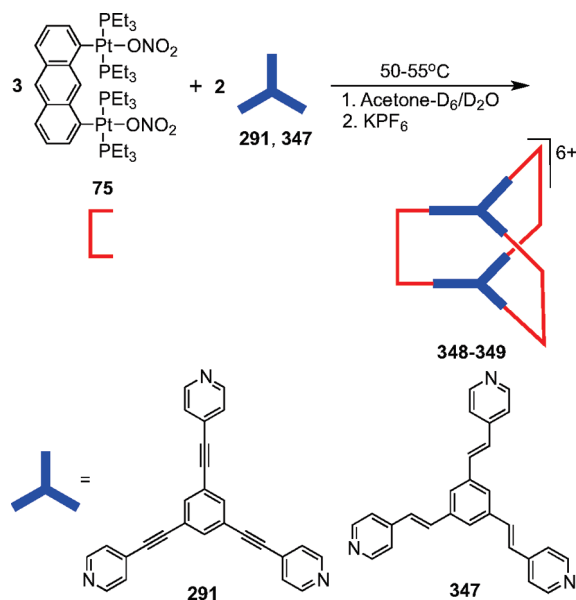
Fujita and co-workers have reported a few trigonal prisms using this multicomponent self-assembly approach. For example, the self-assembly of the 90° cis-blocked 1, tritopic electron-poor triazine panel 2,4,6-tri(4-pyridyl)-1,3,5-triazine (**285**), and pyrazine, which acts as bidentate pillar, led to the formation of trigonal-prism **344** (Scheme 91).<sup>409</sup> The charged metal ion hinges endow the cages with water solubility. In this three-component self-assembly approach there is the possibility of the formation of smaller analogues, such as molecular tetrahedra and squares, from the combination of individual donors with the metal acceptors. However, large aromatic molecules such as coronene (**343**) effectively template the selective formation of the trigonal prism and can be removed after assembly by simple extraction with organic solvents. Prism **344** remains stable after removal of the template and allows the intercalation of various organic molecules. In the presence of 1,3-diketone the ketone is found to exist only in its enol form, suggesting a stabilization effect of prism **344**, as confirmed by NMR spectroscopy.<sup>409</sup> The pyrazine pillar can be replaced by tetramethyl-4,4'-bipyridine or longer 1,4-bis(2,6-dimethylpyridin-4-yl)benzene which results in cages **345** and **346** with larger cavities for stacking of 2 and 3 equiv of aromatic guests, coronene,<sup>410</sup> perylene,<sup>410</sup> and porphene<sup>411</sup> and mononuclear M(II) complexes<sup>412</sup> (M = Pt, Pd, and Cu). Use of an elongated 4,4'-bipyridine extends the cavity of the cage to an ideal size for the accommodation of three guest molecules.<sup>411</sup> The stacking of these aromatic molecules within the cavity is driven and controlled solely by noncovalent interactions.

Using a two-component approach, Stang and co-workers have designed trigonal prisms **348** and **349** using a 0° Pt-based molecular clip (**75**) as the acceptor unit in combination with planar tripodal linkers **291** and **347** by a 3:2 self-assembly reaction (Scheme 92).<sup>413</sup> The structures of these macrobicyclic species were established with multinuclear NMR and ESI-MS. Although several M<sub>3</sub>L<sub>2</sub> prismatic cages using flexible ligands have been reported,<sup>414</sup> they often require the use of templates to assemble in solution or assemble only in the solid state. Use of these rigid donors and acceptors has made it possible to synthesize prismatic cages in the absence of templates. Building upon this strategy, Ko and co-workers<sup>115</sup> have reported the formation of trigonal prisms using a bulkier Pt<sub>2</sub> molecular clip in a 3:2 self-assembly reaction with several tritopic planar donors.

Scheme 91



Scheme 92



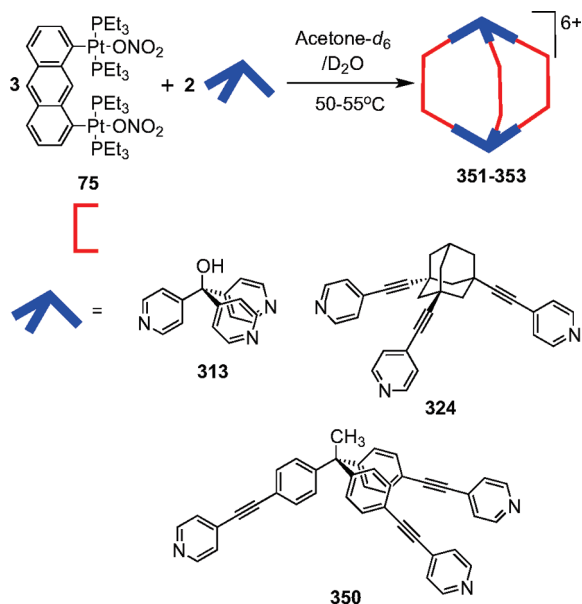
Multinuclear NMR and mass spectral data confirmed the formation of trigonal prisms. The use of isocyanide as the linker also led to the facile formation of molecular trigonal prisms. In a complementary approach, the use of tritopic planar  $\text{Pt}_3$  acceptors in combination with  $0^\circ$  organic clips has also led to the formation of several trigonal prisms in a 2:3 self-assembly processes.<sup>415,416</sup> These  $\pi$ -electron-rich fluorescent cages showed efficient quenching of fluorescence intensity both in solution and solid state in the presence of planar oxidizing nitroaromatics, which are the

chemical signatures of many commercially available explosives. The cages have open spaces to accommodate electron-deficient small nitroaromatics, and the bulky  $\text{PEt}_3$  groups help to avoid intermolecular stacking, thus preventing self-quenching of fluorescence. The solution fluorescence was quenched efficiently by adding nitroaromatics such as dinitrotoluene and trinitrotoluene.<sup>415,416</sup>

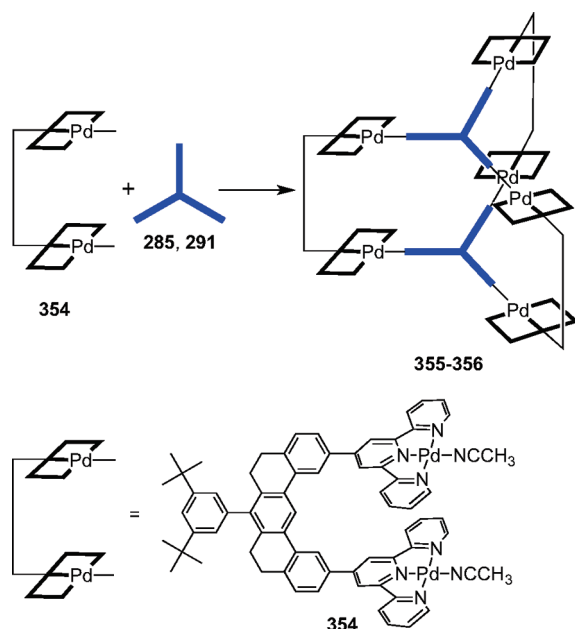
Distorted trigonal prisms 351–353 were also designed by using trigonal-pyramidal acceptors 313, 324, and 350 in conjunction with the  $0^\circ$   $\text{Pt}$ -based molecular clip (75) in a 2:3 molar ratio (Scheme 93).<sup>417</sup> NMR and mass spectrometric results, along with single-crystal X-ray analysis, established that the sizes of the propeller-type 3D structures range from  $1 \times 2 \text{ nm}^2$  to  $1 \times 4 \text{ nm}^2$ . The formation of the smallest of these prisms, 351, was accompanied by the entrapment of a nitrate ion inside its molecular cavity. The  $\text{PF}_6^-$  salt of the largest prism of this series, 353, however, crystallizes with no counteranion inside the cage. A complementary approach using a  $0^\circ$  donor organic molecular clip also led to the assembly of similar molecular prisms.<sup>418</sup> Tetrahedral carbon, silicon, and phosphorus were used as structure-defining elements in these coordination-based cages. Multinuclear NMR, elemental analysis, and ESI-FT-ICR-MS established the formations of these structures.

Bosnich et al.<sup>419</sup> have constructed trigonal prisms from a palladium-based cleft, 354, that contains cofacially disposed terpyridyl-Pd units. The 1:1 reaction of planar tritopic linkers, 285 and 291, with 354 led to the quantitative formation of trigonal prisms 355 and 356 (Scheme 94). Multinuclear NMR and ESI-MS data confirmed the formations of the prisms. These supramolecular trigonal prisms, each bearing three molecular clefts, are shown to form 1:6 and 1:7 host–guest complexes with 9-methylanthracene, and one of the prisms also forms a 1:2 host–guest complex with a tritopic trianthracene guest that registers with the recognition sites of the host.

Scheme 93

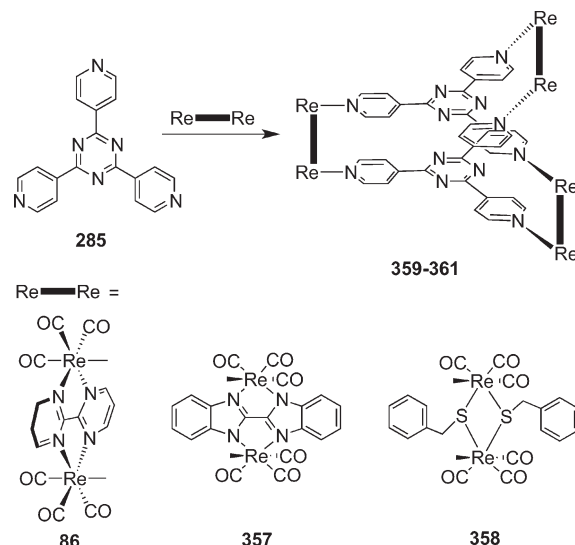


Scheme 94



A number of Re(I)-, Ru(II)-, Ir(I)-, and Rh(I)-based metalloprisms with tridentate triazine ligand, 2,4,6-tri(4-pyridyl)-1,3,5-triazine (**285**) possessing N,N'- or O,O'-donor spacers acting as pillars have also been reported. Hupp et al.<sup>177</sup> reported the synthesis of trigonal-prism **359** by using the bimetallic edge **86** prepared from *fac*-Re(CO)<sub>3</sub>Cl and 2,2-bipyrimidine ligands and subsequently reacting these edges with triazine ligand **285** (Scheme 95). Alternately, the trigonal-prism **359** can be assembled in a one-step process by treating Re(CO)<sub>5</sub>(OTf) and 2,2-bipyrimidine with **285** in a 6:3:2 ratio in THF.<sup>420</sup> The use of 2,2'-bis(benzimidazolate) (**357**) or a pair of benzylthiol-based (**358**) bimetallic edges led to the formation of trigonal prisms

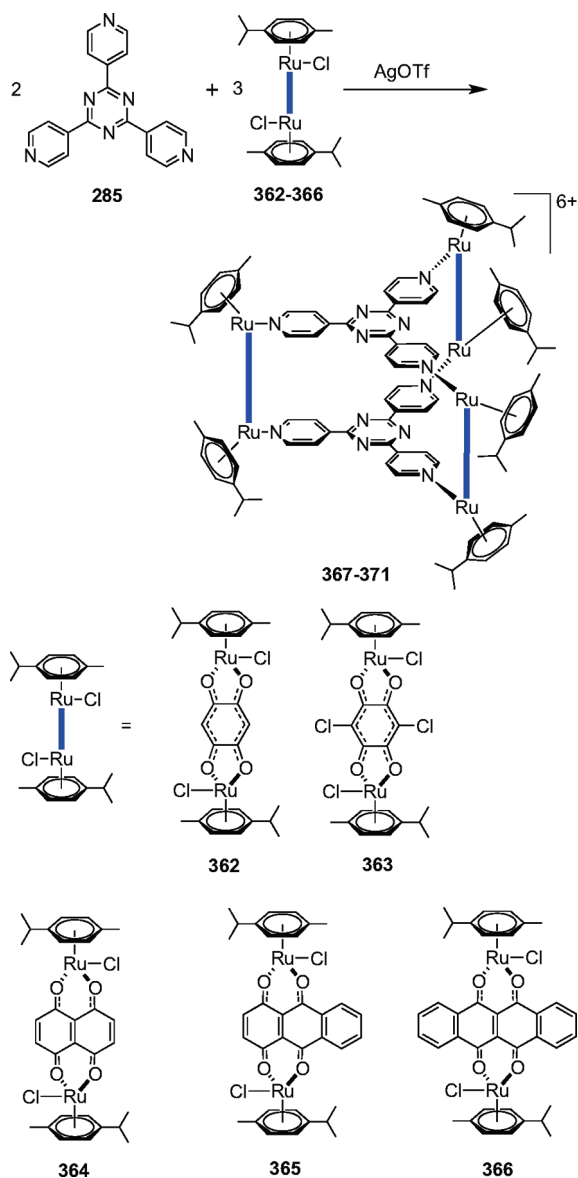
Scheme 95



**360** and **361**, respectively (Scheme 95).<sup>421</sup> The prisms **360** and **361**, in their singly reduced form, are comprised of highly coupled mixed valence systems with orbitally degenerate organic redox centers. The orbital degeneracy of the redox sites of **285** has pronounced effects on light-induced (IT) charge redistribution within the molecules. The self-assembly of Re<sub>2</sub>(CO)<sub>10</sub> and triazine panel **285** in ROH (R = C<sub>4</sub>H<sub>9</sub>, C<sub>8</sub>H<sub>17</sub>, C<sub>12</sub>H<sub>25</sub>), using solvothermal methods at elevated temperatures, led to the formation of thermodynamically stable trigonal cages in excellent yields.<sup>422</sup> In an extension of the methodology, indigo was used as the organic pillar to assemble a trigonal prism in good yield.<sup>423</sup> The structural features of this metalloprism showed very strong  $\pi$ - $\pi$  interactions between the  $\pi$ -clouds of **285** to pull the inner core of the prism inward with a distance one-half of that of the outer core. In THF, the metalloprism displayed intense bands in the near-UV region (200–300 nm) due to  $\pi$ - $\pi^*$  transitions of both **285** and indigo ligands.

Several trigonal-prismatic cationic cages in which six ( $\eta^6$ -arene)-ruthenium(II), ( $\eta^5$ -pentamethylcyclopentadienyl)rhodium(I), or ( $\eta^5$ -pentamethylcyclopentadienyl)iridium(I) units are held together by two trigonal 2,4,6-tri(4-pyridyl)-1,3,5-triazine panels (**285**) and three dichloro<sup>424,425</sup> or oxalate<sup>426,427</sup> bridges were also reported. An extension of this principle led to the construction of larger cationic hexanuclear metalloprisms from *p*-cymene or hexamethylbenzene (C<sub>6</sub>Me<sub>6</sub>) ruthenium building blocks and 2,5-dihydroxy-1,4-benzoquinonato (dhbq) or 2,5-dichloro-3,6-dihydroxy-1,4-benzoquinonato (dchq) or 5,8-dihydroxy-1,4-naphthoquinonato (dhnq) or 9,10-dihydroxy-1,4-anthraquinonato (dhaq), or 6,11-dihydroxynaphthacene-5,12-dionato (dhtq) bridges.<sup>428,429</sup> For example, treatment of diruthenium bridges **362**–**366** with **285** in a 3:2 molar ratio led to the formation of cationic trigonal prisms [Ru<sub>6</sub>(*p*-cymene)<sub>6</sub>(**285**)<sub>2</sub>(dhbq)<sub>3</sub>]<sup>6+</sup> (**367**), [Ru<sub>6</sub>(*p*-cymene)<sub>6</sub>(**285**)<sub>2</sub>(dchq)<sub>3</sub>]<sup>6+</sup> (**368**), [Ru<sub>6</sub>(*p*-cymene)<sub>6</sub>(**285**)<sub>2</sub>(dhnq)<sub>3</sub>]<sup>6+</sup> (**369**), [Ru<sub>6</sub>(*p*-cymene)<sub>6</sub>(**285**)<sub>2</sub>(dhaq)<sub>3</sub>]<sup>6+</sup> (**370**), and [Ru<sub>6</sub>(*p*-cymene)<sub>6</sub>(**285**)<sub>2</sub>(dhtq)<sub>3</sub>]<sup>6+</sup> (**371**) (Scheme 96). Similarly, use of 2,4,6-tri(3-pyridyl)-1,3,5-triazine as the trigonal panel instead of **285** in conjunction with dhnq or dhtq bridges has also led to the formation of hexanuclear arene ruthenium complexes with trigonal-prismatic architecture.<sup>430</sup> These prisms

Scheme 96



were capable of encapsulating various aromatic molecules to form the corresponding inclusion systems as established from one-dimensional ROESY  $^1\text{H}$  NMR experiments, mass spectrometry, and single-crystal structure analysis. The self-assembly of these cationic prisms was also achieved in the presence of  $\text{Pt}(\text{acac})_2$  or  $\text{Pd}(\text{acac})_2$  [ $\text{acac}$  = acetylacetonate] to yield  $\text{Pd}(\text{acac})_2$  or  $\text{Pt}(\text{acac})_2$  encapsulated prisms in almost identical isolated yields.<sup>431</sup> The formation of the  $\text{Pd}(\text{acac})_2/\text{Pt}(\text{acac})_2$  encapsulated cages was monitored by NMR and finally by X-ray structure determination. Interestingly, the use of an oxygen-donor tritopic panel, 1,3,5-benzenetricarboxylate, instead of N-donor panels in combination with oxalate-bridged diruthenium unit has led to the assembly of an incomplete  $\text{Ru}^{\text{II}}_8$  trigonal prism, which exhibits a remarkable shape-selective binding affinity for neutral phenolic compounds via hydrogen-bonding interactions.<sup>432</sup>

Along the same line, Severin et al.<sup>433</sup> designed a trigonal prism having an adaptable cavity size. Using a carboxylate-based diruthenium unit in combination with tritopic ligand **285**, the formation

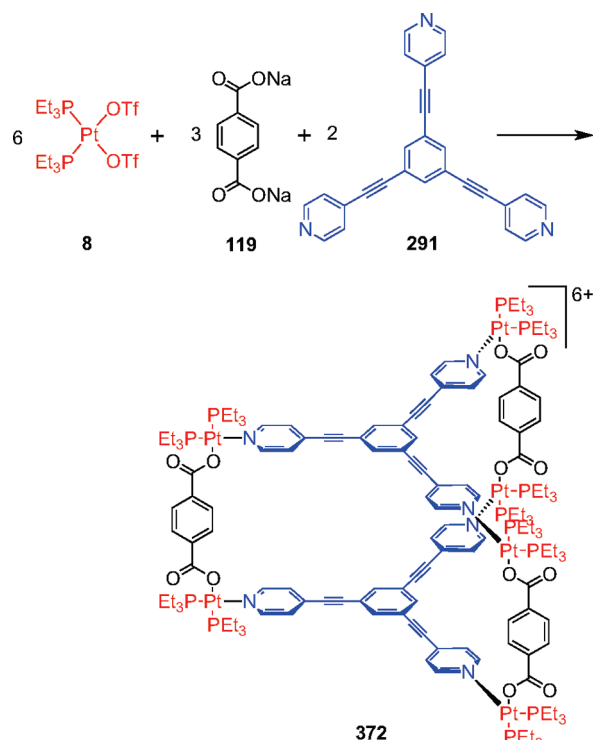
of a trigonal-prismatic cage was achieved. The cage can adopt two distinct conformations: a compressed antiprismatic structure without an internal cavity and an elongated structure having a trigonal-prismatic geometry that is able to accommodate two coronene molecules as guests. The modulation of the cavity space from nearly zero to more than 500 Å was achieved by a conformational change in the flexible ligand rather than the more commonly observed guest-induced constitutional rearrangement.

Hupp et al. have designed supramolecular porphyrinic prisms featuring three, six, or nine porphyrin panels via coordination-driven self-assembly. These molecular prisms were formed by reversible coordination of planar tritopic panels to the  $\text{Zn}(\text{II})$  sites of the porphyrinic dimers and trimers.<sup>434,435</sup> However, due to the weaker Zn-ligand bonds, these assemblies dissociated in highly polar solvents or at high dilution. The use of templated ring-closure metathesis (tRCM) to permanently “set” the structure resulted in the formation of both metalated and metal-free torsionally rigid, irreversible porphyrin prisms.<sup>436</sup> A 3:2 molar ratio reaction of a zinc diporphyrin conjugated through a butadiyne linker and 2,4,6-tri(4-pyridyl)-1,3,5-triazine (**285**) or triethynylpyridylbenzene (**291**) panels preorganizes these panels into assemblies that are ready for ring-closure metathesis. The tRCM using a first generation Grubb’s catalyst afforded the trigonal prisms in high yield. The tridentate panels are important for the formation of the corresponding prisms. Würthner and co-workers described the characterization of a porphyrin-based assembly based on zinc porphyrins as planar units induced by coordination to a bispyridyl-functionalized perylene bisimide.<sup>437,438</sup> The perylene bisimide ligands act as pillars via two axial coordination bonds with the porphyrinic  $\text{Zn}(\text{II})$  ions, fixing the planes of the porphyrin units in a nearly cofacial orientation and inducing the formation of molecular rectangles and trigonal-prism-like structures.

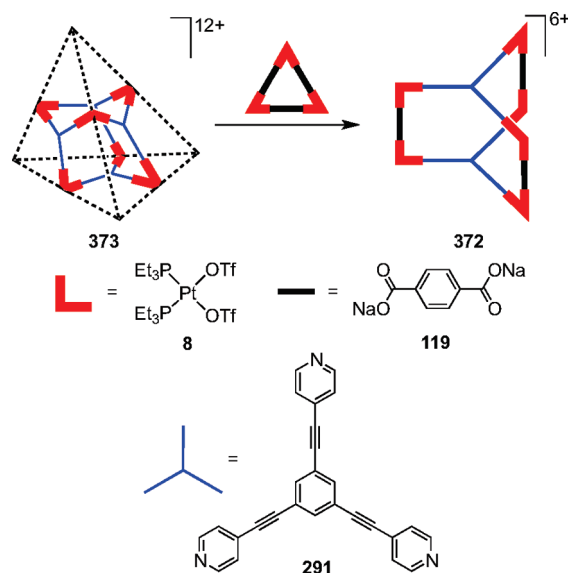
A novel approach toward the construction of heteroleptic trigonal prisms was recently demonstrated from a three-component reaction of carboxylate and pyridyl donor ligands with platinum acceptors.<sup>439</sup> Such multicomponent, selective self-assembly represents a unique assembly process in which multiple, varying components can selectively recognize and combine to generate only one discrete structure within a mixture. Self-assembly of *cis*- $[\text{Pt}(\text{PEt}_3)(\text{OTf})_2]$  (**8**) with linear dicarboxylate **119** and tris(ethynylpyridyl)benzene (**291**) in 6:3:2 molar ratio led to supramolecular trigonal-prism **372** as the predominant species after equilibration (Scheme 97). Multinuclear ( $^{31}\text{P}$  and  $^1\text{H}$ ) NMR spectroscopy, ESI-MS, and PGSE NMR measurements, along with the computational simulations, established the selective self-assembly of heteroleptic trigonal-prism **372**. The self-assembly process is directed, possibly, by a charge separation effect, whereby the anionic carboxylate ligand and a neutral pyridyl donor favor a heteroligated motif upon coordination with  $\text{Pt}(\text{II})$  centers rather than relying only on the stoichiometry and directionality of their molecular components. Furthermore, this selective self-assembly can be achieved via supramolecule-to-supramolecule transformations wherein a homoleptic truncated tetrahedron **373** can be transformed into the heteroleptic trigonal-prism **372** by addition of a solution of homoleptic neutral triangle having carboxylate ligands as the edges (Scheme 98).<sup>439</sup> Similar supramolecule-to-supramolecule transformations in self-assembled polygons,<sup>440,441</sup> helicates<sup>442</sup> and cavitand cages<sup>443</sup> via coordination-driven assembly based on thermodynamic or kinetic control have also been observed. In a complementary approach, heteroleptic  $\text{Pd}(\text{II})$ -based trigonal



Scheme 97



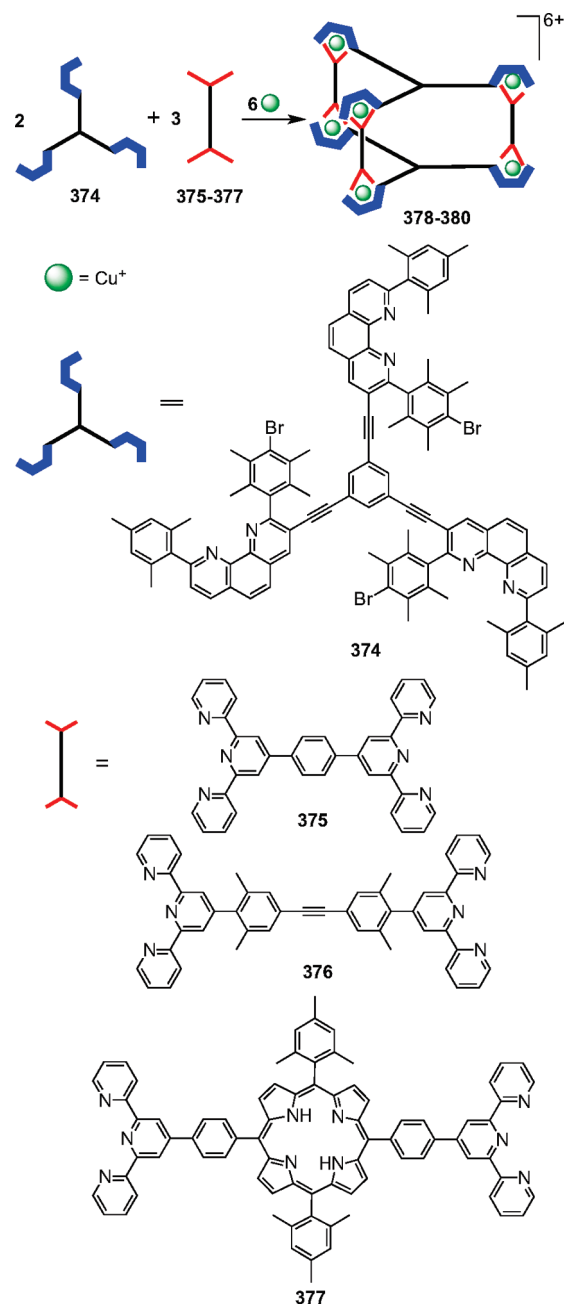
Scheme 98



prisms were assembled using tritopic carboxylates and linear ditopic pyridyl ligands in conjunction with  $90^\circ$  Pd(II) as an acceptor.<sup>444</sup> Isolation of the guest-free cage as well as guest-induced selective formation of the encapsulated cage was achieved using this paradigm.

Using a three-component self-assembly approach, Schmittel et al.<sup>445</sup> designed molecular trigonal prisms from tritopic trisphenanthroline (374) and various bis-terpyridine ligands 375–377. The reaction of 374 with  $[\text{Cu}(\text{MeCN})_4]\text{PF}_6$  in dichloromethane,

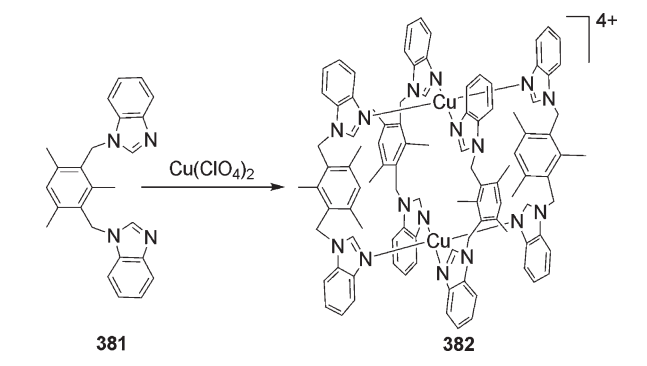
Scheme 99



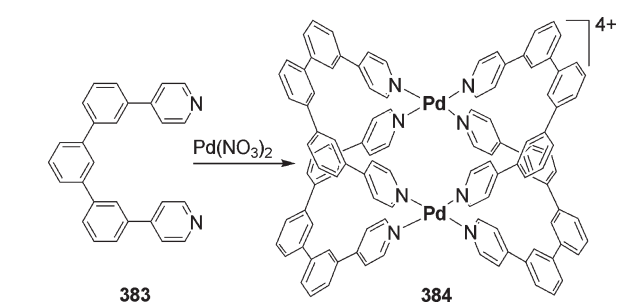
followed by the addition of bis-terpyridine ligands 375–377, led to the formation of heteroleptic trigonal prisms  $[\text{Cu}_6(374)_2(\text{X})_3]^{6+}$  ( $\text{X} = 375–377$ ), 378–380 (Scheme 99). These prisms exist in a dynamic equilibrium with smaller oligomers as determined from NMR and mass spectrometric studies. However, the use of trispyridines as templates drives the equilibrium completely toward the trigonal prisms. In a complementary approach, use of a trispyridine as the tritopic panel with bis-phenanthroline as the pillar also led to the formation of molecular nanoprisms.<sup>446</sup>

**4.2.4. Tetragonal Prisms.** A number of tetragonal prisms have been assembled in recent years using various design paradigms. One of the earliest  $\text{M}_2\text{L}_4$  cages having a tetragonal prismatic architecture was reported by Atwood and co-workers<sup>447</sup> wherein two octahedral Cu(II) ions were bridged by four bispyridyl

Scheme 100

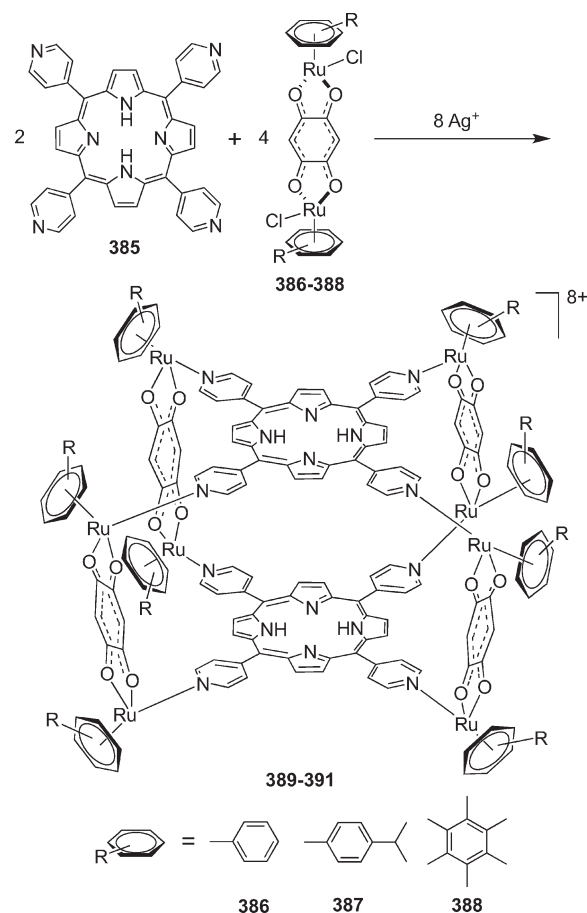


Scheme 101



bidentate building units. While all four equatorial positions of each Cu(II) were coordinated by the pyridyl nitrogens of the ligands, the axial positions were occupied by water molecules. The use of semirigid ligands in conjunction with Cu(II) ions has also led to the assembly of tetragonal prisms. A 1:2 reaction of Cu(II) ion with semirigid bisbenzimidazole ligand **381** led to the formation of cationic tetragonal prism  $[\text{Cu}_2(\text{381})_4]^{4+} \cdot 4\text{ClO}_4^-$  **382** having  $S_4$  symmetry (Scheme 100).<sup>448</sup> Single-crystal X-ray structural analysis showed that the ligand **381** adopts a syn conformation in order to bridge two Cu(II) ions. Each of the Cu(II) ions are held by the benzimidazole arms of the four different ligands via Cu–N coordination to metal ions in a square-planar geometry. The  $\text{ClO}_4^-$  counterion resides in the cavity of the cage. Under similar conditions, the use of  $\text{NiCl}_2$  led to the formation of a neutral tetragonal prism  $[\text{Ni}_2(\text{381})_4]\text{Cl}_2 \cdot \text{H}_2\text{O}$ .<sup>449</sup> The use of ditopic, semirigid ligands that contain long central bases and two pyridyl coordinating rings linked by methylene groups, 2,6-bis(3-pyridylmethyl)hexahydro-4,8-ethenopyrrolo[3,4-*f*]isoindole-1,3,5,7-tetrone also led to a  $\text{M}_2\text{L}_4$  tetragonal prism.<sup>450</sup> Twisted dinuclear Cu(II) cages of the  $\text{M}_2\text{L}_4$  type with an encapsulated chloride between the metal centers were also reported.<sup>451</sup> Use of other metal ions with preferred square-planar coordination geometries, such as Pd(II), have also led to the formation of tetragonal-prismatic cage structures. Fujita and co-workers<sup>452</sup> have reported a Pd(II)-based  $\text{M}_2\text{L}_4$  cage using a rigid organic clip-type donor with naked square-planar  $\text{Pd}^{2+}$  as tetratopic acceptors.  $\text{Pd}(\text{NO}_3)_2$  yielded the tetragonal cage **384** upon 2:4 self-assembly with a bidentate pyridyl ligand, **383** (Scheme 101), which was characterized by NMR and single-crystal X-ray structural analysis. An analogous dinuclear Pd(II)  $\text{M}_2\text{L}_4$  tetragonal cage encapsulating both anionic<sup>453</sup> and cationic<sup>454</sup> guest molecules inside the cavity was also investigated.

Scheme 102



Therrien et al.<sup>455</sup> have reported a series of cationic tetragonal prisms incorporating a dhhq ligand instead of an oxalato bridge. The tetragonal prisms, having general formula  $[\text{Ru}_8(\eta^6\text{-arene})_8(\mu\text{-tppH}_2)_2(\text{dhhq})_4]^{8+}$  (**389**, arene =  $\text{C}_6\text{H}_5\text{Me}$ ; **390**, arene =  $p\text{-cymene}$ ; **391**, arene =  $\text{C}_6\text{Me}_6$ ), were assembled by a 1:2 reaction between 5,10,15,20-tetra(4-pyridyl)porphyrin (tppH<sub>2</sub>, **385**) and ruthenium building blocks **386–388** bridged by a dhhq ligand (Scheme 102). Similarly, toluene or  $p\text{-cymene}$  ruthenium building blocks bridged by the dhhq ligand and connected by a zinc porphyrin 5,10,15,20-tetra(4-pyridyl)porphyrinzinc(II) (tppZn) tetradentate ligand led to the formation of tetragonal prisms:  $[\text{Ru}_8(\text{C}_6\text{H}_5\text{Me})_8(\mu\text{-tppZn})_2(\text{dhhq})_4]^{8+}$  and  $[\text{Ru}_8(p\text{-cymene})_8(\mu\text{-tppZn})_2(\text{dhhq})_4]^{8+}$ .<sup>456</sup> These supramolecular tetragonal prisms interact strongly with duplex and human telomeric quadruplex DNA.

Using the same design principle, Jin and co-workers<sup>457</sup> have reported tetragonal prisms incorporating tetra-4-pyridylporphyrin as a tetrapic donor in combination with oxalato-bridged half-sandwich Ir(III), Rh(III), and Ru(II) connectors. Single-crystal X-ray structure analysis of the  $\text{Ru}_8$  tetragonal prism  $[\text{Ru}_8(p\text{-cymene})_8(\mu\text{-tppH}_2)_2(\mu\text{-C}_2\text{O}_4)_4]^{8+}$  (Figure 34; tppH<sub>2</sub> = 5,10,15,20-tetra-4-pyridylporphyrin, **385**) showed the complex possessed helical chirality with a porphyrin–porphyrin separation of 4 Å. The open space volume inside the prism was approximately 800 Å<sup>3</sup>. The cavity of the octanuclear prism was too small to accommodate a guest molecule, and strong  $\pi$ -stacking interactions between two porphyrin panels were observed. As a

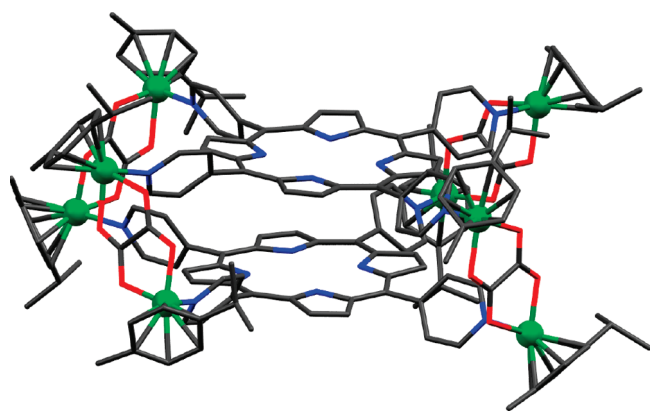
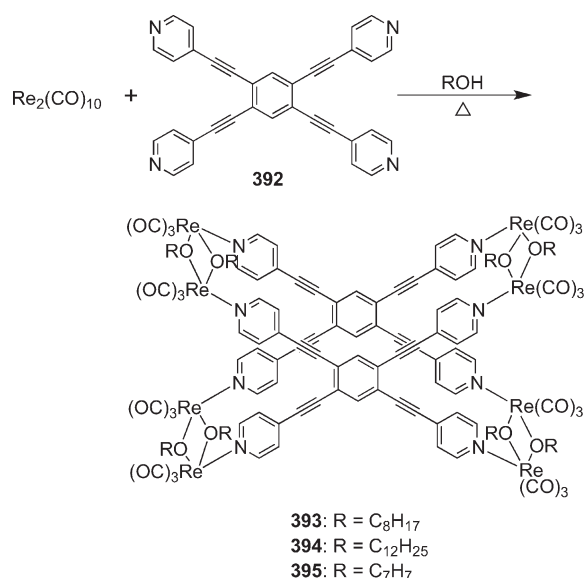


**Figure 34.** Single-crystal X-ray structure of  $\text{Ru}_8$  tetragonal prism  $[\text{Ru}_8(p\text{-cymene})_8(\mu\text{-tppH}_2)_2(\mu\text{-C}_2\text{O}_4)_4]^{8+}$ . Color code: green, Ru; red, O; blue, N; gray, C.

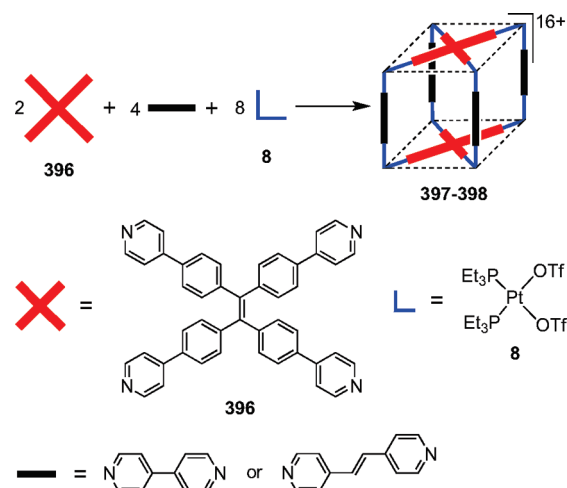
**Scheme 103**



consequence of the twist in the oxalato clips, two porphyrin panels, although being approximately parallel, are twisted along their normal vector and thus give rise to two helical isomers. Chiral discrimination of these enantiomers can be achieved by using anionic chiral  $\Lambda$ -BINPHAT as NMR solvating agent.<sup>458</sup>

Lu and co-workers<sup>459</sup> have reported a series of octametallic tetragonal prismatic cages,  $[\{(\text{CO})_3\text{Re}(\mu_2\text{-OR})_2\text{Re}(\text{CO})_3\}_4(\mu_4\text{-tpeb})_2]$  (**393**,  $\text{R} = \text{-C}_8\text{H}_{17}$ ; **394**,  $\text{R} = \text{-C}_{12}\text{H}_{25}$ ; **395**,  $\text{R} = \text{-C}_7\text{H}_7$ ) obtained in excellent yields at elevated temperatures under solvothermal conditions by mixing  $\text{Re}_2(\text{CO})_{10}$  and the tetradentate ligand 1,2,4,5-tetraethynyl(4-pyridyl)benzene (tpeb, **392**), in a 2:1 ratio in high boiling alcohols (Scheme 103). These prisms **393–395** were the first examples of neutral luminescent molecular tetragonal prisms possessing eight octahedral Re(I) centers and two different kinds of ligands. Single-crystal X-ray structural studies on **393** established that two tpeb ligands were coordinated to four  $[(\text{CO})_3\text{Re}(\mu_2\text{-OCH}_2\text{C}_6\text{H}_5)_2\text{Re}(\text{CO})_3]$  edge moieties, thereby forming a tetragonal prism. Molecular recognition studies revealed that these prisms engage in host–guest interactions with pyrene molecules.

**Scheme 104**



Discrete tetragonal prisms were constructed via a multicomponent coordination-driven self-assembly approach from a combination of a tetraphenylethylene-based tetratopic donor **396**, a linear dipyridine donor, and a  $90^\circ$  platinum metal complex in appropriate stoichiometric ratios in the absence of any template.<sup>460</sup> The 1:2:4 reaction of **396**, 4,4'-bipyridine or (*E*)-1,2-di(4-pyridyl)ethane and **8** in  $\text{CDCl}_3/\text{CD}_3\text{NO}_2$  led to the formation of tetragonal prisms **397** and **398** (Scheme 104). Heteroleptic tetragonal prisms were assembled from tetratopic donor **396** and 5,10,15,20-tetra-4-pyridylporphyrin (tppH<sub>2</sub>) ligand using sodium terephthalate as the pillar with **8** as the acceptor.<sup>439</sup> These heteroleptic prisms can be achieved through supramolecule-to-supramolecule conversion from their homoleptic counterparts. Using this methodology, the self-assembly of supramolecular hexagonal prisms has also been achieved upon mixing a hexakis[4-(4-pyridyl)phenyl]benzene donor ligands and carboxylate donor ligands such as sodium terephthalate, sodium (1,10-biphenyl)-4,4'-dicarboxylate, and sodium 4,4'-(diazene-1,2-diyl)dibenzoate with **8** in a 1:3:6 ratio.<sup>461</sup> Recently, the combination of tetraphenylethylene-based tetratopic donor **396** and ditopic bipyridine or carboxylate ligands functionalized with hydroxyl or amine groups, hydrophobic alkyl chains, or electrochemically active ferrocene was reported to yield a suite of self-assembled tetragonal prisms under mild conditions.<sup>462</sup> These metallacages were characterized by multinuclear NMR ( $^{31}\text{P}$  and  $^1\text{H}$ ) and ESI-MS. Their shapes and sizes were established using molecular force field simulations and PGSE NMR experiments.

**4.2.5. Molecular Boxes.** Tetratopic building units, in combination with a  $90^\circ$  acceptor, may generate several discrete molecular architectures ranging from a trifacial box to higher analogues or even molecular cubes (Figure 35). Though the smallest homologue (trifacial box) is the entropically most preferred isomer, higher analogues like cubes, tetrafacial boxes, and even hexagonal barrels have been reported.

The coordination-driven self-assembly of several trifacial boxes was achieved using rationally designed tetrapyridyl star connectors with  $90^\circ$  platinum linkers.<sup>463</sup> The 1:2 combination of tetratopic planar donors **302**, **392**, **399**, and **400** with *cis*-[Pt(PEt<sub>3</sub>)(OTf)<sub>2</sub>] (**38**) in nitromethane led to the formation of trigonal prisms **401–404** (Scheme 105). This face-directed approach gives high yields without template assistance.

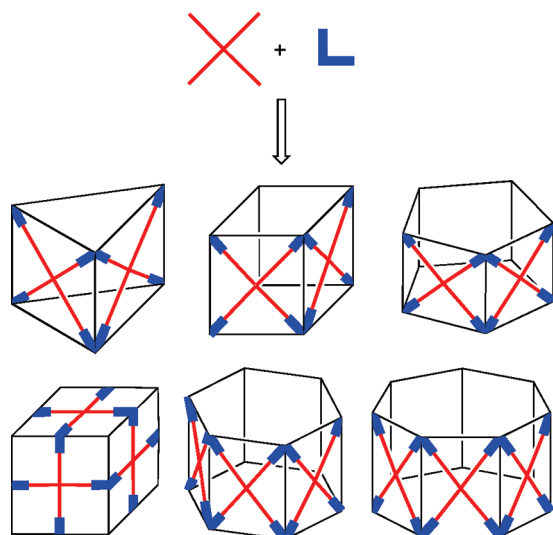
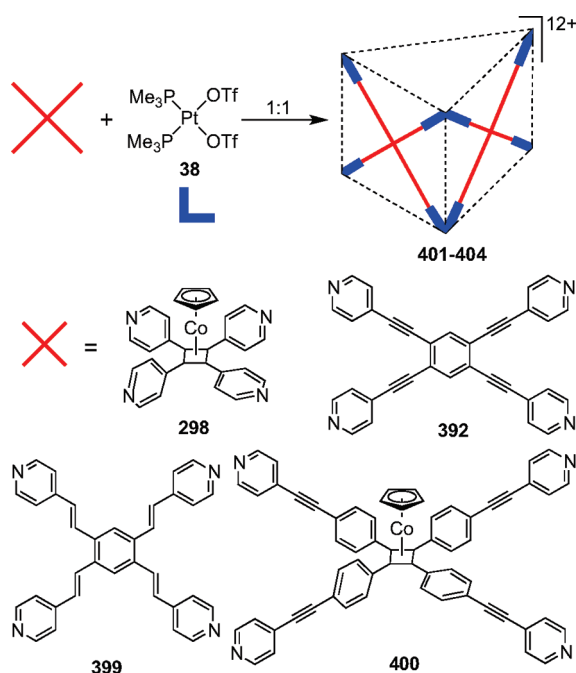


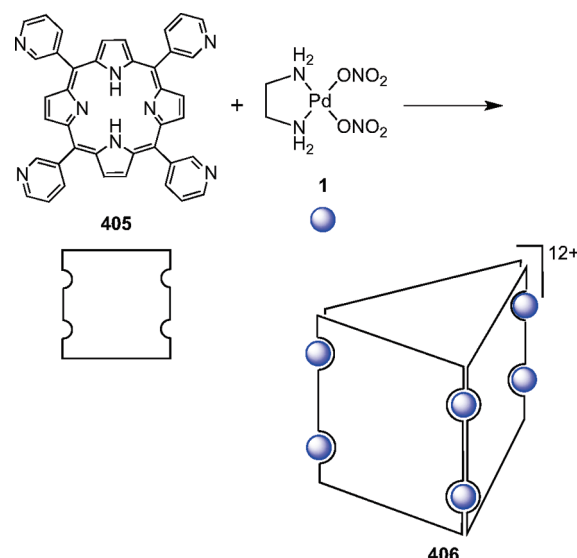
**Figure 35.** Few possible discrete architectures from 1:2 self-assembly of tetratopic donor with 90° acceptor.

**Scheme 105**



Each trifacial box consists of three tetrapyridyl star connectors that span the faces with Pt(II) hinges clipping the vertices. The prisms have been characterized by multinuclear ( $^1\text{H}$  and  $^{31}\text{P}$ ) and DOSY NMR and dual electrospray ionization–Fourier transform–ion cyclotron resonance–mass spectrometry (dual ESI-FT-ICR-MS). The use of a conformationally chiral star connector, **302**, leads to a face-based conformationally chiral prism (**401**) when the connector arm ends attached to a vertex have a strongly correlated twist sense and chirality is communicated across polyhedral faces, edges, and vertices. Molecular mechanics studies suggested that in the smallest trifacial box **401**, collective effects dominate and the all-P and all-M conformers are strongly favored. One-dimensional EXCHSY NMR studies revealed

**Scheme 106**



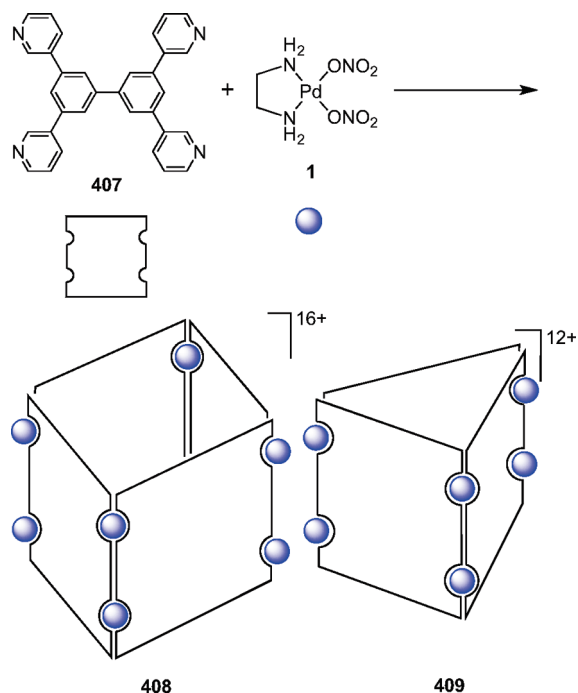
pyridine edge interconversion processes in **401**–**404** compatible with pyridine rotation around the Pt–N bond. Theoretical studies showed that the largest trifacial box, **404**, displayed a highly unusual kinetic behavior during the pyridine ligand rotation.<sup>464</sup>

Fujita and co-workers have employed zinc tetra-3-pyridylporphyrin (**405**) in conjunction with  $[\text{Pd}(\text{en})(\text{NO}_3)_2]$  (**1**) to assemble a  $\text{M}_6\text{L}_3$  trifacial box, (**406**; Scheme 106), utilizing the coordination-driven face-directed self-assembly paradigm.<sup>28</sup>  $^1\text{H}$  NMR, ESI-MS, and X-ray analyses confirmed the formation of the prismatic structure. The crystal structure of **406** showed that the three porphyrin-based ligands span the faces of the prism with six palladium atoms occupying the apical positions. Addition of a pyrene guest molecule for encapsulation triggered a conformational change in host **406** from  $D_{3h}$  to  $C_2$  symmetry. The treatment of a tetrapyridyl rectangular molecular panel, **407**, with **1** at 50 °C for 4 d in  $\text{D}_2\text{O}/\text{CD}_3\text{OD}$  led to the formation of tetrafacial box **408** as the major product (Scheme 107).<sup>465</sup> As determined from NMR and CSI-MS studies, tetrafacial box **408** exists in a dynamic equilibrium with several other products ranging from a trifacial box to a penta-facial box. However, this product equilibrium can be tweaked to favor the quantitative formation of trifacial box **409** through use of biphenyl as a template in the assembly reaction. The use of a 60° donor, 1,2-bis(4-ethynylpyridine)benzene, in combination with  $\text{Pd}(\text{NO}_3)_2$  yielded the solvato-controlled assembly of trifacial  $\text{M}_3\text{L}_6$  and tetrafacial  $\text{M}_4\text{L}_8$  open boxes. Due to the lability of  $\text{Pd}(\text{II})$ –N bonds, a facile interconversion between  $\text{M}_3\text{L}_6$  and  $\text{M}_4\text{L}_8$  boxes was observed by removal or addition of solvent.<sup>466</sup> Addition of  $\text{CD}_3\text{CN}$  to a solution of  $\text{M}_4\text{L}_8$  in  $\text{DMSO}-d_6$  promoted the smooth conversion of complex  $\text{M}_4\text{L}_8$  into a  $\text{M}_3\text{L}_6$  box, as revealed by  $^1\text{H}$  NMR spectroscopy.

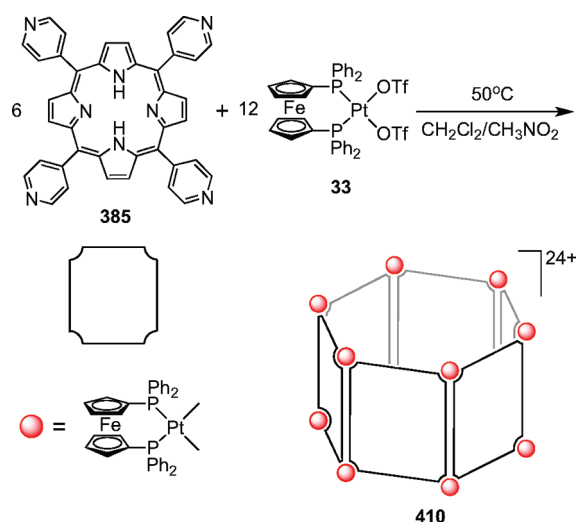
A hexagonal barrel was reported using  $\text{tppH}_2$  (**385**) in combination with a 90° Pt(II) acceptor.<sup>29</sup> The molecular box  $[\{\text{cis}-(\text{dppf})\text{Pt}\}_2(\text{tppH}_2)_6]^{24+}$  (**410**;  $\text{dppf}$  = 1,1-bis(diphenylphosphino)ferrocene) was obtained in quantitative yield by treatment of a solution of  $\text{tppH}_2$  in dichloromethane with 2 equiv of  $\text{cis}[\text{Pt}(\text{dppf})(\text{OTf})_2]$  (**33**) in nitromethane (Scheme 108). NMR and single-crystal X-ray diffraction studies established the exclusive formation of this hexagonal Fe–Pt heterometallic barrel. Structural analysis



Scheme 107



Scheme 108



revealed the formation of a hollow barrel of  $2.7 \text{ nm} \times 2.7 \text{ nm} \times 1.9 \text{ nm}$  dimensions with an internal void volume of around  $13\,550 \text{ \AA}^3$ . In contrast to the self-assembly reactions in which similar tetratopic donors in conjunction with  $90^\circ$  Pt(II) acceptors give trifacial boxes,<sup>463</sup> the use of bulky dppf ligands to cap the  $90^\circ$  Pt(II) acceptor led to the assembly of a wider hexagonal box.

**4.2.6. Molecular Spheres.** A molecular sphere/ball can be formulated as eight trigonal curved surfaces and six square-planar centers. Proper selection of tripodal ligands which can fit on these trigonal faces, in conjunction with square-planar metal centers, may generate molecular balls by an 8:6 face-directed self-assembly. An early example of a coordinatively saturated  $\text{Pd}_6$  molecular ball was reported by Liu and Tong.<sup>467</sup> A flexible tripodal imidazole

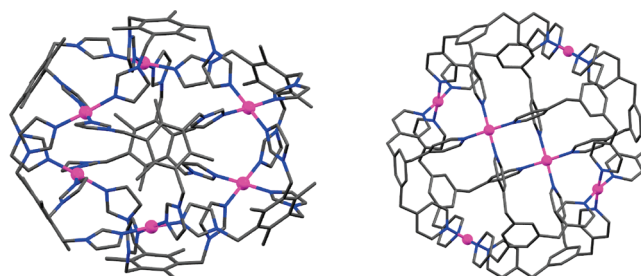
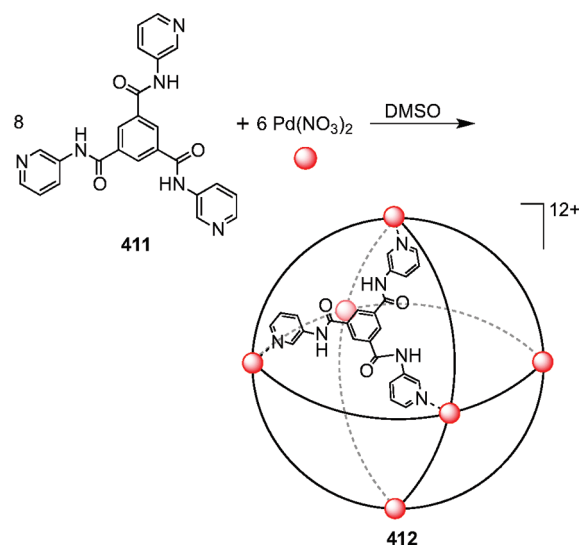


**Figure 36.** Molecular structure of  $\text{M}_6\text{L}_8$  molecular spheres  $[\text{Pd}_6(\text{titmb})_8]^{12+}$  and  $[\text{Pd}_6(322)_8]^{12+}$ . Color code: pink, Pd; blue, N; gray, C.

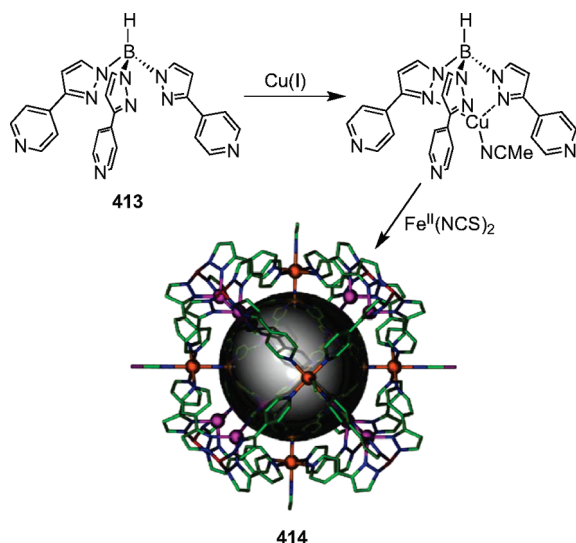
Scheme 109



donor ligand (titmb = 1,3,5-bis(imidazol-1-ylmethyl)-2,4,6-trimethylbenzene) produced a nanometer sized  $\text{M}_6\text{L}_8$  molecular sphere  $[\text{Pd}_6(\text{titmb})_8]^{12+}$  upon treatment with  $\text{PdCl}_2$  (Figure 36). The inner cavity of the ball was determined to be  $1000 \text{ \AA}^3$ , which was enough to accommodate eight  $\text{Cl}^-$  ions inside the ball. Despite the possibility of several conformational isomeric forms due to the flexibility of the ligand, only one configuration was adopted in the structure. An analogous molecular sphere  $[\text{Pd}_6(322)_8]^{12+}$  was reported by Fujita and co-workers using a flexible tripodal pyridyl ligand 1,3,5-tris(4-pyridylmethyl)benzene (322) in combination with  $\text{Pd}(\text{NO}_3)_2$  (Figure 36).<sup>468</sup> The average distance between axially located Pd(II) centers was  $15.2 \text{ \AA}$  and that between equatorial centers was  $10.7 \text{ \AA}$ . The distance between the central benzene rings of the ligands situated at the terminus of the 3-fold axis was  $19.2 \text{ \AA}$ . The same group also prepared a neutral, nanometer-sized metallo-supramolecular sphere  $[\text{Ni}_6(\text{tpst})_8\text{Cl}_{12}]$  (tpst = 2,4,6-tris[(4-pyridyl)sulfanylmethyl]-1,3,5-triazine) from an assembly reaction of  $\text{NiCl}_2$  and the tpst ligand in DMF.<sup>469</sup>

Using a similar approach, a nanosized molecular sphere  $[\text{Pd}_6(\text{tpbc})_8]^{12+}$  **412** (tpbc =  $N,N',N''$ -tri(3-pyridinyl)-1,3,5-benzenetricarboxamide) was reported independently by Lah et al.<sup>470</sup> and Ghosh and Mukherjee<sup>471</sup> using suitably designed  $\text{C}_3$ -symmetric triangular ligands as facial components and  $\text{C}_4$ -symmetric Pd(II) metal ions as corner linkers. Treatment of 4 equiv of tpbc (**411**) with 3 equiv of  $\text{Pd}(\text{NO}_3)_2$  in  $\text{DMSO}-d_6$  led to the quantitative self-assembly of a single product (**412**; Scheme 109) as determined by  $^1\text{H}$  NMR spectroscopic studies.

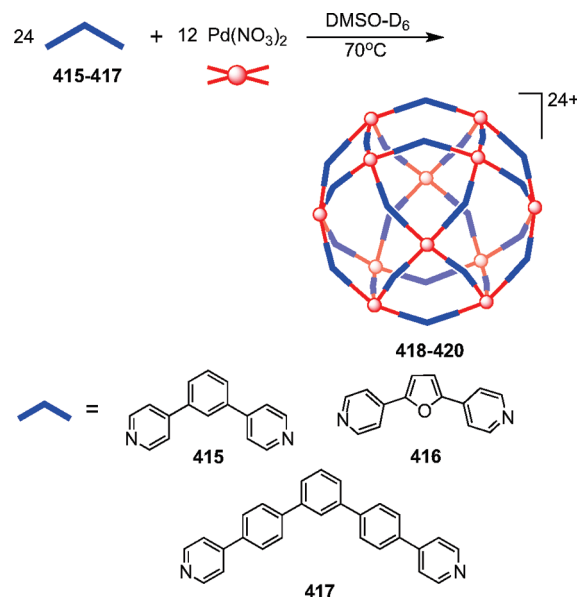
Scheme 110



X-ray crystallographic studies<sup>470</sup> revealed that the nitrogen donor atom at the meta position of the carboxamido pyridinyl group and the tilted pyridyl versus the facial plane of the ligand both provide the needed curvature for the formation of a molecular sphere. Along similar lines, a  $\text{Pd(II)}$ -based molecular sphere,  $[\text{Pd}_6(\text{tppe})_8]^{12+}$ , incorporating ester functionalities, was assembled using a  $\text{C}_3$  symmetric tripodal linker,  $N,N',N''$ -tris(4-pyridylmethyl) trimesic ester (tppe), with  $\text{Pd}(\text{NO}_3)_2$  in a 4:3 molar ratio. NMR, ESI-MS, TEM, and MM2 force-field calculations support the formation of the nanoball with eight trigonal faces occupied by  $\text{C}_3$  symmetric donor linkers. Host–guest studies on molecular sphere  $[\text{Pd}_6(\text{tppe})_8]^{12+}$  showed efficient encapsulation of  $\text{Et}_4\text{N}^+$  cations despite the sphere's high positive charge.<sup>471</sup>

Batten and co-workers<sup>472</sup> have reported a new approach for preparing bimetallic molecular balls using tripodal metalloligands in combination with metal centers of appropriate coordination environments. This efficient, one-pot assembly process involves two distinct steps. First, the central tris(pyrazolyl)hydroborate core of the bifunctional ligand,  $[\text{tris}\{3-(4\text{-pyridyl})\text{-1-pyrazolyl}\}\text{hydroborate}]$  (**413**) is utilized in an in situ, preorganizational step to form the neutral metalloligand  $[\text{Cu}^{\text{I}}(\text{413})(\text{CH}_3\text{CN})]$  (Scheme 110). This building block conformationally locks an otherwise flexible organic ligand, thereby providing directionality to the peripheral 4-pyridyl donor groups for further reaction with an octahedral metal ion. In the second step, crystallization of the discrete nanoball species  $[\{\text{Cu}^{\text{I}}(\text{413})(\text{CH}_3\text{CN})\}_8\{\text{Fe}^{\text{II}}(\text{NCS})_2\}_{10/3}\{\text{Fe}^{\text{II}}(\text{NCS})(\text{CH}_3\text{CN})\}_{8/3}\cdot(\text{ClO}_4)_{8/3}\cdot(\text{CH}_3\text{CN})_n]$  (**414**) occurs by self-assembly upon addition of  $\text{Fe}^{\text{II}}$  ions and a thiocyanate salt. Single-crystal X-ray structural studies revealed that nanoball **414** possesses a rigid  $[\text{Fe}^{\text{II}}\{\text{Cu}^{\text{I}}(\text{413})\}]$  shell in which the octahedral arrangement of  $\text{Fe}^{\text{II}}$  ions and cubic arrangement of  $\text{Cu}^{\text{I}}$  ions forms a distorted rhombic dodecahedron. The fact that  $\text{Fe}^{\text{II}}$  ions exist in two different magnetic environments helps the nanoball reversibly switch between HS and LS states triggered by thermal, light, and guest perturbation. Treatment of metalloligand  $[\text{Cu}^{\text{I}}(\text{413})(\text{CH}_3\text{CN})]$  with a range of divalent metal salts ( $\text{MX}_2$ ) ( $\text{M}^{\text{II}} = \text{Cu}, \text{Mn}, \text{Zn}, \text{Cd}, \text{Fe}$ ;  $\text{X} = \text{ClO}_4^-, \text{NO}_3^-, \text{BF}_4^-$ ) gave a series of nanoballs of the general formula  $[(\text{413})\text{-Cu}^{\text{I}}(\text{MeCN})_8\text{M}^{\text{II}}_6(\text{X})_{10}(\text{MeCN})_2](\text{X})_2 \cdot x\text{MeCN}$ , producing isostructural crystalline samples in a matter of hours.<sup>473</sup>

Scheme 111



These porous nanoballs showed hydrogen gas adsorption as well as solvent adsorption behavior in the solid state.

Unlike the approach used in previous examples of face-directed molecular balls, Fujita and co-workers have revealed a new strategy using edge-directed self-assembly. In this approach, 12  $\text{Pd(II)}$  square-planar metal ions were assembled with 24 units of rigid bent dipyridyl linkers **415–417** to obtain spherical hollow structures **418–420** (Scheme 111).<sup>474</sup>  $^1\text{H}$  NMR and CSI-MS studies confirmed the formation of  $\text{M}_{12}\text{L}_{24}$  molecular spheres. X-ray structural studies on **418** revealed that the spheres have cuboctahedron symmetry in which each of the 12  $\text{Pd(II)}$  atoms occupy the 12 vertices, while the dipyridyl bridging ligands span the 24 edges. Related molecular spheres having cuboctahedral symmetry with copper(II) dinuclear tetracarboxylate junctions have also been reported.<sup>475</sup>

Interestingly, when a ligand analogous to **416**, dipyridylthiophene, was used in conjunction with  $\text{Pd(II)}$  square-planar metal ions, it resulted in the formation of 72-component self-assembled giant  $\text{Pd}_{24}\text{L}_{48}$  coordination spheres using 24 palladium ions ( $\text{Pd}$ ) and 48 curved bridging ligands ( $\text{L}$ ).<sup>476</sup> X-ray crystallographic analysis showed that the  $\text{Pd}_{24}\text{L}_{48}$  coordination sphere (Figure 37) forms a rhombicuboctahedron, which is an Archimedean solid with eight triangular and 18 rectangular faces (26 in total), with one triangle and three rectangles meeting at each vertex. Each of the 48 curved bridging ligands span the edges while 24 metal ions occupy the vertices. Although the ligand dipyridylthiophene differs very little from **416**, the difference in ligand bend angle from  $127^\circ$  in **416** to  $149^\circ$  in dipyridylthiophene, stemming from longer  $\text{C–S}$  bonds ( $1.80 \text{ \AA}$ ) in thiophene as compared with the  $\text{C–O}$  bonds ( $1.39 \text{ \AA}$ ) in furan, accounts for the difference in the final polyhedral geometry. Furthermore, a self-organization study using a mixture of both the bent ligands with  $\text{Pd(II)}$  ions, where the ligand ratio was varied to reflect the continuous modulation of mean ligand angle from  $149$  to  $127^\circ$ , revealed that a slight change in the mean ligand bend angle critically switches the final structure between  $\text{M}_{24}\text{L}_{48}$  and  $\text{M}_{12}\text{L}_{24}$  coordination spheres.

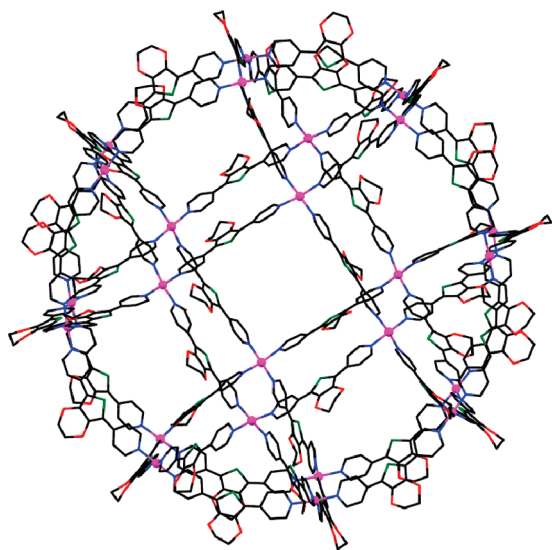


**Figure 37.** X-ray crystal structure of  $\text{Pd}_{24}\text{L}_{48}$ .  $\text{PF}_6^-$  counterions and protons are omitted for clarity. Color code: pink, Pd; red, O; blue, N; green, S; gray, C.

### 4.3. Chiral Systems

Chirality is an inherent property of almost all biomolecules since they are made up of building blocks that are chiral in nature. Almost all biochemical reactions that occur in nature are stereospecific and extremely efficient. Thus, the creation of chiral, 3D spaces for carrying out enantioselective reactions, molecular recognition, and catalysis in confined cavities using natural systems for motivation is a much sought after goal. In recent years, discrete, chiral 3D supramolecules of finite sizes have been assembled by means of weak intermolecular noncovalent interactions<sup>477</sup> as well as metal–ligand coordination.<sup>478</sup> These assemblies have proved themselves as powerful tools to aid in the understanding and exploration of chirality and its effects in host–guest interactions, chemosensing, and enantioselective catalysis.

All Platonic and Archimedean solids, along with prisms and antiprisms, with the exception of snub cube and snub dodecahedra, are inherently achiral. However, chirality can be introduced in these architectures through coordination-driven self-assembly by removing symmetry elements: centers of inversions and mirror planes. This can be achieved through different design strategies: (a) through the use of achiral building blocks where chirality arises at the metal center due to strong mechanical coupling between metal sites through the ligands used, resulting in exclusive homochiral assemblies; (b) using achiral components where chirality is introduced as a consequence of the twisting of the ligands; (c) using enantiopure or racemic scaffolds to assemble chiral supramolecules (the stereogenic center may be incorporated into the organic ligand bridging the metal centers or on an auxiliary ligand); (d) through the encapsulation of a guest molecule within the cavity which perturbs the architecture to lose symmetry elements, thereby making it chiral.

Among the chiral supramolecular architectures, tetrahedral assemblies are perhaps the most extensively studied. Saalfrank et al. reported the earliest example of a chiral supramolecular tetrahedron as described above (section 4.1.1).<sup>329,330</sup> The ternuclear magnesium(II) assembly,  $[(\text{NH}_4)_4\cap\{\text{Mg}_4(\text{L})_6\}]$  (**270**) was formed as a racemic mixture of homochiral  $\Delta\Delta\Delta\Delta$  and

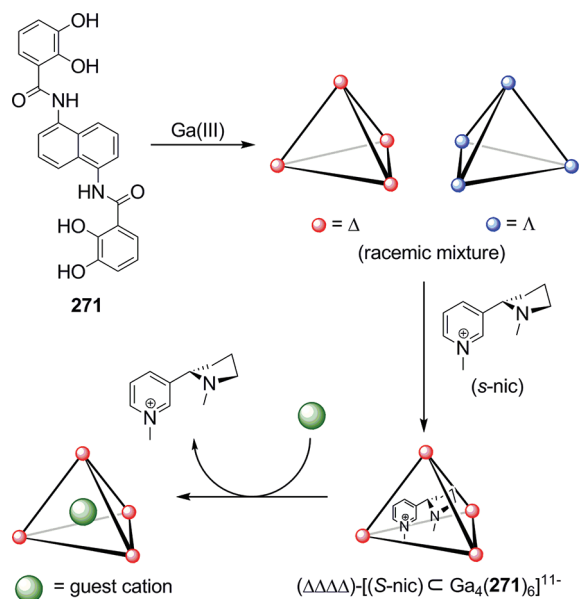
$\Lambda\Lambda\Lambda\Lambda$  ensembles as determined by time-dependent  $^1\text{H}$  NMR spectroscopy. The overall  $T$  symmetry of the ensembles is due to the restricted rotation around the C–C single bonds in the tetracarboxylate ligands, which make the ligands twist in the same sense when coordinating to the four metal centers.<sup>329</sup> The replacement of the R group in the tetracarboxylate ligand (Scheme 77) with hydrogen results in isosturctural homochiral  $\Delta\Delta\Delta\Delta$  and  $\Lambda\Lambda\Lambda\Lambda$  assemblies.<sup>479</sup> Variable-temperature  $^1\text{H}$  NMR studies revealed that the assembly undergoes nondissociative enantiomerization from  $\Delta\Delta\Delta\Delta$  to  $\Lambda\Lambda\Lambda\Lambda$  symmetry without the formation of diastereomeric intermediates.<sup>480</sup> The interconversion involves four simultaneous Bailar twists associated with  $(\Delta)/(\Lambda)$  isomerization at the four octahedral metal centers that are synchronized with the atropenantiomerization process on the four sterically unhindered ligands. When a bulky R group such as  $\text{CO}_2\text{Et}$  in the tetracarboxylate ligand is present, a restriction of the rotation around the central C–C bond in  $\text{L}^{2-}$  occurs, thereby preventing enantiomerization.

Raymond and co-workers designed a series of chiral  $\text{M}_4\text{L}_6$  tetrahedra based on bis-hydroxamate<sup>334,335</sup> and bis-catecholate<sup>336</sup> ligands through the symmetry interaction approach. As described above (section 4.1.1), these tetrahedral anionic cages were assembled from four metal ions such as Ga(III), Al(III), In(III), Fe(III), Ti(IV), Ge(IV), and Sn(IV), which are coordinated by six bifunctional bis-chelating ligands spanning along the edges of the tetrahedra. The chiral environment of the cavities was probed using a monocationic ruthenium(II) half-sandwich complex  $[\text{CpRu}(p\text{-cymene})]^+$  as a guest molecule.<sup>481</sup> The two enantiotropic methyl groups of the isopropyl substituent of *p*-cymene become diastereotopic upon binding with the chiral host and are thus distinguishable, as evidenced by NMR spectroscopy. This implies that the guest is increasingly able to sense the chiral environment of the host molecule.

Though the bis-chelating ligands are achiral in nature, the chirality in these tetrahedral assemblies results from the trisbidentate coordination at each metal center, leading to either a  $\Delta$  or  $\Lambda$  configuration. Due to strong mechanical coupling between the metal centers through the ligands, the chirality is communicated from one vertex to the next, resulting exclusively in homochiral tetrahedra (with either  $\Delta\Delta\Delta\Delta$  or  $\Lambda\Lambda\Lambda\Lambda$  configuration). Depending on the chiralities at the metal centers, these clusters can have idealized  $\text{C}_3$  ( $\Delta\Lambda\Lambda\Lambda/\Lambda\Delta\Delta\Delta$ ),  $\text{S}_4$  ( $\Delta\Delta\Delta\Lambda$ ), or  $T$  ( $\Delta\Delta\Delta\Delta/\Lambda\Lambda\Lambda\Lambda$ ) symmetry. However, the use of achiral components almost always leads to racemic chiral supramolecules due to the lability of the metal–ligand bonds, which facilitate interconversion of the enantiomers. These racemates can be enantiomerically resolved through use of a chiral auxiliary molecule. For example, as shown in Scheme 112, the tetrahedral assembly  $[\text{Ga}_4(\text{271})_6]^{12-}$  preferentially precipitates the diastereomeric ion pair of  $(\Delta\Delta\Delta\Delta)\text{-KH}_3(\text{S-nic})_7[(\text{S-nic}) \subset \text{Ga}_4(\text{271})_6]$  when treated with chiral auxiliary (S)-N-methylnicotinium (S-nic), leaving the soluble  $\Lambda\Lambda\Lambda\Lambda\text{-K}_6(\text{S-nic})_5[(\text{S-nic}) \subset \text{Ga}_4(\text{271})_6]$  species in solution.<sup>482,483</sup> The chiral auxiliary S-nic can then be replaced through ion exchange by an achiral guest cation such as  $\text{NMe}_4^+$  or  $\text{NEt}_4^+$ . The mechanism for chiral resolution of the  $\text{M}_4\text{L}_6$  tetrahedron was shown to be proton-dependent and relies on interactions of the chiral S-nic<sup>+</sup> counterion with the exterior of the anionic host. Interestingly, the  $\text{M}_4\text{L}_6$  tetrahedron  $[\text{NEt}_4 \subset \text{Ga}_4(\text{271})_6]^{11-}$  (**272**) retains the “chiral structural memory”.<sup>484</sup> In a solution of  $(\Delta\Delta\Delta\Delta)\text{-}[\text{NEt}_4 \subset \text{Ga}_4(\text{271})_6]^{11-}$ , as many as three of the six-edge bridging ligands can be replaced by phenyl derivatives while maintaining the original chirality.



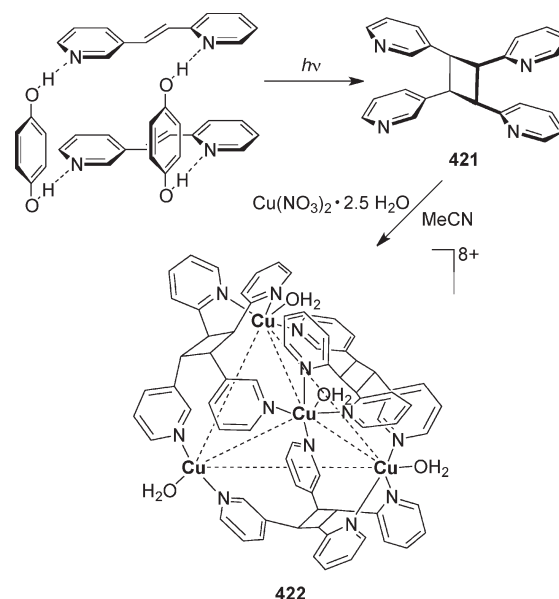
Scheme 112



McCleverty, Ward, and co-workers have assembled chiral  $M_4L_6$  tetrahedral clusters using flexible bispyrazolylpyridine ligands having a central aromatic spacer between the binding sites.<sup>340</sup> These cationic cages are chiral, having noncrystallographic  $T$  symmetry with all four metal centers possessing the same tris-chelate optical configuration with a  $C_3$  axis running through each vertex but no mirror planes.<sup>345</sup> X-ray structural studies have shown that the assemblies crystallize as a racemic homochiral mixture with equal numbers of  $\Delta\Delta\Delta\Delta/\Lambda\Lambda\Lambda\Lambda$  enantiomers. The chiropticity of the internal cavities of the tetrahedral cages of the type  $[Co_4(274)_6(BF_4)]^{7+}$  can be probed by using an enantiopure chiral solvating agent [tris(tetrachlorocatecholato)phosphate(V)] (TRISPHAT).<sup>485</sup> Addition of 2 TRISPHAT  $\Delta$ -1, to a solution of racemic mixtures of  $\Delta\Delta\Delta\Delta$  and  $\Lambda\Lambda\Lambda\Lambda$  enantiomers of  $[Co_4(274)_6(BF_4)]^{7+}$  in 5%  $CD_3NO_2$  in  $CDCl_3$  led to the enantiodifferentiation of the protons of the ligands. The  $^{19}F$  NMR signal (a singlet) for the encapsulated achiral  $BF_4^-$  anion also gets split into two peaks with a separation of 2 ppm between the components arising from the two diastereoisomers. The chiral environment can thus be detected through the enantiodifferentiation of an achiral guest in the chiral cavity. In an alternative approach, diastereoselective formation of a chiral tetrahedral cage has been achieved using a ligand in which a chiral auxiliary,  $\alpha$ -pinene, was appended to a similar flexible bispyrazolylpyridine ligand, having a central 1,2-phenyl aromatic spacer.<sup>486</sup> As evidenced from its  $^1H$  NMR spectrum, the cage exists as a single diastereoisomer in solution and crystallizes as a single diastereoisomer in the acentric space group  $C_2$ .

A number of chiral  $M_4L_4$  tetrahedral cages have been assembled from tris-bidentate chelating ligands and pseudo-octahedral metal ions by the groups of Raymond,<sup>354,358</sup> Saalfrank,<sup>355</sup> Ward,<sup>356,357</sup> and Albrecht.<sup>359,360</sup> The  $C_3$ -symmetric ligands in these cages span the faces of  $M_4L_4$  tetrahedra with octahedral metal ions occupying the vertices. The chirality in these tetrahedral assemblies originates from the tris-bidentate metal chelates, where each metal center can adopt a  $\Delta$  or  $\Lambda$  configuration within each tetranuclear structure. As a result, a  $M_4L_4$  tetrahedron can adopt  $T$  ( $\Delta\Delta\Delta\Delta$  or  $\Lambda\Lambda\Lambda\Lambda$ ),  $C_3$  ( $\Delta\Delta\Delta\Lambda$  or  $\Lambda\Lambda\Lambda\Delta$ ), or  $S_4$

Scheme 113



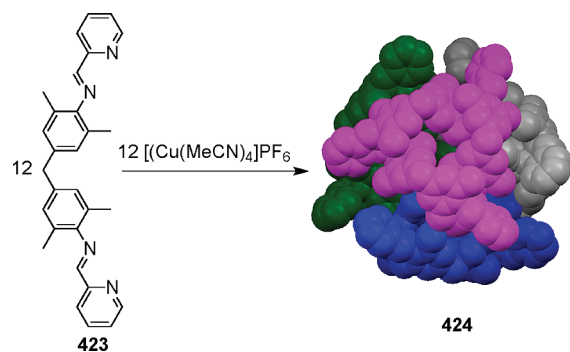
( $\Delta\Delta\Delta\Lambda$ ) symmetry. The chiral induction studies carried out on  $[Ga_4(278)_4]^{12-}$  showed that the chiral auxiliary  $S$ -nic can induce an enantiomeric excess in a racemic population of  $[Ga_4(278)_4]^{12-}$  tetrahedra.<sup>358</sup> Larger  $M_4L_4$  clusters from analogous tris-bidentate chelating ligands having phenylene spacers fail to show enantiomeric enrichment due to the rotational freedom of the phenylene spacers in the ligand.

Achiral tetratopic ligands derived from hydrogen bond-directed solid-state synthesis have also been used to assemble chiral polyhedral cages. A linear template based on resorcinol was used to direct a regiocontrolled synthesis of tetrapyrrolic ligand **421** from *trans*-1-(2-pyridyl)-2-(2-pyridyl)ethylene.<sup>487</sup> Addition of an acetonitrile solution of **421** to an acetonitrile solution of  $Cu(NO_3)_2 \cdot 2.5 H_2O$  led to the formation of a chiral tetrahedral assembly  $[Cu_4(421)_4(H_2O)_4]^{8+}$  (**422**; Scheme 113). X-ray structural studies revealed that each of the four  $Cu(II)$  ions occupies a corner of the tetrahedron. Similar tetratopic ligands derived from *trans*-1-(2-pyridyl)-2-(4-pyridyl)ethylene have earlier been shown to assemble with  $Cu(II)$  ions to form a hexanuclear cage structure that conforms to a trigonal antiprism.<sup>488</sup>

Chiral molecular assemblies have also been achieved using achiral components in which chirality arises as a consequence of the way the organic ligands are twisted in space. For example, Robson et al.<sup>489</sup> and Müller et al.<sup>490</sup> reported chiral truncated tetrahedra having  $M_6L_4$  stoichiometries utilizing guanidine-based ligands. The chirality in these assemblies originated from the screwlike orientation of the ligands upon coordination to the metal centers at each face of the tetrahedra. The reaction of  $CdCl_2$  with tris[(*S*-bromo-2-hydroxybenzylidene)amino]guanidinium chloride,  $[H_6Br_3L]Cl$  in methanol in the presence of  $Et_4NCl$ , and  $Et_3N$  led to the formation of chiral  $M_6L_4$  tetrahedra.<sup>490</sup> X-ray structural studies revealed that each cadmium atom lies in a square-pyramidal center with three of the basal coordination sites occupied by a ligand and one  $Cl^-$ . The fifth site was occupied by a phenolate oxygen atom from the neighboring  $[(CdCl)_3-(H_6Br_3L)]$  triangular panel, formed upon the binding of three  $CdCl$  units. This led to the formation of the chiral cage



Scheme 114



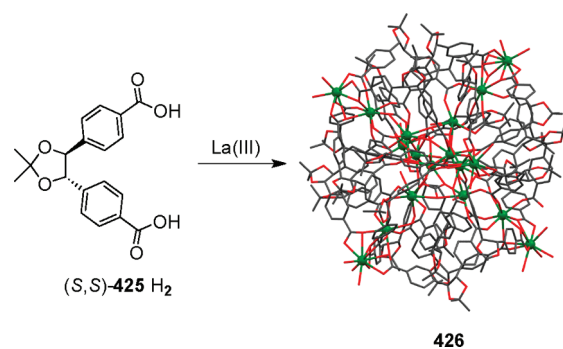
$(\text{Et}_4\text{N})_5(\text{Et}_3\text{NH})_3[\{(\text{CdCl})_3(\text{H}_6\text{Br}_3\text{L})\}_4]$ . Of the eight counterions, one  $[\text{Et}_4\text{N}]^+$  gets trapped in the cavity of the tetrahedron. These guanidine-based ligands have also been used to assemble a chiral trigonal bipyramid<sup>491</sup> and a molecular octahedron  $[\{\text{Pd}_3\text{L}\}_8\{\mu\text{-(bar)}\}_{12}]^{16-}$  (310).<sup>388</sup>

Hannon and co-workers<sup>492</sup> have reported the assembly of a  $\text{M}_{12}\text{L}_{12}$  chiral ball (424) from bis-bidentate ligand 423 and Cu(I) ions. X-ray structural studies revealed that three bis-bidentate ligands (423) assembled to form a chiral trinuclear circular helicate  $\{\text{Cu}_3(\text{423})_3\}^{3+}$  with a Cu(I) ion occupying the vertices of the triangle in a four-coordinate pseudotetrahedral environment. Four of these bowl-shaped circular helicates  $\{\text{Cu}_3(\text{423})_3\}^{3+}$  aggregate to form a tetrameric ball-shaped molecular assembly  $[\{\text{Cu}_3(\text{423})_3\}_4]^{12+}$  (424) held together by  $\text{CH}-\pi$  interactions (Scheme 114). The chirality of each triangular circular helicate makes the overall ball-shaped structure chiral. The chirality of 424 is due to the propeller-type twist arrangement of the pyridyl rings of each triangle.

Molecular scaffolds that are intrinsically chiral have been used as both enantiopure and racemic mixtures to assemble chiral supramolecular assemblies. The chiral center may be introduced into the bridging ligand and/or on the auxiliaries attached to the metal center. Using the directional bonding approach,  $\text{M}_6\text{L}_4$  adamantanoids have been assembled using enantiopure chiral building blocks having stereogenic centers in their carbon backbones. For example, the presence of a chiral center on the ligand backbone makes adamantanoids 341 and 324 chiral.<sup>406</sup> Their stereogenic centers reduce the overall symmetry of the adamantanoids from  $T_d$  symmetry, as expected for achiral species, to  $D_2$  symmetry. A racemic mixture of binaphthalene-based ligands with lanthanide salts led to chiral adamantanoids having perfect  $T$  symmetry, as a result of the  $\text{C}_2$ -symmetric nature of the ligand and  $\text{C}_3$ -symmetric lanthanide centers.<sup>408</sup> Cui et al.<sup>493</sup> reported the synthesis of distereoselective tetrahedral cages using the enantiopure atropisomeric biphenyl bridging ligand 5,5',6,6'-tetramethyl-3,3'-diketone-2,2'-bis(methoxy-methoxy)biphenyl and  $\text{C}_3$ -symmetric metal ions. A 3:2 molar reaction of the bridging ligand with  $\text{M}(\text{III})$  chloride ( $\text{M} = \text{Fe}, \text{Ga}$ ) in DMF, followed by layering the solution with methanol, afforded the homochiral ( $\Delta\Delta\Delta\Delta$ ) or ( $\Lambda\Lambda\Lambda\Lambda$ )  $\text{M}_4\text{L}_6$  tetrahedral cages in moderate yields. These cages demonstrated a high enantioselective ability to resolve small racemic alcohols by crystallization inclusion.

Jeong et al.<sup>494</sup> reported a chiral nanoball encapsulating lanthanum ions in a ferritin-like assembly. The enantiopure carboxylate ligand (S,S)-425, synthesized from 4,4'-dibromostilbene through

Scheme 115

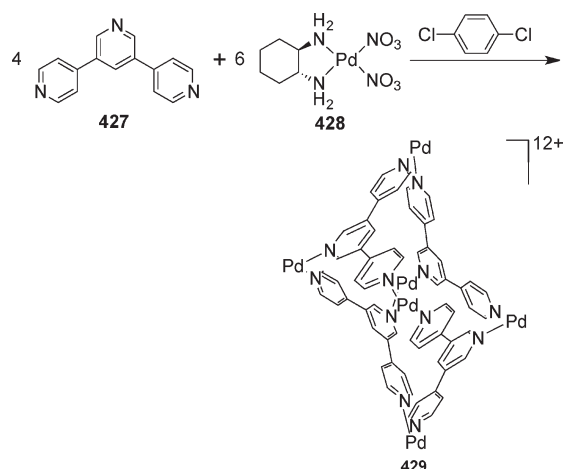


Sharpless asymmetric dihydroxylation, assembled into a molecular cluster having the formula  $[\text{La}_{18}\{(\text{S,S})\text{-425}\}_{24}(\text{CO}_3)_2(\text{H}_2\text{O})_{32}]^{2+}$  (426; Scheme 115) in the presence of  $\text{LaCl}_3 \cdot 6\text{H}_2\text{O}$ . X-ray structural studies showed that 24 ligands encompass 18 metal ions in the assembly. The ball consists of six  $\text{La}_3[(\text{S,S})\text{-425}]_4$  units which are related by pseudo-octahedral symmetry. Each unit is further interconnected with another four equatorial units by four organic ligands, completing the assembly. These ferritin-like chiral assemblies form double helices in the solid state with single-handedness.

Stang and co-workers<sup>365</sup> were able to assemble chiral  $\text{M}_6\text{L}_4$  truncated tetrahedra by introducing stereogenic centers on the auxiliary ligands attached to metal donor units. A 3:2 combination of  $[\text{M}(\text{R-BINAP})(\text{OTf})_2]$  ( $\text{M} = \text{Pd}$  (177) or  $\text{Pt}$  (178), BINAP = 2,2'-bis(diphenylphosphino)-1,1'-binaphthalene) and tridentate ligand 1,3,5-tris[(4-pyridyl)ethynyl]benzene (291) led to the formation of an assembly having a truncated tetrahedral geometry with  $T$  symmetry. Both NMR and ESI-FT-ICR-MS studies established the formation of these assemblies. Similarly, utilizing the  $[(\text{R})\text{-}(+)\text{-BINAP}]\text{Pd}(\text{II})$  bistriflate as a chiral donor unit, Ikeda et al.<sup>495</sup> assembled Zn-based porphyrins bearing four pyridyl groups into a chiral  $\text{M}_4\text{L}_2$  square-prismatic supramolecule possessing  $D_{4h}$  symmetry. Chirality in these assemblies arises due to the chiral auxiliaries present on the periphery of each cage. Fujita et al.<sup>496</sup> have used chiral (R,R)-diaminocyclohexane as an auxiliary attached to a Pd(II) center to assemble  $\text{C}_2$  chiral  $\text{M}_6\text{L}_4$  truncated tetrahedra. A chiral  $\text{M}_6\text{L}_4$  cage, 429, was assembled from the  $D_{2h}$ -symmetric pyridyl ligand, 427, with  $90^\circ$  *cis*-[(R,R)-diaminocyclohexane] $\text{Pd}(\text{NO}_3)_2$  (428) in the presence of 1,4-dichlorobenzene (Scheme 116). The self-assembly process was driven by the template-effect of the aromatic guest molecule.  $^1\text{H}$  NMR studies revealed the formation of two diastereomers in a 1.3:1 ratio. With (S,S)-diaminocyclohexane auxiliary ligands, the resulting assembly showed a negative Cotton effect.

Chirality in a supramolecular assembly can also be induced through encapsulation of guest molecules into the achiral assembly, triggering a conformational change from achiral to chiral. Hiraoka and Fujita observed that the inclusion of flat, achiral 1,3,5-benzenetricarboxylic acids as guest molecules distorts trigonal-bipyramidal cage 323 (Scheme 85) into a chiral cage.<sup>497</sup> The chirality of this asymmetric cage was shown by complexation of *R*-mandelic acid, which induces diastereomeric organization resulting in *P*- and *M*-cages. Furthermore, the observation of two diastereomers also indicated that no racemization takes place on the NMR time scale. Notably, diastereomers

Scheme 116



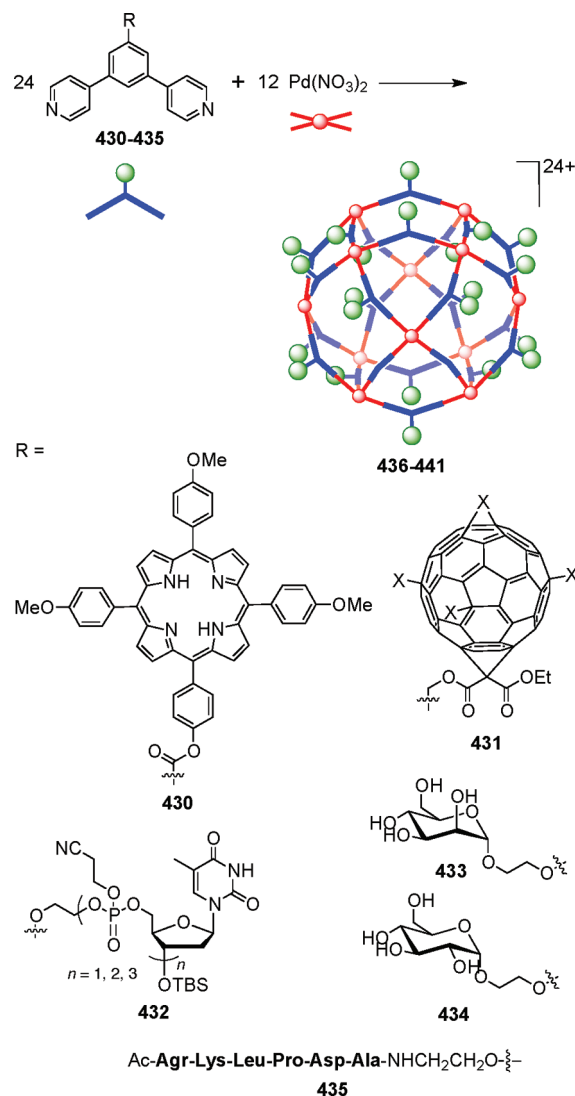
were not observed when racemic mandelic acid was used. Encapsulation of a spherical guest such as  $\text{CBrCl}_3$  or  $\text{CBr}_4$  led to the formation of an achiral trigonal-bipyramidal cage under similar conditions. This was explained through molecular modeling studies wherein it was observed that the asymmetric cage possesses flat internal cavities while the symmetric cage possesses spherical cavities. The same group also observed a conformational change from  $D_{3h}$  symmetry to  $C_2$  symmetry in a porphyrin-based  $\text{M}_6\text{L}_3$  trifacial box (**406**; Scheme 106) upon encapsulation of pyrene as a guest molecule.<sup>28</sup>

#### 4.4. Functionalized Systems

The functionalization of 3D supramolecular assemblies has been intensively investigated over the past few years with an aim to develop nanoscale ensembles that can emulate biological systems and can find applications in various fields such as host–guest chemistry, cavity directed synthesis, catalysis, photonics, redox activity, magnetic behavior, self-organization, and sensing.<sup>230</sup> Although various functionalized nanoscopic systems have been developed through conventional covalent synthesis, when issues such as the control of functional groups and structural precision, the ability to perform selective encapsulation, and synthetic ease and building-block versatility come into question, coordination-driven self-assembly emerges as a powerful tool to assemble 3D functional supramolecules with relative ease. The conformational rigidity of supramolecular ensembles allows for greater structural control and positioning of functional groups on the tectons to form novel, multifunctional structures. Precise control over the number, location, orientation, and relative distribution of functional moieties is possible in these systems. Using the directional bonding approach, functional groups have been introduced both on the exterior and interior of supramolecules.<sup>231</sup>

Exo-functionalization of metallacages can be achieved by the attachment of a functional moiety on the convex side of a building block. This positions the groups on the periphery of the resulting self-assembled suprastructure. Fujita and co-workers have designed a number of  $\text{Pd}_{12}\text{L}_{24}$  exo-functionalized molecular spheres (Scheme 117) decorated with many different functional groups on the surface by simply attaching the desired moiety to the convex dipyrindyl ligands (**430**–**435**). In one early example, metal porphyrins and fullerene nanoballs were introduced on the periphery of a  $\text{Pd}_{12}\text{L}_{24}$  sphere (**436** and **437**).<sup>474</sup>

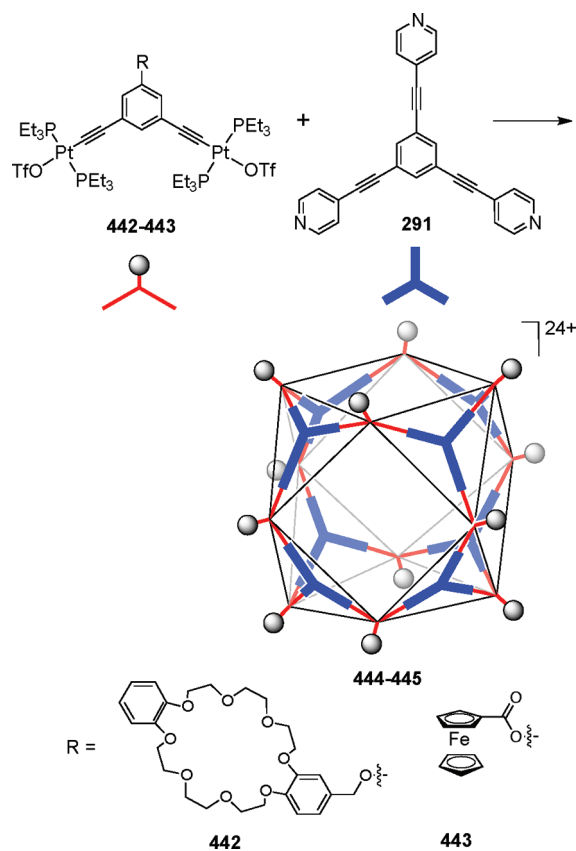
Scheme 117



Similarly, attachment of saccharide groups at the periphery led to saccharide-coated  $\text{Pd}_{12}\text{L}_{24}$  molecular spheres that form aggregates upon interaction with proteins.<sup>498</sup> Studies with concanavalin A, which is a well-known lectin that selectively recognizes  $\alpha$ -mannopyranoside and  $\alpha$ -glucopyranoside at its four binding sites, showed the formation of aggregates with  $\alpha$ -mannopyranoside- and  $\alpha$ -glucopyranoside-coated  $\text{Pd}_{12}\text{L}_{24}$  spheres **439** and **440**, respectively, but not with  $\alpha$ -galactopyranoside- or  $\beta$ -glucopyranoside-coated ones, indicating that concanavalin A can recognize the terminal saccharide units of  $\text{Pd}_{12}\text{L}_{24}$  molecular spheres. Recently, the same group also reported the facile preparation of self-assembled  $\text{Pd}_{12}\text{L}_{24}$  spherical complexes **438** and **441** with their surface modified with oligonucleotide chains<sup>499</sup> and hexapeptide aptamers (Arg–Lys–Leu–Pro–Asp–Ala), respectively.<sup>500</sup> The oligonucleotide-coated spheres can recognize complementary nucleobases through Watson–Crick base pair formation. These well-defined DNA nanoparticles templated by self-assembled  $\text{Pd}_{12}\text{L}_{24}$  molecular spheres may lead to systems that can recognize natural DNA in aqueous media.

Stang et al. reported the construction of multifunctional cuboctahedra having crown ether and ferrocene as functional groups

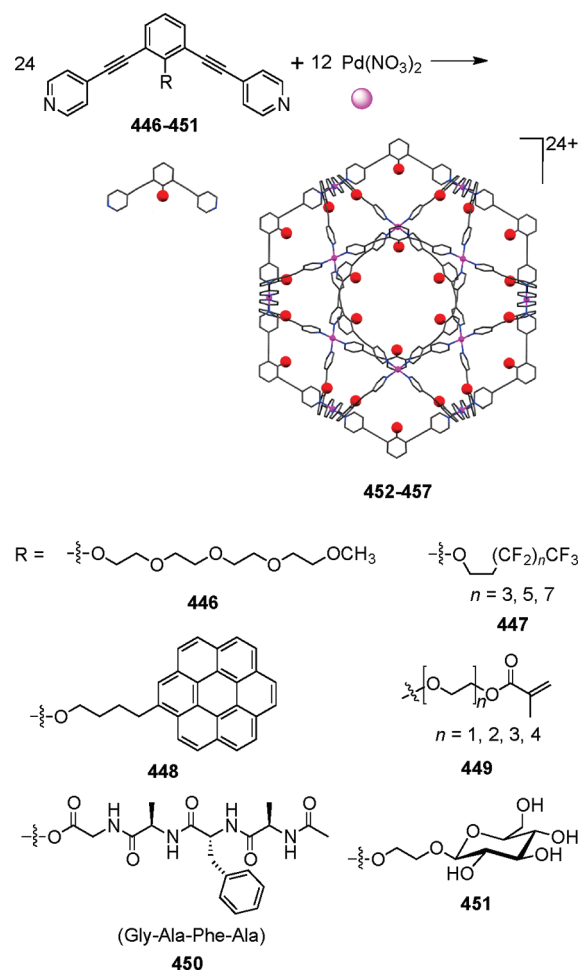
Scheme 118



on the periphery (Scheme 118).<sup>501</sup> Treatment of 120° exo-functionalized acceptors **442** and **443** with the planar tritopic donor 1,3,5-tris(4-pyridylethynyl)benzene (**314**) in 3:2 resulted in the formation of cuboctahedral complexes **444** and **445** with 12 pendant crown ether or ferrocene groups, respectively, at the vertices. Multinuclear NMR (<sup>1</sup>H and <sup>31</sup>P), ESI-MS, and cyclic voltammetric studies established the structures of the complexes. Both functionalized supramolecular systems were obtained in high yield and all of the functional units retained their functional fidelity while surrounding a nanoscopic hollow “core” environment ideal for guest encapsulation. The multiferrocenyl cuboctahedron molecule shows a single redox couple indicating that the redox species react more or less independently of one another. These assemblies may find uses as multielectron catalysts and sensors. Also, the complementary recognition properties of the peripheral crown ether hosts and the interior cavity of the crown ether functionalized cuboctahedron may be used to develop both an exo and endo receptor.

Endohedral functionalization of supramolecular architectures can be achieved by covalently attaching a functional moiety on the concave side of a directional building block, precisely orienting the group inward. Fujita et al. assembled a variety of discrete, endo-functionalized Pd<sub>12</sub>L<sub>24</sub> molecular spheres (**452–457**) by combining 12 naked Pd(II) ions with 24 bis-4-pyridyl ligands (**446–451**) involving two acetylene spacers (Scheme 119). The acetylene spacers play an important role in the overall architecture of the resulting ensembles. In addition to providing a larger cavity space as compared to that in exohedral Pd<sub>12</sub>L<sub>24</sub> cages assembled using dipyridyl ligands **430–435**, the

Scheme 119



acetylene spacers prevent the ligands from adopting unfavorable nonplanar conformations, which are caused by steric repulsion between the pyridyl groups and the core benzene ring in the absence of the spacer. The large cavities of the Pd<sub>12</sub>L<sub>24</sub> molecular spheres allow for the introduction of a variety of pendant functional moieties such as oligo(ethylene oxide) chain (**452**),<sup>502</sup> perfluoroalkyl chain (**453**),<sup>503</sup> extended aromatic system (**454**),<sup>504</sup> polymerizable methyl methacrylate (**455**),<sup>505</sup> sodium *p*-styrene-sulfonate units,<sup>506</sup> peptide (**456**),<sup>507</sup> and sugar (**457**) lining the interior surface. The well-defined nanoscale cavities of these functionalized assemblies have helped in the understanding and illustration of interesting properties otherwise not observable under standard conditions. For example, the attachment of perfluoroalkyl chains generated a fluorophilic nanophase within the cavity, allowing it to solubilize up to approximately eight perfluoroalkane molecules per spherical complex. Their solubility can be tuned by varying the length of the pendant perfluoroalkyl chains.<sup>503</sup> Lining the inner surface with extended aromatic systems such as coronene created an aromatic nanophase resulting in increased solubility of fullerenes, which are sparingly soluble in most solvents.<sup>504</sup> Fujita and co-workers also prepared Pd<sub>12</sub>L<sub>24</sub> molecular spheres (**455**) that can confine 24 methyl methacrylate (MMA) units at their internal cavities.<sup>505</sup> These monomer units can be polymerized to PMMA through radical polymerization using 2,2'-azobis(isobutyronitrile) (AIBN) as a

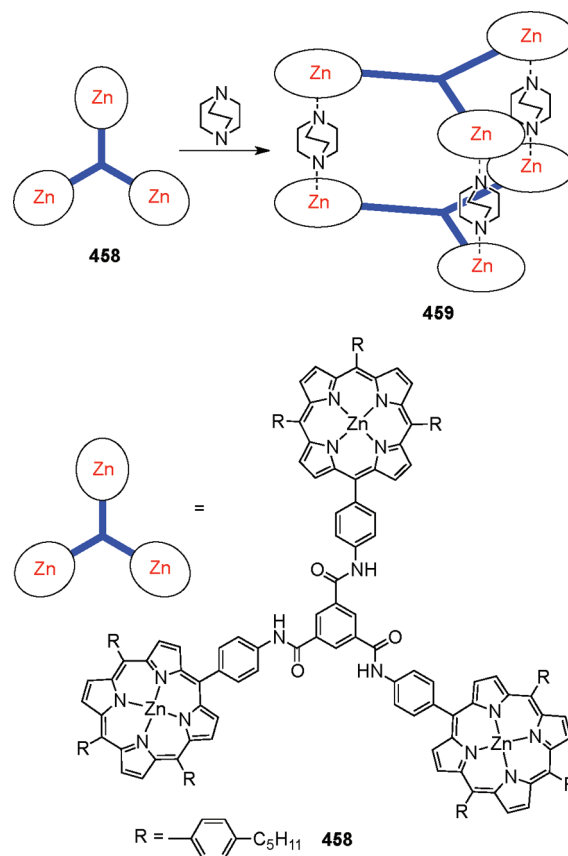
radical initiator. The sphere with tri(ethylene oxide) linkers afforded the best efficiency, with 73% conversion. These nanomolecular materials may find applications as high-density data storage materials.

One of the key challenges in materials science is to gain a high degree of control over the size and shape of nanoparticles. Recently, Fujita and co-workers<sup>508</sup> succeeded in restricting the size and shape of growing silica nanoparticles by using a Pd<sub>12</sub>L<sub>24</sub> molecular cage (**457**) whose inner surface was lined with sugar residues, creating an environment for the sol–gel condensation of tetramethoxysilane. The hydrophilic cavity of the cage served as an endo-template for the condensation process to give monodispersed silica nanoparticles with diameters of 2–4 nm relative to the dimensions of the Pd<sub>12</sub>L<sub>24</sub> spheres (2–4 nm). As monitored by NMR spectroscopy, signals corresponding to free siloxane disappeared during the reaction, whereas a signal arising from methanol appeared and increased in intensity, indicating the formation of condensation products. The sol–gel condensation process took place within the endo-template rather than on the bulk solvent, as evidenced by the homogeneity of the solution. Remarkably, the polydispersities of the silica nanoparticles achieved with this method approached unity, with  $M_w/M_n < 1.01$ . Recently, the Pd<sub>12</sub>L<sub>24</sub> molecular cage **457**, whose inner surface was lined with sugar residues, was also utilized to generate core–shell SiO<sub>2</sub>/TiO<sub>2</sub> and SiO<sub>2</sub>/ZrO<sub>2</sub> nanoparticles with high monodisperse molecular weight distributions ( $M_w/M_n < 1.01$ ) as characterized by TEM and MS analyses.<sup>509</sup>

Similarly, tethering of azobenzene units<sup>510</sup> created a confined and well-defined hydrophobic phase inside the cavity of a Pd<sub>12</sub>L<sub>24</sub> self-assembled spherical complex. The hydrophobicity of the cavity can be switched through the photoisomerization of appended azobenzene chromophores. Azobenzenes are well-known to undergo *cis*–*trans* isomerization upon irradiation with UV light resulting in large changes in size and polarity. The use of a hydrophobic guest, 1-pyrenecarboxaldehyde, as a probe showed that the hydrophobic environment of the confined cavity becomes less hydrophobic due to the reversible isomerization of tethered azobenzene. Likewise, lining the inner surface of a Pd<sub>12</sub>L<sub>24</sub> cage with alkyl chains<sup>511</sup> allowed the solubilization of hydrophobic dyes such as Nile red in polar solvents.

Recently, endo-functionalized Pd<sub>12</sub>L<sub>24</sub> (L = 2,6-bis(4-pyridylethynyl)toluene) molecular spheres were shown to assemble into large, monolayered, hollow, vesicle-like blackberry structures in polar solvents.<sup>512</sup> As established from laser-light scattering studies, these Pd<sub>12</sub>L<sub>24</sub> cationic cages self-assemble into larger structures in DMSO-*d*<sub>6</sub> mediated by both electrostatic and hydrophobic interactions similar to viral-capsid formation in biological systems. A continuous increase in total scattered intensity from the solution in static light scattering (SLS) studies indicated the formation of large self-assembled structures. Dynamic light scattering (DLS) studies revealed that the large assemblies have a narrow size distribution. The very similar values of average radius of gyration ( $R_g$ ) and average hydrodynamic radius ( $R_h$ ) obtained from light-scattering studies indicated the formation of large hollow spherical structures. Like viral-capsids, these assemblies form monolayer spheres with individual nanocages evenly distributed in the wall of the vesicle-like structures. The vesicle-like structures formed by the nanocages also responded to external stimuli (i.e., ionic strength and solvent polarity) and subsequently changed their sizes. Similar spontaneous self-assembly of M<sub>4</sub>L<sub>6</sub> truncated tetrahedral cages [(en)Pd<sub>6</sub>L<sub>4</sub>](NO<sub>3</sub>)<sub>12</sub> (**286**, L = 2,4,6-tris(4-pyridyl)triazine)

Scheme 120



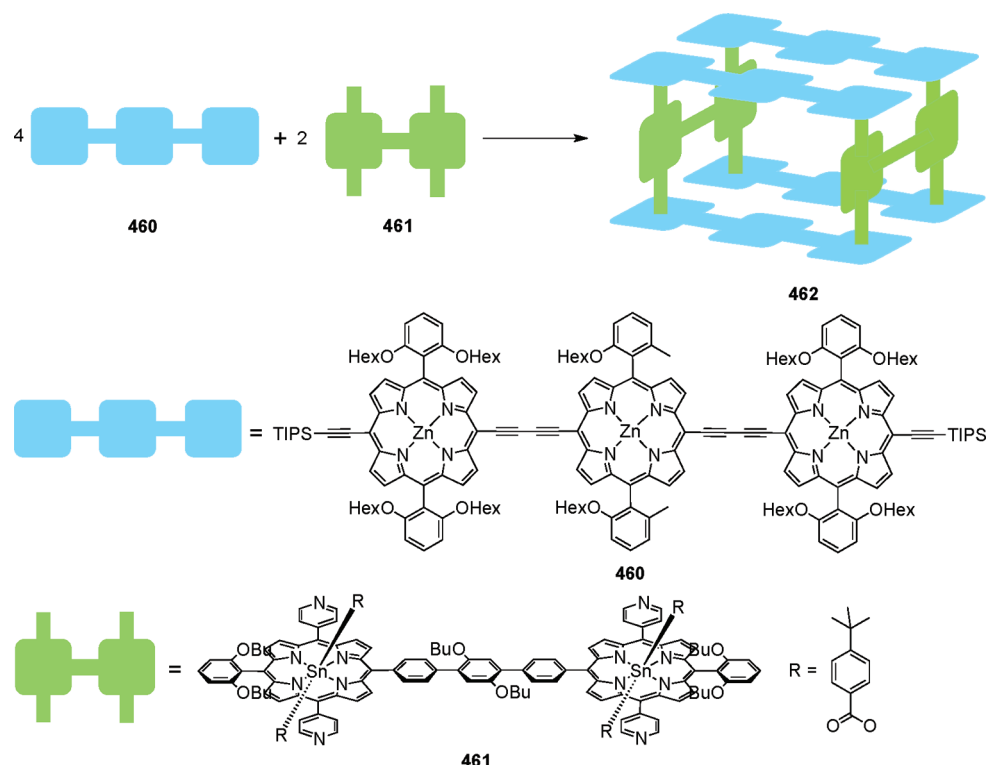
into large monodisperse hollow vesicle-like structures was also observed in dilute solutions.<sup>513</sup>

Self-assembly of trimeric zinc(II) porphyrin units into trigonal-prismatic architectures was achieved by using linear ditopic N-donor ligands such as 1,4-diazabicyclo[2.2.2]octane (DABCO), 4,4'-bipyridine and 5,15-(4-pyridyl)-10,20-phenylporphyrin (4'-*trans*-DPPy). These ligands act as pillars via two axial coordination bonds with the porphyrinic Zn(II) ions, locking the planes of the porphyrin units in an almost cofacial orientation.<sup>514,515</sup> For example, treatment of zinc(II) tris-porphyrin (**458**) with DABCO in a 2:3 ratio led to the formation coordination cage (**459**; Scheme 120). Measurement of stability constants using UV–visible and <sup>1</sup>H NMR spectroscopic studies revealed that, in the presence of an excess of the ditopic N-donor ligand, these coordination cages fall apart to give open species. At micromolar concentrations, the formation of a fully assembled coordination cage was highly favored over the formation of intermediate species stabilized by fewer interactions. In contrast, at millimolar concentrations, the relative stability of intermediate species increased, leading to a stepwise self-assembly process. The presence of a 2:2 intermediate was identified using <sup>1</sup>H NMR spectroscopy. Cage **459** was found to effectively recognize benzene-1,3,5-tricarboxamide derivatives through hydrogen-bonding and aromatic interactions.

Reek and co-workers also reported a similar DABCO-induced porphyrinic architecture using a zinc(II) tris-porphyrin phosphite ligand. Self-assembly of two zinc(II) tris-porphyrin phosphite ligands with three ditopic DABCO ligands led to the formation of a trigonal-prismatic cage.<sup>516</sup> The cage can encapsulate an active



Scheme 121



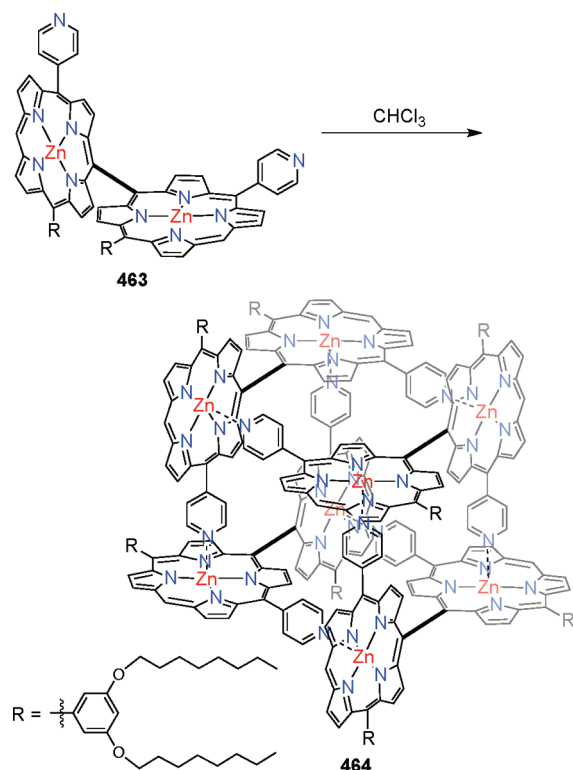
Rh(I) catalytic center through coordination to the phosphorus atoms of the zinc(II) tris-porphyrin phosphite panels. Remarkably, the cage showed high selectivity for linear aldehydes in the rhodium-catalyzed hydroformylation of 1-octene. Similar porphyrin cages were assembled by the same group through a ligand-templated approach wherein bifunctional phosphine ligands possess groups to form cages through coordination to porphyrinic Zn(II) ions while also complexing an active transition metal center for regioselective catalytic applications (vide infra).<sup>18,19</sup>

Hupp and co-workers demonstrated an elegant way to assemble cavity-tailored porphyrinic boxes through coordination-driven self-assembly. Treatment of porphyrinic trimer **460** with pyridine-derivatized porphyrin dimer **461** in a 2:1 ratio led to the generation of a symmetrical 16-porphyrin box, **462** (Scheme 121).<sup>517</sup> Chemically orthogonal metalation of **460**, with Zn(II) and **461** with Sn(IV) ensured that self-recognition between trimers or dimers was avoided. The steric demand of the axial *tert*-butyl benzoate groups on **461** ensured that four of them were directed inward so as to force the dimeric units **461** to link selectively with the first and third porphyrins of **460**, leaving the central Zn sites unoccupied. NMR (<sup>1</sup>H and PGSE) and UV–visible spectroscopy established the exclusive formation of the porphyrinic box **462**. Solution-phase small-angle X-ray scattering (SAXS) measurements confirmed the formation of monodisperse assemblies of precisely the size expected from model box structures. The large cavity ( $22 \times 14 \times 10 \text{ \AA}^3$ ) of the assembly was exploited for both size-selective and enantioselective catalysis. Introduction of bulky R groups such as 3',5'-bis(4-*tert*-butylphenyl)biphenyl-4-carboxylates on porphyrin dimer **461** produced an unusual twisted box. The steric crowding makes the dimer incapable of combining with trimeric unit, **460**, thus forming a porphyrinic box having the architecture of **462**.

Osuka et al. have extensively investigated the formation of a number of supramolecular porphyrin boxes via enantiomeric self-sorting of racemic 4-pyridyl appended meso–meso-linked zinc(II) diporphyrins.<sup>518</sup> As established by <sup>1</sup>H NMR and CSI-MS studies, meso–meso-linked zinc(II) diporphyrin units (**463**) quantitatively self-assembled into supramolecular porphyrinic box **464** in CDCl<sub>3</sub> (Scheme 122).<sup>519</sup> Due to the presence of different *meso*-aryl substituents, the diporphyrin unit **463** is intrinsically chiral, and hence two enantiomers (R and S) are present in equal abundance in solution. Accordingly, both (R)-**464** and (S)-**464** porphyrin boxes were formed in solution through homochiral self-sorting from their respective (R)-**463** and (S)-**463** isomers. The optical resolution of these chiral boxes was achieved with a chiral HPLC setup. Nanoscale porphyrin box **464** has a cavity dimension of  $22 \times 14 \times 10 \text{ \AA}^3$ . Extension of the pyridyl arms of the zinc(II) diporphyrin units led to the formation of boxes with larger dimensions. These porphyrin boxes were demonstrated to serve as well-defined light-harvesting models, exhibiting excitation energy hopping rates that depend on the vertical distance between the meso–meso-linked zinc(II) diporphyrin subunits.<sup>520</sup> The 90° dihedral angle between the diporphyrin and the 4-pyridyl groups played a key role toward the formation of the box-shaped assemblies.

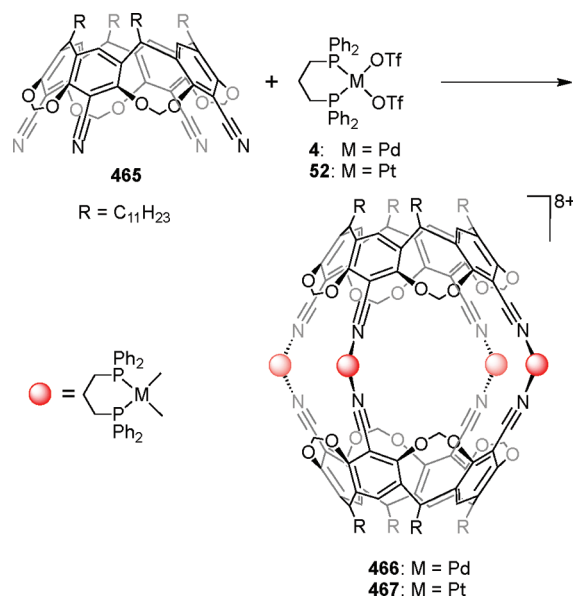
Cavitands, which have half-bowl-shaped structures, can be used as building blocks for supramolecular cages. Early groundbreaking works of Cram demonstrated that covalent linking of two cavitand bowls in a “rim-to-rim” manner resulted in the generation of the closed-shell host molecules, named carcerands and hemicarcerands, that could accommodate complementary guest molecules or ions.<sup>521</sup> More recently, attention has been turned toward the development of larger covalent cavitand cages, which can lead to higher order supramolecules that incorporate a

Scheme 122



greater number of cavita nd hosts.<sup>522</sup> Incorporation of donor groups at the apical positions on the rim of cavita nds makes them interesting molecular building blocks for the self-assembly of coordination-driven metallacages, and the majority of these cavita nd-based assemblies involve tetrasubstituted cavita nds connected by metal centers.<sup>234</sup> In 1997, Jacopozzi and Dalcanele reported the first metal-directed, dimeric cavita nd-based coordination cages (**466** and **467**) from a 1:2 reaction of tetracyano cavita nds **465** with  $[M(dppp)(OTf)_2]$  ( $M = Pd$  (**4**),  $Pt$  (**52**)) at room temperature (Scheme 123).<sup>523</sup> The X-ray crystal structure of **466** showed the presence of an encapsulated triflate ion within the cage. A further comprehensive study on a series of similar cavita nd-based coordination cages showed that the self-assembly process depends on a  $P-M-P$  angle close to  $90^\circ$  between the chelating ligand and the metal precursor ( $Pd$  and  $Pt$ ), weakly coordinated counterions, and preorganization of the tetradentate cavita nd ligand.<sup>524,525</sup> Calorimetric measurements on the formation of these cages together with dynamic NMR ( $^1H$ ,  $^{19}F$ , PGSE, NOE, and EXSY) experiments helped determine the thermodynamics, interionic structure, kinetic stability, and degree of anion encapsulation in these assemblies. The introduction of phenyl spacers to tetracyano cavita nd **465** led to the formation of cavita nd cages with larger internal cavities of nanoscopic dimensions.<sup>526</sup> In this case, as monitored by  $^{19}F$  NMR spectroscopy, no permanent inclusion of triflate ion was observed due to the rapid exchange with the external counterions because of the larger dimensions of the lateral portals. Heteronuclear cavita nd-based coordination cages were also assembled from a tetrasubstituted cavita nd having one 4-pyridylethynyl and three 4-cyanophenyl donor groups at the apical positions with  $Pd(II)$  and  $Pt(II)$  as the metal centers.<sup>527</sup>

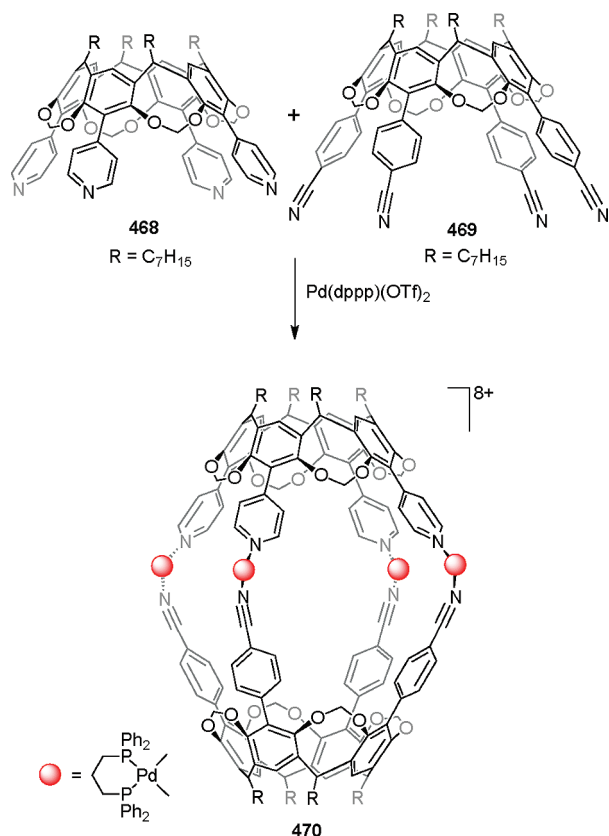
Scheme 123



Using a different synthetic route Kobayashi et al. were able to introduce pyridyl, pyridylethynyl, and cyanophenyl groups on the apical positions of the cavita nds to assemble both dimeric homo- and heterocavita nd cages via metal coordination based on thermodynamic and kinetic control.<sup>443,528</sup> A 1:1:4 mixture of tetra(4-pyridyl)-cavita nd (**468**), tetrakis(4-cyanophenyl)-cavita nd (**469**) and  $Pd(dppp)(OTf)_2$  (**4**) in  $CDCl_3$  selectively self-assembled into thermodynamically stable heterocavita nd cage **470** (Scheme 124). Interestingly, a 1:1:4 mixture of tetrakis(4-cyanophenyl)-cavita nd (**469**), tetrakis(4-pyridylethynyl)-cavita nd, and  $Pd(dppp)(OTf)_2$  (**4**) gave rise to only homocavita nds in  $CDCl_3$ , indicating that a combination of factors such as coordination ability and steric demand of cavita nd ligands can control the selective self-assembly of homo- or heterocavita nd coordination cage. The fact that tetra(4-pyridyl)-cavita nd, **468**, failed to form any discrete assembly as compared to tetrakis(4-pyridylethynyl)-cavita nd, which formed homocavita nd assembly, indicated that tetra(4-pyridyl)-cavita nd, **468**, is sterically more hindered than the tetrakis(4-pyridylethynyl)-cavita nd. Similarly, a 1:1:4 mixture of cyanophenyl-cavita nd, pyridylethynyl-cavita nd, and  $Pd(dppp)(OTf)_2$  self-assembled into the kinetically as well as thermodynamically most stable homo(pyridylethynyl)-cavita nd cage and most labile homo(cyanophenyl)-cavita nd cage in a 1:1 ratio as determined by  $^1H$  NMR spectroscopy. However, heating the reaction mixture at  $50^\circ C$  for 2 h shifts the thermodynamic equilibrium toward heterocavita nd assembly.

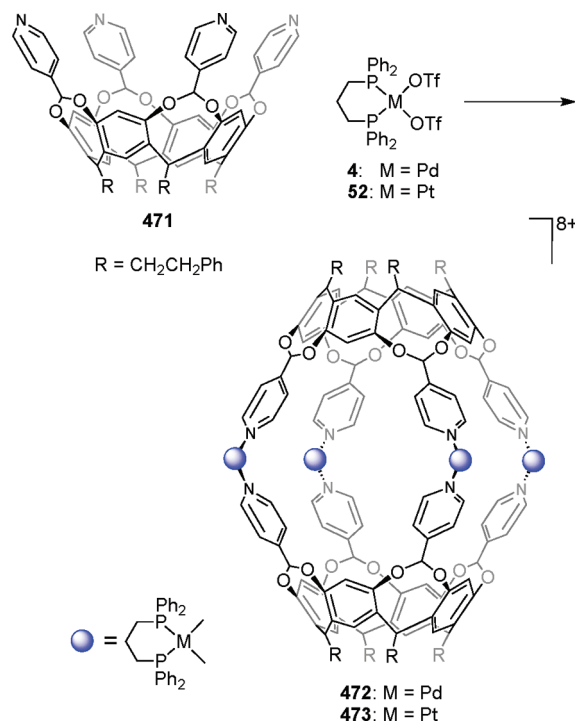
Other examples of coordination-driven self-assembly of cavita nd-based  $Pd(II)$  and  $Pt(II)$  dimeric cages were shown by Lim and Hong using tetrasubstituted cavita nds having flexible pyridyl donors at the apical positions of the cavita nds.<sup>529,530</sup> Formation of these cavita nd cages was affected by subtle changes in the solvent system. While interclipped homocavita nd cages were readily formed in organic solvents (acetone,  $CH_2Cl_2$ , or  $CHCl_3$ ), intracapped supramolecular bowls were formed in aqueous solutions.<sup>531</sup> Subsequent studies using nitromethane as a solvent showed the existence of a dynamic equilibrium between the interclipped homocavita nd cage and the intracapped supramolecular bowl.<sup>532</sup>  $^1H$  NMR and CSI-MS studies confirmed the

Scheme 124



coexistence of two ensembles in nitromethane. Variable-temperature <sup>1</sup>H NMR studies have shown that the conversion from the interclipped homocavitand cage to the intracapped bowl is entropically favored and enthalpically disfavored. Haino et al. introduced phenyl–bipyridine donors at the apical positions of cavitands to form stable dimeric cages via coordination of four Ag(I) metal centers.<sup>533</sup> Each metal center coordinates with two bipyridine units in a tetrahedral fashion. The large internal cavity of the cavitand cage allowed for the selective encapsulation of large aromatics as well as aliphatic mono- and diacetates as guest molecules. The detailed thermodynamic studies on guest encapsulation revealed that both CH– $\pi$  interactions between the methyl groups on the guest termini and the aromatic cavity and desolvation of the inner cavity play a key role in guest encapsulation.<sup>534</sup> Attachment of iminodiacetate moieties at the apical position of resorcinarene-based cavitands followed by treatment with CoCl<sub>2</sub> or FeCl<sub>2</sub> under basic conditions led to the formation of dimeric coordination cages consisting of four octahedrally coordinated metal ions holding together two cavitand scaffolds.<sup>535,536</sup> X-ray structural studies on both cages revealed that each metal ion is coordinated to two doubly deprotonated iminodiacetate moieties, resulting in octaanionic complexes. These pH-dependent, water-soluble cages were found to selectively encapsulate a wide variety of guests including aromatic molecules, alkanes, alkenes, haloalkanes, and alcohols.<sup>537</sup> For example, in the case of the Co(II) cavitand cage, the encapsulation preference for *p*-xylene was 26 700 times more favorable as compared to that of *o*-xylene or *m*-xylene. Calorimetric studies have shown that guest molecules having optimum sizes, shapes, and polarities occupy the greatest percentage of

Scheme 125



cavity space and have the greatest number of favorable bonding interactions with the internal cavity of the cage.<sup>538</sup>

In an alternative design strategy, pendant donor groups were introduced as bridges between the phenolic OH groups of resorcinarene scaffolds. Treatment of tetrasubstituted cavitand 471 with [M(dppp)(OTf)<sub>2</sub>] (M = Pd (4), Pt (52)) in a 1:2 molar ratio at room temperature led to the formation of coordination cages 472 and 473, respectively (Scheme 125).<sup>539,540</sup> The formation of the cages was established by multinuclear NMR (<sup>1</sup>H and <sup>31</sup>P) and mass (ESI and MALDI-TOF) spectrometry and by single-crystal X-ray structural studies in case of cavitand cage 472. Cage 472 has a large internal cavity of ca. 840 Å<sup>3</sup>, ideal for the encapsulation of guest molecules such as fullerenes. Cavitand cages with larger cavity dimensions were similarly assembled using a tetrasubstituted cavitand ligand having a phenyl spacer between the methylene bridge and pyridine donor unit.<sup>541</sup> Host–guest studies using cage 472 as host gave a 1:1 host–guest complex (472 ⊃ guest) with methano[60]fullerene derivatives as evidenced in <sup>1</sup>H NMR and ESI-MS studies.<sup>540</sup>

Since the early studies by Ikeda and Shinkai<sup>542</sup> on metal-mediated self-assembly of calix[4]arene-based dimeric cages, a number of novel coordination cages using tetrasubstituted calix[4]arenes in conjunction with various metal ions have been reported. Hunter and co-workers assembled DABCO-induced calixarene–porphyrin cages utilizing calixarenes having two and four pendant zinc(II) porphyrin units.<sup>543</sup> While the calix–bisporphyrin formed a 2:2 complex with DABCO, calix–tetraporphyrin formed four different complexes depending on the stoichiometry and concentration of DABCO. Careful titration experiments, coupled with a combination of UV–visible and <sup>1</sup>H NMR spectroscopy, revealed that, during the course of a titration, all four intramolecular and intermolecular calix–tetraporphyrin–DABCO sandwich complexes were populated,



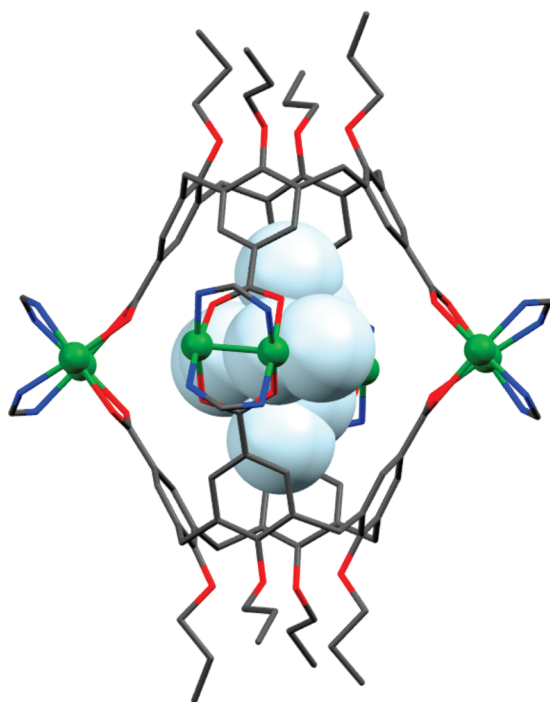


**Figure 38.** Single-crystal X-ray structure of  $\{\text{NEt}_4 \subset [\text{cis-Rh}_2(\text{DAniF})_2(\text{H}_2\text{O})_{1/2}(\text{MeCN})_{1/2}]_4[\text{calix}[4]\text{arene}(\text{CO}_2)_4]_2\}^+$ . The anisyl groups of all formamidinate ligands and the axial ligands (two  $\text{H}_2\text{O}$  and two MeCN molecules which occupy one axial position of each of the four  $\text{Rh}_2^{4+}$  units) have been removed for clarity. Color code: green, Rh; red, O; blue, N; gray, C.

and only at a precise calix–tetraporphyrin:DABCO ratio of 2:4 was the dimeric cage assembly observed.

Cotton et al. reported a dimeric calixarene coordination cage using a calixarene scaffold,  $\text{calix}[4]\text{arene}(\text{CO}_2)_4$ , functionalized with four carboxylic acid groups.<sup>544</sup> Two tetrasubstituted calixarene subunits,  $\text{calix}[4]\text{arene}(\text{CO}_2)_4$ , were assembled via four  $[\text{Rh}_2(\text{DAniF})_2]^{2+}$  ( $\text{DAniF} = N,N'$ -di-*p*-anisylformamidinate) dimetallic corner units to give dimeric cage  $\{\text{NEt}_4 \subset [\text{cis-Rh}_2(\text{DAniF})_2(\text{H}_2\text{O})_{1/2}(\text{MeCN})_{1/2}]_4[\text{calix}[4]\text{arene}(\text{CO}_2)_4]_2\}\text{BF}_4$ , with a tetraethylammonium cation trapped inside the cavity.  $^1\text{H}$  NMR, IR, mass spectrometry, and X-ray crystallographic studies established the formation of the dimeric cage having  $\text{NEt}_4^+$  as an entrapped cation. Figure 38 presents the single-crystal X-ray structure of dimeric cage  $\{\text{NEt}_4 \subset [\text{cis-Rh}_2(\text{DAniF})_2(\text{H}_2\text{O})_{1/2}(\text{MeCN})_{1/2}]_4[\text{calix}[4]\text{arene}(\text{CO}_2)_4]_2\}^+$ .

Cavitand-based trimeric and tetrameric cages via coordination-driven self-assembly were first reported by Beer and co-workers. Tetrasubstituted dithiocarbamate functionalized cavitands were assembled into trimeric and tetrameric cavitand cages with late transition metals (Ni, Pd, Cu, Au, Zn, and Cd).<sup>545,546</sup> The coordination geometry of the transition metal used dictated the architecture that was adopted. X-ray crystallographic studies showed that square-planar coordination geometries result in tetrameric cages, whereas square-based pyramidal metal geometries favor trimeric architectures. Thus, while Zn(II) and Cd(II) formed trimeric cages, with Cu(II), a tetrameric cage was observed. Ni(II), Pd(II), and Au(II) also formed tetranuclear cages. These cavitand cages possess large internal cavity dimensions suitable for encapsulation of  $\text{C}_{60}$  and  $\text{C}_{70}$  fullerenes. Host–guest studies

using these cages as hosts have showed the formation of strong 1:1 host–guest complexes with fullerenes, with the Cd(II) trimeric cage being the best host system.<sup>547</sup> Electrochemical, NMR, and molecular modeling studies suggested that the electronic character of dithiocarbamate sulfur donor atom, which was affected by the nature of the metal ions, dictated the binding efficiency of the electron-deficient fullerene guests. A hexameric spheroidal cavitand cage based on cavitand–terpyridine subunits was assembled from a reaction between a tetrasubstituted terpyridyl–phenyl cavitand with  $[\text{Zn}(\text{NCMe}_6)]_2[\text{TFPB}]_2$  (TFPB = tetrakis(3,5-bis(trifluoromethyl)phenyl)borate) containing lipophilic anions, which enhanced the solubility of the highly charged assembly in nonpolar organic solvents.<sup>548</sup> The hexameric assembly was characterized by ESI-MS, elemental analysis, small-angle X-ray scattering (SAXS), and diffusion NMR spectroscopy.

#### 4.5. Applications and Uses of 3D Cages

The past decade has seen remarkable progress in the application and use of 3D cages, designed primarily through metal–ligand coordination<sup>8–19</sup> and hydrogen bonding,<sup>549</sup> in diverse fields such as host–guest chemistry and molecular recognition, reactivity modulation, catalysis, and biology. Three-dimensional cages engineered via the coordination-driven self-assembly paradigms have a distinct advantage over conventional covalent container molecules due to the synthetic ease with which the coordination cages can be realized, the availability of a large library of building blocks, and the ability to exhibit selective guest encapsulations. The strong and highly directional nature of metal–ligand interactions results in the formation of stable and rigid coordination cages with well-defined internal cavities. The confined nanospaces within the enclosed cavities in these coordination cages create unique environments and geometric constraints different from the bulk media. It is this localized microenvironment that allows access to hitherto inaccessible molecules and stabilization of short-lived intermediates and leads to unusual reactions.

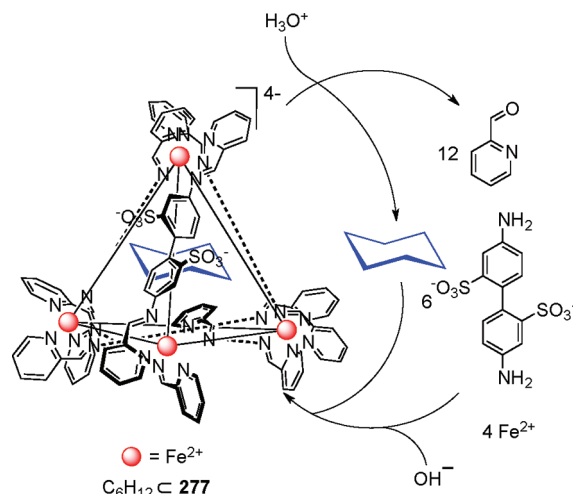
**4.5.1. Host–Guest Chemistry.** Host–guest studies using discrete 3D supramolecular cages having well-defined cavities as hosts for the selective binding of guest molecules play a crucial role in understanding the underlying mechanism, thermodynamics, and specific interactions involved in guest binding. The fundamental knowledge thus gained forms the basis for molecular recognition and sensor applications, allowing the chemistry of supramolecular ensembles to be expanded into the field of catalysis and drug delivery. A variety of 3D supramolecular cages have been utilized to encapsulate multiple numbers of guests driven both by specific interactions between the guest and host, as well as nonspecific, weak, supramolecular interactions such as Coulombic, van der Waals, hydrogen bonding, ion-association forces, and steric interactions. Furthermore, a synergistic combination of charge, dielectric, shape, size, and solvation also dictate the guest binding preferences in host molecules. Mechanistic studies have shown that in these systems the guest encapsulation is entropically driven and operates either through an associative mechanism, where the guest replaces the noncovalently bound molecules/solvents from the cavity in a concerted fashion, or through a dissociative mechanism, where guest egress yields an “empty” assembly which is trapped by an incoming guest.<sup>550</sup>

**4.5.1.1. Molecular Encapsulation and Recognition.** In the context of host–guest studies, Raymond and co-workers utilized a series of anionic tetrahedral  $\text{M}_4\text{L}_6$  ( $\text{M} = \text{Ga}^{\text{III}}$ ,  $\text{Al}^{\text{III}}$ ,  $\text{In}^{\text{III}}$ ,  $\text{Fe}^{\text{III}}$ ,  $\text{Ti}^{\text{IV}}$ , and  $\text{Sn}^{\text{IV}}$ ) cages wherein the metal atoms occupying the



corners of a tetrahedron were bridged by six bis-catecholate-based ligands having  $C_2$  symmetry.<sup>9,336</sup> Although composed of achiral components, these tetrahedral assemblies are intrinsically chiral due to the strong mechanical coupling between the metal centers, resulting in homochiral assemblies of  $\Delta\Delta\Delta\Delta$  or  $\Lambda\Lambda\Lambda\Lambda$  configuration. The tetrahedral assembly  $[\text{Ga}_4(\mathbf{271})_6]^{12-}$ , derived from naphthalene-based bis-catecholate ligand **271**, was used extensively as host due to its favorable properties, including its solubility in water, structural integrity during guest exchange, and non-interconvertible and resolvable enantiomers. The anionic tetrahedral assembly  $[\text{Ga}_4(\mathbf{271})_6]^{12-}$  was soluble in various polar solvents and contains a hydrophobic cavity volume of 450 Å. The assembly could selectively encapsulate a variety of monocationic guests such as  $\text{NMe}_4^+$ ,  $\text{NEt}_4^+$ ,  $\text{Me}_2\text{Pr}_2\text{N}^+$ ,  $\text{Pr}_4\text{N}^+$ , and  $\text{PEt}_4^+$  with remarkable discrimination to form host–guest complexes  $[\text{guest} \subset \text{Ga}_4(\mathbf{271})_6]^{11-}$ . The affinity of the guest molecules for the cavity depends on their size, hydrophobicity, enthalpy of desolvation, and charge.<sup>337</sup> X-ray crystallographic analyses to probe the host–guest interactions in  $[\text{M}_4\text{L}_6]^{n-}$  cages of different metals ( $\text{M} = \text{Ga}^{\text{III}}$ ,  $\text{Fe}^{\text{III}}$ ,  $\text{Ti}^{\text{IV}}$ ) and different encapsulated guests ( $\text{NEt}^{4+}$ ,  $\text{BnNMe}^{3+}$ ,  $\text{Cp}_2\text{Co}^+$ ,  $\text{Cp}^*\text{Co}^+$ ) showed that the nature of the metal ions has little impact on the assemblies. However, the encapsulated guests significantly distort the sizes and shapes of the interior cavities of the assemblies.<sup>551</sup> Studies to understand the guest encapsulation into  $[\text{Ga}_4(\mathbf{271})_6]^{12-}$  through van't Hoff thermodynamic analysis showed that the encapsulation of cationic guests is an endothermic process with positive  $\Delta H$  and  $\Delta S$  values. Spontaneous, entropically driven processes are a consequence of the desolvation of bound waters from the solvation shell of the guest and release of water from the cavity host into the bulk solvent, thus paying an enthalpic penalty through entropic gains.<sup>337</sup> Further studies using a series of guests ranging from simple alkylammonium cations to complex organometallic iridium species have confirmed that guest encapsulation in polar protic solvents involved initial desolvation of the guest with concomitant entropy–enthalpy compensation effects due to the rearrangement of the hydrogen bond network in solution.<sup>552</sup> A recent study using a combination of NMR, UV–visible, and isothermal titration calorimetry has shown<sup>553</sup> remarkable differences between the internal and external binding of simple alkylammonium cations,  $\text{NEt}^{4+}$  and  $\text{NMe}^{4+}$  into  $[\text{Ga}_4(\mathbf{271})_6]^{12-}$ . The encapsulation process was entropically driven while external binding was enthalpically driven and involved ion association<sup>554</sup> and the loss of degrees of freedom as a consequence of the high charge and hydrophilic outer space of the cage. Mechanistic studies to elucidate the guest exchange process in these tetranuclear assemblies using  $[\text{Ga}_4(\mathbf{271})_6]^{12-}$  as the host for a series of tetraalkylammonium, phosphonium, and organometallic cations have shown that, unlike hydrogen-bonded cages,<sup>549</sup> guest exchange in these tetrahedral cages occurs by the expansion of the cage apertures without metal–ligand bond rupture.  $^1\text{H}$  NMR kinetic studies have shown that the rate of guest exchange is significantly retarded with sterically demanding  $\text{Cp}^*\text{Co}^+$  as the anionic guest compared to smaller guests such as  $\text{NMe}^{4+}$ ,  $\text{NEt}^{4+}$ , and  $\text{CoCp}^{2+}$ .<sup>555</sup> This indicated that the steric repulsions that must be overcome by the guest in order to escape increases with guest size and rigidity. Furthermore, guest exchange in hosts composed of more inert metal–ligand bonds was as facile as guest exchange in more labile analogues, suggesting that the exchange was independent of metal–ligand interactions. Computational studies revealed that guest exchange takes place through one of the four  $C_3$  apertures

Scheme 126



at the center of each face of the tetrahedron. Further kinetic studies of the host–guest dynamics of  $[\text{Ga}_4(\mathbf{271})_6]^{12-}$  suggested a nondissociative mechanism.<sup>556</sup> The fact that larger guests have much more negative  $\Delta S^\ddagger$  values than their smaller counterparts substantiate the squeezing of the guests through host apertures rather than bond rupture.

Nitschke and co-workers designed an anionic tetrahedral cage, **277**, through a combination of dynamic covalent and metal ligand coordination bonds, which could reversibly disassemble and reassemble upon application of an external stimulus.<sup>349</sup> A change in pH of the aqueous solution of **277** having cyclohexane as a guest induced a reversible opening of the cage (Scheme 126). Addition of *p*-toluenesulfonic acid made the cage come apart and liberate the cyclohexane guest. Changing the solution pH to a basic regime by addition of sodium bicarbonate induced the reassembly of the cage. Tetrahedral cage **277** was effectively used to store the potent greenhouse gas  $\text{SF}_6$  in aqueous solution.<sup>557</sup> The stored payload could be released in a controlled fashion through different physical and chemical stimuli such as temperature, pH, and imine exchange reactions. However, in contrast to tetrahedral host cage  $[\text{Ga}_4(\mathbf{271})_6]^{12-}$ , it failed to encapsulate  $\text{NMe}^{4+}$  and other small alkylammonium cations despite being anionic and having an ideal shape and size. Recently, the same group designed a  $\text{M}_8\text{L}_6$  porphyrin-based cubic cage that can efficiently encapsulate large aromatic guest molecules such as coronene and fullerenes.<sup>383</sup> Addition of excess of coronene to the  $\text{M}_8\text{L}_6$  cube led to the formation of host–guest complexes in which exactly 3 equiv of this flat, aromatic guest were encapsulated per host, as confirmed by NMR spectroscopy, ESI-MS, and microanalysis. The cube also showed selective binding affinity for fullerenes. From a commercially available fullerene soot, the cube selectively encapsulated  $\text{C}_{70}$ ,  $\text{C}_{76}$ ,  $\text{C}_{78}$ , and  $\text{C}_{84}$  to form 1:1 host–guest complexes.

Raymond, Bergman, and co-workers were also able to encapsulate neutral, hydrophobic guests including *n*-alkanes, cycloalkanes, arenes, and enantiopure terpenoids into a tetrahedral host,  $[\text{Ga}_4(\mathbf{271})_6]^{12-}$ , in aqueous solution.<sup>558,559</sup> The driving force for the binding of these neutral guests was attributed to a hydrophobic effect. The molecular host assembly selectively encapsulated different substitutional isomers of disubstituted benzenes with ortho-substitution leading to the encapsulation

of two guests, while meta- or para-substitution lead to the encapsulation of only one guest. Therrien et al. were able to encapsulate different planar aromatic molecules such as phenanthrene, pyrene, fluoranthene, benzo[e]pyrene, triphenylene, and coronene into the hydrophobic cavity of a series of cationic (arene)ruthenium-based trigonal prisms  $[\text{Ru}_6(\eta^6\text{-p-cymene})_6\text{-(285)}_2(\text{OO} \cap \text{OO})_3]^{6+}$  **363–367** [ $\text{OO} \cap \text{OO} = \text{dhbq, dchq, dhng, dhaq, or dhtq}$ ] by using them as templating guests.<sup>428,429</sup> Empty trigonal-prismatic cages **363–367** have been used for host–guest studies and have shown that small aromatic molecules (phenanthrene and pyrene) show rapid inclusion into the hydrophobic cavities of the cages upon gradual addition of guests. However, molecules that are too large to exit the portal of the cages get permanently incarcerated, thus giving rise to stable carceplex systems.

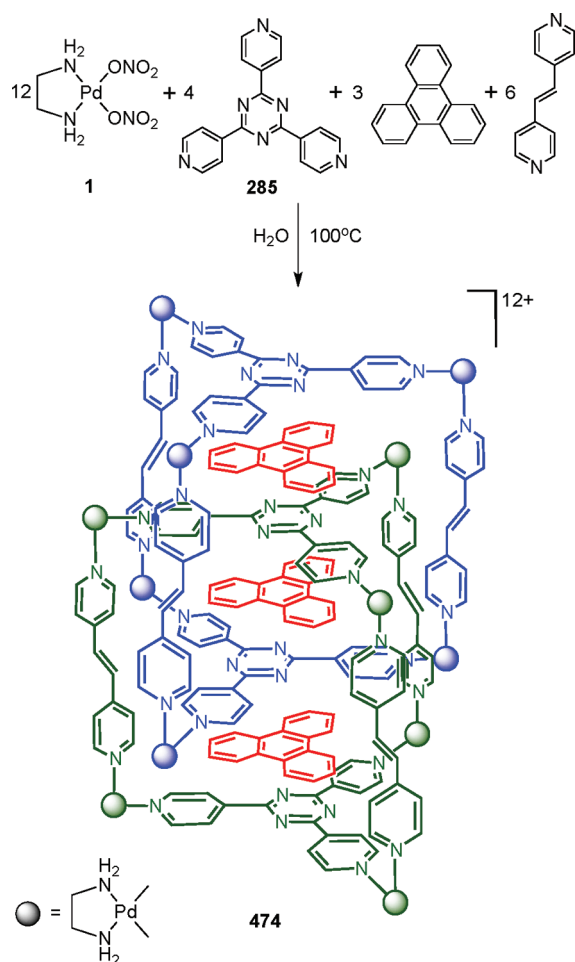
Lindoy et al. have recently reported the selective encapsulation of a  $[\text{Fe}^{\text{III}}\text{Cl}_4]^-$  anion over a  $[\text{Fe}^{\text{II}}\text{Cl}_4]^{2-}$  anion within the central cavity of a tetrahedral cage of the type  $[\text{Fe}^{\text{II}}_4\text{L}_6]^{8+}$  ( $\text{L} = \text{S}, \text{S}'''$ -dimethyl-2,2':5',5'':2'',2'''-quaterpyridine).<sup>560</sup> The treatment of quaterpyridine ligand **L** with  $\text{FeCl}_2 \cdot \text{SH}_2\text{O}$  in acetonitrile at reflux for 24 h followed by the addition of  $\text{KPF}_6$  led to the isolation of an  $[\text{Fe}^{\text{III}}\text{Cl}_4]^-$  encapsulated tetranuclear cage  $[\text{Fe}^{\text{II}}_4\text{L}_6 \supset \text{Fe}^{\text{III}}\text{Cl}_4](\text{PF}_6)_7$  as established from  $^1\text{H}$  NMR, microanalysis, and X-ray crystallography. The crystal structure of  $[\text{Fe}^{\text{II}}_4\text{L}_6 \supset \text{Fe}^{\text{III}}\text{Cl}_4](\text{PF}_6)_7$  showed that  $[\text{Fe}^{\text{III}}\text{Cl}_4]^-$  occupies the central cavity and has a perfect tetrahedral symmetry with  $\text{Cl–Fe–Cl}$  bond angles of  $109.5^\circ$ . It is noteworthy that the tetrahedral cage  $[\text{Fe}^{\text{II}}_4\text{L}_6]^{8+}$  selectively extracts a  $[\text{Fe}^{\text{III}}\text{Cl}_4]^-$  anion from a mix of  $\text{Fe}^{\text{II}}$  and/or  $\text{Fe}^{\text{III}}$  chloro species undoubtedly present in the solution. Such an observation is consistent with the earlier observation by Raymond and co-workers<sup>337</sup> where they found that larger enthalpy of desolvation associated with doubly charged species significantly hampers their encapsulation within a confined cavity, making it less favorable. The same system was earlier shown to encapsulate both  $\text{BF}_4^-$  and  $\text{PF}_6^-$  counteranions within the central cavity with marked selectivity for  $\text{PF}_6^-$  over  $\text{BF}_4^-$ .<sup>348</sup>

Fujita and co-workers have extensively investigated self-assembled trigonal-prismatic cages constructed from a combination of end-capped  $\text{Pd}(\text{II})$  ions as hinges, two tridentate planar panels and N-donor bidentate pillars for the intercalation of flat aromatic molecules (Scheme 102).<sup>561</sup> For example, the trigonal-prism **344**, pillared by pyrazine, could encapsulate one coronene molecule, stabilized through  $\pi$ – $\pi$  interactions with the host assembly in aqueous media.<sup>409</sup> The aromatic molecule, coronene, acts as templating agent in the selective formation of the trigonal-prism architecture and can be removed after assembly through extraction with  $\text{CHCl}_3$ . The efficient intercalation of planar guest molecules within the cavity of **344** was applied to control the equilibration between keto and enol forms of 1,3-bis(4-methoxyphenyl)propane-1,3-dione. As confirmed by  $^1\text{H}$ ,  $^{13}\text{C}$ , and COSY NMR spectra, exclusive enolization was observed due to the selective encapsulation of the planar enol form over the nonplanar keto form. The cavity space of these trigonal prisms can be altered by changing the length of the pillars, thus facilitating encapsulation of more than one flat, aromatic molecule inside the cavity.<sup>410</sup> The extended cavity afforded through the use of longer pillars, 2,2',6,6'-tetramethyl-4,4'-bipyridine and 1,4-bis(2,6-dimethyl-4-pyridyl)benzene, results in cages **345** and **346**, respectively, ideal for stacking of 2 or 3 equiv of an aromatic templated guest. Thus, 2 equiv of electron-rich aromatic guests such as pyrene, coronene, or porphine form

acceptor–donor–donor–acceptor (A–D–D–A) quadruple stacks through charge-transfer interactions with donor guests sandwiched between electron-poor triazine panels in cage **345**. Recently, a dissymmetrical hetero A–D–A–A quadruple stack was also obtained with two different guest molecules, triphenylene and naphthalenediimide, using trigonal-prism **345** as a host.<sup>562</sup> Cage **346** showed quintuple (A–D–A–D–A) stacking with an intercalated triazine panel and two coronene or porphine molecules.<sup>410,411</sup> The use of a less electron-rich, planar red fluorescent dye, tetraazaporphine, led to templated encapsulation of 3 equiv of tetraazaporphines.<sup>563</sup> The host–guest complex **346**  $\supset$  (azaporphine)<sub>3</sub> was highly soluble in water as compared to free tetraazaporphine, which was sparingly soluble in aqueous solutions. Fluorescent studies with the **344**  $\supset$  (tetraazaporphine) system showed that tetraazaporphine retains its fluorescent properties upon encapsulation, in contrast to those in aqueous solution, which quench due to aggregation.<sup>564</sup> The fact that tetraazaporphine retained its fluorescent properties indicated there is a minimal charge-transfer interaction between the host and the guest molecule. Interestingly, reversible quenching of the fluorescence was achieved in aqueous solution through the addition of  $\text{NEt}_3$ , leading to the abstraction of an acidic proton from the tetraazaporphine, forming a nonemissive **344**  $\supset$  (tetraazaporphine) species, which then can be treated with acid to reestablish emission. The selective encapsulation of tetraazaporphine/porphine stacks allowed for the generation of metal-containing homo- and heteroarrays  $\text{Cu}(\text{II})\text{–M–Cu}(\text{II})$  ( $\text{M} = \text{Cu}(\text{II})$  or  $\text{Pd}(\text{II})$ ).<sup>563</sup> The inclusion complex **345**  $\supset$   $[\text{Cu}(\text{II})\text{–azaporphine}]_3$  showed a ferromagnetically coupled spin–spin interaction between the three copper(II)–azaporphine units, as determined from ESR studies, which revealed a quartet state of the  $\text{Cu}(\text{II})$  centers despite the absence of any covalent or noncovalent bonds between the stacked azaporphine nuclei. The heterometal ion arrays also showed strong metal–metal interactions as indicated by broadening of their ESR spectra.

Fujita and co-workers have also demonstrated the formation of columns of aromatic molecules consisting of seven to nine discretely stacked aromatic molecules. The reaction of organic pillars of appropriate length, planar panel ligands, aromatic planar templating guests, and end-capped  $\text{Pd}(\text{II})$  metal hinges in a suitable ratio led to the quantitative formation of 2-fold interpenetrated self-assembled trigonal-prismatic cages.<sup>565</sup> For example, combination of *trans*-1,2-bis(4-pyridyl)ethene (bpe) as a pillar, triazine panel **285**, triphenylene as a aromatic templating guest, and **1** in a 6:4:3:12 molar ratio in aqueous solution gave a 2-fold interpenetrated self-assembled trigonal-prismatic cage (**474**; Scheme 127) containing three triphenylene guest molecules sandwiched between four triazine panels. The  $^1\text{H}$  NMR spectrum, which showed two sets of signals in a 2:1 ratio for the intercalated triphenylene guest, and CSI-MS studies, indicated the formation of a septet aromatic stacked motif, **474**. X-ray crystallographic studies using a (tmen) $\text{Pd}(\text{II})$  hinge and pyrene as guest confirmed the formation of septet (A–D–A–D–A–D–A) aromatic stacked architectures. Adjusting the pillar lengths facilitated the assembly of taller octuplet (A–D–A–D–D–A–D–A) and nonuplet (A–D–A–D–D–D–A–D–A) stacks. These discrete, interpenetrating, self-assembled hosts were utilized as “magnetic aligners” to orient a small organic molecule in a magnetic field.<sup>566</sup> Septet columnar stacks with solubilizing side chains showed aggregation at higher concentrations in aqueous solution via intermolecular hydrophobic and  $\pi$ – $\pi$  interactions.<sup>567</sup>

Scheme 127



The entrapped molecules within the cavities of the trigonal prisms are unrestrained and have rotational freedom within the cages. This enabled encapsulated guests to display unique stacking and orientation preferences, depending upon the number of stacked guests. Three highly polarized aromatic guest molecules, pyrene-4,5-dione, formed a triple-layered host–guest complex when mixed with triazine panels, end-capped Pt(II) as hinges and *trans*-1,2-bis(4-pyridyl)ethylene (bpe) as pillars.<sup>568</sup> The pyrene-4,5-dione molecules rotated freely within the cage, as indicated by the <sup>1</sup>H NMR resonances which suggest high symmetry. However, in the solid state, three pyrene-4,5-dione molecules stack in a staggered fashion by 120° with respect to each other (Figure 39). By adopting such an orientation, the dione triple stack achieves a negligible overall dipole moment. By systematically altering the pillar heights, the number of stacking molecules can be controlled without restricting the orientation of the guests.<sup>569</sup> When the number of stacks was even, the dione molecules adopted a head to tail orientation to cancel the local and net dipole moments. In odd-numbered stacks the net dipole is canceled at the expense of local dipole interactions.

Using the same approach as described above, Fujita et al. engineered discrete, stacked arrays of planar transition metal complexes via d–d interactions between the metal centers for studying interesting chemical phenomena otherwise unobservable in infinite assemblies, in crystalline or liquid crystalline phases.<sup>561</sup>

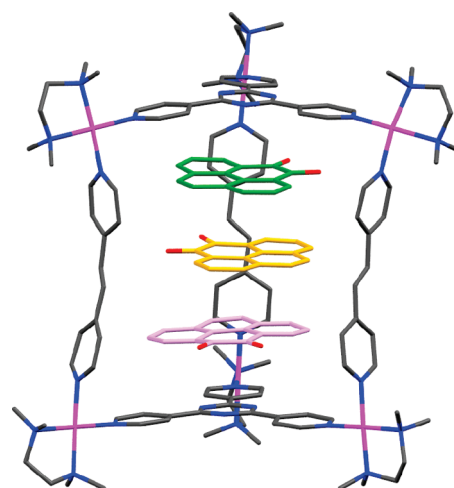


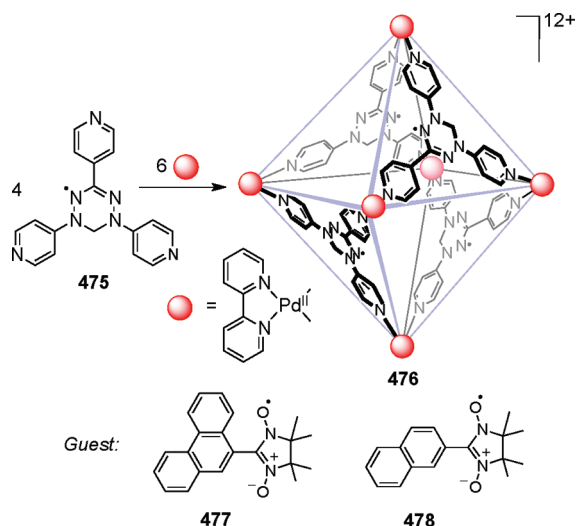
**Figure 39.** X-ray crystal structure of three pyrene-4,5-dione molecules stacked in a 120° twisted fashion in a trigonal-prism cage. Solvents (H<sub>2</sub>O) and counteranions (NO<sub>3</sub>) are omitted for clarity. Color code: pink, Pd; red, O; blue, N; gray, C.

For example, the suspension of 2 equiv of planar M(acac)<sub>2</sub> (M = Pt<sup>2+</sup>, Pd<sup>2+</sup>, or Cu<sup>2+</sup>, acac = acetylacetonate) in an aqueous solution of trigonal-prismatic cage **345** led to the formation of host–guest complexes **345** ⊃ [M(acac)<sub>2</sub>]<sub>2</sub>.<sup>412</sup> X-ray crystallographic analysis and UV–visible measurements of host–guest complex **345** ⊃ [Pt(acac)<sub>2</sub>]<sub>2</sub> showed strong Pt(II)–Pt(II) d–d interactions. The inclusion complex **345** ⊃ [Cu(acac)<sub>2</sub>]<sub>2</sub> showed spin–spin interactions as evidenced by a broadening of ESR signals at low temperature and Cu(II)–Cu(II) interactions involving nonbonding stacking of two d<sub>x<sup>2</sup>–y<sup>2</sup></sub> orbitals. Recently, three-dimensional *m* × *n* stacked arrays of discrete, planar polynuclear metal complexes were assembled within the cavity of trigonal prismatic cages.<sup>570</sup> Cyclic trinuclear Au(I) complexes [3 × 2] and [3 × 3] Au(I) clusters were encapsulated along the C<sub>3</sub> axis of trigonal-prismatic cages to form 3D columnar metal arrays. Therrien et al. have also achieved the encapsulation of M(acac)<sub>2</sub> (M = Pt or Pd) as guests into the hydrophobic cavity of an (arene)ruthenium-based trigonal-prism [Ru<sub>6</sub>(*p*-cymene)<sub>6</sub>-(285)<sub>2</sub>(dhbq)<sub>3</sub>]<sup>6+</sup> (**367**) using M(acac)<sub>2</sub> as a templating guest.<sup>431</sup> Studies of their cytotoxicity toward cancer cells revealed that these inclusion complexes **367** ⊃ [M(acac)<sub>2</sub>]<sub>2</sub> were more active as compared to the free cage or Pd/Pt(acac)<sub>2</sub> complexes.

The host–guest complexes containing square-planar Ni(II) and Co(II) complexes as guest in trigonal-prismatic hosts **344**–**346** showed interesting spin-crossover phenomena without changing the coordination number or geometry of the metal complexes.<sup>571</sup> The encapsulation of the square-planar low-spin Ni<sup>II</sup>(acen) (acen = *N,N'*-ethylenebis(acetylacetonateiminato)) complex in cages **344** and **345** gave inclusion complexes **344** ⊃ [Ni<sup>II</sup>(acen)] and **345** ⊃ [Ni<sup>II</sup>(acen)]<sub>2</sub>, respectively. <sup>1</sup>H NMR and CSI-MS confirmed their stoichiometry. Upon encapsulation, the spin state of Ni<sup>II</sup>(acen) changed from low-spin to high-spin, as indicated by magnetic measurements. SQUID measurements showed paramagnetic behavior, confirming the high-spin state of the complex within the host assembly. X-ray structural studies on the 1:2 host–guest complex **345** ⊃ [Ni<sup>II</sup>(acen)]<sub>2</sub> revealed that the square-planar geometries of the two Ni<sup>II</sup>(acen) guests were perfectly preserved. The two planar molecules were twisted by 150° due to steric repulsion of the methyl groups of



Scheme 128

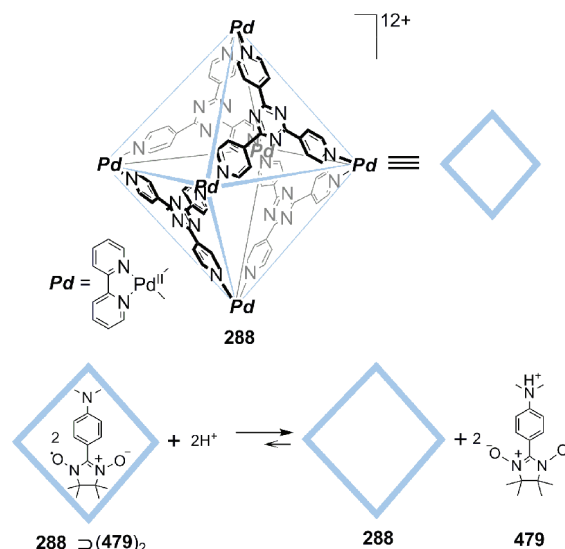


the acen moieties. A spin-crossover phenomenon was also observed when  $\text{Co}^{\text{II}}$ (tetraazaporphine) was intercalated along with two coronenes into **346** to give inclusion complex **346**  $\supset$  [coronene  $\cdot$   $\text{Ni}^{\text{II}}$ (acen)  $\cdot$  coronene]. The anisotropic and temperature-dependent nature of the ESR signal is indicative of the involvement of a high-spin state. The observed spin-crossover of the  $\text{Ni}^{\text{II}}$  and  $\text{Co}^{\text{II}}$  complexes, upon entrapment in the host cages, was ascribed to interactions between the metal  $d_{z^2}$  orbital and the  $\pi$  orbitals of aromatic cage panels or coguests.

To study the noncovalent spin–spin interaction between the host and the guest, Fujita et al. designed spin cages by replacing the typical triazine panels **285** with verdazyl panels **475**.<sup>572,573</sup> The trigonal-prismatic-shaped cage assembled efficiently from a mixture of verdazyl panels, (en) $\text{Pd}^{\text{II}}$  hinges, and pyrazine pillars.<sup>572</sup> The encapsulation of triphenylene by this host showed spin exchange interactions between the two parallel panels with verdazyl cores, as evidenced by the broadening of the ESR signal at room temperature. At low temperature, the ESR spectrum showed characteristics of magnetic dipole interactions. Noncovalent host–guest spin–spin interactions were also observed when  $\text{Cu}(\text{acac})_2$  was encapsulated as a guest. The ESR studies of the resulting inclusion complex clearly indicated that the  $\text{Cu}^{\text{II}}$  center magnetically interacts with the radical panel of the cage. Similarly, a  $\text{M}_6\text{L}_4$  tetrahedral spin cage (**476**) was assembled by using a 2,2'-bipyridine-capped  $\text{Pd}^{\text{II}}$  complex with a verdazyl radical ligand, **475**, in place of triazine panels (Scheme 128). The cage demonstrated host–guest spin–spin interactions.<sup>573</sup> The four spin centers of cage **476** showed intramolecular magnetic interactions indicated by the broadening of the ESR signal as compared with free ligand **475**, which showed hyperfine splitting. Upon the encapsulation of a stable nitrosyl radical, **477**, the 1:1 host–guest inclusion complex **476**  $\supset$  **477** showed antiferromagnetic spin–spin host–guest interactions. Similar treatment of **478** with spin cage **476** formed a 1:2 host–guest complex **476**  $\supset$  (**478**)<sub>2</sub> which showed enhanced magnetic interactions through host–guest and guest–guest interactions.

Fujita and co-workers also demonstrated that the confined cavities of the  $\text{M}_6\text{L}_4$  coordination cages could induce through-space spin–spin interactions between encapsulated stable organic radicals in solution. When stable organic nitrosyl radical **478** was

Scheme 129

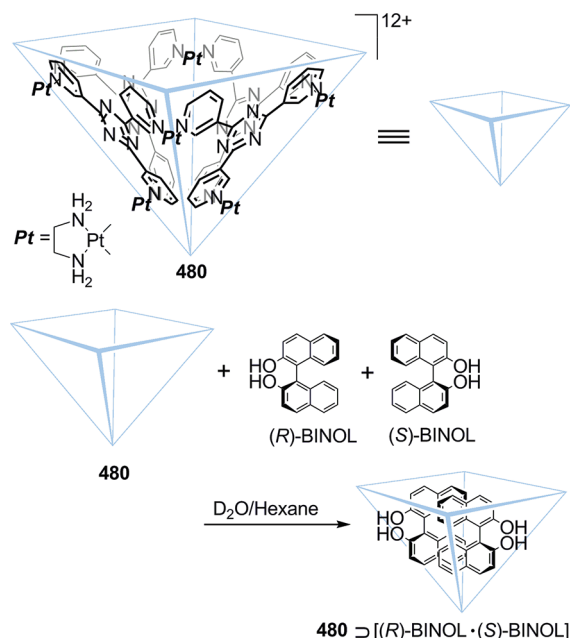


encapsulated in self-assembled cage **288**, a 1:2 host–guest complex **288**  $\supset$  (**478**)<sub>2</sub> was formed.<sup>574</sup> Due to the restriction imposed by the confined cavity of the cage, two organic radicals were forced to be close to each other within the cavity. Such close encapsulation induced through-space spin–spin interactions between the two radicals, as observed by ESR spectroscopy. The ESR spectrum of **288**  $\supset$  (**478**)<sub>2</sub>, in both solution and the solid state, showed a broadened signal assignable to a dimeric aggregate of radical **478** in a triplet state, stemming from an intermolecular spin–spin interaction. The quantity of the triplet state generated by encapsulation also increases with an increase in the affinity of the radical to the cage.<sup>575</sup> Since these organic radicals are held together only through weak hydrophobic forces, the through-space spin–spin interactions are sensitive to external stimuli such as temperature and pH. The use of an organic radical having an amine group (**479**), which can be protonated, reduced the affinity of the radical to the cage due to cationic repulsions (Scheme 129).<sup>576</sup> As a result, the encapsulated organic radicals were released from the **288**  $\supset$  (**479**)<sub>2</sub> 1:2 inclusion complex into an acidic solution, as indicated by the disappearance of the signal for the triplet state in the ESR spectrum of the host–guest complex in solution. Upon treatment with  $\text{K}_2\text{CO}_3$ , the triplet signal reappeared, signaling the reencapsulation of the radicals into the host.

Enantioselective recognition and resolution of chiral guest molecules was also exploited using self-assembled coordination cages having well-defined cavities. Raymond et al. utilized the homochiral tetrahedral assembly  $[\text{Ga}_4(\text{271})_6]^{12-}$  as a host for the chiral recognition of half-sandwich organometallic species of a general formula  $[\text{Cp}^*\text{Ru}(\eta^4\text{-diene})(\text{H}_2\text{O})]\text{Cl}$  ( $\text{Cp}^* = \text{C}_5(\text{CH}_3)_5$ ).<sup>577</sup> The combination of an aqueous solution of racemic  $[\text{Ga}_4(\text{271})_6]^{12-}$  with an ethereal layer of racemic  $\text{Cp}^*\text{Ru}(\eta^4\text{-diene})\text{Cl}$  led to the formation of a 1:1 host–guest complex,  $[\text{Ga}_4(\text{271})_6] \supset [\text{Cp}^*\text{Ru}(\eta^4\text{-diene})(\text{H}_2\text{O})]^{11-}$ , with two diastereomeric pairs of enantiomeric host–guest complexes ( $\Delta/\text{R}$ ,  $\Lambda/\text{S}$  and  $\Delta/\text{S}$ ,  $\Lambda/\text{R}$ ). When  $\text{Cp}^*\text{Ru}(2\text{-ethylbutadiene})\text{Cl}$  was used as the encapsulated guest, the ensemble showed a diastereomeric excess of 70%. Studying the scope of enantioselective recognition with a series of 1- and 2-substituted diene containing complexes revealed that the encapsulation process was controlled not only



Scheme 130

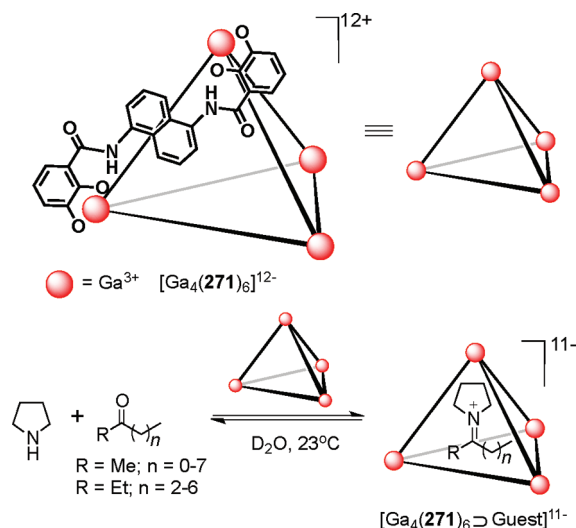


by the guest's size but also by its shape. Using enatiopure host cage  $\Lambda\Lambda\Lambda\Lambda$ -[Ga<sub>4</sub>(271)<sub>6</sub>]<sup>12-</sup> with Cp<sup>\*</sup>Ru(2-ethylbutadiene)Cl as a guest in a 1:2 ratio led to the quantitative formation of  $\Lambda\Lambda\Lambda\Lambda$ -[Ga<sub>4</sub>(271)<sub>6</sub>] ⊃ [Cp<sup>\*</sup>Ru(η<sup>4</sup>-diene)(H<sub>2</sub>O)]<sup>11-</sup>.

Fujita and co-workers utilized a bowl-shaped host **480**,<sup>27</sup> assembled from the reaction of planar triazine panels tris(3-pyridyl)triazine and (en)Pd<sup>II</sup> hinges in a 6:3 ratio, to study the preferential encapsulation of a homochiral pair of 1,1'-binaphthyl-2,2'-diol (BINOL).<sup>578</sup> Treatment of an aqueous solution of the bowl-shaped host, **480**, with an organic solution of (S)-BINOL at a 50% enantiomeric excess led to the formation of a 1:2 host–guest complex with 1 equiv each of (S)-BINOL and (R)-BINOL selectively encapsulated within the cavity of **480** (Scheme 130). The efficient heterorecognition of enantiomers afforded a significant enantiomeric enrichment of BINOL in the organic phase from 50 to 81%.

**4.5.1.2. Stabilization of Reactive Molecules and Intermediates.** Ever since the early pioneering work of Cram and co-workers, where a covalently constructed carcerand derived from calix[4]arene was able to stabilize cyclobutadiene,<sup>579</sup> there has been a sustained interest in designing molecular containers that can incarcerate unstable molecules and reactive intermediates within their cavities.<sup>521,522</sup> The unique microenvironment that exists within a cavity protects otherwise unrealizable molecules and intermediates from the bulk phase, making them amenable to detection and characterization. Raymond and co-workers have utilized a homochiral tetrahedral assembly, [Ga<sub>4</sub>(271)<sub>6</sub>]<sup>12-</sup>, to stabilize phosphonium,<sup>580,581</sup> diazonium,<sup>582</sup> tropylium,<sup>582</sup> and iminium<sup>583</sup> ions and organometallic reactive intermediates.<sup>584</sup> Reactive phosphonium ions [R<sup>1</sup> MeC(OH)PR<sub>3</sub>]<sup>+</sup> generated by the reaction of phosphines and ketones in acidic medium can be stabilized by encapsulation as guests within the tetrahedral assembly, [Ga<sub>4</sub>(271)<sub>6</sub>]<sup>12-</sup>, in aqueous solution.<sup>580</sup> Although these phosphonium ions have a transient existence in an aqueous medium, entrapment within the hydrophobic cavity of the cage increases their lifetimes considerably. Encapsulation of a range of phosphonium ions showed that the sizes and shapes of the guest

Scheme 131



cations play a vital role in the stability of the inclusion complexes. The stability of the phosphonium cations also increases with decreasing pH of the solutions. Similarly, tetrahedral assembly [Ga<sub>4</sub>(271)<sub>6</sub>]<sup>12-</sup> effectively encapsulated diazonium and tropylium cations within its hydrophobic cavity.<sup>582</sup> The combination of a tetrafluoroborate diazonium salt and [Ga<sub>4</sub>(271)<sub>6</sub>]<sup>12-</sup> in aqueous solution resulted in the formation of a 1:1 host–guest complex. Subsequent addition of 2,4-pentanedione showed no reaction, indicating stabilization of the diazonium ion within the cage.

Iminium ions generated in situ from amines and ketones have a transient stability in aqueous solutions at neutral or basic pH.<sup>583</sup> However, stabilization of such ions in water can be achieved via encapsulation within the hydrophobic cavity of the tetrahedral assembly, [Ga<sub>4</sub>(271)<sub>6</sub>]<sup>12-</sup>. For example, reaction of pyrrolidine with a wide variety of ketones in the presence of tetrahedral cage [Ga<sub>4</sub>(271)<sub>6</sub>]<sup>12-</sup> in aqueous solutions led to the formation of an encapsulated iminium ion complex (Scheme 131). Once encapsulated, these iminium ions were stable for months at room temperature. In the absence of host [Ga<sub>4</sub>(271)<sub>6</sub>]<sup>12-</sup>, no iminium ion could be observed by <sup>1</sup>H NMR spectroscopy. The binding efficiency of the iminium cations depended on their size, shape, charge, and hydrophobicity. Encapsulation of proton-bound amine homodimers in self-assembled host cage [Ga<sub>4</sub>(271)<sub>6</sub>]<sup>12-</sup> was achieved in water. These homodimers are otherwise not observable in aqueous medium.<sup>585</sup> A wide range of cyclic amines showed a proton-bound homodimer for *N*-alkyl aziridines, azetidines, pyrrolidines, and piperidines. Cyclic amines were chosen as guests due to their reduced degrees of rotational freedom, which attenuates the entropic price paid for encapsulation of multiple guests. Theoretical calculations suggest that formation of proton-bonding homodimers is highly enthalpically favorable.

Expanding on the incarceration of water-sensitive guests, Raymond, Bergman, and co-workers investigated the stabilization of reactive organometallic intermediates inside the self-assembled host [Ga<sub>4</sub>(271)<sub>6</sub>]<sup>12-</sup>.<sup>584</sup> [CpRuCl(cod)] (cod = 1,5-cyclooctadiene), a catalyst for C–C bond formation that undergoes halide dissociation in polar media to form a cationic solvated species [CpRu(cod)(H<sub>2</sub>O)]<sup>+</sup>. Surprisingly, suspending [CpRuCl(cod)] in an aqueous solution containing tetrahedral host [Ga<sub>4</sub>(271)<sub>6</sub>]<sup>12-</sup> resulted in the formation of an unusual 1:1 host–guest

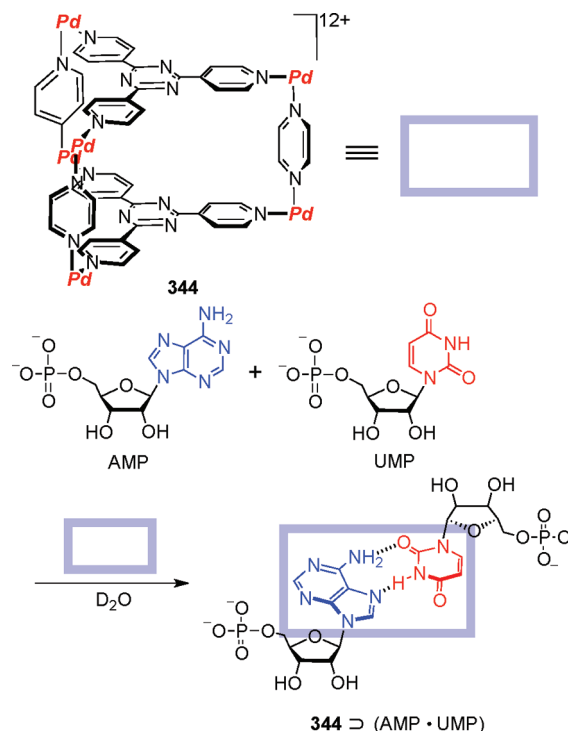
complex  $[\text{Ga}_4(271)_6 \supset \text{CpRu}(1,3,5\text{-octatriene})]^{11-}$  containing a highly unstable 16-electron ruthenium complex  $[\text{CpRu}(1,3,5\text{-octatriene})]^+$  within the cavity. The encapsulation provided enough binding energy to prevent the decomposition of the reactive species for several weeks. The incarcerated complex,  $[\text{CpRu}(1,3,5\text{-octatriene})]^+$ , still retained its reactivity and reacted stoichiometrically with CO to form  $[\text{CpRu}(\text{cod})(\text{CO})]^+$ . The addition of CO was believed to happen inside the cavity of the cage.

Fujita and co-workers were able to generate, stabilize, and characterize elusive organometallic species within the confined cavity of the self-assembled coordination cage **287**.<sup>586</sup> Treatment of an aqueous solution of coordination cage **287** with an excess amount of stable organometallic complex  $\text{Cp}'\text{Mn}(\text{CO})_3$  ( $\text{Cp}'$  = methylcyclopentadienyl) gave a 1:4 host–guest complex **287**  $\supset$   $[\text{Cp}'\text{Mn}(\text{CO})_3]_4$ . Photoirradiation of crystals of **287**  $\supset$   $[\text{Cp}'\text{Mn}(\text{CO})_3]_4$  at 100 K generated a 16-electron coordinatively unsaturated species  $\text{Cp}'\text{Mn}(\text{CO})_2$  in situ due to the dissociation of a single CO from one of the four guest molecules. The unsaturated manganese species  $\text{Cp}'\text{Mn}(\text{CO})_2$  retains its pyramidal geometry within the cage. Earlier, the same group was able to isolate and characterize reactive intermediates of a polycondensation reaction of trialkoxysilanes using tetrahedral coordination cage **286**.<sup>587,588</sup> Unstable cyclic silanol trimers formed during the polycondensation reaction were stabilized within the cavity of the coordination cage. The stability of the reactive species was attributed to its large size and rigidity, making it unable to escape the cavity of the cage. Modulating the cavity space through the use of a variety of coordination cages led to the observation of other short-lived species generated in the polycondensation of trialkoxysilanes.

In aqueous medium, short nucleotide fragments such as mono- and dinucleotides do not form stable hydrogen-bonded base pairs at molecularities less than four, due to competition from water. However, within the hydrophobic confines of biomolecules, even very short nucleotides can selectively form base pairs during translation, replication, and transcription. Fujita et al. have recently achieved the selective formation of stable mono- and dinucleotides in water using self-assembled trigonal-prismatic cages.<sup>589,590</sup> In the presence of coordination cage **344**, 5'-adenosine monophosphate (AMP) and 5'-uridine monophosphate (UMP) formed a 1:2 host–guest complex **344**  $\supset$  (AMP·UMP) in aqueous solution (Scheme 132), as indicated by an upfield shift of the nucleobase proton resonances in the <sup>1</sup>H NMR spectrum. The encapsulation of AMP–UMP base pairs was driven by a combination of hydrophobic, electrostatic, and  $\pi$ – $\pi$  interactions.

X-ray crystal structural studies of the encapsulated base pair revealed that it is not linked through the usual Watson–Crick hydrogen bonding observed in duplexes, but rather through an anti-Hoogsteen hydrogen-bonding pattern usually observed in triplexes.<sup>15</sup> <sup>15</sup>N NMR spectroscopic studies also supported the formation of anti-Hoogsteen nucleobase pairs within the cavity of the cage. Similarly, dinucleoside monophosphate duplexes were formed when an aqueous solution of thymidyl-(3'-5')-2'-deoxyadenosine (TA) was stirred with the 4,4'-bipyridine pillared cage having an extended cavity to form a 1:2 host–guest complex. NMR (1D and NOESY) spectroscopic studies suggested the formation of a discrete base paired (TA)<sub>2</sub> dimer through anti-Hoogsteen hydrogen bonding within the cavity. The X-ray crystal structure of the host–guest complex, however, showed an infinite network, whereas dinucleotides formed hydrogen-bonded chains threaded through adjacent host cages.

Scheme 132

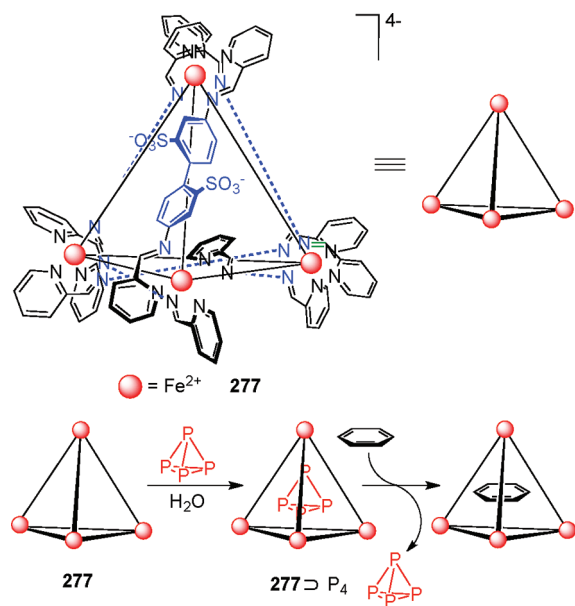


The authors suggested that the two structures (discrete and polymeric) were in equilibrium with discrete species being dominant in solution, while the polymeric structure was trapped in the solid state.

Nitschke et al. utilized a self-assembled, water-soluble tetrahedral cage (**277**) to encapsulate highly pyrophoric white phosphorus  $\text{P}_4$ , thus making it inert and air-stable.<sup>591</sup> Uptake of  $\text{P}_4$  within the hydrophobic cavity of **277** of the anionic cage was observed in aqueous solution. <sup>1</sup>H NMR and X-ray crystallographic studies indicated the incorporation of  $\text{P}_4$  through the formation of a 1:1 host–guest complex **277**  $\supset$   $\text{P}_4$  (Scheme 133). The host–guest complex remained stable upon exposure to air for 4 months. Despite oxygen molecules' smaller size than  $\text{P}_4$  molecules, suggesting that they could gain access to the interior of the cage,  $\text{O}_2$  did not react with  $\text{P}_4$  confined within the cavity. The reason for such an unusual behavior was attributed to the unavailability of space to form the reaction intermediates inside the cavity during the steps of phosphorus oxidation. The incarcerated  $\text{P}_4$  molecule could be easily released by layering an aqueous solution of host–guest complex **277**  $\supset$   $\text{P}_4$  with benzene, causing benzene molecules to replace  $\text{P}_4$  as the guests.

**4.5.2. Cavity Controlled Reactions.** Self-assembled coordination cages have been successfully applied as nanovessels for carrying out various stoichiometric and catalytic reactions. A wide variety of reactions such as thermal, photochemical, and encapsulated transition metal catalyzed reactions have been shown to occur within the nanospaces of coordination cages. The unique microenvironment created within the nanometer-sized cavities of these assemblies, due to their specific sizes, shapes, and hydrophobicities, can force substrates to adopt unusual conformations often unobservable in bulk phases through  $\pi$ -stacking and hydrophobic effects. Furthermore, the stabilization of transition states and reactive intermediates within

Scheme 133



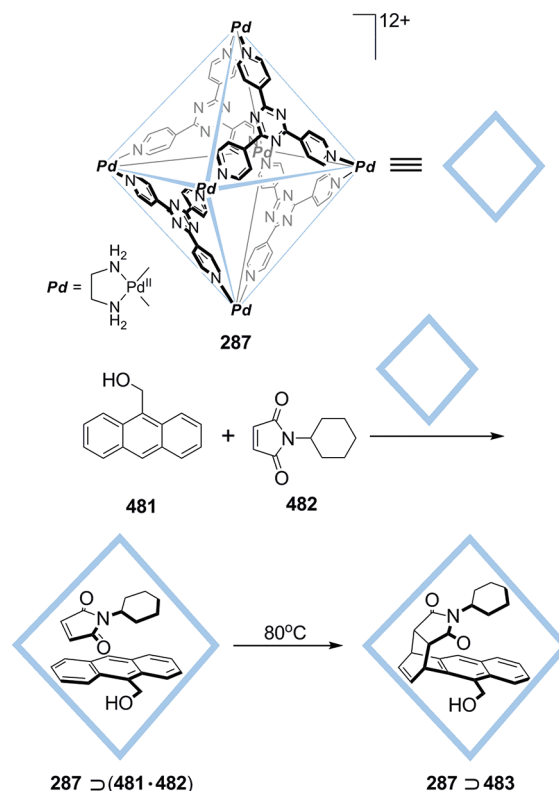
the cavities can also change the course of the reaction by manipulating the reaction energetics. Protection of these species from the bulk phase, similar to enzyme pockets, blocks the bulk reaction pathway, leading to new, unusual regio-, chemo-, and stereoselective products.

**4.5.2.1. Cavity Controlled Stoichiometric Reactions.** Fujita and co-workers utilized steric constriction within the nanospaces of coordination cages to achieve unusual regio- and stereoselective Diels–Alder reactions between anthracenes and maleimides.<sup>592</sup> For example, suspending a mixture of 9-hydroxymethylantracene **481** and *N*-cyclohexylmaleimide **482** in an aqueous solution of a stoichiometric amount of coordination cage **287** resulted in the formation of 1:2 host–guest complex **287** ⊃ (**481**·**482**). Upon heating the reaction mixture to 80 °C, unusual stereo- and regioselective formation of a [2 + 2] cycloaddition product, **483**, was observed in more than 98% yield (Scheme 134). NMR and X-ray crystallographic studies of **287** ⊃ **482** revealed the formation of a *syn*-1,4-Diels–Alder adduct via a reaction at the terminal anthracene ring. The observation of such an unusual Diels–Alder reaction was due to coordination cage **287** enforcing the two substrates to adopt specific orientations, thus preventing interactions at the expected 9,10 position of the anthracene.

Similarly, otherwise inert arenes also underwent unusual [2 + 2] and [2 + 4] thermal cycloaddition reactions within the cavities of analogous palladium and platinum tetrahedral cages.<sup>593</sup> Highly stable aromatic molecules, such as triphenylene, perylene, substituted naphthalenes, acenaphthylene, and 1*H*-cyclopenta[1]-phenanthrene, afforded the corresponding [2 + 2] and [2 + 4] endo Diels–Alder adducts with *N*-cyclohexylmaleimide (**482**) in good yields.<sup>594,595</sup> The steric demand of the *N*-cyclohexyl group on **482** is important as it directs the preorganization of the substrates within the hydrophobic cavity, thus promoting energetically unfavorable stereo- and regioselective reactions.

Fujita and co-workers investigated cavity-directed, highly stereoselective photodimerization of olefins mediated by self-assembled coordination cages. For example, when excess amounts of the

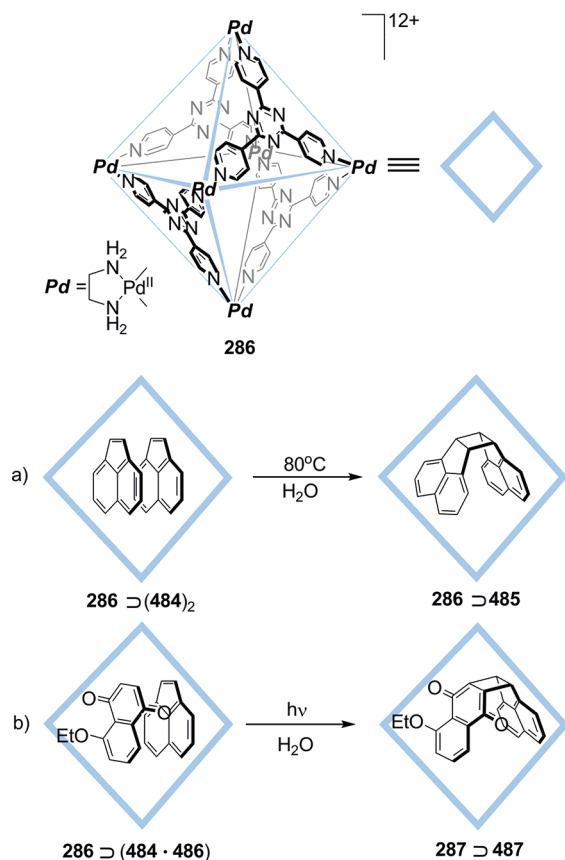
Scheme 134



bulky olefin acenaphthylene (**484**) were suspended in an aqueous solution of coordination cage **286**, formation of a 1:2 host–guest complex **286** ⊃ (**484**)<sub>2</sub> was observed, as indicated by the upfield shift of the <sup>1</sup>H NMR signals corresponding to the encapsulated guest molecules (Scheme 135a).<sup>596</sup> Photoirradiation of this host–guest complex led to the exclusive formation of the *syn* dimer **485** in quantitative yield. Similarly, encapsulation of two molecules of 1-methylacenaphthylene followed by irradiation gave exclusively the head-to-tail *syn* dimer. Exclusive formation of *syn* dimer **485** was also observed, even in the presence of sensitizers such as xanthine dyes, although the sensitized reactions generally go through triplet states.<sup>597</sup> X-ray structural analyses of **286** ⊃ (**484**)<sub>2</sub> and **286** ⊃ **485** both before and after [2 + 2] photodimerization allowed in situ crystallographic tracking of the photochemical transformation.<sup>598</sup> Before photoirradiation, the two encapsulated substrate molecules interacted with the cage through  $\pi$ -interactions and were disordered over three positions at 240 K, providing a fluidlike environment even in the crystalline state. This allowed the guest molecule to thermally tumble within the host cavity. Nevertheless, quantitative formation of *syn* dimer **485** was observed upon irradiation at 240 K, as revealed by the single-crystal X-ray structure of **287** ⊃ **485**. Bowl-shaped host **480** also showed the exclusive formation of the *syn* dimer in more than 98% yield in the [2 + 2] photodimerization of naphthoquinones.<sup>596</sup> X-ray structural studies of the dimer-encapsulated cage revealed a *syn* conformation for the dimer, which was held through  $\pi$ – $\pi$  and CH– $\pi$  interactions. Ramamurthy et al., working with coordination cage **286**, also investigated the [2 + 2] photodimerization of *trans*-cinnamic acid esters in water.<sup>599</sup> Irradiation of a series of *trans*-cinnamic acid methyl esters encapsulated host–guest complexes showed mostly the formation of *syn*



Scheme 135



head-to-head dimers in a range of 21–63% yields along with the corresponding monomeric isomerization products. In two cases, however, anti head-to-tail dimers were also observed, indicating that substituents can also play a role in the packing of the substrates and thus the photochemical outcome of the reaction. A series of derivatives of coumarin also led to the exclusive formation of syn head-to-head dimers with coordination cage 286 as the nanovessel for the [2 + 2] photodimerization reaction.<sup>600</sup> Selective [2 + 2] cross-photodimerization was also investigated using self-assembled coordination cage 286 as a host in aqueous medium.<sup>601</sup> Such reactions are challenging, as the host cage must selectively and pairwise recognize two different olefins in a proper orientation for the cross-photodimerization to occur. Suspension of acenaphthylene 484 and 5-ethoxynaphthoquinone 486 in an aqueous solution at  $80^\circ\text{C}$  in the presence of coordination cage host 286 led to the formation a 1:2 host guest complex,  $287 \supset (484 \cdot 486)$ , as determined by the upfield shift of the signals due to the encapsulated guests in the  $^1\text{H}$  NMR spectra. Upon photoirradiation with a mercury lamp, a hetero-syn-dimer 487 was obtained in 92% yield (Scheme 135b). However, olefins having smaller or no substituents gave both hetero- and homodimers. The steric bulk of the substrate is essential for preorganization of the substrate within the host cavity, which prevents the formation of other possible products. Thus, the use of sterically demanding *N*-cyclohexylmaleimide and its derivatives afforded a [2 + 2] photodimerization with planar arenes such as acenaphthylene, pyrene, phenanthrene, and fluoranthene.<sup>594,601</sup> Chiral induction of an asymmetric [2 + 2] cross-photoaddition was also observed with chiral cages analogous

to 286 by replacing the ethylenediamine end cap on each Pd center with chiral diamines.<sup>602</sup> The [2 + 2] cross-photoaddition reaction of *N*-cyclohexylmaleimide and fluoranthene led to the formation of a [2 + 2] product with an enantiomeric excess of up to 50%. The remote chiral auxiliaries induce chiral deformation of the central cavity through deformation of the triazine panels.

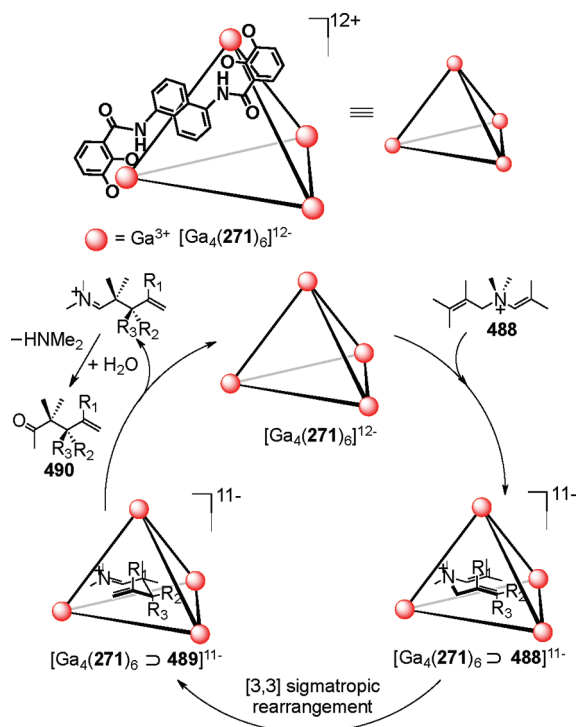
The confined cavity of a coordination cage was also utilized to suppress the photocleavage of  $\alpha$ -diketones to give cyclization products through kinetically unfavorable pathways.<sup>603</sup> Typically,  $\alpha$ -diketones undergo homolytic cleavage followed by degradation upon photoirradiation. However, encapsulation of benzil, a  $\alpha$ -diketone, within the cavity of coordination cage 287 gave a 1:2 host–guest complex which, upon irradiation, gave unusual rearranged products with an overall yield of 52%, indicating that homolytic cleavage is completely suppressed and a kinetically unfavorable pathway becomes dominant. The photomediated 1,4-radical addition of *o*-quinones to a bulky toluene derivative was also observed within the cavity of self-assembled host 286.<sup>604</sup> The photoexcited quinone abstracts a proton from the neighboring methyl group of the toluene derivative to generate a benzylic radical and semiquinone radicals, which subsequently recombine to selectively produce the 1,4-adduct in 70% yield.

Fujita and co-workers have also achieved the oxidation of alkanes through photochemical excitations of self-assembled coordination cage 287.<sup>605</sup> It is important to note here that the host cage actively participates by influencing the reaction pathway rather than remaining an inert and passive component. To explore the photoresponsible nature of cage 287, an inert alkane guest, adamantane, was encapsulated to give a 1:4 host–guest complex  $287 \supset (\text{adamantane})_4$ . Upon irradiation under aerobic conditions, regioselective oxidation of adamantane afforded 1-adamantylhydroperoxide and 1-adamantanol in 24% yield (or 96%, assuming that only one guest is oxidized per cavity). Detailed spectroscopic, electrochemical, and theoretical studies revealed that host–guest complex  $287 \supset (\text{adamantane})_4$  was well-suited for photoinduced electron transfer.<sup>606</sup> The electron-poor triazine panels accept an electron from the encapsulated adamantane to give rise to an adamantyl radical. Subsequent quenching of the adamantyl radical by oxygen or water resulted in the formation of oxidation products 1-adamantylhydroperoxide and 1-adamantanol. Tight host–guest contact brings triazine panels close to the adamantane molecules, thus promoting unusual photoinduced electron transfer.

Encapsulation of half-sandwich iridium complexes within the cavity of supramolecular host cage  $[\text{Ga}_4(271)_6]^{12-}$  showed selective C–H bond activation of aldehydes.<sup>607</sup> The addition of monocationic iridium complex  $[\text{Cp}^*(\text{PMe}_3)\text{Ir}(\text{Me})(\text{C}_2\text{H}_4)]^+$  and tetrahedral cage  $[\text{Ga}_4(271)_6]^{12-}$  in aqueous medium led to quantitative encapsulation resulting in a 1:1 host–guest complex  $272 \supset [\text{Cp}^*(\text{PMe}_3)\text{Ir}(\text{Me})(\text{C}_2\text{H}_4)]$ , as indicated by the upfield NMR shifts of the resonances of guest molecule. Heating an aqueous solution of host–guest complex  $[\text{Ga}_4(271)_6]^{12-} \supset [\text{Cp}^*(\text{PMe}_3)\text{Ir}(\text{Me})(\text{C}_2\text{H}_4)]$  and acetaldehyde at  $75^\circ\text{C}$  led to the formation of a new encapsulated product,  $[\text{Cp}^*(\text{PMe}_3)\text{Ir}(\text{Me})(\text{CO})]$ , which resulted from the C–H bond activation of the acetaldehyde. Substrate scope and mechanistic studies showed that size and shape selectivities play vital roles in the encapsulated C–H bond activation reactions.<sup>608</sup> The fact that the dissociation of the guest was slower than the rate of C–H bond activation indicated that the reactions occur within the cavity of the host–guest assembly. Kinetic studies revealed that the iridium guest dissociation proceeds through a strongly bound



Scheme 136



ion pair intermediate through a two-step process in which the guest exits the cavity but remains bound to the outside of the host cage before fully dissociating from the host.

**4.5.2.2. Cavity Controlled Catalytic Reactions.** Self-assembled coordination cages can be efficient reaction nanovessels for various catalytic reactions. The unique microenvironments of the hydrophobic cavities coupled with the size- and shape-defined nanospaces drive reactions often unobservable in bulk solution. However, in many such cavity-mediated reactions, strong complexation and/or the large size of the reaction product traps it within the cavity, resulting in a low catalytic turnover. Judicious choice of the host and substrate can prevent such product inhibition, leading to truly catalytic systems. Raymond and co-workers demonstrated that the problem of product inhibition might be circumvented through prudent choice of compatible hosts and guests. The anionic self-assembled cage  $[\text{Ga}_4(271)_6]^{12-}$  was shown to act as a true catalytic host in the unimolecular aza-Cope rearrangement of enamonium cations in aqueous medium.<sup>609</sup> Enamonium cation **488**, the reaction substrate for the cationic aza-Cope rearrangement reaction, are analogous to the known<sup>337</sup> strong binding ammonium cationic guest  $\text{NMe}_2\text{Pr}^{2+}$  and thus effectively bind within the cavity of anionic self-assembled cage  $[\text{Ga}_4(271)_6]^{12-}$  to form 1:1 inclusion complex  $[\text{Ga}_4(271)_6 \cdot 488]^{11-}$  (Scheme 136). Subsequent  $[3,3]$  sigmatropic rearrangement led to the formation of iminium cation **489**, which escape from the interior of the cavity to an exterior binding site where they undergo hydrolysis to give the corresponding  $\gamma, \delta$ -unsaturated aldehyde (**490**) with turnover numbers (TON) of ca. 8. Since the neutral molecules are bound weakly within the cavity of the host assembly  $[\text{Ga}_4(271)_6]^{12-}$ , neutral aldehydes were rapidly displaced from the cavity by the cationic substrate molecules, preventing product inhibition.

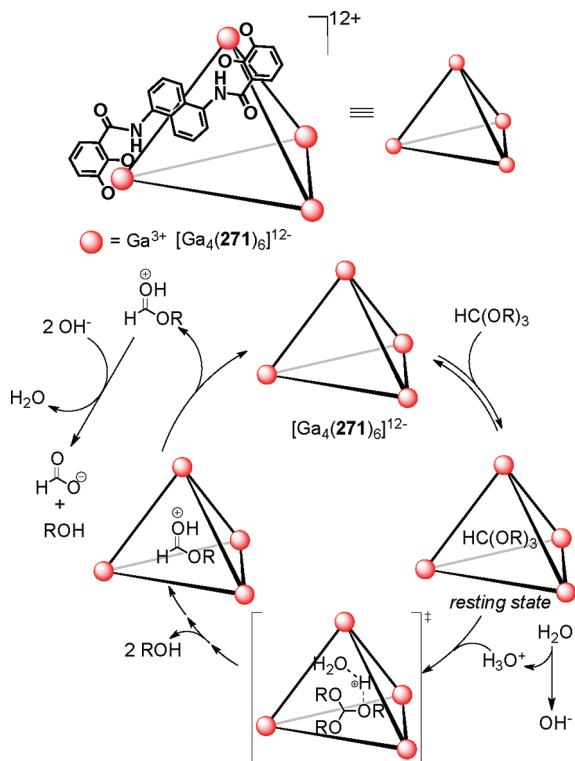
When enamonium ions were substituted unsymmetrically ( $\text{R}_2 \neq \text{R}_3$ ), the rearrangement generated a chiral center, resulting

in the formation of chiral product aldehydes. A series of prochiral enamonium tosylates, upon treatment with catalytic amounts of  $(\text{NMe}_4)_{12}[\Delta\Delta\Delta\Delta\text{-Ga}_4(271)_6]$ , resulted in the asymmetric induction of a catalyzed aza-Cope rearrangement.<sup>610</sup> The enantioselectivities achieved for the products were highly dependent on the substrate size and charge. Detailed substrate scope and mechanistic studies revealed that, upon encapsulation, the confined cavity of the host assembly enforces the substrates to adopt reactive conformations, as evidenced by kinetic, activation parameter, and quantitative NOE studies, thus accelerating the rate of rearrangement by factors up to 3 orders of magnitude.<sup>611</sup> Extension of the study to the rearrangement of less reactive propargyl enamonium cationic substrates showed rate accelerations by factors of up to 184 as compared with the background reaction rate.<sup>612</sup> Determination of the kinetic parameters revealed that the catalytic reactions follow the Michaelis–Menten model of enzyme kinetics. Activation parameters indicated the reasons for the rate acceleration were due to a more positive value of  $\Delta S^\ddagger$ .

Raymond, Bergman, and co-workers recently achieved a reaction rate acceleration by a factor of  $10^6$ , comparable in size to those observed in the domain of enzymatic catalysis. The tetrahedral self-assembled cage  $[\text{Ga}_4(271)_6]^{12-}$  was shown to accelerate the Nazarov cyclization of pentadiols.<sup>613</sup> Suspension of 10 equiv of 3,4,5-trimethylhepta-2,5-dien-4-ol in an aqueous solution of coordination cage  $[\text{Ga}_4(271)_6]^{12-}$  at 50 °C resulted in the quantitative formation of the Nazarov cyclized product, pentamethylcyclopentadiene. The pseudo-first-order reaction rate was, however, impeded due the competitive binding of the cyclized product within the host cavity, leading to product inhibition. This problem was avoided by using maleimide as a trapping agent for the cyclized product. The resulting Diels–Alder adducts have less affinity for the host as compared to the substrate, accordingly restoring the pseudo-first-order kinetic behavior. The rate-determining step for the reaction was found to be the rearrangement of the encapsulated substrate to adopt a bent conformation prior to or at the transition state. Thus, the constricted environment within the cavity of  $[\text{Ga}_4(271)_6]^{12-}$  facilitates a million-fold rate enhancement due to the combination of an increase in the basicity of the alcohol functionality upon encapsulation, preorganization of the bound substrate, and stabilization of the transition state of the electrocyclic reaction.

In previous studies, the same group demonstrated that tetrahedral cage  $[\text{Ga}_4(271)_6]^{12-}$  could mediate acid-catalyzed reactions within its cavity in basic solutions. Due to the high binding affinity of cationic guest molecules over neutral species, addition of neutral guests leads to thermodynamically driven encapsulation and stabilization of the corresponding protonated species within the cavity of the anionic cage. Since hydrolysis of orthoformates goes through a protonated reactive intermediate, orthoformates  $\text{HC}(\text{OR})_3$  undergo rapid hydrolysis to the corresponding formates in the presence of a catalytic amount of coordination cage  $[\text{Ga}_4(271)_6]^{12-}$  in a basic aqueous solution (pH 11).<sup>614</sup> The catalytic cycle for the process is shown in Scheme 137. Initially, orthoformate gets encapsulated within the hydrophobic cavity of the cage to give a 1:1 inclusion complex,  $[\text{Ga}_4(271)_6]^{12-} \cdot [\text{HC}(\text{OR})_3]$ . The protonated ester  $\text{HC}(\text{O})\text{OR}$ , generated through protonation from water, is subsequently hydrolyzed by  $\text{OH}^-$  to the formate ion. Mechanistic studies revealed that electrostatic and hydrophobic effects drive the initial encapsulation of the neutral guest. Protonation of the substrate within the cavity through proton transfer from water is the rate-limiting step. Determination of the kinetic and activation

Scheme 137



parameters revealed that the hydrolysis follows Michaelis–Menten kinetics in parallel to enzymatic pathways. The observed entropy of activation and solvent isotope effect suggested that the initial step of the hydrolysis proceeded through an  $\text{A-S}_{\text{E}}2$  mechanism in contrast to an  $\text{A-1}$  mechanism for orthoformate hydrolysis in bulk solution. A kinetic analysis of the rate constants in comparison with the uncatalyzed reaction showed a  $10^3$ -fold rate acceleration. For tri-*n*-orthoformate, a 3900-fold acceleration was observed.<sup>615</sup> Similarly, the acid-catalyzed hydrolysis of acetals was also investigated using tetrahedral self-assembled coordination cage  $[\text{Ga}_4(271)_6]^{12-}$ . Acetals are stable in neutral and basic media and require Brønsted or Lewis acid catalysts for their hydrolysis. This makes tetrahedral cage  $[\text{Ga}_4(271)_6]^{12-}$  an ideal catalytic host for the reaction. For example, addition of 2,2-dimethoxypropane as a substrate in a basic aqueous solution containing a catalytic amount of  $[\text{Ga}_4(271)_6]^{12-}$  at pH 10 showed the expected hydrolyzed products.<sup>616,617</sup> Mechanistic studies revealed that the mechanism of hydrolysis takes place inside the assembly and proceeds through an  $\text{A-2}$  mechanism, in contrast to the  $\text{A-1}$  mechanism operating in the uncatalyzed reaction. The rate-limiting step of the reaction involves negative entropy of activation and an inverse solvent isotope effect.

As discussed above, the Diels–Alder cycloaddition reaction between substituted anthracenes with *N*-cyclohexylmaleimide in aqueous medium requires use of a stoichiometric amount of coordination cage to mediate the reaction, due to the strong complexation of the product to the host molecule.<sup>592</sup> However, the same reaction proceeded catalytically upon use of bowl-shaped cage **480** as the host. For example, in the presence of a catalytic amount of coordination cage **480** (10 mol %), 9-hydroxymethylanthracene (**481**) with *N*-phenylmaleimide efficiently produced the Diels–Alder adduct with good TON (ca. 10).<sup>592</sup>

In this reaction, however, a conventional 9,10-adduct was formed in contrast to the unusual 1,4-adduct observed when coordination cage **287** was used. The open hydrophobic cavity of bowl **480** ensured facile encapsulation of the substrate molecules through hydrophobic,  $\pi$ -stacking and/or charge-transfer interactions. The bent shape of the anthracene moiety in the resulting adducts hampers  $\pi$ -stacking within the host cage, thus reducing the affinity to the host as compared to the substrates. This enables substrate molecules to displace adducts and maintain the catalytic cycle.

Self-assembled coordination cages having encapsulated active organometallic catalysts have led to new and hitherto unobserved reactions. Encapsulation of a catalyst within the cavity of self-assembled host cage may alter its activity through changes in its structure, giving rise to different properties. The rate-determining step in a catalytic cycle of a known organometallic catalyst may also be altered due to encapsulation, leading to new selectivities. Raymond, Bergman, and co-workers utilized self-assembled tetrahedral cage  $[\text{Ga}_4(271)_6]^{12-}$  to encapsulate an active rhodium complex to investigate the catalytic isomerization of allylic alcohols.<sup>618</sup> A combination of the tetrahedral cage  $[\text{Ga}_4(271)_6]^{12-}$  and small bisphosphine rhodium complexes of the general formula  $[(\text{P-P})\text{Rh}(\text{diene})]\text{BF}_4$  ( $\text{P-P} = \text{PMe}_3$  or 1,2-bis(dimethylphosphino)ethane (dmpe), diene = 1,5-cyclooctadiene (COD), or norbornadiene (NBD)) in aqueous solution led to the formation of discrete 1:1 inclusion complexes  $[\text{Ga}_4(271)_6 \supset \{(\text{P-P})\text{Rh}(\text{diene})\}]^{11-}$ . Upfield shifting of the NMR resonances of the encapsulated guest molecules indicated the formation of a host–guest assembly. The encapsulated catalyst precursor was hydrogenated to generate a reactive catalyst,  $[\text{Ga}_4(271)_6 \supset \{(\text{P-P})\text{Rh}(\text{OD}_2)_2\}]^{11-}$ . Upon addition of allylic alcohol to this activated, catalytic host–guest assembly, the corresponding isomerized products were formed within 30 min at room temperature. While the shape and size selection of the catalytic host–guest assembly allowed encapsulation of small and unsubstituted allylic alcohols, it prevented encapsulation of large and branched substrates by denying access to the active site of the catalyst. Apertures of the host–guest assembly regulate the encapsulations of substrate molecules. Recently, gold(I)–phosphine complexes encapsulated by a self-assembled tetrahedral cage  $[\text{Ga}_4(271)_6]^{12-}$  were utilized to investigate the intramolecular hydroalkoxylation of allenes.<sup>619</sup> The combination of  $\text{Me}_3\text{PAuBr}$  with the tetrahedral cage  $[\text{Ga}_4(271)_6]^{12-}$  in  $\text{D}_2\text{O}$  or MeOD led to the formation of a discrete 1:1 inclusion complex  $[\text{Ga}_4(271)_6 \supset (\text{Me}_3\text{PAu}^+)]^{11-}$  as observed by  $^1\text{H}$  NMR spectroscopy. Addition of 6-methylhepta-4,5-dien-1-ol to an aqueous solution of  $[\text{Ga}_4(271)_6 \supset (\text{Me}_3\text{PAu}^+)]^{11-}$  showed 48% conversion of the allene to the desired cyclized product after 18 h at room temperature. In contrast,  $\text{Me}_3\text{PAuBr}$  under similar reaction conditions gives only an 11% yield of cyclized product after 18 h. This reaction constitutes an elegant example of the enhancement of catalytic activity of an organometallic complex in which the reactivity and lifetime of the catalyst are both enhanced by supramolecular encapsulation.

Fujita et al. utilized coordination cage **286** as a phase-transfer catalyst because of its amphiphilic nature in the Wacker-type oxidation of styrene and its derivatives. For example, the addition of styrene to an aqueous solution containing a catalytic amount of **286** led to the formation of host–guest system  $\text{286} \supset (\text{styrene})_n$  ( $n = \text{ca. } 3$ ) as indicated by its  $^1\text{H}$  NMR spectrum. Subsequent addition of a catalytic amount of  $[\text{Pd}(\text{en})(\text{NO}_3)_2]$  followed by heating at  $80^\circ\text{C}$  for 24 h gave acetophenone in an

82% yield with a TON of 8. The oxidation proceeds through a biphasic reaction wherein styrene is encapsulated by the host cage and then transferred into the aqueous phase where it is oxidized to acetophenone by the Pd(II) reagent. The reaction product, acetophenone, being less hydrophobic, was displaced from the host cavity by the substrate molecules.<sup>620</sup> Similarly, coordination cage **287** catalyzed the Wacker-type oxidation of linear alkenols.<sup>621</sup>

Hupp and co-workers utilized a supramolecular porphyrinic box as catalyst for selective olefin epoxidation and enantioselective sulfoxidation.<sup>622</sup> The cavity-tailored supramolecular catalytic box consists of 18 porphyrin units—four zinc(II) porphyrin trimers, two tin(IV) porphyrin dimers, and one manganese(III) porphyrin dimer. The catalytically active manganese(III) porphyrin dimer unit was encapsulated within the rigid porphyrin box cavity that was tailored with carboxylate ligands via a self-sorting process. A competitive study of size-selective epoxidation between *cis*-stilbene and *cis*-3,3',5,5'-tetra(*tert*-butyl)stilbene showed that *cis*-stilbene was 5.5-fold more reactive than sterically bulky *cis*-3,3',5,5'-tetra(*tert*-butyl)stilbene. The steric bulk of the carboxylate ligands present on the adjacent tin(IV) porphyrin dimer inhibits the access of the larger olefin to the Mn(III) catalytic center resulting in size-selective catalysis. When the cavity was modified with a chiral amino acid ligand, *N*-acetyl-D-phenylalanine, on the Sn(IV) dimer, an enantioselective sulfoxidation of methyl *p*-tolyl sulfide with an enantiomeric excess of 12% ee was observed. Remarkably, the sense of chiral excess was reversed when *N*-acetyl-L-phenylalanine was used. No enantiomeric excess was observed when the free manganese(III) porphyrin dimer was used in the presence of free tin(IV) porphyrin dimer.

Recently, a trigonal-bipyramidal cage was utilized as a catalyst for Suzuki-Miyaura C—C cross-coupling reactions.<sup>623</sup> The molecular cage  $[\{(Me_4en)Pd\}_3L_2](BF_4)_6$  ( $L = 1,3,5$ -tris(isonicotinoyloxyethyl)cyanurate), assembled from a reaction of  $(Me_4en)Pd(BF_4)_2$  and 1,3,5-tris(isonicotinoyloxyethyl)cyanurate, has a truncated trigonal-bipyramidal architecture with a  $C_{3h}$  symmetry point group. Each *L* occupies a pyramid, and three Pd(II) ions lie in equatorial positions with a single, disordered water molecule nestled into the cavity. Both  $[\{(Me_4en)Pd\}_3L_2 \supset H_2O]^{6+}$  and desolvated  $[\{(Me_4en)Pd\}_3L_2]^{6+}$  efficiently catalyzed C—C cross-coupling reactions in *N,N*-dimethylformamide with  $K_2CO_3$  as a base without phosphine or any other additives. The cage  $[\{(Me_4en)Pd\}_3L_2 \supset H_2O]^{6+}$  gave higher yield of the cross-coupled product compared to  $[\{(Me_4en)Pd\}_3L_2]^{6+}$  due to the water-assisted effects of the Suzuki-Miyaura C—C cross-coupling reaction.

**4.5.3. Biological Applications.** Biological applications of self-assembled supramolecular ensembles are still in their infancy. Only in the past few years have researchers begun to apply coordination-driven self-assembled supramolecular ensembles toward biological applications by building functional structures that mimic the complex recognition, regulatory, and other properties of biological systems. Incorporation of biological functionalities into these supramolecular structures and control of their relative arrangements have led to the observation of interesting phenomena. Furthermore, these self-assembled supramolecular metallacages are increasingly being applied to hitherto underexplored biochemical and biomedical applications.<sup>624</sup>

The binding of proteins regulates the expression of genetic information encoded in DNA in a reversible and noncovalent manner through weak interactions. Thus, the study of noncovalent

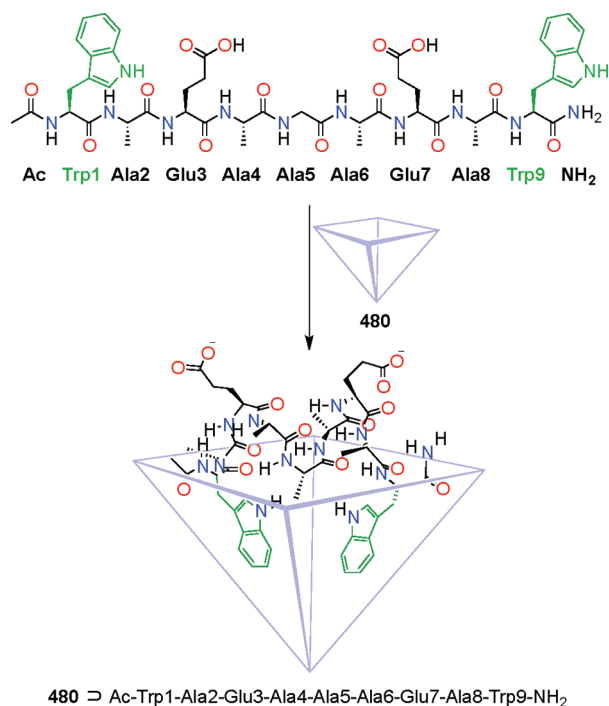
interactions of DNA with synthetic, small molecules may provide insight into DNA structure control by proteins. Supramolecular chemistry allows the design of DNA-binding agents of similar dimensions to protein DNA-recognition motifs.<sup>624</sup> Furthermore, such studies are also of great importance toward effective drug design and development. Hannon and co-workers have extensively studied supramolecular DNA recognition by coordination-driven metallohelicities. The supramolecular triple helicates  $[M_2L_3]^{2n+}$  ( $n$  = charge on each metal) were assembled through the interaction of metal ions with bis(pyridylimine) ligands (*L*) having diphenylmethane spacer.<sup>625</sup> As determined from induced circular dichroism, linear dichroism, AFM, NMR, and computational studies, racemic  $[Fe^{II}_2L_3]^{4+}$  was found to interact with DNA in a single binding mode consistent with major groove binding, an often preferred site for recognition by protein, and induces DNA bending and intramolecular coiling.<sup>626,627</sup> The enantiomers of  $[Fe^{II}_2L_3]^{4+}$  bind differently with DNA. The *M* enantiomers bind the major groove with partial insertion of one chelate between DNA bases. *P* isomers bind in the minor groove, spanning the two phosphate backbones.<sup>628</sup> However, an extension of the structure of the triple helicate through ligand modulation affects the DNA binding ability significantly. The extended helicates, having two ketimine spacers, do not bind to DNA, as established from induced circular dichroism studies.<sup>629</sup> This is due to the loss of CH— $\pi$  interactions among the ligand strands resulting in the disruption of the relay of chiral information between the two metal centers, leading to the formation of a mixture of rac and meso isomers, with the meso isomer being dominant. A dicationic Cu(I) double helicate  $[Cu^I_2L_2]^{2+}$  binds less strongly to DNA and in a slightly different orientation as compared to tetracationic helicate  $[Fe^{II}_2L_3]^{4+}$ .<sup>630</sup> This indicates that the charge, size, and shape of the helicates serve as important parameters for effective DNA binding. The same group also observed a rare mode of DNA recognition wherein the tetracationic helicate  $[Fe^{II}_2L_3]^{4+}$  interacts with a palindromic DNA hexanucleotide. X-ray structural studies revealed that the helicate binds into the central trigonal hydrophobic cavity of a three-way DNA junction.<sup>631</sup>

G-quadruplex DNA structures based on guanine quartets are found in the telomeric and transcriptional regulatory regions of chromosomes. In cancer cells, the telomeres are elongated by the enzyme telomerase, thereby conferring immortality to the cancerous cell line. Thus, molecules that can bind specifically to quadruplex DNA may lead to potential anticancer drugs.<sup>322</sup> Therrien et al. studied the interaction of arene ruthenium-based tetragonal coordination cages  $[Ru_8(\eta^6\text{-arene})_8(\mu\text{-tppH}_2)_2\text{-(dqb)}_4]^{8+}$  (**389**, arene =  $C_6H_5Me$ ; **390**, arene = *p*-cymene) and  $[Ru_8(\eta^6\text{-arene})_8(\mu\text{-tppZn})_2\text{-(dqb)}_4]^{8+}$  with both duplex and quadruplex DNA.<sup>456</sup> A fluorescence intercalation displacement assay (FID) and surface Plasmon resonance (SPR) study showed that the metallacages bind strongly to telomeric and *c-myc* DNA. Although SPR results indicated that these cages bind more strongly with quadruplex DNA than duplex DNA, selectivity for quadruplex over duplex DNA was modest, supposedly due to the high cationic charge of the tetragonal cages, which increases nonspecific binding of DNA via electrostatic interaction.

In the context of recognition and folding of peptides, Fujita et al. utilized a variety of self-assembled molecular cages as hosts. Using tetrahedral cage **287** as a supramolecular host, sequence-selective recognition of oligopeptides within the hydrophobic cavity of was observed in aqueous media.<sup>632</sup> Coordination cage **287** showed a strong and specific binding affinity toward



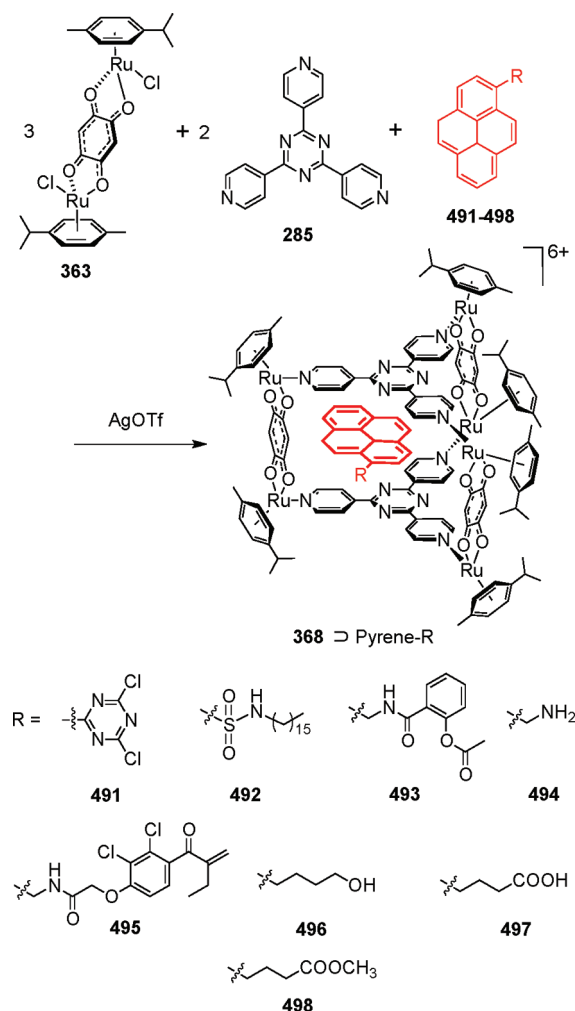
Scheme 138



Ac-Trp-Trp-Ala-NH<sub>2</sub> over other sequences of tripeptides. A tetrapeptide and hexapeptide possessing the Trp-Trp-Ala sequence also bind strongly to tetrahedral cage **287**. The specific binding affinity for the Trp-Trp-Ala sequence was attributed to efficient  $\pi$ - $\pi$  interactions between the indole rings of Trp residues and triazine panels of the host cage. Likewise, the bowl-shaped host, **480**, encapsulated a nine-residue peptide (Ac-Trp1-Ala2-Glu3-Ala4-Ala5-Ala6-Glu7-Ala8-Trp9-NH<sub>2</sub>) inside the hydrophobic pocket in aqueous solution (Scheme 138).<sup>633,634</sup> The binding of the peptide within the cavity induced and stabilized a  $\alpha$ -helix conformation. <sup>1</sup>H NMR titration studies revealed that the two terminal tryptophan residues (Trp1 and Trp9) bind to the bowl leading to a 1:1 host-guest complex. TOCSY and NOESY measurements, coupled with molecular modeling, revealed that the 9-mer peptide adopts an  $\alpha$ -helical conformation with two Trp residues deeply buried into the hydrophobic pocket. However, the 2:1 host-guest complex, wherein two bowls wrapped the whole 9-mer residue, was predominantly formed in the presence of an excess amount of cage. Varying the hydrophobic residues in the short oligopeptides revealed that the aromatic-aromatic interactions are the key driving force for enclathration.<sup>635</sup> Further studies using a trifacial cage by the same group have showed that it has a remarkable ability to fold Ala-Ala-Ala sequences into  $\beta$ -turns via encapsulation in the hydrophobic cavity.<sup>636,637</sup> This result demonstrated that peptide recognition within the large cavity of self-assembled cages is a powerful method to produce the secondary structures of peptides, even if the peptide fragment is considerably short.

Recently, Therrien and co-workers have utilized a trigonal prism, [Ru<sub>6</sub>(*p*-cymene)<sub>6</sub>(**285**)<sub>2</sub>(dhbq)<sub>3</sub>]<sup>6+</sup> (**367**), as a prototype for a drug delivery system. Cage **367** can act as a carrier for cisplatin, and its high charge potentially facilitates uptake in cancer cells, although it leaches rapidly from the hydrophobic pocket in water.<sup>431</sup> However, more hydrophobic complexes

Scheme 139



[M(acac)<sub>2</sub>] (M = Pd, Pt) are strongly immobilized within **367**, while being almost insoluble in water in their free form under ambient conditions. The cage **367** was moderately cytotoxic toward human ovarian A2780 cancer cells, while the encapsulated cages were more active. The platinum-containing species was about twice as active as the empty cage, and the palladium-entrapped species was more than 1 order of magnitude more cytotoxic. Recently, a series of biologically relevant, planar hydrophobic pyrenyl guest (pyrene-R) molecules (**491-498**) were encapsulated within the hydrophobic cavity of cage **367** to form 1:1 cationic host-guest complexes [367  $\supset$  pyrene-R]<sup>6+</sup>, as evidenced by <sup>1</sup>H NMR and ESI-MS studies (Scheme 139).<sup>638</sup> The in vitro anticancer activity of these water-soluble systems showed that these inclusion complexes were more cytotoxic than the empty cage itself. Cytotoxicity studies of empty cage **367** on human ovarian A2780 cancer cells using an MTT assay, which measures mitochondrial dehydrogenase activity as an indication of cell viability, showed it to be moderately active. However, encapsulation of pyrenyl derivatives within the cavity of the cage **367** either increases or has negligible effect on the cytotoxicity. The host-guest complex [367  $\supset$  **492**]<sup>6+</sup> and [367  $\supset$  **493**]<sup>6+</sup> have IC<sub>50</sub> values of 2  $\pm$  0.6 and 3  $\pm$  1.1  $\mu$ M, respectively, that are comparable to the IC<sub>50</sub> value of cisplatin (1.6  $\mu$ M). Similar anti-proliferative activity studies on both A2780 (cisplatin sensitive)



and A2780cisR (cisplatin resistant) human ovarian cancer cells using porphyrin-based open arene ruthenium assemblies showed that both the charge and the length of the spacer between the porphyrin panels significantly affect the cytotoxic activity.<sup>639</sup> The ability of the trigonal-prism **367** to deliver guest molecules into the A2780 cells was studied using the host–guest complex  $[367 \supset 491]^{6+}$ .<sup>640</sup> The uptake and release of guest molecule **491** was monitored by means of flow cytometry. Once incarcerated within the cavity of the cage, the natural fluorescence of the guest molecule was quenched. The freed molecules were monitored by fluorescence spectroscopy following incubation of  $[367 \supset 491]^{6+}$  with A2780 cell lines. Efficient uptake and release of the incarcerated payload was observed from the cages. The rate of uptake and release was found to be dependent on the incubation time and concentration of the host–guest complex. Recently, the same group studied the effect of sizes of the guest molecules on cytotoxicity by encapsulating a series of large pyrenyl-containing dendrimers of different generations within hexanuclear arene-ruthenium cage  $[\text{Ru}_6(p\text{-cymene})_6(\mathbf{285})_2(\text{dhnq})_3]^{6+}$  (**370**;  $\text{dhnq} = 5,8\text{-dihydroxy-1,4-naphthoquinonato}$ ).<sup>641</sup> The cytotoxicity of the host–guest systems, with the pyrenyl moiety being encapsulated in the hydrophobic cavity of the cage and the dendritic functional group dangling outward, was evaluated on human ovarian A2780 and A2780cisR cancer cell lines. The host–guest systems show similar cytotoxicity to the empty metalloprism **370** and remain intact before internalization by the cancer cells. This demonstrated that metallacage host systems were able to deliver a hydrophobic payload with large appendages into cancer cells.

A similar hexanuclear arene ruthenium complex  $[\text{Ru}_6(p\text{-cymene})_6(\mathbf{291})_2(\text{dhnq})_3]^{6+}$  having a trigonal-prismatic architecture assembled from dinuclear arene ruthenium complexes  $[\text{Ru}_2(\eta^6\text{-}p\text{-cymene})_2(\mu\text{-OO} \cap \text{OO})_2(\text{OTf})_2]$  ( $\text{OO} \cap \text{OO} = \text{dhnq}$ ) and 1,3,5-tris(4-pyridylethynyl)benzene (**291**) also showed effective growth inhibition activity in SK-hep-1 (liver cancer), HeLa (ovary cancer), HCT-15 (colon cancer), A549 (lung cancer), and MDA-MB-231 (breast cancer) tumor cell assays.<sup>642</sup> The cage showed low micromolar inhibition against all cancer cell lines. In particular, the hexanuclear cage  $[\text{Ru}_6(p\text{-cymene})_6(\mathbf{291})_2(\text{dhnq})_3]^{6+}$  was found to inhibit the proliferation of A549 cells with an  $\text{IC}_{50}$  of  $3.4 \mu\text{M}$ , which is comparable to the effect seen with cisplatin ( $\text{IC}_{50} = 2.4 \mu\text{M}$ ). Mechanistic studies to understand the antiproliferative effect of the nanocage suggested that the anticancer activity through apoptosis originated from the interaction of the cytotoxic  $\text{dhnq}$  with  $[(p\text{-cymene})\text{RuCl}(\mu\text{-Cl})_2]$  which was enhanced in the nanocage due to increased nuclearity and by the presence of the extended  $\pi$ -conjugated system.

## 5. MISCELLANEOUS

### 5.1. Self-Selection and Self-Sorting in Coordination-Driven Self-Assembly

Of late, there has been a paradigm shift from supramolecular preorganization to more complex systems where the system undergoes self-organization through self-selection and self-sorting to generate one or more well-defined and ordered supramolecular architectures.<sup>14,643–647</sup> Self-selections of structurally “instructed” components allow controlled assemblies from complex mixtures of components following specific programs. Nature provides an amazingly wide array of successful examples of complex structures designed through self-organization using noncovalent interactions. For example, in the biosynthesis of

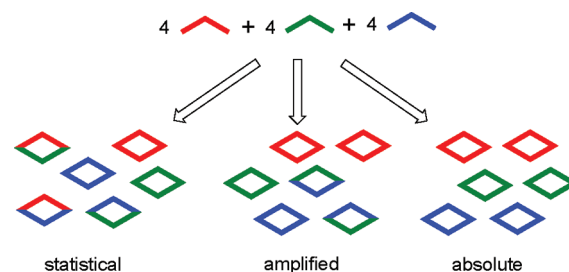


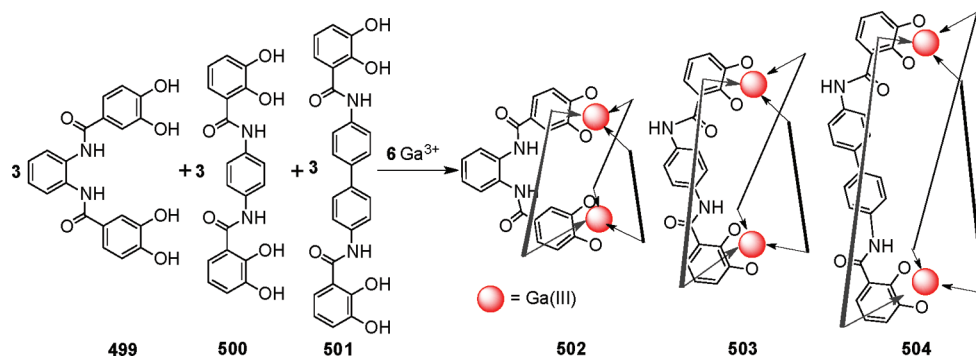
**Figure 40.** Representation of differing extents of self-organization phenomena that can occur within a complex mixture of subunits.

lipid membranes, proteins, nucleic acids, protein aggregates, and virus particles, nature utilizes the noncovalent information stored within the structural and electronic properties of the components to self-assemble them into the preferred biomolecules. In fact self-organization is the driving force that led up to the evolution of the biological world from inanimate matter.

Coordination-driven self-assembly paradigms have been extensively used by the research groups of Lehn,<sup>643</sup> Raymond,<sup>644</sup> Albrecht,<sup>645</sup> Stang,<sup>646</sup> Severin,<sup>647</sup> and others<sup>14</sup> over the past decade to develop and understand the phenomena of self-organization that occurs in nature and biological systems. Wide ranges of complex synthetic mixtures were investigated that undergo varying degrees of self-organization. The facile kinetic reversibility of metal–ligand coordination that drives systems to the formation of thermodynamically favorable collections of supramolecular ensembles is the cornerstone of such synthetic strategies. Several other factors such as temperature, concentration, association constants of complementary pairs, and the presence of competitors, however, also play a vital role in controlling the extent of self-organization phenomena in these systems. Depending on the extent of self-organization occurring in a complex mixture of subunits, the process can range from a statistical mixture of different supramolecules to amplified organization, where some supramolecules are formed in greater ratios than others and to absolute self-organization and the exclusive formation of discrete supramolecules (Figure 40).<sup>646</sup>

Coordination-driven self-assembly, with its highly modular character, along with the extensive library of individual molecular subunits of varying size, geometry, and physical properties that have been prepared in recent years, has allowed the study of self-organization in both 2D and 3D supramolecular architectures. In this paradigm, by combining multiple rigid acceptor and donor subunits, the directional nature of the coordination-driven self-assembly protocols can be used to study the phenomena of self-selection and self-sorting under mild conditions. In one of the earliest demonstrations of self-selection, in 1993, Lehn et al.<sup>648</sup> described the spontaneous formation of metal helices from a mixture of ligands triggered by a metal ion. Upon treatment with Cu(I) ions, mixtures of oligo(2,2′)-bipyridine strands containing 2–5 bipyridine units led to the formation of double helicates without significant crossover. Similarly, when a mixture of the two different tris-bipyridine ligands was allowed to react with Cu(I) and Ni(II) ions, only a double helicate and a triple helicate were formed. The process represents a self-recognition involving the preferential binding of like metal ions by like ligand strands in a mixture to selectively assemble into the corresponding helicates. Caulder and Raymond<sup>649</sup> have shown that naked metal ions can act as a trigger for the self-organized assembly of rationally designed bis(catecholamide) ligands of different lengths (**499–501**).

Scheme 140

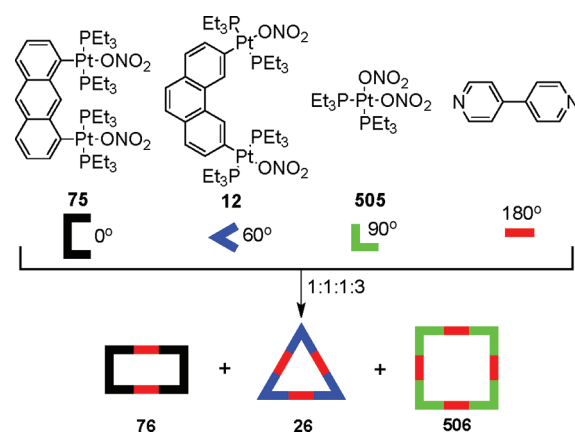


These structurally instructed rigid bis(catecholamide) ligands, in the presence of the  $\text{Ga(III)}$  ions, undergo facile self-organization, resulting in a highly ordered system of helicates (**502**–**504**) in solution (Scheme 140). Albrecht and co-workers have also observed that rigid oligo-*p*-phenylene-type dicatchol ligands having different lengths undergo template-directed self-organization to dinuclear  $\text{Ti(IV)}$ -based triple stranded  $\text{M}_2\text{L}_3$  helicates in the presence of appropriate counterions ( $\text{M} = \text{Li}, \text{Na}, \text{K}$ , or  $\text{NH}_4^+$ ).<sup>650,651</sup> Ligands having similar geometric preferences do not lead to self-organization. Self-assembly of heterodinuclear triple-stranded helicates was achieved on the basis of metal selection by “geometric discrimination”.<sup>652</sup>

One of the earliest examples of the self-sorting of molecular components resulting in the absolute self-organization into discrete supramolecular rectangles via the directional bonding approach was demonstrated by Hupp and co-workers.<sup>108</sup> The combination of a metal precursor with two rigid linear linkers of differing lengths should, in the absence of any driving bias, result in a statistical mixture of two molecular squares of different sizes and a rectangle. However, the combination of the octahedral  $\text{Re(CO)}_5\text{Cl}$  as the corner unit and linear pyridyl linkers of different lengths, namely, pyrazine and 4,4'-bipyridine, led to the exclusive formation of only two types of molecular squares rather than a statistical mixture of squares and rectangle.

Stang et al. extensively studied self-organization of platinum-based 2D and 3D metallacycles and metallacages.<sup>646</sup> Square-planar platinum(II) metal acceptors of varying angles between the coordination sites ranging from 0 to  $90^\circ$  with electron-rich pyridyl donors were used as molecular subunits. It was shown that by a careful modulation of the intrinsic geometric parameters of the molecular subunits (angle, size, and relative orientation of coordination centers), absolute self-organization could be achieved without introducing any external effectors and the process could be applied to a diverse set of coordinative supramolecules. As shown in Scheme 141, the use of square-planar platinum(II) acceptors **75**, **12**, and **505** having 0, 60, and  $90^\circ$  angles between their coordination sites in conjunction with a  $180^\circ$  linear pyridyl donor ligand, 4,4'-bipyridine in 1:1:1:3 molar ratio resulted in the absolute self-organization into the discrete supramolecular rectangle **76**, triangle **26**, and square **506**, respectively.<sup>653</sup> Although a random combination of different subunits was observed initially as determined by NMR and ESI-MS, prolonged reaction led to fully equilibrated mixtures of the discrete individual assemblies. The major driving force for the selective formation of the discrete polygons was the angular

Scheme 141

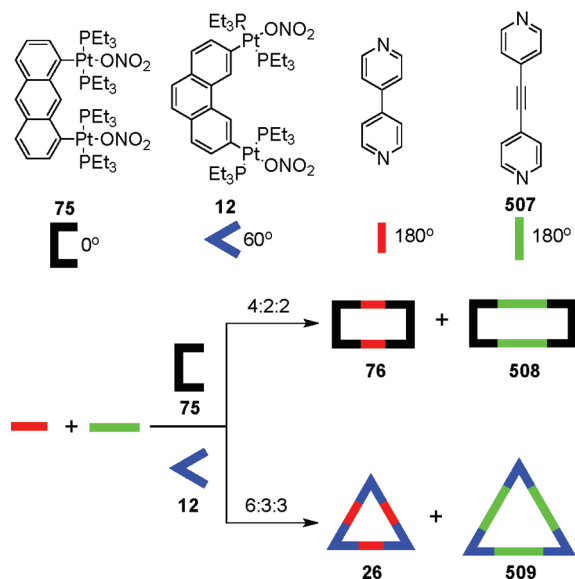


differences in the organoplatinum acceptor units. The size of the resulting assembly can also direct the absolute self-organization of 2D and 3D supramolecular ensembles.<sup>654</sup> For example, mixing two pyridyl donors of different lengths, 4,4'-bipyridine and 1,2-bis(4-pyridyl)ethyne (**507**), with diplatinum acceptors **75** and **12** having 0 and  $60^\circ$  angles leads to molecular rectangles (**76**, **508**) and triangles (**26**, **509**), respectively (Scheme 142).

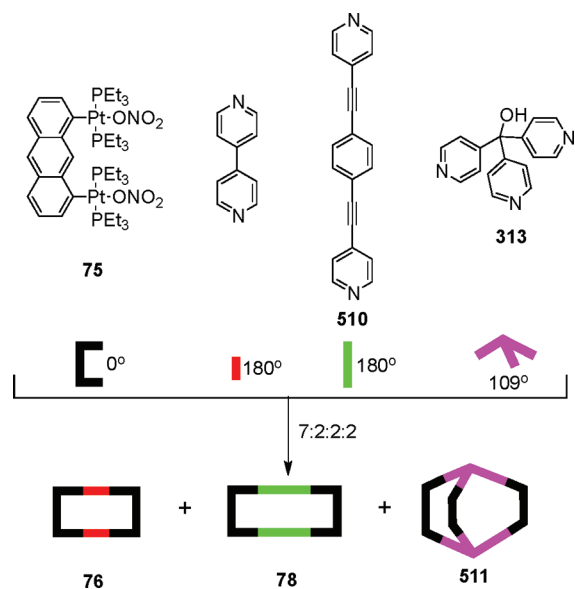
The combination of different subunits of varying size, shape, and dimensions also leads to absolute self-organization into discrete supramolecules.<sup>655</sup> A complex 7:2:2:2 mixture of  $0^\circ$  diplatinum(II) acceptor (**75**) with three donors, 4,4'-bipyridine, 1,4-bis(4-pyridylethynyl)benzene, and tris(4-pyridyl)methanol (**313**), differing in size, shape, and orientation of the coordination sites has been successfully assembled exclusively into discrete structures—rectangles (**76** and **78**) and a distorted trigonal prism (**511**)—demonstrating the strength and utility of the directional bonding approach in studying self-organization (Scheme 143). Besides these structural and geometric factors, the reaction temperature and choice of solvent also determines the extent of self-organization.<sup>655</sup> It is interesting to note that, in all of the examples cited above, absolute self-organization occurs in acetone/water (1:1) solvent mixture, but not in dichloromethane.

Similarly, the formation of discrete 3D polyhedra from multiple subunits in a complex mixture was also investigated.<sup>656</sup> The self-recognition process was found to be strongly dependent upon the structural information stored within individual building blocks, i.e., geometry, directionality, and rigidity. In addition, the

Scheme 142

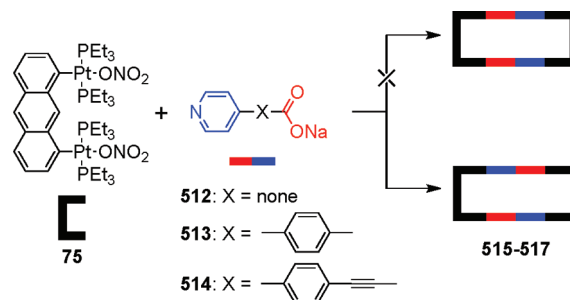


Scheme 143



thermodynamic stability of the products also played a great role in the self-recognition process. Self-recognition and self-assembly were achieved as the kinetically labile Pt–N bond allowed for the dynamic exchange of complementary molecular components by internal rearrangement, exchange, extrusion, and incorporation of different components, through which intermediate assemblies are self-selected and proof-read in order to generate the most thermodynamically preferred 3D cages. In fact, constitutional dynamic exchange of complementary molecular components in coordination-driven self-assembly was recently shown using ESI-MS for molecular polygons.<sup>657</sup> Treatment of <sup>1</sup>H and <sup>2</sup>D isotope-labeled 4,4'-bipyridines with 60° diplatinum(II) acceptors (12) gave the corresponding molecular triangles. Mixing these two homoisotopic triangles resulted in ligand exchange to give heteroisotopic triangles. Similarly, mixing of

Scheme 144

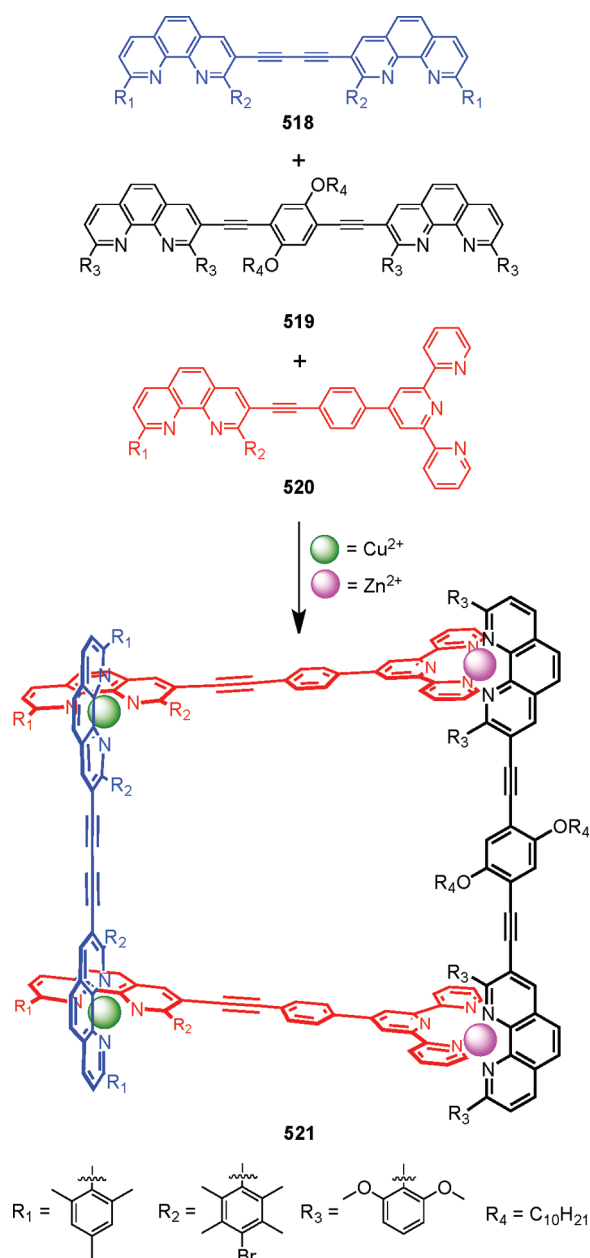


homoisotopic rectangles generated from 60° diplatinum(II) acceptors (75) and <sup>1</sup>H and <sup>2</sup>D isotope-labeled 4,4'-bipyridines also resulted in heteroisotopic rectangles. Formation of these heteroisotopic polygons was established on the basis of quantitative mass spectroscopic results. The exchange process was found to be dependent upon the temperature, solvent, and the nature of the counteranions.

Self-organization during self-assembly of a series of linear bispyridyl donors functionalized with hydrophobic alkyl (C<sub>6</sub>H<sub>13</sub>, C<sub>12</sub>H<sub>25</sub>, and C<sub>18</sub>H<sub>37</sub>) chains or hydrophilic (di-, tri-, or tetra-)ethylene glycol chains with complementary 0° di-Pt(II) acceptors into supramolecular rectangles was also explored.<sup>658</sup> The connectivity and location of functional groups on the bispyridyl ligands ensured that they did not interfere sterically or electronically with their respective binding sites. Employing carefully controlled reaction conditions so that the only means of self-organization during self-assembly was through “second-order” effects arising from the distal functional groups themselves, it was observed that increasing the chain length drove the self-assembly process toward amplified self-organization.

Ambidentate ligands having two different binding sites have been used to demonstrate absolute self-sorting in the self-selection of a single linkage isomeric product. The combination of molecular clip 75 with ambidentate pyridyl carboxylate ligands 512–514 led to the assembly of the most symmetrical isomers, 515–517, with isooriented (i.e., each Pt atom is bound to a pyridyl nitrogen and a carboxylate oxygen atom), ligands, despite the possibility of formation of two isomeric rectangles (Scheme 144).<sup>659</sup> Similarly, self-selection for the symmetric supramolecular rectangles was observed when molecular clip 75 was treated with linear ambidentate ligand, N-(4-pyridyl)isonicotinamide (30), in a 1:1 ratio.<sup>112</sup> It was also found that steric interactions among the substituents present on the subunits in a complex mixture of ditopic ligands could drive the process of self-organized assembly from statistical to absolute organization.<sup>660</sup> By preparing a number of unsymmetric bis(4-pyridyl)acetylene ligands with one of the two pyridyl moieties substituted with 2,6-dimethyl-, 2-chloro-, and 3,5-dichloro- substituents and treating them with the 90° *cis*-[Pd(PMe<sub>3</sub>)<sub>2</sub>(NO<sub>3</sub>)<sub>2</sub>] acceptor, it was shown that the asymmetry of the linear donors leads to four different supramolecular squares, depending upon the relative orientations of each squares' constituent donors. In keeping with the previous observation of molecular rectangles, in the case of molecular triangles also, due to the different bonding connectivity of the ambidentate ligands, two linkage isomeric triangles were expected. However, when the 90° heterobimetallic *cis*-[Pt(dppf)(OTf)<sub>2</sub>] (32; dppf = diphenylphosphinoferrrocene) acceptor was treated with unsymmetrical ambidentate ligand,

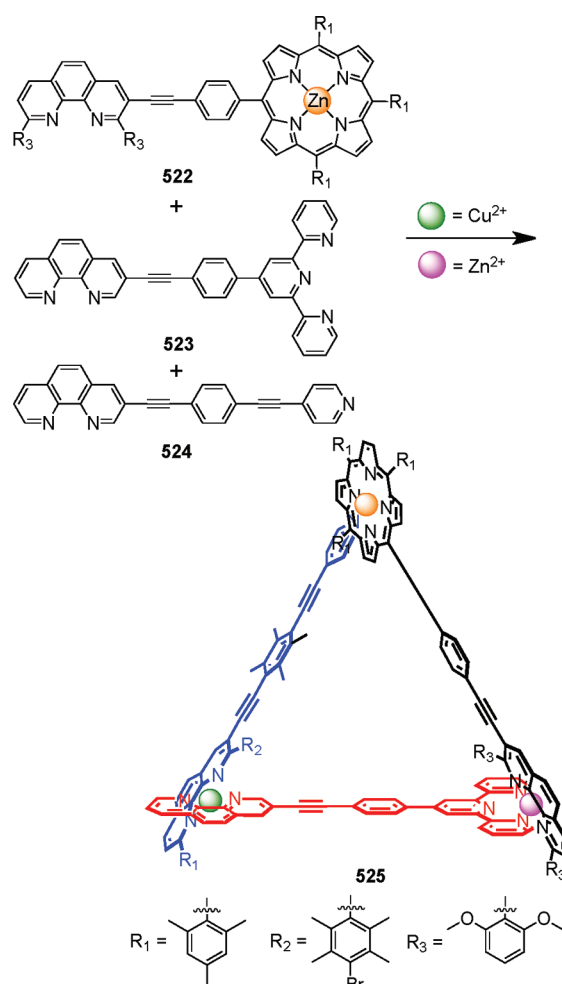
Scheme 145



sodium isonicotinate, a symmetric molecular triangle was obtained as exclusive product.<sup>59</sup> Similarly, sodium pyrimidinecarboxylate in conjunction with **32** led to the self-selection for the symmetrical isomer.<sup>58</sup> As determined from  $^{31}\text{P}$  and  $^1\text{H}$  NMR, ESI-MS, and X-ray crystallography, of the two possible linkage isomers, the most symmetrical one, in which all the ambidentate ligands are isooriented, was observed. The driving force for such absolute self-sorting is the enthalpic gain achieved by heteroligation at each Pd center. Furthermore, by orienting the ligands in an alternating fashion, the geometric strains on the triangles are relieved. The combined effect of these driving factors leads to the thermodynamically preferred metallacycles.

Schmitt et al. have demonstrated multicomponent integrative self-sorting leading to the formation of trapezoids,<sup>661</sup> triangles,<sup>662</sup>

Scheme 146



and ladders.<sup>663</sup> For example, the isosceles trapezoid **521** was constructed through sequential addition of the specifically designed ligands—two bisphenanthroline ligands **518** and **519** with varied length serve as the shorter edge of the trapezoid while the phenanthroline-terpyridine hybrid ligand, **520**, serves as the longer edge of trapezoid **521** (Scheme 145).<sup>661</sup> First, a mixture of **519** and **520** were treated with Zn(II) followed by the addition of **518** and Cu(I). NMR and ESI-MS studies confirmed the exclusive formation of the macrocycle. Steric effects,  $\pi$ – $\pi$  interactions, electronic effects, and metal–ion interactions play a vital role in controlling the self-sorting process. Similarly, a molecular triangle assembles from five-components via self-sorting from related building units.<sup>662</sup>

Recently, the same group also demonstrated the assembly of a tris-heterometallic scalene triangle with three different self-assembled corners from an eight-component algorithm via self-sorting.<sup>664</sup> The combination of a phenanthroline–porphyrin hybrid ligand (**522**), terpyridine–phenanthroline ligand (**523**), phenanthroline–pyridine hybrid (**524**), Zn<sup>2+</sup>, and Cu<sup>+</sup> in 1:1:1:1:1 ratio under reflux condition for 2 h in acetonitrile/DCM (2:1) led to the formation of scalene triangle [CuZn-(**522**)(**523**)(**524**)](OTf)<sub>2</sub>(PF<sub>6</sub>) (**525**; Scheme 146). The exclusive formation of triangle **525** was established by ESI-MS,  $^1\text{H}$  NMR, DOSY, DPV, and elemental analysis. Steric and electronic effects,  $\pi$ – $\pi$  interactions, and metal–ion interactions drive the



3-fold complete self-sorting process, which leads to the assembly of a single species in solution.

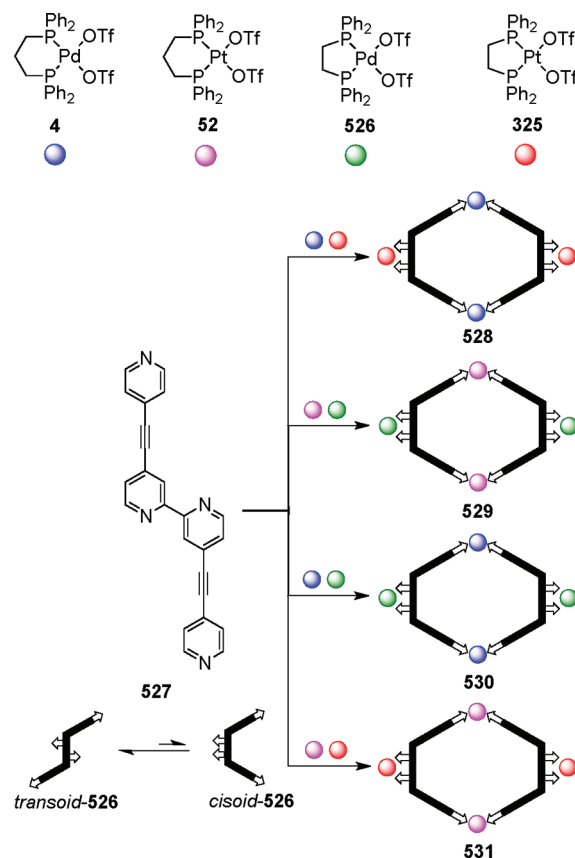
Schalley et al. have also successfully demonstrated the concept of integrative self-sorting with a hetero[3]pseudorotaxane as a model system.<sup>665</sup> The synthesis of a hetero[3]rotaxane with an efficient cascade-stoppering system was achieved from a four-component mixture. In a similar study<sup>666</sup> of a four-component self-sorting system of crown ethers and ammonium ions, six building blocks were designed in which two identical or different binding sites are incorporated. These building blocks, when mixed in many different ways, led to distinctly different pseudorotaxane assemblies. The self-sorting process integrates all building blocks in specific places so that this approach permits one to exert positional control and can widely influence the resulting assemblies with respect to the details of their structures.

In an interesting study, the same group recently demonstrated a thermodynamically controlled self-assembly of hetero-bimetallic metallo-supramolecular macrocycles through self-sorting caused by different ancillary ligands present on the cis-blocked Pd(II) and Pt(II) metal centers.<sup>667</sup> The self-sorting of metallo-supramolecular macrocycles was investigated using a tetratopic ligand (**527**) that has two different metal-binding sites, a central 2,2'-bipyridine core, which act as a chelate ligand, and two terminal pyridine coordination sites, which mediate assembly formation. Treatment of **527** with  $M(\text{dppp})(\text{OTf})_2$  [ $M = \text{Pd}$  (**4**),  $\text{Pt}$  (**52**);  $\text{dppp}$  = diphenylphosphinopropane] and/or  $M(\text{dppe})(\text{OTf})_2$  [ $M = \text{Pd}$  (**526**),  $\text{Pt}$  (**325**);  $\text{dppe}$  = diphenylphosphinoethane] in all four possible combinations led to a high-fidelity self-sorting upon equilibration for 3 days, resulting in the generation of two self-sorted heterobimetallic (**528** and **529**) and two homobimetallic (**530** and **531**) macrocycles (Scheme 147). <sup>31</sup>P NMR and tandem mass spectrometric experiments provided the evidence for the formulation of the macrocycles. In all four macrocycles, ( $\text{dppp})\text{M}^{\text{II}}$  hinge coordinates to the pyridines. The ( $\text{dppe})\text{M}^{\text{II}}$  is displaced from the pyridine and binds exclusively to the bipyridine sites when thermodynamic equilibrium is achieved. Thus, a difference of merely one methylene group incorporated in the ancillary ligands induced high-fidelity self-sorting.

Osuka et al. have investigated high-fidelity homochiral self-sorting in porphyrin-based systems where *meso*-pyridyl-appended zinc(II) porphyrins assemble to form macrocycles and cages of different dimensions. Due to the restricted rotation around the *meso*–*meso* linkages, 4-pyridyl-appended *meso*–*meso*-linked zinc(II) diporphyrins exist as both *R* and *S* enantiomers in solution, leading to formation of the corresponding homochiral (*R*)- and (*S*)-porphyrin boxes through self-sorting.<sup>520</sup> The homochiral self-sorting behaviors of *meso*-cinchonemide (3,4-pyridinedicarboximide)-appended zinc(II) porphyrin and 10,10'-cinchonemide-appended *meso*–*meso*-linked zinc(II) diporphyrins in noncoordinating solvents were also investigated.<sup>668</sup> While the former undergoes complete assembly to yield its trimer, the latter led to trimeric, tetrameric, and pentameric rings, through rigorous homochiral self-sorting processes, due to the presence of three stable conformers with respect to the orientation of the pyridyl nitrogen atoms. Similarly, *meso*–*meso*'-bis(5-azaindol-2-yl)-appended zinc(II) porphyrin formed a trimeric fluorescent assembly that consisted of three single atropisomers due to the facile rotation of the 5-azaindol-2-yl substituent and effective trapping via self-sorting assembling by complementary coordination.<sup>669</sup>

Severin and co-workers have demonstrated the self-sorting process to generate dynamic combinatorial libraries based on

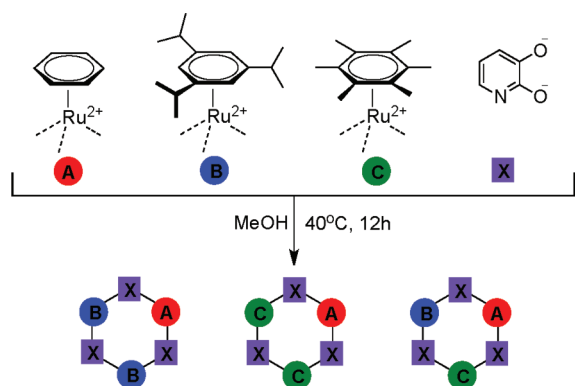
Scheme 147



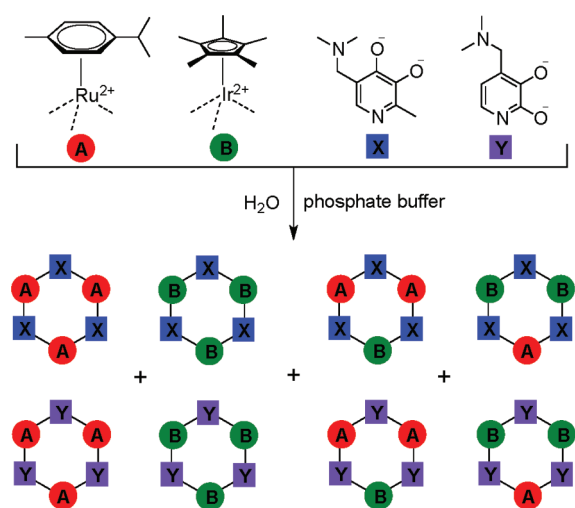
half-sandwich complexes having triangular topologies.<sup>647</sup> A combinatorial assembly of three Ru half-sandwich complexes having sterically different  $\pi$ -ligands—a small benzene ligand, a large 1,3,5-triisopropylbenzene ligand, and a very large hexamethylbenzene ligand with 2,3-dihydroxypyridine—gave only three species in significant amount out of 10 possible products.<sup>670</sup> From a thermodynamic point of view, the trinuclear metalla-macrocycles with the smallest steric congestion, i.e., the compound with three (benzene)Ru fragments, is expected to be most stable. However, in the equilibrated mixture, all three macrocycles contained only one (benzene)Ru fragment (Scheme 148). This demonstrated that a higher thermodynamic stability of a dynamic combinatorial library member does not necessarily correlate to an elevated concentration. A more complex mixture containing half-sandwich metal building blocks [ $\{\text{Ru}(p\text{-cymene})\text{Cl}_2\}_2$ ], and [ $\{\text{Ir}(\text{Cp}^*)\text{Cl}_2\}_2$ ] and two different dihydroxypyridine ligands in buffered aqueous solution form a dynamic combinatorial library with unique network topology.<sup>671</sup> Upon mixing, these complexes undergo scrambling reactions to give only eight out of a possible 24 macrocycles (Scheme 149). The eight different complexes can be divided into two partially orthogonal sublibraries. Within these sublibraries, an exchange of metal fragments and ligands is possible, but communication between the sublibraries is restricted to an exchange of metal fragments.

Nitschke and co-workers have investigated self-sorting phenomena by using the dynamic nature of both metal–ligand coordination and reversible imine bond formation.<sup>14</sup> For example, when 2-formylpyridine (**275**) and benzaldehyde-2-sulfonate (**532**) were mixed with a diamine (**533**) in aqueous medium, a

Scheme 148



Scheme 149



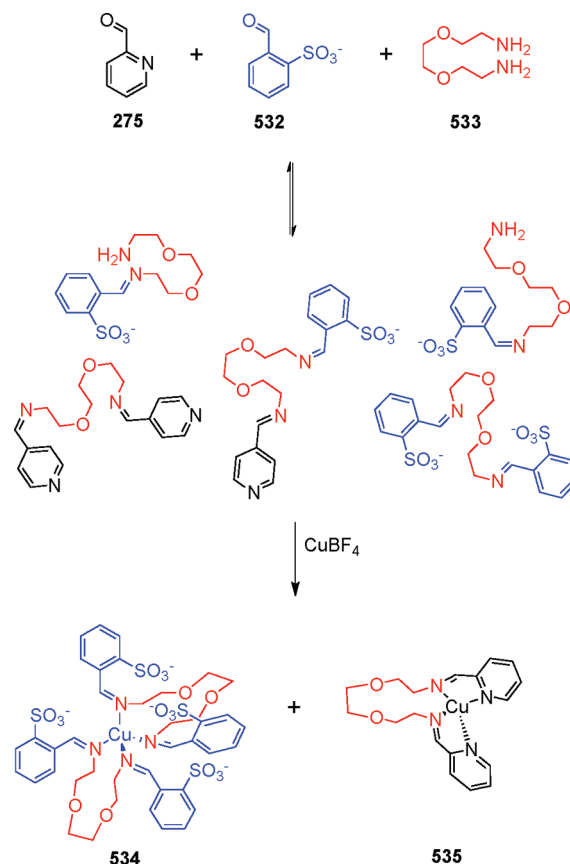
complex library of ligands was generated in dynamic equilibrium with the starting materials.<sup>672</sup> However, addition of CuBF<sub>4</sub> triggered a collapse of the library leading to the formation of only two self-sorted supramolecules **534** and **535** (Scheme 150). Formation of any other structures is both entropically and enthalpically unfavorable.

Similar self-organization phenomena were observed when 2-aminoquinoline and 4-chloroaniline were mixed with the phenanthroline dialdehyde to generate a dynamic library of ligands which subsequently collapse to form dicopper and tricopper helicates upon addition of copper(I).<sup>673</sup> Use of two different metals, Cu(I) and Fe(II), also induced a dynamic combinatorial library of 11 structures to self-organize into only two discrete supramolecules.<sup>674</sup> The efficiency and selectivity of self-organization could be correlated with the electronic nature of the substituted amine subunits, which were studied using Hammett  $\sigma_{\text{para}}$  values, and on the coordination geometries of the metal ions used.<sup>675</sup>

## 5.2. Surface Confined Ensembles

Over the past decade, a great deal of attention has been paid to assembling metallo-supramolecular macrocycles and metallacages on solid supports to understand the factors that govern and control the assembly process on surfaces and accordingly

Scheme 150



develop materials with novel properties.<sup>20–22</sup> As delineated in previous sections, metallo-supramolecular assemblies having novel electronic, magnetic, photophysical, redox, and catalytic properties have been extensively investigated in solution using a wide variety solution-phase analytical techniques. However, in the solution phase, supramolecular assemblies generally lack coherence in their orientation, alignment, and packing order, prohibiting the large-scale uniformity and coordination required for advanced functional materials. On the other hand, assembling supramolecules on surfaces imparts a high degree of coherence and uniformity for fabrication of nanostructures and nanodevices for material applications. Various substrates such as SiO<sub>2</sub>, Cu(100), gold, indium–tin oxide (ITO), and highly ordered pyrolytic graphite (HOPG) have been used to prepare metallo-supramolecular adlayers. Scanning probe techniques, in particular scanning tunneling microscopy (STM) and atomic force microscopy (AFM), have been commonly used to study the formation and properties of such surface-confined self-assembled molecular systems.

Hupp and co-workers have extensively studied film- and membrane-based porous materials derived from surface-confined metallo-supramolecular assemblies for molecular sieving and chemosensing.<sup>20</sup> In their initial studies in this area, microporous thin films composed of discrete Re(I)-based metallo-supramolecular squares were prepared on inert conductive platforms such as gold, glassy carbon, ITO, and platinum to act as electrodes to evaluate the size-selective transport of small molecules and complexes.<sup>676,677</sup> Re(I)-based porphyrin and pyrazine-containing molecular squares were assembled on permeable polyester membranes, and their thickness (~25 nm), morphology,

and crystallinity were characterized by low-resolution optical microscopy and by AFM measurements.<sup>269,678</sup> These film-coated electrodes, when exposed to solutions containing redox-active probe molecules and complexes of various sizes, led to size-selective transport across the membrane as determined from their voltammetric responses. Only those species capable of permeating the film showed faradic current flow. More robust films have been obtained by assembling phosphonate-functionalized Re(I) porphyrinic squares on ZrP-modified ITO and SiO<sub>2</sub> surfaces.<sup>679,680</sup> The high affinity of Zr(IV) for phosphonate allowed for layer-by-layer assembly either by direct attachment of the octaphosphonated squares to metal-oxide surfaces or by first derivatizing the supporting surfaces with zirconium binding ligands. This layer-by-layer assembly approach allowed precise control over the film thickness as well as the morphology by overriding the defects associated with vapor deposition. Interdigitated phosphonated porphyrinic molecular squares with phosphonated perylenedimides through layer-by-layer assembly on ZrP-coated ITO surfaces has led to bulk heterojunctions. When employed in photovoltaics, these molecularly interlaced heterojunctions generate photocurrent with visible light.<sup>270,271</sup> In aqueous I<sub>3</sub><sup>−</sup>/I<sup>−</sup> solutions these photoelectrochemical cells produce cathodic photocurrents, in contrast to generally observed anodic photocurrents with conventional dye-sensitized solar cells. Microporous thin films (~50–400 nm) composed of discrete, cavity-containing Mn(I)- and Re(I)-based molecular rectangles assembled on electrically conductive ITO-coated glass slides yielded a collection of needle-shaped structures that were readily visualized via low-resolution optical microscopy and AFM measurements.<sup>681</sup> These rectangle-based thin film materials displayed both size- and shape-selective membrane transport behavior when placed in contact with aqueous solutions of redox-active probes. Only those probes that were short and narrow in at least one dimension were allowed to permeate through the membrane. The shape selectivity, however, was found to be through intramolecular rather than intermolecular cavities. Quantitative and semiquantitative measurement using rotating disk electrode (RDE) voltammetry and scanning electrochemical microscopy (SECM), respectively, showed that the transport was roughly 2 orders of magnitude slower than observed in thin films of molecular squares featuring similar-sized cavities.

Wan and co-workers have investigated the self-organization of supramolecular metallacycles and metallacages on Au(111) and HOPG surfaces by scanning tunneling microscopy (STM).<sup>21</sup> Well-ordered self-organized architectures with three metallo-supramolecular assemblies, a square, a rectangle, and a three-dimensional cage, on Au(111) surfaces were fabricated.<sup>682</sup> The self-assembled adlayers were prepared by immersing the Au beads in an ethanol solution of the respective assemblies. These supramolecular assemblies adsorb on Au(111) surfaces and self-organize to form highly ordered adlayers with distinct conformations that are consistent with their chemical structures. For example, the metallo-supramolecular square [Pt(dppp)(4,4'-bipyridine)]<sub>4</sub>(PF<sub>6</sub>)<sub>8</sub> spontaneously adsorbed on the Au(111) surface to give regular rows of squares lying flat on the surface and extending in the A and B directions, forming 90° angles (Figure 41). The dimensions of each molecular square were determined from the STM image and found to be 2.1 ± 0.1 nm on each side, consistent with the size previously determined from X-ray crystallography.<sup>292</sup> Molecular rectangles, [{(1,8-bis[trans-Pt-(PEt<sub>3</sub>)<sub>2</sub>]anthracene)}<sub>2</sub>(4,4'-bipyridine)<sub>2</sub>]<sup>4+</sup> (**76**) also assembled into well-ordered arrays on Au(111) surfaces. Similarly, adsorption

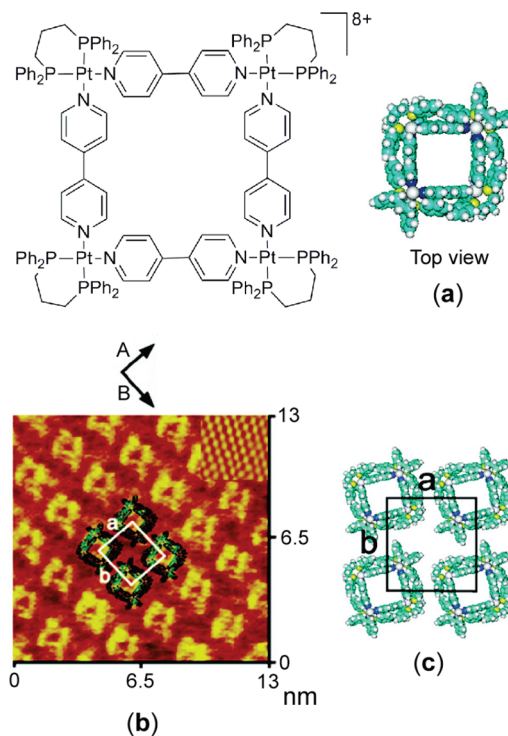


**Figure 41.** (a) Space-filling model of molecular square [Pt(dppp)(4,4'-bipyridine)]<sub>4</sub>(PF<sub>6</sub>)<sub>8</sub>, (b) high-resolution STM images of the adlayer of square on Au(111), and (c) structural model of the adlayer.

of bis-terpyridine-based [2 × 2] grid-type Zn(II) and Co(II) assemblies on HOPG surfaces led to well-organized adlayers.<sup>683,684</sup>

Schalley and co-workers also studied the assembly of a metallo-supramolecular square [Pt(en)(4,4'-bipyridine)]<sub>4</sub>(NO<sub>3</sub>)<sub>8</sub> on Cu(100) surfaces modified with a chloride adsorbate layer.<sup>685</sup> Chloride-covered Cu(100) surfaces were prepared by adsorbing chloride anions on positively polarized Cu(100) electrode from chloride-containing electrolytes. The adsorbed chloride layer adopted the symmetry of the copper substrate and essentially retained its full charge upon adsorption. The negatively charged chloride layer caused the cationic squares to adsorb and lie flat on the electrode surface. While adsorbate–substrate interactions were driven by attractive electrostatic interactions, lateral ordering was governed by van der Waals interactions. However, due to the acidic conditions used to prepare the surface, the square slowly opened up and chainlike oligomers coadsorbed. On HOPG surfaces the molecular squares showed a striped pattern in the STM images. Self-organization of Fréchet-type dendron-functionalized Pd(II)- and Pt(II)-based metallo-supramolecular squares on mica and HOPG surfaces were also investigated by the same group.<sup>251</sup> AFM studies on the materials revealed two distinctly different morphological arrays of adsorbed self-assembled dendronized squares depending on the solvent in which the sample was applied to the surface. When ethanol solutions of squares were used, towerlike aggregates appeared on both mica and HOPG surfaces. When ethanol/acetone solutions of the dendronized squares were used for deposition, the mica surface showed similar towerlike aggregation. However, on a HOPG surface, a mixed solvent solution showed formation of monolayers. Thus, a balance between surface–dendrimer and dendrimer–dendrimer interactions plays a vital role in driving such self-organization.



In addition to 2D metallacycles, 3D metallacages were also shown to form well-ordered adlayers on Au(111).<sup>682</sup> The distorted trigonal prism,  $[(1,8\text{-bis}(\text{trans-Pt}(\text{PEt}_3)_2)\text{anthracene})_3\text{-(tris(4-pyridyl)methanol)}_2](\text{PF}_6)_5(\text{NO}_3)$  self-organized into two-dimensional array with regular molecular rows. The cages oriented themselves in such a way that their propeller “blades” were interdigitated along the A direction while along the A–B diagonal, the faces of their bis-Pt(II) anthracenyl moieties aligned roughly parallel. Such an arrangement maximized intermolecular van der Waals interactions, thereby providing stability to the adlayers. Self-organization of a supramolecular chiral trifacial box (**401**) on Au(111) showed domain-separated monolayers.<sup>686</sup> The self-assembled adlayers were prepared by suspending gold beads in a racemic mixture of the trifacial box, **401**, in ethanol. Upon adsorption of the racemic mixture on Au(111), each enantiomer formed separate, well-ordered, locally chiral domains of MMM and PPP helical enantiomers. The supramolecules lie edge-down on the Au(111) surface while projecting one of their three flat faces upward. A similar manifestation of chirality into separate enantiomerically pure domains on Cu(100) surfaces modified with a chloride adsorbate layer was also observed with Pt(II)-chiral molecular rhomboids, **198**.<sup>216</sup> STM experiments revealed spontaneous separation of enantiomers at the surface resulting in enantiomerically pure domains when a racemic mixture was used. Only one well-defined orientation with respect to the underlying substrate was observed when enantiomerically pure rhomboids were adsorbed.

The nature of the substrate used for deposition of the supramolecular assemblies was found to profoundly affect the morphology of self-organization on surfaces. For example, the supramolecular rectangles (**79**) shown in Figure 42a self-assemble in an “face-on” geometry on Au(111) surfaces, while on the HOPG surface the same molecules self-assemble in an “edge-on” geometry.<sup>687</sup> When gold beads were immersed in a  $10^{-6}$  M solution of **79** in toluene, a uniform, well-ordered molecular adlayer with few defects was observed. STM images showed that the rectangles lie flat on the Au(111) surface, forming linear chains (Figure 42b). In contrast, on HOPG surface, the long edges of the rectangle stand on the surface, forming a 2D molecular network (Figure 42d). The observation that supramolecular rectangle **79** adopted two different orientations on Au(111) and HOPG surfaces demonstrated that molecular adlayers of coordination-driven self-assemblies could be dominated by the nature of their solid supports. The substrate–adsorbate interaction is much stronger in the case of Au(111) due to the strong Au– $\pi$  interactions that are maximized when the rectangles lie flat on the surface. The self-organization on HOPG surfaces, on the other hand, was primarily governed by intermolecular  $\pi$ – $\pi$  and van der Waals interactions between the adjacent rectangles, forcing them to adopt a close-packed 2D molecular network.

Molecular templates have been found to promote the monodispersion of a well-ordered array of supramolecular assemblies that otherwise form disordered adlayers on surfaces. For example, use of the triple-armed amphiphile, 1,3,5-tris(10-carboxydecyloxy)-benzene (TCDB) as template for coadsorption with supramolecular rectangles  $[(1,8\text{-bis}[\text{trans-Pt}(\text{PEt}_3)_2]\text{anthracene})_2(4,4'\text{-bipyridine})_2]^{4+}$  (**76**) led to the formation of well-distributed and monodispersed adlayers on a HOPG surface, which otherwise form disordered adlayers.<sup>688</sup> The judicious choice of template is vital as various interactions such as tetplate–template, adsorbate–template, template–surface, and adsorbate–surface along with

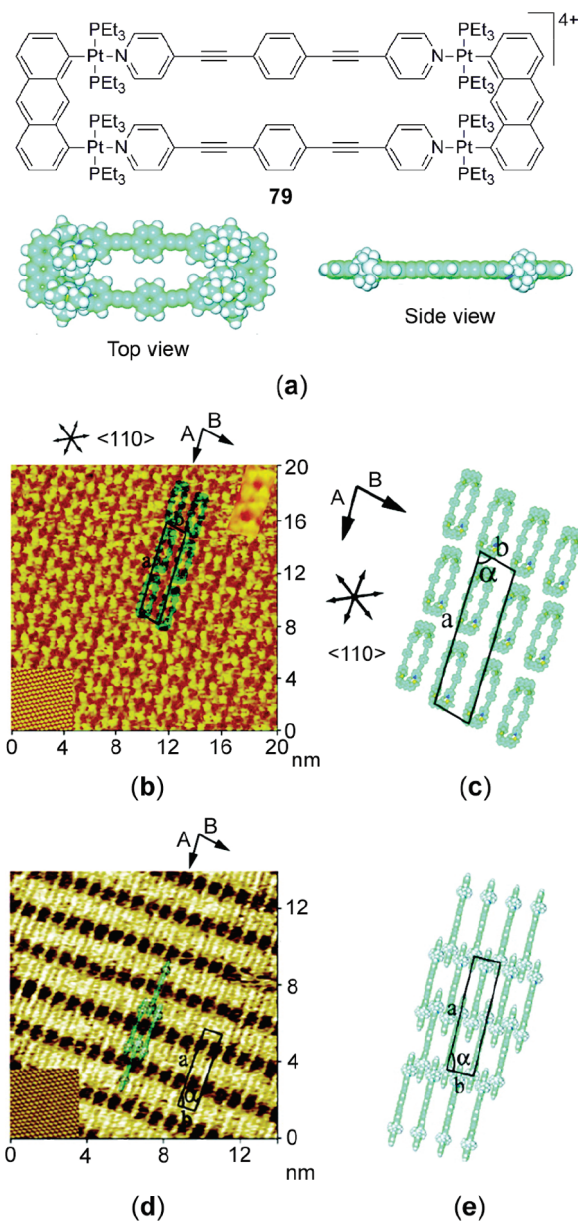


**Figure 42.** (a) Space-filling models of molecular rectangle **79**, (b) high-resolution STM images of the adlayer of **79** on Au(111), (c) structural model of the adlayer on Au(111), (d) high-resolution STM images of the adlayer of **79** on HOPG, and (e) structural model of the adlayer on HOPG surface.

appropriate size complementarities act as driving forces for templation and monodispersion. An ethanolic solution containing a 1:3 mixture of TCDB and molecular rectangle **76** deposited on a HOPG surface gave a well-ordered assembly. STM images showed that the rectangles were entrapped in the molecular template, thus forming the ordered adlayer. Similarly, use of shape-persistent arylene–ethynylene–butadiynylene macrocycles as templates for co-deposition with molecular square  $[\text{Pt}(\text{dppp})(4,4'\text{-bipyridine})_4](\text{PF}_6)_8$  or molecular rectangle **76** allowed for 2D ordered arrays on HOPG surfaces.<sup>689</sup> For each underlying shape-persistent macrocycle, one metallacycle has been detected, indicating that the structural information of the macrocycle layer was perfectly transformed to the guest molecules.



Dalcanale and co-workers have reported the generation of cavitand-based coordination cages directly on surfaces by using self-assembled monolayers on gold.<sup>690,691</sup> The formation of the molecular cages was monitored directly by atomic force microscopy (AFM). Self-assembled monolayers of a cavitand, functionalized with four cyano groups at the apical positions on the upper rim and four alkylthioether groups on the lower rim, were prepared by adsorption on gold surfaces at 60 °C from an EtOH/CHCl<sub>3</sub> solution for 12 h.<sup>690</sup> Monolayers of self-assembled coordination cages were obtained by soaking the self-assembled monolayers of cavitands in a solution of [M(dppp)(OTf)<sub>2</sub>] (M = Pd, Pt) and tetracyano-substituted cavitand **465**. The self-assembly process was monitored by directly measuring the height profile of these cages by means of AFM using substrates containing internal height references prepared by microcontact printing. Similarly, larger cavitand-based coordination cages were assembled on gold surfaces through metal-induced coordination by using a cavitand having four tolylpyridyl groups at the bridgehead positions on its upper rim and four 11-mercaptopundecanol groups on its lower rim.<sup>691</sup> Reversible disassembly of the resulting coordination cages could also be achieved by exposing the monolayers of the cages to a solution of triethylamine in ethanol for 1 h. Triethylamine was able to shift the equilibrium toward the formation of [Pd(dppp)(NEt<sub>3</sub>)<sub>2</sub>(OTf)<sub>2</sub>] and free cavitand by competing with the Pd coordination centers. AFM studies indicated that more than half of the cages were disassembled, leaving free cavitand molecules.

### 5.3. Novel Characterization Methods

The growth of coordination-driven self-assembly over the past decade has been spurred to some extent by the immense technological advancement made in the characterization tools for supramolecular ensembles. The development of novel characterization methods helped to answer questions associated with these complex architectures held together by coordination bonds. It is equally true that problems faced by supramolecular chemists with characterization served as the impetus for the development of new methodologies and improvement of existing characterization tools to a great extent. Thus, this symbiotic relationship has worked to the benefit of both supramolecular chemistry and analytical chemistry. Today, many novel methods as well as conventional tools, which have improved remarkably in terms of sensitivity, resolution, and precision, are at hand for the characterization of supramolecular ensembles. We present here in the following sections a brief overview on some of the novel techniques that are being increasingly used in recent years in the context of elucidating the structures and properties of coordination-driven metallacycles and metallacages.

**5.3.1. Mass Spectrometry.** Mass spectrometry is perhaps one of the most extensively used tools for the characterization of coordination-driven supramolecular assemblies. In addition to analytical characterization of supramolecules with respect to their exact masses, isotopic patterns, charge states, stoichiometries, and impurities, mass spectrometry can provide a wealth of informations about the structures, fragmentation pathways, reactivities, and thermodynamic properties of supramolecular ensembles.<sup>692,693</sup> Many of the commonly available ionization techniques such as fast atom bombardment and matrix-assisted laser desorption/ionization are incompatible with supramolecular assemblies that contain noncovalent bonds because these ionization methods are intrinsically harsh and impart large internal energy to the ions of the analyte

molecule, consequently leading to fragmentation to a significant extent.

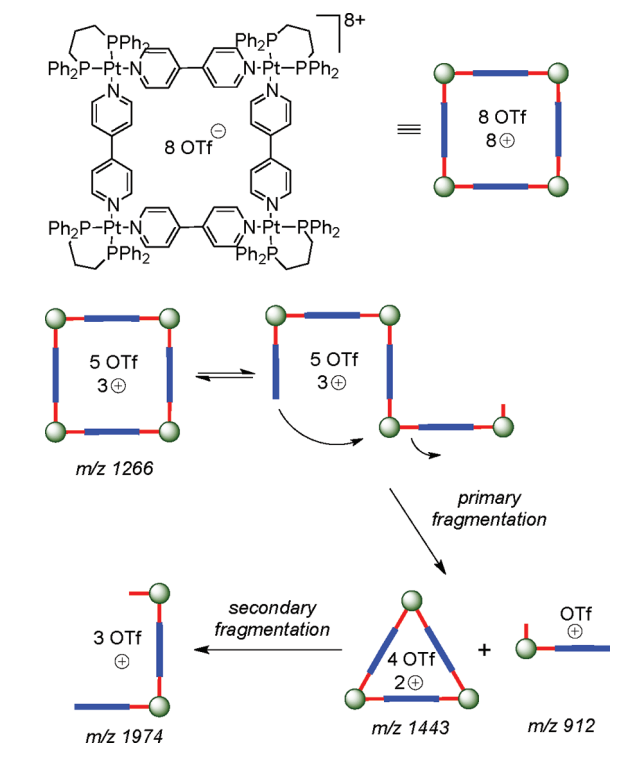
Electrospray ionization,<sup>694</sup> which is a soft ionization technique, has emerged in the past decade as an indispensable tool for analyzing supramolecular assemblies that contain noncovalent bonds.<sup>695</sup> ESI works by generating charged droplets through dispersion by electrospray from a solution of the desired analyte. The small droplets, through evaporation of solvents, shrink and as a result of Coulombic repulsion undergo fission into even smaller droplets until desolvated ions are formed. The advantage of ESI is that it keeps the internal energy of the ions low and thus not only suppresses extensive fragmentation but also make the intact ionization of noncovalent ensembles feasible. Moreover, the analyte can be ionized from almost any suitable solution, provided that a charge is present in the complex or can be delivered to it during ionization. The combination of ESI sources with time-of-flight mass analyzer was developed to increase the ion separation time so that much higher mass accuracy and resolution could be achieved. Similarly, combination of ESI sources with Fourier transform–ion cyclotron resonance systems allows one to investigate the isotope patterns in a broad distribution of different charge states with high accuracy and resolution. These sophisticated techniques, especially ESI-MS, have been extensively used to analyze a wide variety of supramolecular assemblies.<sup>693</sup>

Cold-spray ionization–mass spectrometry, a gentler alternative to ESI-MS, was developed to characterize labile self-assembled species.<sup>696</sup> The fundamental difference between ESI-MS and CSI-MS is that, in CSI, the ion source and desolvation chamber operate at low temperature. While ESI-MS is not suitable for these compounds because of their instability, CSI-MS affords multiply charged molecular ions with attached solvent molecules and, thus, analytical data on molecular mass, charge state, and isotope pattern are easily obtained. Fujita and co-workers have used this technique to characterize a large number of metallacycles and metallacages.<sup>696</sup>

Another softer variant of ESI-MS, sonic spray ionization–mass spectrometry (SSI-MS), allows fragile compounds to remain unfragmented during ionization and results in singly charged species.<sup>697,698</sup> The two ionization techniques differ in the way the solvent droplets are formed, the solution concentrations and flow rates required, the magnitude of the applied voltage, and the method of ion production. In SSI, the ion source involves two capillaries, one nested inside the other. While the inner capillary introduces a solution of analyte, the outer capillary provides a coaxial nitrogen gas flow to facilitate droplet nebulization. SSI-MS is typically operated at atmospheric pressure and without applying an electric potential to the source. The soft-ionization method reduces the fragmentation of noncovalent assemblies, fragile analytes, and thermodynamically labile ensembles. For example, transition metal (Fe<sup>3+</sup>, Co<sup>2+</sup>, and Cu<sup>2+</sup>) induced, resorcinarene-based coordination cages were characterized via SSI-MS.<sup>699</sup> In contrast to ESI-MS, which shows multiply charged peaks, SSI-MS spectra showed monocharged ion peaks, making the identification of the cages straightforward.

In recent years, researchers have increasingly focused on using mass spectrometry as a tool for studying various aspects of coordination-driven supramolecular systems such as host–guest chemistry, fragmentation and reactivity in solution and gas phase, and structural elucidation, through tandem mass spectroscopic experiments.<sup>693</sup> Müller et al. have studied the encapsulation of guest cations within the cavity of a metallo-supramolecular cage

Scheme 151



having  $M_6L_4$  truncated tetrahedral topology.<sup>490</sup> A remarkable difference between ESI-FT-ICR-MS of  $M_6L_4$  tetrahedron  $[(\text{CdCl})_3(\text{H}_6\text{Br}_3\text{L})]^{8+}$  ( $\text{H}_6\text{Br}_3\text{L}$  = tris[(5-bromo-2-hydroxybenzylidene)amino]guanidinium) encapsulating  $\text{NEt}_4^+$  or  $\text{NEt}_3\text{H}^+$  ions as templating guest was observed. When  $\text{NEt}_4^+$  was encapsulated, it exactly filled up the internal space and signals for each charge state accompanied by successive losses of  $\text{NEt}_4\text{Cl}$  or by exchange of  $\text{NEt}_4^+$  against  $\text{H}^+$  appeared in the mass spectrum. The simulated isotopic pattern also agreed with the experimental one. When  $\text{NEt}_3\text{H}^+$  acted as guest, an additional signal due to water molecule was observed indicating that  $\text{NEt}_3\text{H}^+$  leaves enough space for an additional water molecule, which is coencapsulated in the cavity of the tetrahedron.

Tandem MS experiments have also led to the elucidation of structure and the energetics of fragmentation process in metallo-supramolecular assemblies. Fragmentation pathways of the metallo-supramolecular square<sup>25</sup>  $[\text{Pt}(\text{dppp})(4,4'\text{-bipyridine})]_4^{8+}$  ( $\text{OTf}$ )<sub>8</sub> have been studied by Schalley et al. by carefully mass-selecting triply charged squares in the gas phase via tandem MS experiments.<sup>700</sup> Infrared multiphoton dissociation (IRMPD) spectra of Pt(II) squares in their +3 charged state in the gas phase have been recorded on a ESI-FT-ICR mass spectrometer. The mass spectrum showed a doubly charged 3:3 complex ( $m/z$  1443) and a singly charged 1:1 complex ( $m/z$  912) of Pt(II) corners and bipyridines as primary products. No doubly charged 2:2 complex was observed, indicating that no fragmentation into two half-squares occurred, although the same number of metal–nitrogen bonds needed to be broken (Scheme 151). Instead, a singly charged half-square was formed from the 3:3 complex ( $m/z$  1974) as a secondary fragmentation product. The reason for the preference of one pathway over the other has been explained by invoking a rear-attack mechanism. When irradiated by the IR lasers, the internal energy of the ions increases, leading

to an opening of the first bond. This gives rise to a chainlike conformer where an uncomplexed pyridine end can attack at the third metal center, thus forming a new M–N bond while facilitating the cleavage of a M–N bond to form species having  $m/z$  1443 and 912. Although not observed in the solution phase by NMR experiments, triangles were formed under the gas-phase conditions. To understand the effect of charge repulsion on the fragmentation pathway, tandem MS experiments performed with +5 charged states of the same squares showed strong dependencies of fragmentation patterns on the parent ions' charge states.<sup>701</sup> For species with a lower number of charges, expulsions of edge ligands prevailed, whereas charge separation pathways dominated over the dissociation pathways for more highly charged species.

Tandem MS experiments carried out on Pt(II)- and Pd(II)-based chiral molecular rhomboids also provided access to fragmentation processes that are difficult to study in the condensed phase.<sup>216</sup> To understand the fragmentation behavior of the rhomboids in the gas phase, the ions of interest were mass-selected in the FT-ICR cell and subjected to a collision-induced decay (CID) experiment. CID experiments revealed that doubly charged 2:2 complexes fragment into two identical, singly charged species followed by C–H and C–C bond activation mediated by coordinatively unsaturated metal centers. The observed  $\beta$ -hydrogen shift was analogous to ones encountered in transition-metal-mediated catalytic processes such as the Heck reaction.

Ion mobility spectrometry–mass spectrometry (IMS-MS),<sup>702</sup> a widely used method for studying conformations of protein and other large biomolecules,<sup>703</sup> has been recently used to obtain the structures of coordination-driven metallo-supramolecular assemblies that cannot be unambiguously characterized through traditional methods such as X-ray crystallography or NMR spectroscopy. Wesdemiotis, Newkome, and co-workers used traveling wave IMS-MS to obtain qualitative conformational information and high-resolution mass spectra for Cd(I), Fe(II), and Ru(II) metallocycles.<sup>704,705</sup> Traveling wave IMS-MS, which enables two-dimensional gas-phase separation and complete deconvolution of the isotope patterns of ions with the same  $m/z$  value, facilitates the structural analysis for self-assembled supramolecules.<sup>706</sup> With traveling wave IMS-MS, ions with different charges and shapes are separated on the basis of their drift time in the ion mobility device, thus avoiding the isomer superposition prevalent in regular ESI-MS or Fourier transform mass spectrometry. The separated structures or charge states are subsequently characterized by their mass spectra and their fragmentation patterns in tandem mass spectra. Bowers and co-workers have used drift cell IMS-MS to obtain absolute cross-sections of a number of coordination-driven supramolecular assemblies.<sup>707</sup> Ion-mobility studies on a molecular rectangle,<sup>109</sup>  $[(1,8\text{-bis}(\text{trans-Pt}(\text{PET}_3)_2)\text{-anthracene})_2(4,4'\text{-bipyridine})_2](\text{PF}_6)_4$ , and a molecular triangle,<sup>55</sup>  $[(3,6\text{-bis}(\text{trans-Pt}(\text{PET}_3)_2)\text{phenanthrene})_3(4,4'\text{-bipyridine})_3](\text{PF}_6)_6$ , gave cross-sections that matched well with the values obtained from their corresponding single-crystal X-ray structures. For a trifacial prismatic box,<sup>463</sup>  $[(\text{cis-Pt}(\text{PET}_3)_2)_6(\text{tetrakis}(4\text{-pyridyl})\text{-cyclobutadienecyclopentadienylcobalt(II)})_3](\text{OTf})_{12}$ , the experimental cross-section values obtained from IMS-MS agreed well with the calculated cross-sections from molecular modeling studies. These studies indicate that IMS-MS can be a powerful new tool in supramolecular structure determination and is complementary to existing methods such as X-ray and NMR.

**5.3.2. Solution-Phase X-ray Measurement.** One of the major challenges that was and is still faced by supramolecular chemists is the inability to characterize the supramolecules

structurally. The structural complexity, conformational flexibility, and nanoscale dimensions of supramolecular architectures often makes them difficult to crystallize and therefore limits the use of classical single-crystal X-ray diffraction methods. Although multinuclear NMR and mass spectroscopy provides information about the general features and composition of the supramolecular architectures, these techniques do not provide direct structural information. Application of multidimensional NMR techniques, widely used to deduce conformations of biomolecules, is limited in supramolecular assemblies due to the presence of repetitive, chemically analogous groups in the building blocks.

Solution-phase X-ray measurements provide an extraordinarily useful means to characterize supramolecular architectures whose structures and sizes cannot be determined by traditional crystallographic, spectroscopic, and mass spectrometric methods. In addition, this method provides insight into the formation, shape, and structure of the supramolecular species in solution. Since many of the applications of supramolecular assemblies are in solution phase, the knowledge of their structural conformations in solution, which can sometimes significantly vary from their solid-state structures, can better explain the fundamental principles involved at the atomic scale. X-ray solution scattering in both the small-angle (SAXS) and wide-angle (WAXS) regimes have been extensively used to understand structural conformations of biological macromolecules such as proteins in solution.<sup>708</sup> While SAXS allows for low-resolution structural characterization of macromolecules in solution, WAXS afford a high-resolution pattern that approaches that of conventional X-ray crystallographic measurements, thus providing atomic scale insight into the structure and conformational dynamics of macromolecules in solution.

In recent years, solution-phase X-ray scattering experiments in conjunction with coordinate-based molecular modeling have been used to elucidate solution-phase structures of coordination-driven self-assembled architectures. WAXS have been used to obtain direct structural information on supramolecular Pt(II)-based molecular triangle,<sup>55</sup> [(3,6-bis(*trans*-Pt(PET<sub>3</sub>)<sub>2</sub>)phenanthrene)<sub>3</sub>-(4,4'-bipyridine)<sub>3</sub>](PF<sub>6</sub>)<sub>6</sub>, molecular rectangle<sup>109</sup> [(1,8-bis(*trans*-Pt(PET<sub>3</sub>)<sub>2</sub>)anthracene)<sub>2</sub>-(4,4'-bipyridine)<sub>2</sub>](PF<sub>6</sub>)<sub>4</sub>, and trigonal prism<sup>417</sup> [(1,8-bis(*trans*-Pt(PET<sub>3</sub>)<sub>2</sub>)anthracene)<sub>3</sub>-(tris(4-pyridyl)-methanol)<sub>2</sub>](PF<sub>6</sub>)<sub>4</sub> in solution.<sup>709</sup> X-ray scattering patterns recorded for the low-angle region (0.12–2.48 Å<sup>−1</sup>) that compared well with their calculated patterns indicated that the supramolecules retained their shape when dissolved in nitromethane solution. Scattering patterns obtained from a large-angle region (0.19–16 Å<sup>−1</sup>) gave platinum–platinum distances and coordination number, and the results correlated well with the theoretical calculations. Although the solution-phase structures of these assemblies are similar to that in the crystalline solid state, they are significantly less rigid in solution as indicated by smaller diagonal platinum–platinum interaction as compared to that seen in single-crystal X-ray data.

Tiede and co-workers determined the solution-phase structure of a series of Re(I)-based supramolecular squares using WAXS experiments.<sup>710</sup> WAXS patterns recorded for the molecular squares showed a strong interference pattern corresponding to rhenium spacing within the discrete squares. The observed interference patterns are markers of the overall macrocycle structure, molecular motions, configurational flexibility, and solvent interactions. The radius of gyration (*R<sub>g</sub>*) values obtained from scattering patterns agreed well with the sizes of the squares calculated from molecular modeling studies. The Re–Re edge

distances determined from pair distribution function (PDF) patterns also matched well with the model and solid-state X-ray structures. The solution-phase WAXS pattern recorded for small and conformationally rigid molecular square<sup>711</sup> [(Re(CO)<sub>3</sub>Cl)(pyrazine)]<sub>4</sub> showed a good match with the scattering pattern calculated from the single-crystal X-ray structure. Interestingly, the analogous molecular square [(Re(CO)<sub>3</sub>Cl)-(4,4'-bipyridine)]<sub>4</sub>, which has two different X-ray structures—one with a flat geometry<sup>711</sup> and the other with a puckered butterfly form<sup>676</sup>—showed a solution-phase structure that differs from either of the two solid-state structures. The solution-phase structure appeared to be a bimodal distribution of conformers that are interrelated by a butterfly-type motion spanning about 25° in the improper Re–Re–Re–Re torsion angle.

Hupp and co-workers have used solution-phase X-ray scattering measurements to obtain structures of porphyrin-based supramolecular assemblies in solution. SAXS patterns obtained for a series of supramolecular porphyrinic prisms assembled from Zn(II)-containing porphyrin monomers, dimers, or trimers gave *R<sub>g</sub>* values that agreed well with the values calculated from modeling studies.<sup>434</sup> WAXS measurements to obtain information about interatomic spacing within the assemblies showed Zn–Zn interactions unique to prism assemblies. Likewise, the structures of other porphyrinic assemblies such as a tetrameric zinc(II) porphyrin assembly<sup>276</sup> and cavity-tailored porphyrin boxes<sup>517</sup> in solution were ascertained using solution-phase X-ray scattering measurements. Similarly, Tiede et al. were able to structurally characterize a hexameric, diphenylene-linked zinc(II) porphyrin macrocycle and the corresponding host–guest complex formed by inclusion of a tripyridyl guest in solution using X-ray scattering measurements.<sup>712,713</sup> X-ray scattering patterns coupled with pair distance function (PDF) analyses revealed that the hexameric assembly is structurally nonrigid and exists as a distribution of conformers. The host assembly underwent an expansion upon guest inclusion.

#### 5.4. Photophysical Studies Using Laser Spectroscopy

Self-assembly, which provides a facile way to assemble a large number of molecules into highly organized supramolecular architectures, has been applied to assemble chromophores and electroactive molecules for use as molecular devices and machines in nanoscale dimensions.<sup>714</sup> These novel materials have found applications in molecular electronics, photonics, and photovoltaics. In these multichromophoric assemblies, collective excitations at multiple sites contribute to the observed optical behavior. A wide variety of two- and three-dimensional supramolecular systems containing perylene imide and diimide dyes, and porphyrins have been assembled to study the electron transport and charge separation processes.<sup>715</sup> Recently, various spectroscopic techniques such as transient absorption, two-photon absorption, steady-state fluorescence, and time-resolved fluorescence have been used to explore the charge-transfer and photophysical properties of self-assembled metallacycles and metallacages.

The crystal structure of the LH2 light-harvesting antenna system of purple photosynthetic bacteria *Rhodospseudomonas acidophila* revealed a circularly arranged chromophoric assembly of bacteriochlorophylls, leading to considerable efforts to develop biomimetic artificial photosynthetic systems that may offer insights into the photophysics of energy collection and transfer in these proteins.<sup>715</sup> Multiporphyrin ensembles can function as light-harvesting antennae as in natural photosynthetic systems if sufficiently fast electron transfer between the porphyrin subunits



can be achieved. The most common approach to achieve efficient electron transfer is to design ensembles that have photoactive porphyrin moieties and electron-deficient chromophores. Photophysical studies on self-assembled zinc(II) trisporphyrin prisms having 1,4-diazabicyclo[2.2.2]octane (DABCO), 4,4'-bipyridine, and 5,15-(4-pyridyl)-10,20-phenylporphyrin (4'-*trans*-DPyP) as pillars have shown efficient photoinduced energy transfer from the triporphyrin unit to the pillars upon excitation of both components within the assemblies.<sup>515</sup> Luminescence experiments showed that when 4'-*trans*-DPyP was used as a pillar, a highly efficient photoinduced electron transfer (96% efficiency) from the triporphyrin units to the 4'-*trans*-DPyP pillars occurred. The analogous trigonal prisms having ditopic N-donor ligands based on perylene tetracarboxylic acid bisimide also showed efficient photoinduced electron transfer from the zinc porphyrin units to the axially coordinated bisimide pillars, occurring from the singlet excited states localized on both chromophores.<sup>437</sup>

Photoinduced energy-transfer processes have also been observed in self-assembled porphyrin/peryene bisimide ensembles.<sup>438</sup> The metallo-supramolecular ensembles (ZnMC)<sub>2</sub>(PBI)<sub>2</sub> were prepared by axial coordination of *N,N'*-dipyridyl-functionalized perylene bisimide (PBI) dyes to the zinc ion centers of two [2 + 2] porphyrin metallacycles (ZnMC) [*trans,cis,cis*-RuCl<sub>2</sub>(CO)<sub>2</sub>-(Zn·4'-*cis*-DPyP)]<sub>2</sub>. These complexes were structurally characterized by single-crystal X-ray crystallography.<sup>716</sup> Ultrafast absorption techniques showed that the observed photophysical behaviors depended on the substituents present at the bay area of the PBI pillars. When a *tert*-butylphenoxy substituent was present, efficient quenching of both perylene bisimide and the zinc porphyrin chromophores was observed, leading to a charge-separated state, PBI<sup>−</sup>–Zn<sup>+</sup>, in which a perylene bisimide unit was reduced and zinc porphyrin was oxidized. In contrast, PBI-bearing pyrrolidinyl substituents led to singlet energy transfer from the zinc porphyrin chromophores to the perylene bisimide units with an efficiency of 0.7. This value was due to a competing quenching mechanism, leading to PBI<sup>−</sup>–Zn<sup>+</sup>.<sup>438</sup>

Wasielowski and co-workers investigated energy-transfer processes in a cyclic self-assembled zinc(II) porphyrin tetramer by transient absorption measurements using femtosecond laser pulses. A cyclic tetramer self-assembled from *meso*-ethynylpyridyl-functionalized zinc(II) porphyrin showed efficient electron transfer between the porphyrin units.<sup>276</sup> The electron-transfer rate was found to be ~8 times faster than the analogous zinc(II) porphyrin tetramers.<sup>717,718</sup> A self-assembled cyclic zinc chlorophyll tetramer exhibited an ultrafast intramolecular energy-transfer rate as determined from femtosecond singlet–singlet annihilation and transient absorption anisotropy studies.<sup>719</sup> The cyclic tetramer upon excitation with 120 fs laser pulses yielded its lowest singlet excited state in which the rate of energy transfer was ~20 times faster than the tetramer in the ground state. However, this ultrafast energy-transfer rate is still ~10 times slower than what is observed in the photosynthetic proteins. This difference is attributed to the larger transition dipole moment found in chlorophyll as compared to porphyrin. Thus, subtle changes in the structures of assemblies can profoundly affect electron-transfer rates.

Extending this concept, butadiyne-linked zinc(II) chlorophyll and porphyrin dimers were assembled into trigonal prisms to study the photophysics of electron-transfer dynamics.<sup>720</sup> The butadiyne-linked dimers, upon treatment with 3-fold symmetric ligands such as triethynylpyridine, assembled into prismatic structures in which the dimers comprised the faces of the prism. The incorporation of butadiyne linkages increased the ability of these dimers to

absorb the solar spectrum over a broad range of wavelengths. The prismatic architecture restricted the rotation of the macrocycles about the joining butadiyne bond. Photoexcitation of these prismatic assemblies, using femtosecond transient absorption spectroscopy, revealed efficient, through-space energy transfer between the macrocyclic dimers within the prisms. Use of a 3-fold symmetric ligand possessing longer arms gave larger trigonal prisms, resulting in more efficient energy transfers between the prism faces.

Recently, ultrafast excited-state relaxation dynamics of a number of Pt(II)-containing self-assembled metallacycles and metallacages were studied using femtosecond measurements of fluorescence upconversion and transient absorption spectra.<sup>721</sup> In the case of the metallacycles, the charge-transfer dynamics and intersystem crossing were found to be dependent on the geometries and dimensions of the metallacycles. For rectangular anthracene-containing metallacycles, the electronic coupling between adjacent ligands was relatively weak, whereas for the triangular phenanthrene-containing structures, there was a clear interaction between the conjugated ligand and the metal center. The photophysical properties of the coordination-driven self-assembled metallo-supramolecular rhomboids having donor ligands 1,2-bis(3-pyridyl)ethyne and 1,4-bis(3-pyridyl)-1,3-butadiyne were also investigated by the use of both time-resolved fluorescence spectroscopy and quantum chemistry calculations.<sup>722</sup> Steady-state absorption and fluorescence as well as the time-correlated single photon counting techniques revealed that the nature of the excited states for these metallo-supramolecular rhomboids varies with the acetylene chain length of the donor ligands and with the different conformers. Thus, the results demonstrate that differences in the dimensionality and structure of the metallacycles results in different optical properties, which may be utilized in the design of nonlinear optical materials and potential longer lived excited-state materials for further electronic applications.

## 6. CONCLUSIONS AND PROGNOSTICATION

As described above, coordination-driven self-assembly is a vibrant, active field. It is evident that considerable progress has been made since the beginnings of the field some 2 decades ago. Early work involved the self-assembly of helicates, grids, and other infinite ensembles. Out of this area evolved the self-assembly of finite closed systems, both two-dimensional and three-dimensional with well-defined shapes and sizes, that is the topic of this review. Early work in this field focused on the development of rational methodologies for the self-assembly of predesigned systems along with their characterization. At the start, only architectures based on just two components were prepared primarily involving Pt and Pd pyridine interactions. However, other transition metals and different donor units were rapidly adopted. As it was and still is a challenge to get suitable single crystals of these large systems with cavities filled with solvent for X-ray structure analysis, proper characterization was and remains a challenge. Multinuclear, high-resolution NMR and electrospray mass spectrometry are the primary and essential tools for proper characterization along with X-ray and more recently synchrotron X-ray methods.

As seen in this review, considerable progress has been made in our understanding of these abiological, coordination-based self-assembly processes. Moreover, multicomponent self-assembly along with self-sorting and self-organization has been developed. However, the greatest progress, mostly in the past half-dozen



years, has been in the uses and applications of these self-assembled metallacycles and metallacages. Both 2D and 3D systems have been used in chemosensing and host–guest chemistry. Particularly interesting are Fujita's use of 3D cages for the encapsulation of reactive species as described above. However, the most recent and arguably interesting applications have been in catalysis, use as microreactors and biological applications. In particular Raymond and Bergman have elegantly exploited the cavities of self-assembled 3D cages for enzyme-like catalysis as detailed in section 4.5.2. Likewise, Fujita and co-workers have used 3D cages as nanoreaction vessels to carry out unusual reactions as described in the preceding sections. In the past couple of years the biological applications of self-assembled metallacycles and metallacages have been described. Particularly relevant are the antitumor studies of Therrien and co-workers and the investigation of Sleiman and co-workers on nucleic acid interactions.

It is clear that coordination-driven self-assembly will continue to be an active area of research and an important component of supramolecular chemistry and nanoscience. Future developments are likely to involve the formation and characterization of even more complex ensembles and their applications. In particular we are likely to see further advances in multicomponent self-assembly of functionalized systems. Emphasis will likely be on applications and uses both in material science and biochemical and biomedical areas. More sophisticated sensors as well as better and more useful catalytic applications will undoubtedly emerge. Likewise, the biomedical applications of these systems, such as potential antitumor agents, protein and nucleic acid interactions, and so on are new vistas that will see increasing activity. Self-assembly in general, and coordination-driven self-assembly in particular, will play an important role in the “bottom-up” manufacturing of novel materials in the evolving nanotechnology arena. Likewise, similarity and evolving synergy between coordination-driven self-assembly of metallacages and MOFs will lead to new developments and applications.

## AUTHOR INFORMATION

### Corresponding Author

\*E-mail: rajesh@chem.utah.edu (R.C.); stang@chem.utah.edu (P.J.S.); and psm@ipc.iisc.ernet.in (P.S.M.).

## BIOGRAPHIES

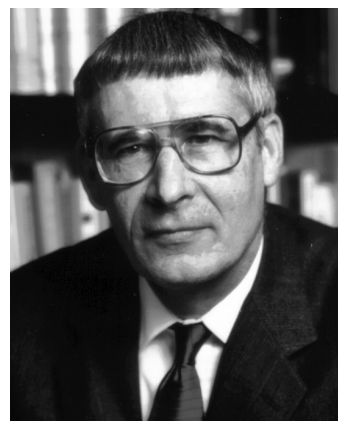


Rajesh Chakrabarty was born and grew up in Manipur, India. He received his Ph.D. from Gauhati University working with

Prof. Birinchi K. Das focusing on homogeneous and heterogeneous catalysis using metal–oxo clusters. He then moved to the Indian Institute of Science, Bangalore, as a CSIR Research Associate to work with Dr. Partha Sarathi Mukherjee in the field of supramolecular chemistry. Since the fall of 2009, Rajesh has been working in the group of Prof. Peter J. Stang as post-doctoral fellow at the University of Utah. His current research interests include functionalization of supramolecules for biological applications.



Partha Sarathi Mukherjee was born in 1973 in West Bengal, India. He earned his B.Sc. with honors in chemistry from Burdwan University in 1995 and M.Sc. in chemistry in 1998 from Jadavpur University. He did his Ph.D. from the Indian Association for the Cultivation of Science in 2002 working with Prof. N. Ray Chaudhuri and his postdoctoral from University of Utah with Prof. Peter J. Stang. In 2004 he moved to University of Goettingen to work with Prof. Herbert W. Roesky as a Humboldt fellow. He has been at the Indian Institute of Science, Bangalore, since July 2005, where he is currently an Associate Professor. His current research interests are in the areas of self-assembly of functional molecular architectures, organometallic materials, and magnetic clusters/polyclusters. He is the recipient of a young scientist medal of the Indian National Science Academy, Associateship of the Indian Academy of Sciences, and Microsoft Research outstanding young faculty award. Dr. Mukherjee has published 78 original papers in peer-reviewed journals.



Peter J. Stang is a Distinguished Professor of Chemistry at the University of Utah, as well as the Editor of the *Journal of Americal Chemical Society*. He is a member of the U.S. National Academy of Sciences and a Foreign Member of the Chinese (CAS) and

Hungarian Academies of Sciences. He was recently listed by the Times Higher Education among the 100 top chemists, who had the highest citation impact scores (citations/papers for the decade of 2000–2010).

## ACKNOWLEDGMENT

P.J.S. thanks the NIH and NSF for continued financial support over the years of our studies in coordination-driven self-assembly. P.S.M. thanks the Department of Science and Technology (DST), India, for the financial support. We thank Dr. Timothy R. Cook for help with editing the paper.

## REFERENCES

- (1) Pedersen, C. J. *Angew. Chem., Int. Ed. Engl.* **1988**, *27*, 1021.
- (2) Lehn, J.-M. *Angew. Chem., Int. Ed. Engl.* **1988**, *27*, 89.
- (3) Cram, D. J. *Angew. Chem., Int. Ed. Engl.* **1988**, *27*, 1009.
- (4) (a) Steed, J. W.; Turner, D. R.; Wallace, K. J. *Core Concepts in Supramolecular Chemistry and Nanochemistry*; John Wiley & Sons: West Sussex, U.K., 2007. (b) Steed, J. W.; Atwood, J. L. *Supramolecular Chemistry*; John Wiley & Sons: West Sussex, U.K., 2000.
- (5) Lehn, J.-M. *Supramolecular Chemistry: Concepts and Perspectives*; VCH: Weinheim, Germany, 1995.
- (6) Sauvage, J.-P.; Dietrich-Buchecker, C., Eds. *Molecular Catenanes, Rotaxanes, and Knots: A Journey Through the World of Molecular Topology*; Wiley-VCH: Weinheim, Germany, 1999.
- (7) For recent reviews see: (a) Beves, J. E.; Leigh, D. A. *Nat. Chem.* **2010**, *2*, 708. (b) Fang, L.; Olson, M. A.; Benítez, D.; Tkatchouk, E.; Goddard, W. A., III; Stoddart, J. F. *Chem. Soc. Rev.* **2010**, *39*, 17. (c) Durot, S.; Reviriego, F.; Sauvage, J.-P. *Dalton Trans.* **2010**, *39*, 10557. (d) Faiz, J. A.; Heitz, V.; Sauvage, J.-P. *Chem. Soc. Rev.* **2009**, *38*, 422. (e) Crowley, J. D.; Goldup, S. M.; Lee, A.-L.; Leigh, D. A.; McBurney, R. T. *Chem. Soc. Rev.* **2009**, *38*, 1530. (f) Balzani, V.; Credi, A.; Venturi, M. *Chem. Soc. Rev.* **2009**, *38*, 1542. (g) Stoddart, J. F. *Chem. Soc. Rev.* **2009**, *38*, 1802. (h) Champin, B.; Mobian, P.; Sauvage, J.-P. *Chem. Soc. Rev.* **2007**, *36*, 358. (i) Sauvage, J.-P. *Chem. Commun. (Cambridge, U.K.)* **2005**, 1507. (j) Bonnet, S.; Collin, J.-P.; Koizumi, M.; Mobian, P.; Sauvage, J.-P. *Adv. Mater.* **2006**, *18*, 1239. (k) Dietrich-Buchecker, C.; Colasson, B. X.; Sauvage, J.-P. *Top. Curr. Chem.* **2005**, *249*, 261. (l) Ruben, M.; Rojo, J.; Romero-Salguero, F. J.; Uppadine, L. H.; Lehn, J.-M. *Angew. Chem., Int. Ed.* **2004**, *43*, 3644.
- (8) Reviews: (a) Stang, P. J. *J. Org. Chem.* **2009**, *74*, 2. (b) Northrop, B. H.; Chercka, D.; Stang, P. J. *Tetrahedron* **2008**, *64*, 11495. (c) Seidel, S. R.; Stang, P. J. *Acc. Chem. Res.* **2002**, *35*, 972. (d) Leininger, S.; Olenyuk, B.; Stang, P. J. *Chem. Rev.* **2000**, *100*, 853. (e) Stang, P. J. *Chem.—Eur. J.* **1998**, *4*, 19. (f) Olenyuk, B.; Fechtenkötter, A.; Stang, P. J. *J. Chem. Soc., Dalton Trans.* **1998**, 1707. (g) Stang, P. J.; Olenyuk, B. *Acc. Chem. Res.* **1997**, *30*, 502.
- (9) Reviews: (a) Caulder, D. L.; Raymond, K. N. *J. Chem. Soc., Dalton Trans.* **1999**, 1185. (b) Caulder, D. L.; Raymond, K. N. *Acc. Chem. Res.* **1999**, *32*, 975. (c) Caulder, D. L.; Brückner, C.; Powers, R. E.; König, S.; Parac, T. N.; Leary, J. A.; Raymond, K. N. *J. Am. Chem. Soc.* **2001**, *123*, 8923.
- (10) Reviews: (a) Fujita, M.; Tominaga, M.; Hori, A.; Therrien, B. *Acc. Chem. Res.* **2005**, *38*, 371. (b) Fujita, M.; Umemoto, K.; Yoshizawa, M.; Fujita, N.; Kusakawa, T.; Biradha, K. *Chem. Commun. (Cambridge, U.K.)* **2001**, 509. (c) Fujita, M. *Struct. Bonding (Berlin, Ger.)* **2000**, *96*, 177. (d) Fujita, M. *Chem. Soc. Rev.* **1998**, *27*, 417.
- (11) Reviews: (a) Oliveri, C. G.; Ulmann, P. A.; Wiester, M. J.; Mirkin, C. A. *Acc. Chem. Res.* **2008**, *41*, 1618. (b) Gianneschi, N. C.; Masar, M. S., III; Mirkin, C. A. *Acc. Chem. Res.* **2005**, *38*, 825. (c) Holliday, B. J.; Mirkin, C. A. *Angew. Chem., Int. Ed.* **2001**, *40*, 2022.
- (12) Reviews: (a) Cotton, F. A.; Lin, C.; Murillo, C. A. *Proc. Natl. Acad. Sci. U. S. A.* **2002**, *99*, 4810. (b) Cotton, F. A.; Lin, C.; Murillo, C. A. *Acc. Chem. Res.* **2001**, *34*, 759.
- (13) De, S.; Mahata, K.; Schmittel, M. *Chem. Soc. Rev.* **2010**, *39*, 1555.
- (14) Reviews: (a) Nitschke, J. R. *Acc. Chem. Res.* **2007**, *40*, 103. (b) Safont-Sempere, M. M.; Fernández, G.; Würthner, F. *Chem. Rev.* **2011**, DOI: 10.1021/cr100357h.
- (15) Reviews: (a) Wiester, M. J.; Ulmann, P. A.; Mirkin, C. A. *Angew. Chem., Int. Ed.* **2011**, *50*, 114. (b) Breiner, B.; Clegg, J. K.; Nitschke, J. R. *Chem. Sci.* **2011**, *2*, 51. (c) Laughrey, Z.; Gibb, B. C. *Chem. Soc. Rev.* **2011**, *40*, 363. (d) Saalfrank, R. W.; Maid, H.; Scheurer, A. *Angew. Chem., Int. Ed.* **2008**, *47*, 8794. (e) Ruben, M.; Lehn, J.-M.; Müller, P. *Chem. Soc. Rev.* **2006**, *35*, 1056. (f) Schmittel, M.; Kalsani, V. *Top. Curr. Chem.* **2005**, *245*, 1. (g) Collin, J.-P.; Heitz, V.; Sauvage, J.-P. *Top. Curr. Chem.* **2005**, *262*, 29. (h) You, C.-C.; Dobrawa, R.; Saha-Möller, C. R.; Würthner, F. *Top. Curr. Chem.* **2005**, *258*, 39.
- (16) Reviews: (a) Yoshizawa, M.; Fujita, M. *Bull. Chem. Soc. Jpn.* **2010**, *83*, 609. (b) Yoshizawa, M.; Klosterman, J. K.; Fujita, M. *Angew. Chem., Int. Ed.* **2009**, *48*, 3418. (c) Maurizot, V.; Yoshizawa, M.; Kawano, M.; Fujita, M. *Dalton Trans.* **2006**, 2750.
- (17) Reviews: (a) Pluth, M. D.; Bergman, R. G.; Raymond, K. N. *Acc. Chem. Res.* **2009**, *42*, 1650. (b) Fiedler, D.; Leung, D. H.; Bergman, R. G.; Raymond, K. N. *Acc. Chem. Res.* **2005**, *38*, 351. (c) Davis, A. V.; Yeh, R. M.; Raymond, K. N. *Proc. Natl. Acad. Sci. U. S. A.* **2002**, *99*, 4793.
- (18) van Leeuwen, P. W. N. M., Ed. *Supramolecular Catalysis*; Wiley-VCH: Weinheim, Germany, 2008.
- (19) Reviews: (a) Meeuwissen, J.; Reek, J. N. H. *Nat. Chem.* **2010**, *2*, 615. (b) Koblenz, T. S.; Wassenaar, J.; Reek, J. N. H. *Chem. Soc. Rev.* **2008**, *37*, 247. (c) Kleij, A. W.; Reek, J. N. H. *Chem.—Eur. J.* **2006**, *12*, 4218. (d) Wilkinson, M. J.; van Leeuwen, P. W. N. M.; Reek, J. N. H. *Org. Biomol. Chem.* **2005**, *3*, 2371.
- (20) Reviews: (a) Hupp, J. T. *Struct. Bonding (Berlin, Ger.)* **2006**, *121*, 145. (b) Snurr, R. Q.; Hupp, J. T.; Nguyen, S. T. *AIChE J.* **2004**, *50*, 1090. (c) Nguyen, S. T.; Gin, D. L.; Hupp, J. T.; Zhang, X. *Proc. Natl. Acad. Sci. U. S. A.* **2001**, *98*, 11849. (d) Dinolfo, P. H.; Hupp, J. T. *Chem. Mater.* **2001**, *13*, 3113.
- (21) Li, S.-S.; Northrop, B. H.; Yuan, Q.-H.; Wan, L.-J.; Stang, P. J. *Acc. Chem. Res.* **2009**, *42*, 249.
- (22) Kudernac, T.; Lei, S.; Elemans, J. A. A. W.; De Feyter, S. *Chem. Soc. Rev.* **2009**, *38*, 402.
- (23) Fujita, M.; Yazaki, J.; Ogura, K. *J. Am. Chem. Soc.* **1990**, *112*, 5645.
- (24) Fujita, M.; Yazaki, J.; Ogura, K. *Chem. Lett.* **1991**, 1031.
- (25) Stang, P. J.; Cao, D. H. *J. Am. Chem. Soc.* **1994**, *116*, 4981.
- (26) Fujita, M.; Oguro, D.; Miyazawa, M.; Oka, H.; Yamaguchi, K.; Ogura, K. *Nature* **1995**, *378*, 469.
- (27) Yu, S.-Y.; Kusakawa, T.; Biradha, K.; Fujita, M. *J. Am. Chem. Soc.* **2000**, *122*, 2665.
- (28) Fujita, N.; Biradha, K.; Fujita, M.; Sakamoto, S.; Yamaguchi, K. *Angew. Chem., Int. Ed.* **2001**, *40*, 1718.
- (29) Bar, A. K.; Chakrabarty, R.; Mostafa, G.; Mukherjee, P. S. *Angew. Chem., Int. Ed.* **2008**, *47*, 8455.
- (30) Review: Pitt, M. A.; Johnson, D. W. *Chem. Soc. Rev.* **2007**, *36*, 1441.
- (31) Fujita, M.; Aoyagi, M.; Ogura, K. *Inorg. Chim. Acta* **1996**, *246*, 53.
- (32) Fujita, M.; Ibukuro, F.; Hagihara, H.; Ogura, K. *Nature* **1994**, *367*, 720.
- (33) Fujita, M.; Ibukuro, F.; Seki, H.; Kamo, O.; Imanari, M.; Ogura, K. *J. Am. Chem. Soc.* **1996**, *118*, 899.
- (34) Fujita, M.; Ibukuro, F.; Yamaguchi, K.; Ogura, K. *J. Am. Chem. Soc.* **1995**, *117*, 4175.
- (35) Lu, J.; Turner, D. R.; Harding, L. P.; Byrne, L. T.; Baker, M. V.; Batten, S. R. *J. Am. Chem. Soc.* **2009**, *131*, 10372.
- (36) Schmitz, M.; Leininger, S.; Fan, J.; Arif, A. M.; Stang, P. J. *Organometallics* **1999**, *18*, 4817.
- (37) Habicher, T.; Nierengarten, J.-F.; Gramlich, V.; Diederich, F. *Angew. Chem., Int. Ed.* **1998**, *37*, 1916.
- (38) Chatterjee, B.; Noveron, J. C.; Resendiz, M. J. E.; Liu, J.; Yamamoto, T.; Parker, D.; Cinke, M.; Nguyen, C. V.; Arif, A. M.; Stang, P. J. *J. Am. Chem. Soc.* **2004**, *126*, 10645.
- (39) Yang, H.-B.; Das, N.; Huang, F.; Hawkrigge, A. M.; Díaz, D. D.; Arif, A. M.; Finn, M. G.; Muddiman, D. C.; Stang, P. J. *J. Org. Chem.* **2006**, *71*, 6644.

- (40) Review:Zangrando, E.; Casanova, M.; Alessio, E. *Chem. Rev.* **2008**, *108*, 4979.
- (41) Murray, H. H.; Raptis, R. G.; Fackler, J. P., Jr. *Inorg. Chem.* **1988**, *27*, 26.
- (42) Raptis, R. G.; Fackler, J. P., Jr. *Inorg. Chem.* **1990**, *29*, 5003.
- (43) For example, see: (a) Dias, H. V. R.; Diyabalanage, H. V. K.; Rawashdeh-Omary, M. A.; Franzman, M. A.; Omary, M. A. *J. Am. Chem. Soc.* **2003**, *125*, 12072. (b) Dias, H. V. R.; Diyabalanage, H. V. K.; Eldabaja, M. G.; Elbjairami, O.; Rawashdeh-Omary, M. A.; Omary, M. A. *J. Am. Chem. Soc.* **2005**, *127*, 7489. (c) Omary, M. A.; Elbjairami, O.; Gamage, C. S. P.; Sherman, K. M.; Dias, H. V. R. *Inorg. Chem.* **2009**, *48*, 1784. (d) Dias, H. V. R.; Gamage, C. S. P.; Keltner, J.; Diyabalanage, H. V. K.; Omari, I.; Eyobo, Y.; Dias, N. R.; Roehr, N.; McKinney, L.; Poth, T. *Inorg. Chem.* **2007**, *46*, 2979.
- (44) Rawashdeh-Omary, M. A.; Rashdan, M. D.; Dharanipathi, S.; Elbjairami, O.; Ramesh, P.; Dias, H. V. R. *Chem. Commun. (Cambridge, U. K.)* **2011**, *47*, 1160.
- (45) Dias, H. V. R.; Singh, S.; Campana, C. F. *Inorg. Chem.* **2008**, *47*, 3943.
- (46) Dias, H. V. R.; Gamage, C. S. P. *Angew. Chem., Int. Ed.* **2007**, *46*, 2192.
- (47) Hall, J. R.; Loeb, S. J.; Shimizu, G. K. H.; Yap, G. P. A. *Angew. Chem., Int. Ed.* **1998**, *37*, 121.
- (48) Espinet, P.; Soulantica, K.; Charmant, J. P. H.; Orpen, A. G. *Chem. Commun. (Cambridge, U. K.)* **2000**, 915.
- (49) Vicente, J.; Chicote, M.-T.; Alvarez-Falcón, M. M.; Jones, P. G. *Chem. Commun. (Cambridge, U. K.)* **2004**, 2658.
- (50) Lippert, B.; Miguel, P. J. S. *Chem. Soc. Rev.* **2011**, DOI: 10.1039/c1cs15090a.
- (51) Schnebeck, R.-D.; Freisinger, E.; Lippert, B. *Chem. Commun. (Cambridge, U. K.)* **1999**, 675.
- (52) Schnebeck, R.-D.; Freisinger, E.; Glahé, F.; Lippert, B. *J. Am. Chem. Soc.* **2000**, *122*, 1381.
- (53) Hwang, S.-H.; Moorefield, C. N.; Fronczek, F. R.; Lukyanova, O.; Echegoyen, L.; Newkome, G. R. *Chem. Commun. (Cambridge, U. K.)* **2005**, 713.
- (54) Romero, F. M.; Ziessel, R.; Dupont-Gervais, A.; Van Dorsselaer, A. *Chem. Commun. (Cambridge, U. K.)* **1996**, 551.
- (55) Kryshchenko, Y. K.; Seidel, S. R.; Arif, A. M.; Stang, P. J. *J. Am. Chem. Soc.* **2003**, *125*, 5193.
- (56) Qin, Z.; Jennings, M. C.; Puddephatt, R. J. *Chem. Commun. (Cambridge, U. K.)* **2001**, 2676.
- (57) Qin, Z.; Jennings, M. C.; Puddephatt, R. J. *Inorg. Chem.* **2003**, *42*, 1956.
- (58) Bar, A. K.; Chakrabarty, R.; Chi, K.-W.; Batten, S. R.; Mukherjee, P. S. *Dalton Trans.* **2009**, 3222.
- (59) Ghosh, S.; Turner, D. R.; Batten, S. R.; Mukherjee, P. S. *Dalton Trans.* **2007**, 1869.
- (60) Teo, P.; Koh, L. L.; Hor, T. S. A. *Inorg. Chem.* **2008**, *47*, 6464.
- (61) Teo, P.; Koh, L. L.; Hor, T. S. A. *Chem. Commun. (Cambridge, U. K.)* **2007**, 2225.
- (62) Park, K.-M.; Kim, S.-Y.; Heo, J.; Whang, D.; Sakamoto, S.; Yamaguchi, K.; Kim, K. J. *J. Am. Chem. Soc.* **2002**, *124*, 2140.
- (63) Schweiger, M.; Seidel, S. R.; Arif, A. M.; Stang, P. J. *Angew. Chem., Int. Ed.* **2001**, *40*, 3467.
- (64) Tzeng, B.-C.; Kuo, J.-H.; Lee, Y.-C.; Lee, G.-H. *Inorg. Chim. Acta* **2008**, *361*, 2515.
- (65) Berben, L. A.; Faia, M. C.; Crawford, N. R. M.; Long, J. R. *Inorg. Chem.* **2006**, *45*, 6378.
- (66) Shan, N.; Vickers, S. J.; Adams, H.; Ward, M. D.; Thomas, J. A. *Angew. Chem., Int. Ed.* **2004**, *43*, 3938.
- (67) Shan, N.; Ingram, J. D.; Easun, T. L.; Vickers, S. J.; Adams, H.; Ward, M. D.; Thomas, J. A. *Dalton Trans.* **2006**, 2900.
- (68) Schmittel, M.; Mahata, K. *Chem. Commun. (Cambridge, U. K.)* **2008**, 2550.
- (69) Schmittel, M.; Mahata, K. *Inorg. Chem.* **2009**, *48*, 822.
- (70) Würthner, F.; You, C.-C.; Saha-Möller, C. R. *Chem. Soc. Rev.* **2004**, *33*, 133.
- (71) Stang, P. J.; Olenyuk, B.; Fan, J.; Arif, A. M. *Organometallics* **1996**, *15*, 904.
- (72) Whiteford, J. A.; Lu, C. V.; Stang, P. J. *J. Am. Chem. Soc.* **1997**, *119*, 2524.
- (73) Stang, P. J.; Cao, D. H.; Chen, K.; Gray, G. M.; Muddiman, D. C.; Smith, R. D. *J. Am. Chem. Soc.* **1997**, *119*, 5163.
- (74) Stang, P. J.; Fan, J.; Olenyuk, B. *Chem. Commun. (Cambridge, U. K.)* **1997**, 1453.
- (75) Stang, P. J.; Chen, K.; Arif, A. M. *J. Am. Chem. Soc.* **1995**, *117*, 8793.
- (76) Manna, J.; Kuehl, C. J.; Whiteford, J. A.; Stang, P. J.; Muddiman, D. C.; Hofstadler, S. A.; Smith, R. D. *J. Am. Chem. Soc.* **1997**, *119*, 11611.
- (77) Goeb, S.; Prusakova, V.; Wang, X.; Vézina, A.; Sallé, M.; Castellano, F. N. *Chem. Commun. (Cambridge, U. K.)* **2011**, *47*, 4397.
- (78) Sun, S. S.; Lees, A. J. *Inorg. Chem.* **2001**, *40*, 3154.
- (79) Würthner, F.; Sautter, A. *Chem. Commun. (Cambridge, U. K.)* **2000**, 445.
- (80) You, C. C.; Würthner, F. *J. Am. Chem. Soc.* **2003**, *125*, 9716.
- (81) Sautter, A.; Kaletas, B. K.; Schmid, D. G.; Dobrawa, R.; Zimine, M.; Jung, G.; van Stokkum, I. H. M.; Cola, L. D.; Williams, R. M.; Würthner, F. *J. Am. Chem. Soc.* **2005**, *127*, 6719.
- (82) Kraft, S.; Hanuschek, E.; Beckhaus, R.; Haase, D.; Saak, W. *Chem.—Eur. J.* **2005**, *11*, 969.
- (83) Theilmann, O.; Saak, W.; Haase, D.; Beckhaus, R. *Organometallics* **2009**, *28*, 2799.
- (84) Janzen, D. E.; Patel, K. N.; VanDerveer, D. G.; Grant, G. J. *Chem. Commun. (Cambridge, U. K.)* **2006**, 3540.
- (85) Teo, P.; Koh, L. L.; Hor, T. S. A. *Inorg. Chem.* **2003**, *42*, 7290.
- (86) Ghosh, S.; Mukherjee, P. S. *Inorg. Chem.* **2009**, *48*, 2605.
- (87) Shanmugaraju, S.; Bar, A. K.; Chi, K.-W.; Mukherjee, P. S. *Organometallics* **2010**, *29*, 2971.
- (88) Gontier, E.; Bellec, N.; Brignou, P.; Gohier, A.; Guerro, M.; Roisnel, T.; Lorcy, D. *Org. Lett.* **2010**, *12*, 2386.
- (89) Gianneschi, N. C.; Mirkin, C. A.; Zakharov, L. N.; Rheingold, A. L. *Inorg. Chem.* **2002**, *41*, 5326.
- (90) Liu, X.; Stern, C. L.; Mirkin, C. A. *Organometallics* **2002**, *21*, 1017.
- (91) Fujita, M.; Sasaki, O.; Mitsunashi, T.; Fujita, T.; Yazaki, J.; Yamaguchi, K.; Ogura, K. *Chem. Commun. (Cambridge, U. K.)* **1996**, 1535.
- (92) Weilandt, T.; Troff, R. W.; Saxell, H.; Rissanen, K.; Schalley, C. A. *Inorg. Chem.* **2008**, *47*, 7588.
- (93) Holló-Sitkei, E.; Tárkányi, G.; Párkányi, L.; Megyes, T.; Besenyey, G. *Eur. J. Inorg. Chem.* **2008**, 1573.
- (94) Ferrer, M.; Mounir, M.; Rossell, O.; Ruiz, E.; Maestro, M. A. *Inorg. Chem.* **2003**, *42*, 5890.
- (95) Ferrer, M.; Gutiérrez, A.; Mounir, M.; Rossell, O.; Ruiz, E.; Rang, A.; Engeser, M. *Inorg. Chem.* **2007**, *46*, 3395.
- (96) Ferrer, M.; Pedrosa, A.; Rodríguez, L.; Rossell, O.; Vilaseca, M. *Inorg. Chem.* **2010**, *49*, 9438.
- (97) Sautter, A.; Schmid, D. G.; Jung, G.; Würthner, F. *J. Am. Chem. Soc.* **2001**, *123*, 5254.
- (98) You, C.-C.; Würthner, F. *J. Am. Chem. Soc.* **2003**, *125*, 9716.
- (99) Würthner, F.; Sautter, A. *Org. Biol. Chem.* **2003**, *1*, 240.
- (100) Schweiger, M.; Seidel, S. R.; Arif, A. M.; Stang, P. J. *Inorg. Chem.* **2002**, *41*, 2556.
- (101) Yamamoto, T.; Arif, A. M.; Stang, P. J. *J. Am. Chem. Soc.* **2003**, *125*, 12309.
- (102) Yu, S.-Y.; Huang, H.-P.; Li, S.-H.; Jiao, Q.; Li, Y.-Z.; Wu, B.; Sei, Y.; Yamaguchi, K.; Pan, Y.-J.; Ma, H.-W. *Inorg. Chem.* **2005**, *44*, 9471.
- (103) Sun, Q.-F.; Wong, K. M.-C.; Liu, L.-X.; Huang, H.-P.; Yu, S.-Y.; Yam, V. W.-W.; Li, Y.-Z.; Pan, Y.-J.; Yu, K.-C. *Inorg. Chem.* **2008**, *47*, 2142.
- (104) Kraus, T.; Buděšínský, M.; Cvačka, J.; Sauvage, J.-P. *Angew. Chem., Int. Ed.* **2006**, *45*, 258.
- (105) Voignier, J.; Frey, J.; Kraus, T.; Buděšínský, M.; Cvačka, J.; Heitz, V.; Sauvage, J.-P. *Chem.—Eur. J.* **2011**, *17*, 5404.
- (106) Champin, B.; Sartor, V.; Sauvage, J.-P. *New J. Chem.* **2008**, *32*, 1048.



- (107) Thanasekaran, P.; Liao, R.-T.; Liu, Y.-H.; Rajendran, T.; Rajagopal, S.; Liu, K.-L. *Coord. Chem. Rev.* **2005**, *249*, 1085.
- (108) Slone, R. V.; Benkstein, K. D.; Bélanger, S.; Hupp, J. T.; Guzei, I. A.; Rheingold, A. L. *Coord. Chem. Rev.* **1998**, *171*, 221.
- (109) Kuehl, C. J.; Huang, S. D.; Stang, P. J. *J. Am. Chem. Soc.* **2001**, *123*, 9634.
- (110) Kaim, W.; Schwederski, B.; Dogan, A.; Fiedler, J.; Kuehl, C. J.; Stang, P. J. *Inorg. Chem.* **2002**, *41*, 4025.
- (111) Resendiz, M. J. E.; Noveron, J. C.; Disteldorf, H.; Fischer, S.; Stang, P. J. *Org. Lett.* **2004**, *6*, 651.
- (112) Ghosh, S.; Mukherjee, P. S. *Dalton Trans.* **2007**, 2542.
- (113) Addicott, C.; Oesterling, I.; Yamamoto, T.; Müllen, K.; Stang, P. J. *J. Org. Chem.* **2005**, *70*, 797.
- (114) Ghosh, S.; Chakrabarty, R.; Mukherjee, P. S. *Inorg. Chem.* **2009**, *48*, 549.
- (115) Kim, D.; Paek, J. H.; Jun, M.-J.; Lee, J. Y.; Kang, S. O.; Ko, J. *Inorg. Chem.* **2005**, *44*, 7886.
- (116) Sommer, R. D.; Rheingold, A. L.; Goshe, A. J.; Bosnich, B. *J. Am. Chem. Soc.* **2001**, *123*, 3940.
- (117) Benkstein, K. D.; Hupp, J. T.; Stern, C. L. *J. Am. Chem. Soc.* **1998**, *120*, 12982.
- (118) Benkstein, K. D.; Stern, C. L.; Splan, K. E.; Johnson, R. C.; Walters, K. A.; Vanhelmont, F. W. M.; Hupp, J. T. *Eur. J. Inorg. Chem.* **2002**, 2818.
- (119) Yan, H.; Süß-Fink, G.; Neels, A.; Stoeckli-Evans, H. J. *Chem. Soc., Dalton Trans.* **1997**, 4345.
- (120) Suzuki, H.; Tajima, N.; Tatsumi, K.; Yamamoto, Y. *Chem. Commun. (Cambridge, U. K.)* **2000**, 1801.
- (121) Review:Therrien, B. *Eur. J. Inorg. Chem.* **2009**, 2445.
- (122) (a) Mattsson, J.; Govindaswamy, P.; Renfrew, A. K.; Dyson, P. J.; Štěpnička, P.; Süß-Fink, G.; Therrien, B. *Organometallics* **2009**, *28*, 4350. (b) Barry, N. P. E.; Edfeld, F.; Therrien, B. *Dalton Trans.* **2011**, *40*, 7172.
- (123) Barry, N. P. E.; Furrer, J.; Freudenreich, J.; Süß-Fink, G.; Therrien, B. *Eur. J. Inorg. Chem.* **2010**, 725.
- (124) Barry, N. P. E.; Furrer, J.; Therrien, B. *Helv. Chim. Acta* **2010**, *93*, 1313.
- (125) Han, Y.-F.; Jia, W.-G.; Lin, Y.-J.; Jin, G.-X. *Organometallics* **2008**, *27*, 5002.
- (126) Han, Y.-F.; Fei, Y.; Jin, G.-X. *Dalton Trans.* **2010**, *39*, 3976.
- (127) Han, Y.-F.; Lin, Y.-J.; Jia, W.-G.; Wang, G.-L.; Jin, G.-X. *Chem. Commun. (Cambridge, U. K.)* **2008**, 1807.
- (128) Barry, N. P. E.; Therrien, B. *Inorg. Chem. Commun.* **2009**, *12*, 465.
- (129) Yu, W.-B.; Han, Y.-F.; Lin, Y.-J.; Jin, G.-X. *Chem.—Eur. J.* **2011**, *17*, 1863.
- (130) Yu, W.-B.; Han, Y.-F.; Lin, Y.-J.; Jin, G.-X. *Organometallics* **2011**, *30*, 3090.
- (131) Beauchamp, D. A.; Leob, S. J. *Chem. Commun. (Cambridge, U. K.)* **2002**, 2484.
- (132) Yue, N. L. S.; Jennings, M. C.; Puddephatt, R. J. *Inorg. Chem.* **2005**, *44*, 1125.
- (133) Lindner, E.; Zong, R.; Eichele, K.; Weisser, U.; Ströbele, M. *Eur. J. Inorg. Chem.* **2003**, 705.
- (134) Stang, P. J.; Persky, N. E.; Manna, J. J. *Am. Chem. Soc.* **1997**, *119*, 4777.
- (135) Leininger, S.; Schmitz, M.; Stang, P. J. *Org. Lett.* **1999**, *1*, 1921.
- (136) Zhao, L.; Ghosh, K.; Zheng, Y.; Lyndon, M. M.; Williams, T. I.; Stang, P. J. *Inorg. Chem.* **2009**, *48*, 5590.
- (137) Hasenknopf, B.; Lehn, J.-M.; Kneisel, B. O.; Baum, G.; Fenske, D. *Angew. Chem., Int. Ed. Engl.* **1996**, *35*, 1838.
- (138) Hasenknopf, B.; Lehn, J.-M.; Boumediene, N.; Dupont-Gervais, A.; Van Dorsselaer, A.; Kneisel, B.; Fenske, D. *J. Am. Chem. Soc.* **1997**, *119*, 10956.
- (139) Campos-Fernández, C. S.; Clérac, R.; Koomen, J. M.; Russell, D. H.; Dunbar, K. R. *J. Am. Chem. Soc.* **2001**, *123*, 773.
- (140) Campos-Fernández, C. S.; Schottel, B. L.; Chifotides, H. T.; Bera, J. K.; Basca, J.; Koomen, J. M.; Russell, D. H.; Dunbar, K. R. *J. Am. Chem. Soc.* **2005**, *127*, 12909.
- (141) Mamula, O.; von Zelewsky, A.; Bernardinelli, G. *Angew. Chem., Int. Ed.* **1998**, *37*, 289.
- (142) Baxter, P. N. W.; Khoury, R. G.; Lehn, J.-M.; Baum, G.; Fenske, D. *Chem.—Eur. J.* **2000**, *6*, 4140.
- (143) Coronado, E.; Galan-Mascaros, J. R.; Gaviña, P.; Martí-Gastaldo, C.; Romero, F. M.; Tatay, S. *Inorg. Chem.* **2008**, *47*, 5197.
- (144) Review:Eryazici, I.; Moorefield, C. N.; Newkome, G. R. *Chem. Rev.* **2008**, *108*, 1834.
- (145) Newkome, G. R.; Cho, T. J.; Moorefield, C. N.; Baker, G. R.; Cush, R.; Russo, P. S. *Angew. Chem., Int. Ed.* **1999**, *38*, 3717.
- (146) Newkome, G. R.; Cho, T. J.; Moorefield, C. N.; Cush, R.; Russo, P. S.; Godínez, L. A.; Saunders, M. J.; Mohapatra, P. *Chem.—Eur. J.* **2002**, *8*, 2946.
- (147) Newkome, G. R.; Cho, T. J.; Moorefield, C. N.; Mohapatra, P. P.; Godínez, L. A. *Chem.—Eur. J.* **2004**, *10*, 1493.
- (148) Perera, S.; Li, X.; Guo, M.; Wesdemiotis, C.; Moorefield, C. N.; Newkome, G. R. *Chem. Commun. (Cambridge, U. K.)* **2011**, *47*, 4658.
- (149) Hwang, S.-H.; Wang, P.; Moorefield, C. N.; Godínez, L. A.; Manríquez, J.; Bustos, E.; Newkome, G. R. *Chem. Commun. (Cambridge, U. K.)* **2005**, 4672.
- (150) Wang, G.-L.; Lin, Y.-J.; Jin, G.-X. *Chem.—Eur. J.* **2011**, *17*, 5578.
- (151) Farrell, J. R.; Mirkin, C. A.; Guzei, I. A.; Liable-Sands, L. M.; Rheingold, A. L. *Angew. Chem., Int. Ed.* **1998**, *37*, 465.
- (152) Liu, X.; Eisenberg, A. H.; Stern, C. L.; Mirkin, C. A. *Inorg. Chem.* **2001**, *40*, 2940.
- (153) Dixon, F. M.; Eisenberg, A. H.; Farrell, J. R.; Mirkin, C. A.; Liable-Sands, L. M.; Rheingold, A. L. *Inorg. Chem.* **2000**, *39*, 3432.
- (154) Masar, M. S., III; Ovchinnikov, M. V.; Mirkin, C. A.; Zakharov, L. N.; Rheingold, A. L. *Inorg. Chem.* **2003**, *42*, 6851.
- (155) Eisenberg, A. H.; Dixon, F. M.; Mirkin, C. A.; Stern, C. L.; Incarvito, C. D.; Rheingold, A. L. *Organometallics* **2001**, *20*, 2052.
- (156) Masar, M. S., III; Mirkin, C. A.; Stern, C. L.; Zakharov, L. N.; Rheingold, A. L. *Inorg. Chem.* **2004**, *43*, 4693.
- (157) Eisenberg, A. H.; Ovchinnikov, M. V.; Mirkin, C. A. *J. Am. Chem. Soc.* **2003**, *125*, 2836.
- (158) Das, N.; Mukherjee, P. S.; Arif, A. M.; Stang, P. J. *J. Am. Chem. Soc.* **2003**, *125*, 13950.
- (159) Mukherjee, P. S.; Das, N.; Kryschenko, Y. K.; Arif, A. M.; Stang, P. J. *J. Am. Chem. Soc.* **2004**, *126*, 2464.
- (160) Das, N.; Ghosh, A.; Arif, A. M.; Stang, P. J. *Inorg. Chem.* **2005**, *44*, 7130.
- (161) Bar, A. K.; Gole, B.; Ghosh, S.; Mukherjee, P. S. *Dalton Trans.* **2009**, 6701.
- (162) Das, N.; Arif, A. M.; Stang, P. J.; Sieger, M.; Sarkar, B.; Kaim, W.; Fiedler, J. *Inorg. Chem.* **2005**, *44*, 5798.
- (163) Severin, K. *Coord. Chem. Rev.* **2003**, *245*, 3.
- (164) Piotrowski, H.; Polborn, K.; Hilt, G.; Severin, K. *J. Am. Chem. Soc.* **2001**, *123*, 2699.
- (165) Lehaire, M.-L.; Scopelliti, R.; Hardeis, L.; Polborn, K.; Mayer, P.; Severin, K. *Inorg. Chem.* **2004**, *43*, 1609.
- (166) Mirtschin, S.; Krasniqi, E.; Scopelliti, R.; Severin, K. *Inorg. Chem.* **2008**, *47*, 6375.
- (167) Brasey, T.; Scopelliti, R.; Severin, K. *Inorg. Chem.* **2005**, *44*, 160.
- (168) Review:Bray, D. J.; Clegg, J. K.; Lindoy, L. F.; Schilter, D. *Adv. Inorg. Chem.* **2006**, *59*, 1.
- (169) Clegg, J. K.; Lindoy, L. F.; McMurtrie, J. C.; Schilter, D. *Dalton Trans.* **2005**, 857.
- (170) Clegg, J. K.; Bray, D. J.; Gloe, K.; Gloe, K.; Hayter, M. J.; Jolliffe, K. A.; Lawrance, G. A.; Meehan, G. V.; McMurtrie, J. C.; Lindoy, L. F.; Wenzel, M. *Dalton Trans.* **2007**, 1719.
- (171) Clegg, J. K.; Lindoy, L. F.; Moubarak, B.; Murray, K. S.; McMurtrie, J. C. *Dalton Trans.* **2004**, 2417.
- (172) Clegg, J. K.; Bray, D. J.; Gloe, K.; Gloe, K.; Jolliffe, K. A.; Lawrance, G. A.; Lindoy, L. F.; Meehan, G. V.; Wenzel, M. *Dalton Trans.* **2008**, 1331.



- (173) Clegg, J. K.; Lindoy, L. F.; McMurtrie, J. C.; Schilter, D. *Dalton Trans.* **2006**, 3114.
- (174) Clegg, J. K.; Gloe, K.; Hayter, M. J.; Kataeva, O.; Lindoy, L. F.; Moubarak, B.; McMurtrie, J. C.; Murray, K. S.; Schilter, D. *Dalton Trans.* **2006**, 3977.
- (175) Clegg, J. K.; Iremonger, S. S.; Hayter, M. J.; Southon, P. D.; Macquart, R. B.; Duriska, M. B.; Jensen, P.; Turner, P.; Jolliffe, K. A.; Kepert, C. J.; Meehan, G. V.; Lindoy, L. F. *Angew. Chem., Int. Ed.* **2010**, *49*, 1075.
- (176) Dinolfo, P. H.; Williams, M. E.; Stern, C. L.; Hupp, J. T. *J. Am. Chem. Soc.* **2004**, *126*, 12989.
- (177) (a) Benkstein, K. D.; Hupp, J. L.; Stern, C. L. *Angew. Chem., Int. Ed.* **2000**, *39*, 2891. (b) Benkstein, K. D.; Hupp, J. T. *Mol. Cryst. Liq. Cryst.* **2000**, *342*, 151.
- (178) Manimaran, B.; Rajendran, T.; Lu, Y.-L.; Lee, G.-H.; Peng, S.-M.; Lu, K.-L. *J. Chem. Soc., Dalton Trans.* **2001**, 515.
- (179) Gupta, D.; Rajakannu, P.; Shankar, B.; Shanmugam, R.; Hussain, F.; Sarkar, B.; Sathiyendiran, M. *Dalton Trans.* **2011**, *40*, 5433.
- (180) Benkstein, K. D.; Hupp, J. T.; Stern, C. L. *Inorg. Chem.* **1998**, *37*, 5404.
- (181) Woessner, S. M.; Helms, J. B.; Shen, Y.; Sullivan, B. P. *Inorg. Chem.* **1998**, *37*, 5406.
- (182) Rajendran, T.; Manimaran, B.; Liao, R.-T.; Lin, R.-J.; Thanasekaran, P.; Lee, G.-H.; Peng, S.-M.; Liu, Y.-H.; Chang, I.-J.; Rajagopal, S.; Lu, K.-L. *Inorg. Chem.* **2003**, *42*, 6388.
- (183) Rajendran, T.; Manimaran, B.; Lee, F.-Y.; Lee, G.-H.; Peng, S.-M.; Wang, C. M.; Lu, K.-L. *Inorg. Chem.* **2000**, *39*, 2016.
- (184) Sun, S.-S.; Lees, A. J. *J. Am. Chem. Soc.* **2000**, *122*, 8956.
- (185) Cotton, F. A.; Daniels, L. M.; Lin, C.; Murillo, C. A. *J. Am. Chem. Soc.* **1999**, *121*, 4538.
- (186) Cotton, F. A.; Lin, C.; Murillo, C. A. *Inorg. Chem.* **2001**, *40*, 478.
- (187) Cotton, F. A.; Daniels, L. M.; Lin, C.; Murillo, C. A.; Yu, S.-Y. *J. Chem. Soc., Dalton Trans.* **2001**, 502.
- (188) Angaridis, P.; Berry, J. F.; Cotton, F. A.; Murillo, C. A.; Wang, X. *J. Am. Chem. Soc.* **2003**, *125*, 10327.
- (189) Bonar-Law, R. P.; McGrath, T. D.; Singh, N.; Bickley, J. F.; Steiner, A. *Chem. Commun. (Cambridge, U. K.)* **1999**, 2457.
- (190) Bickley, J. F.; Bonar-Law, R. P.; Femoni, C.; MacLean, E. J.; Steiner, A.; Teat, S. J. *J. Chem. Soc., Dalton Trans.* **2000**, 4025.
- (191) Schiavo, S. L.; Pocsfalvi, G.; Serroni, S.; Cardiano, P.; Piraino, P. *Eur. J. Inorg. Chem.* **2000**, 1371.
- (192) Cotton, F. A.; Lin, C.; Murillo, C. A. *Inorg. Chem.* **2001**, *40*, 575.
- (193) Cotton, F. A.; Lin, C.; Murillo, C. A. *Inorg. Chem.* **2001**, *40*, 472.
- (194) Cotton, F. A.; Jin, J.-Y.; Li, Z.; Liu, C. Y.; Murillo, C. A. *Dalton Trans.* **2007**, 2328.
- (195) Bera, J. K.; Angaridis, P.; Cotton, F. A.; Petrukhina, M. A.; Fanwick, P. E.; Walton, R. A. *J. Am. Chem. Soc.* **2001**, *123*, 1515.
- (196) Cotton, F. A.; Liu, C. Y.; Murillo, C. A.; Wang, X. *Inorg. Chem.* **2006**, *45*, 2619.
- (197) Cotton, F. A.; Murillo, C. A.; Yu, R. *Dalton Trans.* **2006**, 3900.
- (198) Chisholm, M. H.; Patmore, N. J.; Reed, C. R.; Singh, N. *Inorg. Chem.* **2010**, *49*, 7116.
- (199) Khoshbin, M. S.; Ovchinnikov, M. V.; Mirkin, C. A.; Zakharov, L. N.; Rheingold, A. L. *Inorg. Chem.* **2005**, *44*, 496.
- (200) Reviews: (a) Lee, S. J.; Lin, W. *Acc. Chem. Res.* **2008**, *41*, 521. (b) Leigh, D. A.; Pérez, E. M. *Top. Curr. Chem.* **2006**, *265*, 185. (c) Amabilino, D. B.; Veciana, J. *Top. Curr. Chem.* **2006**, *265*, 253. (d) Mamula, O.; von Zelewsky, A. *Coord. Chem. Rev.* **2003**, *242*, 87.
- (201) Enders, D.; Jaeger, K.-E., Eds. *Asymmetric Synthesis with Chemical and Biological Methods*; Wiley-VCH: New York, 2007.
- (202) Stang, P. J.; Olenyuk, B.; Arif, A. M. *Organometallics* **1995**, *14*, 5281.
- (203) Olenyuk, B.; Whiteford, J. A.; Stang, P. J. *J. Am. Chem. Soc.* **1996**, *118*, 8221.
- (204) Stang, P. J.; Olenyuk, B. *Angew. Chem., Int. Ed. Engl.* **1996**, *35*, 732.
- (205) Fan, J.; Whiteford, J. A.; Olenyuk, B.; Levin, M. D.; Stang, P. J.; Fleischer, E. B. *J. Am. Chem. Soc.* **1999**, *121*, 2741.
- (206) Heo, J.; Jeon, Y.-M.; Mirkin, C. A. *J. Am. Chem. Soc.* **2007**, *129*, 7712.
- (207) Lee, S. J.; Lin, W. *J. Am. Chem. Soc.* **2002**, *124*, 4554.
- (208) Lee, S. J.; Kim, J. S.; Lin, W. *Inorg. Chem.* **2004**, *43*, 6579.
- (209) Lee, S. J.; Hu, A.; Lin, W. *J. Am. Chem. Soc.* **2002**, *124*, 12948.
- (210) Zhang, L.; Niu, Y.-H.; Jen, A. K.-Y.; Lin, W. *Chem. Commun. (Cambridge, U. K.)* **2005**, 1002.
- (211) Lee, S. J.; Luman, C. R.; Castellano, F. N.; Lin, W. *Chem. Commun. (Cambridge, U. K.)* **2003**, 2124.
- (212) Jiang, H.; Lin, W. *J. Am. Chem. Soc.* **2003**, *125*, 8084.
- (213) Jiang, H.; Hu, A.; Lin, W. *Chem. Commun. (Cambridge, U. K.)* **2003**, 96.
- (214) Hua, J.; Lin, W. *Org. Lett.* **2004**, *6*, 861.
- (215) Jiang, H.; Lin, W. *J. Am. Chem. Soc.* **2004**, *126*, 7426.
- (216) Jeong, K. S.; Kim, S. Y.; Shin, U.-S.; Kogej, M.; Hai, N. T. M.; Broekmann, P.; Jeong, N.; Kirchner, B.; Reiher, M.; Schalley, C. A. *J. Am. Chem. Soc.* **2005**, *127*, 17672.
- (217) Jeong, K. S.; Kim, S. Y.; Oh, Y.; Min, D. W.; Kim, J.; Jeong, N. *CrystEngComm* **2007**, *9*, 273.
- (218) Wisser, B.; Chamayou, A.-C.; Miller, R.; Scherer, W.; Janiak, C. *CrystEngComm* **2008**, *10*, 461.
- (219) Rang, A.; Engeser, M.; Maier, N. M.; Nieger, M.; Lindner, W.; Schalley, C. A. *Chem.—Eur. J.* **2008**, *14*, 3855.
- (220) Rang, A.; Nieger, M.; Engeser, M.; Lützen, A.; Schalley, C. A. *Chem. Commun. (Cambridge, U. K.)* **2008**, 4789.
- (221) Das, N.; Ghosh, A.; Singh, O. M.; Stang, P. J. *Org. Lett.* **2006**, *8*, 1701.
- (222) Yeh, R. M.; Raymond, K. N. *Inorg. Chem.* **2006**, *45*, 1130.
- (223) Yamanari, K.; Fukuda, I.; Kawamoto, T.; Kushi, Y.; Fuyuhiko, A.; Kubota, N.; Fukuo, T.; Arakawa, R. *Inorg. Chem.* **1998**, *37*, 5611.
- (224) Zhang, Y.; Wang, S.; Enright, G. D.; Breeze, S. R. *J. Am. Chem. Soc.* **1998**, *120*, 9398.
- (225) Liu, C.-M.; Nordlander, E.; Schmech, D.; Shoemaker, R.; Pierpont, C. G. *Inorg. Chem.* **2004**, *43*, 2114.
- (226) Cotton, F. A.; Murillo, C. A. *Eur. J. Inorg. Chem.* **2006**, 4209.
- (227) Cotton, F. A.; Murillo, C. A.; Wang, X.; Yu, R. *Inorg. Chem.* **2004**, *43*, 8394.
- (228) Cotton, F. A.; Murillo, C. A.; Stiriba, S.-E.; Wang, X.; Yu, R. *Inorg. Chem.* **2005**, *44*, 8223.
- (229) Cotton, F. A.; Murillo, C. A.; Yu, R. *Inorg. Chem.* **2005**, *44*, 8211.
- (230) Reviews: (a) Kumar, A.; Sun, S.-S.; Lees, A. J. *Coord. Chem. Rev.* **2008**, *252*, 922. (b) Cooke, M. W.; Chartrand, D.; Hanan, G. S. *Coord. Chem. Rev.* **2008**, *252*, 903. (c) Amijs, C. H. M.; van Klink, G. P. M.; Van Koten, G. *Dalton Trans.* **2006**, 308. (d) Lützen, A. *Angew. Chem., Int. Ed.* **2005**, *44*, 1000.
- (231) Northrop, B. H.; Yang, H.-B.; Stang, P. J. *Chem. Commun. (Cambridge, U. K.)* **2008**, 5896.
- (232) Chi, K.-W.; Addicot, C.; Stang, P. J. *J. Org. Chem.* **2004**, *69*, 2910.
- (233) Huang, F.; Yang, H.-B.; Das, N.; Maran, U.; Arif, A. M.; Gibson, H. W.; Stang, P. J. *J. Org. Chem.* **2006**, *71*, 6623.
- (234) Pirondini, L.; Dalcanele, E. In *Modern Supramolecular Chemistry: Strategies for Macrocyclic Synthesis*; Diederich, F., Stang, P. J., Tykwinski, R. R., Eds.; Wiley-VCH: Weinheim, Germany, 2008; p 233.
- (235) Menozzi, E.; Busi, M.; Massera, C.; Ugozzoli, F.; Zuccaccia, D.; Macchioni, A.; Dalcanele, E. *J. Org. Chem.* **2006**, *71*, 2617.
- (236) Jude, H.; Sinclair, D. J.; Das, N.; Sherburn, M. S.; Stang, P. J. *J. Org. Chem.* **2006**, *71*, 4155.
- (237) Jude, H.; Disteldorf, H.; Fischer, S.; Wedge, T.; Hawkridge, A. M.; Arif, A. M.; Hawthorne, M. F.; Muddiman, D. C.; Stang, P. J. *J. Am. Chem. Soc.* **2005**, *127*, 12131.
- (238) Das, N.; Stang, P. J.; Arif, A. M.; Campana, C. F. *J. Org. Chem.* **2005**, *70*, 10440.
- (239) Northrop, B. H.; Glöckner, A.; Stang, P. J. *J. Org. Chem.* **2008**, *73*, 1787.

- (240) Thanasekaran, P.; Wu, J.-Y.; Manimaran, B.; Rajendran, T.; Chang, I.-J.; Rajagopal, S.; Lee, G.-H.; Peng, S.-M.; Lu, K.-L. *J. Phys. Chem. A* **2007**, *111*, 10953.
- (241) You, C.-C.; Hippus, C.; Grüne, M.; Würthner, F. *Chem.—Eur. J.* **2006**, *12*, 7510.
- (242) Yang, H.-B.; Ghosh, K.; Northrop, B. H.; Zheng, Y.-R.; Lyndon, M. M.; Muddiman, D. C.; Stang, P. J. *J. Am. Chem. Soc.* **2007**, *129*, 14187.
- (243) Ghosh, K.; Yang, H.-B.; Northrop, B. H.; Lyndon, M. M.; Zheng, Y.-R.; Muddiman, D. C.; Stang, P. J. *J. Am. Chem. Soc.* **2008**, *130*, 5320.
- (244) Reviews: (a) Lee, C. C.; MacKay, J. A.; Fréchet, J. M. J.; Szoka, F. C. *Nat. Biotechnol.* **2005**, *23*, 1517. (b) Boas, U.; Heegaard, P. M. H. *Chem. Soc. Rev.* **2004**, *33*, 43.
- (245) Reviews: (a) Méry, D.; Astruc, D. *Coord. Chem. Rev.* **2006**, *250*, 1965. (b) Berger, A.; Gebbink, R. J. M. K.; van Koten, G. *Top. Organomet. Chem.* **2006**, *20*, 1. (c) Ribaudo, F.; van Leeuwen, P. W. N. M.; Reek, J. N. H. *Top. Organomet. Chem.* **2006**, *20*, 39. (d) Chandler, B. D.; Gilbertson, J. D. *Top. Organomet. Chem.* **2006**, *20*, 97. (e) Hajji, C.; Haag, R. *Top. Organomet. Chem.* **2006**, *20*, 149. (f) van Heerbeek, R.; Kamer, P. C. J.; van Leeuwen, P. W. N. M.; Reek, J. N. H. *Chem. Rev.* **2002**, *102*, 3717. (g) Grayson, S. M.; Fréchet, J. M. J. *Chem. Rev.* **2001**, *101*, 3819.
- (246) Reviews: (a) Astruc, D.; Daniel, M.-C.; Ruiz, J. *Top. Organomet. Chem.* **2006**, *20*, 121. (b) Venturi, M.; Serroni, S.; Juris, A.; Campagna, S.; Balzani, V. *Top. Curr. Chem.* **1998**, *197*, 193. (c) Balzani, V.; Campagna, S.; Denti, G.; Juris, A.; Serroni, S.; Venturi, M. *Acc. Chem. Res.* **1998**, *31*, 26.
- (247) Yang, H.-B.; Das, N.; Huang, F.; Hawkridge, A. M.; Muddiman, D. C.; Stang, P. J. *J. Am. Chem. Soc.* **2006**, *128*, 10014.
- (248) Yang, H.-B.; Hawkridge, A. M.; Huang, S. D.; Das, N.; Bunge, S. D.; Muddiman, D. C.; Stang, P. J. *J. Am. Chem. Soc.* **2007**, *129*, 2120.
- (249) Yang, H.-B.; Northrop, B. H.; Zheng, Y.-R.; Ghosh, K.; Lyndon, M. M.; Muddiman, D. C.; Stang, P. J. *J. Org. Chem.* **2009**, *74*, 3524.
- (250) Yang, H.-B.; Northrop, B. H.; Zheng, Y.-R.; Ghosh, K.; Stang, P. J. *J. Org. Chem.* **2009**, *74*, 7067.
- (251) Baytekin, H. T.; Sahre, M.; Rang, A.; Engeser, M.; Schulz, A.; Schalley, C. A. *Small* **2008**, *4*, 1823.
- (252) Yang, H.-B.; Ghosh, K.; Zhao, Y.; Northrop, B. H.; Lyndon, M. M.; Muddiman, D. C.; White, H. S.; Stang, P. J. *J. Am. Chem. Soc.* **2008**, *130*, 839.
- (253) Ghosh, K.; Zhao, Y.; Yang, H.-B.; Northrop, B. H.; White, H. S.; Stang, P. J. *J. Org. Chem.* **2008**, *73*, 8553.
- (254) Ghosh, K.; Hu, J.; Yang, H. B.; Northrop, B. H.; White, H. S.; Stang, P. J. *J. Org. Chem.* **2009**, *74*, 4828.
- (255) Zhao, G.-Z.; Chen, L.-J.; Wang, C.-H.; Yang, H.-B.; Ghosh, K.; Zheng, Y.-R.; Lyndon, M. M.; Muddiman, D. C.; Stang, P. J. *Organometallics* **2010**, *29*, 6137.
- (256) Xu, X.-D.; Yang, H.-B.; Zheng, Y.-R.; Ghosh, K.; Lyndon, M. M.; Muddiman, D. C.; Stang, P. J. *J. Org. Chem.* **2010**, *75*, 7373.
- (257) Chan, Y.-T.; Moorefield, C. N.; Soler, M.; Newkome, G. R. *Chem.—Eur. J.* **2010**, *16*, 1768.
- (258) Zhao, L.; Ghosh, K.; Zheng, Y.-R.; Stang, P. J. *J. Org. Chem.* **2009**, *74*, 8516.
- (259) Reviews: (a) Beletskaya, I.; Tyurin, V. S.; Tsivadze, A. Y.; Guillard, R.; Stern, C. *Chem. Rev.* **2009**, *109*, 1659. (b) Scandola, F.; Chiorboli, C.; Prodi, A.; Iengo, E.; Alessio, E. *Coord. Chem. Rev.* **2006**, *250*, 1471. (c) Rose, E.; Andrioletti, B.; Zrig, S.; Quelquejau-Ethève, M. *Chem. Soc. Rev.* **2005**, *34*, 573. (d) Iengo, E.; Zangrando, E.; Alessio, E. *Eur. J. Inorg. Chem.* **2003**, 2371.
- (260) Drain, C. M.; Lehn, J.-M. *J. Chem. Soc., Chem. Commun.* **1994**, 2313.
- (261) Iengo, E.; Milani, B.; Zangrando, E.; Geremia, S.; Alessio, E. *Angew. Chem., Int. Ed.* **2000**, *39*, 1096.
- (262) Iengo, E.; Zangrando, E.; Minatel, R.; Alessio, E. *J. Am. Chem. Soc.* **2002**, *124*, 1003.
- (263) Iengo, E.; Zangrando, E.; Bellini, M.; Alessio, E.; Prodi, A.; Chiorboli, C.; Scandola, F. *Inorg. Chem.* **2005**, *44*, 9752.
- (264) Iengo, E.; Scandola, F.; Alessio, E. *Struct. Bonding (Berlin, Ger.)* **2006**, *121*, 105.
- (265) Lee, S. J.; Hupp, J. T. *Coord. Chem. Rev.* **2006**, *250*, 1710.
- (266) Mines, G. A.; Tzeng, B.-C.; Stevenson, K. J.; Li, J.; Hupp, J. T. *Angew. Chem., Int. Ed.* **2002**, *41*, 154.
- (267) Chang, S. H.; Chung, K.-B.; Slone, R. V.; Hupp, J. T. *Synth. Met.* **2001**, *117*, 215.
- (268) Slone, R. V.; Hupp, J. T. *Inorg. Chem.* **1997**, *36*, 5422.
- (269) Czaplewski, K. F.; Hupp, J. T.; Snurr, R. Q. *Adv. Mater.* **2001**, *13*, 1895.
- (270) Splan, K. E.; Massari, A. M.; Hupp, J. T. *J. Phys. Chem. B* **2004**, *108*, 4111.
- (271) Martinson, A. B. F.; Massari, A. M.; Lee, S. J.; Gurney, R. W.; Splan, K. E.; Hupp, J. T.; Nguyen, S. T. *J. Electrochem. Soc.* **2006**, *153*, A527.
- (272) Maeda, C.; Kim, P.; Cho, S.; Park, J. K.; Lim, J. M.; Kim, D.; Vura-Weis, J.; Wasielewski, M. R.; Shinokubo, H.; Osuka, A. *Chem.—Eur. J.* **2010**, *16*, 5052.
- (273) Park, M.; Yoon, M.-C.; Yoon, Z. S.; Hori, T.; Peng, X.; Aratani, N.; Hotta, J.; Uji-i, H.; Sliwa, M.; Hofkens, J.; Osuka, A.; Kim, D. *J. Am. Chem. Soc.* **2007**, *129*, 3539.
- (274) Yang, J.; Park, M.; Yoon, Z. S.; Hori, T.; Peng, X.; Aratani, N.; Dedecker, P.; Hotta, J.; Uji-i, H.; Sliwa, M.; Hofkens, J.; Osuka, A.; Kim, D. *J. Am. Chem. Soc.* **2008**, *130*, 1879.
- (275) Splan, K. E.; Keefe, M. H.; Massari, A. M.; Walters, K. A.; Hupp, J. T. *Inorg. Chem.* **2002**, *41*, 619.
- (276) Jensen, R. A.; Kelley, R. F.; Lee, S. J.; Wasielewski, M. R.; Hupp, J. T.; Tiede, D. M. *Chem. Commun. (Cambridge, U. K.)* **2008**, 1886.
- (277) Reviews: (a) Haak, R. M.; Wezenberg, S. J.; Kleij, A. W. *Chem. Commun. (Cambridge, U. K.)* **2010**, *46*, 2713. (b) Gupta, K. C.; Sutar, A. K. *Coord. Chem. Rev.* **2008**, *252*, 1420. (c) McGarrigle, E. M.; Gilheany, D. G. *Chem. Rev.* **2005**, *105*, 1563. (d) Cozzi, P. G. *Chem. Soc. Rev.* **2004**, *33*, 410. (e) Larrow, J. F.; Jacobsen, E. N. *Top. Organomet. Chem.* **2004**, *6*, 123. (f) Katsuki, T. *Adv. Synth. Catal.* **2002**, *344*, 131.
- (278) Reviews: (a) Kleij, A. W. *Chem.—Eur. J.* **2008**, *14*, 10520. (b) Kleij, A. W. *Dalton Trans.* **2009**, 4635.
- (279) Wezenberg, S. J.; Kleij, A. W. *Angew. Chem., Int. Ed.* **2008**, *47*, 2354.
- (280) See for some examples: (a) Clever, G. H.; Sötl, Y.; Burks, H.; Spahl, W.; Carell, T. *Chem.—Eur. J.* **2006**, *12*, 8708. (b) Clever, G. H.; Polborn, K.; Carell, T. *Angew. Chem., Int. Ed.* **2005**, *44*, 7204. (c) Czaplewski, J. L.; Sheppard, T. L. *Chem. Commun. (Cambridge, U. K.)* **2004**, 2468. (d) Escudero-Adán, E. C.; Benet-Buchholz, J.; Kleij, A. W. *Inorg. Chem.* **2008**, *47*, 4256.
- (281) Sun, S.-S.; Stern, C. L.; Nguyen, S. T.; Hupp, J. T. *J. Am. Chem. Soc.* **2004**, *126*, 6314.
- (282) Splan, K. E.; Massari, A. M.; Morris, G. A.; Sun, S.-S.; Reina, E.; Nguyen, S. T.; Hupp, J. T. *Eur. J. Inorg. Chem.* **2003**, 2348.
- (283) Sun, S.-S.; Anspach, J. A.; Lees, A. J. *Inorg. Chem.* **2002**, *41*, 1862.
- (284) Kleij, A. W.; Kuil, M.; Tooke, D. M.; Lutz, M.; Spek, A. L.; Reek, J. N. H. *Chem.—Eur. J.* **2005**, *11*, 4743.
- (285) Wezenberg, S. J.; Escudero-Adán, E. C.; Benet-Buchholz, J.; Kleij, A. W. *Inorg. Chem.* **2008**, *47*, 2925.
- (286) Kleij, A. W.; Kuil, M.; Tooke, D. M.; Spek, A. L.; Reek, J. N. H. *Inorg. Chem.* **2007**, *46*, 5829.
- (287) Salassa, G.; Castilla, A. M.; Kleij, A. W. *Dalton Trans.* **2011**, *40*, 5236.
- (288) Maverick, A. W.; Buckingham, S. C.; Yao, Q.; Bradbury, J. R.; Stanley, G. G. *J. Am. Chem. Soc.* **1986**, *108*, 7430.
- (289) Maverick, A. W.; Klavetter, F. E. *Inorg. Chem.* **1984**, *23*, 4129.
- (290) Fujita, M.; Yazaki, J.; Ogura, K. *Tetrahedron Lett.* **1991**, *32*, 5589.
- (291) Fujita, M.; Nagao, S.; Iida, M.; Ogata, K.; Ogura, K. *J. Am. Chem. Soc.* **1993**, *115*, 1574.
- (292) Stang, P. J.; Cao, D. H.; Saito, S.; Arif, A. M. *J. Am. Chem. Soc.* **1995**, *117*, 6273.



- (293) Whiteford, J. A.; Stang, P. J.; Huang, S. D. *Inorg. Chem.* **1998**, *37*, 5595.
- (294) Chang, S.-Y.; Um, M.-C.; Uh, H.; Jang, H.-Y.; Jeong, K.-S. *Chem. Commun. (Cambridge, U. K.)* **2003**, 2026.
- (295) Jeong, K.-S.; Cho, Y. L.; Chang, S.-Y.; Park, T.-Y.; Song, J. U. *J. Org. Chem.* **1999**, *64*, 9459.
- (296) Chen, Y.-Q.; Wang, X.-Z.; Shao, X.-B.; Hou, J.-L.; Chen, X.-Z.; Jiang, X.-K.; Li, Z.-T. *Tetrahedron* **2004**, *60*, 10253.
- (297) Sato, H.; Tashiro, K.; Shinmori, H.; Osuka, A.; Murata, Y.; Komatsu, K.; Aida, T. *J. Am. Chem. Soc.* **2005**, *127*, 13086.
- (298) (a) Vajpayee, V.; Kim, H.; Mishra, A.; Mukherjee, P. S.; Stang, P. J.; Lee, M. H.; Kim, H. K.; Chi, K.-W. *Dalton Trans.* **2011**, 40, 3112. (b) Vajpayee, V.; Song, Y. H.; Lee, M. H.; Kim, H.; Wang, M.; Stang, P. J.; Chi, K.-W. *Chem.—Eur. J.* **2011**, *17*, 7837.
- (299) Heo, J.; Mirkin, C. A. *Angew. Chem., Int. Ed.* **2006**, *45*, 941.
- (300) Grote, Z.; Lehaire, M.-L.; Scopelliti, R.; Severin, K. *J. Am. Chem. Soc.* **2003**, *125*, 13638.
- (301) Grote, Z.; Scopelliti, R.; Severin, K. *J. Am. Chem. Soc.* **2004**, *126*, 16959.
- (302) Piotrowski, H.; Hilt, G.; Schulz, A.; Mayer, P.; Polborn, K.; Severin, K. *Chem.—Eur. J.* **2001**, *7*, 3196.
- (303) Lehaire, M.-L.; Scopelliti, R.; Piotrowski, H.; Severin, K. *Angew. Chem., Int. Ed.* **2002**, *41*, 1419.
- (304) Rochat, S.; Grote, Z.; Severin, K. *Org. Biomol. Chem.* **2009**, *7*, 1147.
- (305) Qin, Z.; Jennings, M. C.; Puddephatt, R. J. *Inorg. Chem.* **2002**, *41*, 3967.
- (306) Yue, N.; Qin, Z.; Jennings, M. C.; Eisler, D. J.; Puddephatt, R. J. *Inorg. Chem. Commun.* **2003**, *6*, 1269.
- (307) Yue, N. L. S.; Eisler, D. J.; Jennings, M. C.; Puddephatt, R. J. *Inorg. Chem. Commun.* **2005**, *8*, 31.
- (308) Sathiyendiran, M.; Liao, R.-T.; Thanasekaran, P.; Luo, T.-T.; Venkataramanan, N. S.; Lee, G.-H.; Peng, S.-M.; Lu, K.-L. *Inorg. Chem.* **2006**, *45*, 10052.
- (309) Waiter, C. J.; Anderson, H. L.; Sanders, J. K. M. *J. Chem. Soc., Chem. Commun.* **1993**, 458.
- (310) Mackay, L. G.; Wylie, R. S.; Sanders, J. K. M. *J. Am. Chem. Soc.* **1994**, *116*, 3141.
- (311) Merlau, M. L.; del Pilar Mejia, M.; Nguyen, S. T.; Hupp, J. T. *Angew. Chem., Int. Ed.* **2001**, *40*, 4239.
- (312) Fritsky, I. O.; Ott, R.; Krämer, R. *Angew. Chem., Int. Ed.* **2000**, *39*, 3255.
- (313) Fritsky, I. O.; Ott, R.; Pritzkow, H.; Krämer, R. *Chem.—Eur. J.* **2001**, *7*, 1221.
- (314) Gianneschi, N. C.; Bertin, P. A.; Nguyen, S. T.; Mirkin, C. A.; Zakharov, L. N.; Rheingold, A. L. *J. Am. Chem. Soc.* **2003**, *125*, 10508.
- (315) (a) Gianneschi, N. C.; Nguyen, S. T.; Mirkin, C. A. *J. Am. Chem. Soc.* **2005**, *127*, 1644. (b) Masar, M. S., III; Gianneschi, N. C.; Oliveri, C. G.; Stern, C. L.; Nguyen, S. T.; Mirkin, C. A. *J. Am. Chem. Soc.* **2007**, *129*, 10149.
- (316) Yoon, H. J.; Kuwabara, J.; Kim, J.-H.; Mirkin, C. A. *Science* **2010**, *330*, 66.
- (317) Oliveri, C. G.; Gianneschi, N. C.; Nguyen, S. T.; Mirkin, C. A.; Stern, C. L.; Wawrzak, Z.; Pink, M. *J. Am. Chem. Soc.* **2006**, *128*, 16286.
- (318) Oliveri, C. G.; Heo, J.; Nguyen, S. T.; Mirkin, C. A.; Wawrzak, Z. *Inorg. Chem.* **2007**, *46*, 7716.
- (319) Yoon, H. J.; Heo, J.; Mirkin, C. A. *J. Am. Chem. Soc.* **2007**, *129*, 14182.
- (320) Gianneschi, N. C.; Cho, S.-H.; Nguyen, S. T.; Mirkin, C. A. *Angew. Chem., Int. Ed.* **2004**, *43*, 5503.
- (321) Müller, P.; Baud, C.; Ené, D.; Motallebi, S.; Doyle, M. P.; Brandes, B. D.; Dyatkin, A. B.; See, M. M. *Helv. Chim. Acta* **1995**, *78*, 459.
- (322) Reviews: (a) Franceschin, M. *Eur. J. Org. Chem.* **2009**, 2225. (b) Ou, T.-M.; Lu, Y.-J.; Tan, J.-H.; Huang, Z.-S.; Wong, K.-Y.; Gu, L.-Q. *ChemMedChem* **2008**, *3*, 690. (c) Neidle, S.; Read, M. A. *Biopolymers* **2001**, *56*, 195. (d) Shafer, R. H.; Smirnov, I. *Biopolymers* **2001**, *56*, 209. (e) Han, H.; Hurley, L. H. *Trends Pharmacol. Sci.* **2000**, *21*, 136.
- (323) Kietlyka, R.; Englebienne, P.; Fakhoury, J.; Autexier, C.; Moitessier, N.; Sleiman, H. F. *J. Am. Chem. Soc.* **2008**, *130*, 10040.
- (324) Mounir, M.; Lorenzo, J.; Ferrer, M.; Prieto, M. J.; Rossell, O.; Avilès, F. X.; Moreno, V. *J. Inorg. Biochem.* **2007**, *101*, 660.
- (325) Fyles, T. M.; Tong, C. C. *New J. Chem.* **2007**, *31*, 655.
- (326) Barry, N. P. E.; Edafe, F.; Dyson, P. J.; Therrien, B. *Dalton Trans.* **2010**, 39, 2816.
- (327) Vajpayee, V.; Song, Y. H.; Yang, Y. J.; Kang, S. C.; Kim, H.; Kim, I. S.; Wang, M.; Stang, P. J.; Chi, K.-W. *Organometallics* **2011**, *30*, 3242.
- (328) Ang, W. H.; Grote, Z.; Scopelliti, R.; Juillerat-Jeanneret, L.; Severin, K.; Dyson, P. J. *Organomet. Chem.* **2009**, *694*, 968.
- (329) Saalfrank, R. W.; Stark, A.; Peters, K.; von Schnering, H. G. *Angew. Chem., Int. Ed. Engl.* **1988**, *27*, 851.
- (330) Saalfrank, R. W.; Demleitner, B.; Glaser, H.; Maid, H.; Reihs, S.; Bauer, W.; Maluenga, M.; Hampel, F.; Teichert, M.; Krautscheid, H. *Eur. J. Inorg. Chem.* **2003**, 822.
- (331) Saalfrank, R. W.; Stark, A.; Bremer, M.; Hummel, H.-U. *Angew. Chem., Int. Ed. Engl.* **1990**, *29*, 311.
- (332) Saalfrank, R. W.; Burak, R.; Breit, A.; Stalke, D.; Herbst-Irmer, R.; Daub, J.; Porsch, M.; Bill, E.; Mütter, M.; Trautwein, A. X. *Angew. Chem., Int. Ed. Engl.* **1994**, *33*, 1621.
- (333) Saalfrank, R. W.; Hörner, B.; Stalke, D.; Salbeck, J. *Angew. Chem., Int. Ed. Engl.* **1993**, *32*, 1179.
- (334) Beissel, T.; Powers, R. E.; Raymond, K. N. *Angew. Chem., Int. Ed. Engl.* **1996**, *35*, 1084.
- (335) Beissel, T.; Powers, R. E.; Parac, T. N.; Raymond, K. N. *J. Am. Chem. Soc.* **1999**, *121*, 4200.
- (336) Caulder, D. L.; Powers, R. E.; Parac, T. N.; Raymond, K. N. *Angew. Chem., Int. Ed.* **1998**, *37*, 1840.
- (337) Parac, T. N.; Caulder, D. L.; Raymond, K. N. *J. Am. Chem. Soc.* **1998**, *120*, 8003.
- (338) Johnson, D. W.; Raymond, K. N. *Inorg. Chem.* **2001**, *40*, 5157.
- (339) Biros, S. M.; Yeh, R. M.; Raymond, K. N. *Angew. Chem., Int. Ed.* **2008**, *47*, 6062.
- (340) Review: Ward, M. D. *Chem. Commun. (Cambridge, U. K.)* **2009**, 4487.
- (341) Fleming, J. S.; Mann, K. L. V.; Carraz, C.-A.; Psillakis, E.; Jeffery, J. C.; McCleverty, J. A.; Ward, M. D. *Angew. Chem., Int. Ed.* **1998**, *37*, 1279.
- (342) Paul, R. L.; Bell, Z. R.; Jeffery, J. C.; McCleverty, J. A.; Ward, M. D. *Proc. Natl. Acad. Sci. U. S. A.* **2002**, *99*, 4883.
- (343) Paul, R. L.; Bell, Z. R.; Jeffery, J. C.; Harding, L. P.; McCleverty, J. A.; Ward, M. D. *Polyhedron* **2003**, *22*, 781.
- (344) Tidmarsh, I. S.; Taylor, B. F.; Hardie, M. J.; Russo, L.; Clegg, W.; Ward, M. D. *New J. Chem.* **2009**, *33*, 366.
- (345) Paul, R. L.; Couchman, S. M.; Jeffery, J. C.; McCleverty, J. A.; Reeves, Z. R.; Ward, M. D. *J. Chem. Soc., Dalton Trans.* **2000**, 845.
- (346) (a) Paul, R. L.; Argent, S. P.; Jeffery, J. C.; Harding, L. P.; Lynam, J. M.; Ward, M. D. *Dalton Trans.* **2004**, 3453. (b) Hall, B. R.; Manck, L. E.; Tidmarsh, I. S.; Stephenson, A.; Taylor, B. F.; Blaikie, E. J.; Griend, D. A. V.; Ward, M. D. *Dalton Trans.* **2011**, DOI: 10.1039/c1dt10781j.
- (347) Bell, Z. R.; Jeffery, J. C.; McCleverty, J. A.; Ward, M. D. *Angew. Chem., Int. Ed.* **2002**, *41*, 2515.
- (348) Glasson, C. R. K.; Meehan, G. V.; Clegg, J. K.; Lindoy, L. F.; Turner, P.; Duriska, M. B.; Willis, R. *Chem. Commun. (Cambridge, U. K.)* **2008**, 1190.
- (349) (a) Mal, P.; Schultz, D.; Beyeh, K.; Rissanen, K.; Nitschke, J. R. *Angew. Chem., Int. Ed.* **2008**, *47*, 8297. (b) Meng, W.; Clegg, J. K.; Thoburn, J. D.; Nitschke, J. R. *J. Am. Chem. Soc.* **2011**, DOI: 10.1021/ja205254s.
- (350) Mal, P.; Nitschke, J. R. *Chem. Commun. (Cambridge, U. K.)* **2010**, *46*, 2417.
- (351) Hristova, Y. R.; Smulders, M. M. J.; Clegg, J. K.; Breiner, B.; Nitschke, J. R. *Chem. Sci.* **2011**, *2*, 638.
- (352) Clegg, J. K.; Li, F.; Jolliffe, K. A.; Meehan, G. V.; Lindoy, L. F. *Chem. Commun. (Cambridge, U. K.)* **2011**, *47*, 6042.
- (353) Reviews: (a) Albrecht, M.; Janser, I.; Fröhlich, R. *Chem. Commun. (Cambridge, U. K.)* **2005**, 157. (b) Albrecht, M. *Angew. Chem., Int. Ed.* **1999**, *38*, 3463.

- (354) Brückner, C.; Powers, R. E.; Raymond, K. N. *Angew. Chem., Int. Ed.* **1998**, *37*, 1837.
- (355) Saalfrank, R. W.; Glaser, H.; Demleitner, B.; Hampel, F.; Chowdhry, M. M.; Schünemann, V.; Trautwein, A. X.; Vaughan, G. B. M.; Yeh, R.; Davis, A. V.; Raymond, K. N. *Chem.—Eur. J.* **2002**, *8*, 493.
- (356) Amoroso, A. J.; Jeffery, J. C.; Jones, P. L.; McCleverty, J. A.; Thornton, P.; Ward, M. D. *Angew. Chem., Int. Ed. Engl.* **1995**, *34*, 1343.
- (357) Paul, R. L.; Amoroso, A. J.; Jones, P. L.; Couchman, S. M.; Reeves, Z. R.; Rees, L. H.; Jeffery, J. C.; McCleverty, J. A.; Ward, M. D. *J. Chem. Soc., Dalton Trans.* **1999**, 1563.
- (358) Yeh, R. M.; Xu, J.; Seeber, G.; Raymond, K. N. *Inorg. Chem.* **2005**, *44*, 6228.
- (359) Albrecht, M.; Janser, I.; Meyer, S.; Weis, P.; Fröhlich, R. *Chem. Commun. (Cambridge, U. K.)* **2003**, 2854.
- (360) Albrecht, M.; Janser, I.; Runsink, J.; Raabe, G.; Weis, P.; Fröhlich, R. *Angew. Chem., Int. Ed.* **2004**, *43*, 6662.
- (361) Saalfrank, R. W.; Maid, H.; Scheurer, A.; Heinemann, F. W.; Puchta, R.; Bauer, W.; Stern, D.; Stalke, D. *Angew. Chem., Int. Ed.* **2008**, *47*, 8941.
- (362) Kusukawa, T.; Fujita, M. *J. Am. Chem. Soc.* **2002**, *124*, 13576.
- (363) Yamashita, K.; Kawano, M.; Fujita, M. *Chem. Commun. (Cambridge, U. K.)* **2007**, 4102.
- (364) Leininger, S.; Fan, J.; Schmitz, M.; Stang, P. J. *Proc. Natl. Acad. Sci. U. S. A.* **2000**, *97*, 1380.
- (365) Stang, P. J.; Olenyuk, B.; Muddiman, D. C.; Smith, R. D. *Organometallics* **1997**, *16*, 3094.
- (366) Schweiger, M.; Yamamoto, T.; Stang, P. J.; Bläser, D.; Boese, R. *J. Org. Chem.* **2005**, *70*, 4861.
- (367) Zheng, Y.-R.; Zhao, Z.; Kim, H.; Wang, M.; Ghosh, K.; Pollock, J. B.; Chi, K.-W.; Stang, P. J. *Inorg. Chem.* **2010**, *49*, 10238.
- (368) Granzhan, A.; Riis-Johannessen, T.; Scopelliti, R.; Severin, K. *Angew. Chem., Int. Ed.* **2010**, *49*, 5515.
- (369) Granzhan, A.; Schouwey, C.; Riis-Johannessen, T.; Scopelliti, R.; Severin, K. *J. Am. Chem. Soc.* **2011**, *133*, 7106.
- (370) Roche, S.; Haslam, C.; Adams, H.; Heath, S. L.; Thomas, J. A. *Chem. Commun. (Cambridge, U. K.)* **1998**, 1681.
- (371) Suzuki, K.; Tominaga, M.; Kawano, M.; Fujita, M. *Chem. Commun. (Cambridge, U. K.)* **2009**, 1638.
- (372) Natarajan, R.; Savitha, G.; Moorthy, J. N. *Cryst. Growth Des.* **2005**, *5*, 69.
- (373) Johannessen, S. C.; Brisbois, R. G.; Fischer, J. P.; Grieco, P. A.; Counterman, A. E.; Clemmer, D. E. *J. Am. Chem. Soc.* **2001**, *123*, 3818.
- (374) Klausmeyer, K. K.; Rauchfuss, T. B.; Wilson, S. R. *Angew. Chem., Int. Ed.* **1998**, *37*, 1694.
- (375) Klausmeyer, K. K.; Wilson, S. R.; Rauchfuss, T. B. *J. Am. Chem. Soc.* **1999**, *121*, 2705.
- (376) Lang, J.-P.; Xu, Q.-F.; Chen, Z.-N.; Abrahams, B. F. *J. Am. Chem. Soc.* **2003**, *125*, 12682.
- (377) Heinrich, J. L.; Berseth, P. A.; Long, J. R. *Chem. Commun. (Cambridge, U. K.)* **1998**, 1231.
- (378) Berseth, P. A.; Sokol, J. J.; Shores, M. P.; Heinrich, J. L.; Long, J. R. *J. Am. Chem. Soc.* **2000**, *122*, 9655.
- (379) Sokol, J. J.; Shores, M. P.; Long, J. R. *Inorg. Chem.* **2002**, *41*, 3052.
- (380) Bell, Z. R.; Harding, L. P.; Ward, M. D. *Chem. Commun. (Cambridge, U. K.)* **2003**, 2432.
- (381) Argent, S. P.; Adams, H.; Harding, L. P.; Ward, M. D. *Dalton Trans.* **2006**, 542.
- (382) (a) Tidmarsh, I. S.; Faust, T. B.; Adams, H.; Harding, L. P.; Russo, L.; Clegg, W.; Ward, M. D. *J. Am. Chem. Soc.* **2008**, *130*, 15167. (b) Stephenson, A.; Ward, M. D. *Dalton Trans.* **2011**, 40, 7824. (c) Stephenson, A.; Ward, M. D.; *Dalton Trans.* **2011**, DOI: 10.1039/c1dt10263j.
- (383) Meng, W.; Breiner, B.; Rissanen, K.; Thoburn, J. D.; Clegg, J. K.; Nitschke, J. R. *Angew. Chem., Int. Ed.* **2011**, *50*, 3479.
- (384) Hiraoka, S.; Harano, K.; Shiro, M.; Ozawa, Y.; Yasuda, N.; Toriumi, K.; Shionoya, M. *Angew. Chem., Int. Ed.* **2006**, *45*, 6488.
- (385) Harano, K.; Hiraoka, S.; Shionoya, M. *J. Am. Chem. Soc.* **2007**, *129*, 5300.
- (386) Ronson, T. K.; Fisher, J.; Harding, L. P.; Hardie, M. J. *Angew. Chem., Int. Ed.* **2007**, *46*, 9086.
- (387) Prakash, M. J.; Zou, Y.; Hong, S.; Park, M.; Bui, M.-P. N.; Seong, G. H.; Lah, M. S. *Inorg. Chem.* **2009**, *48*, 1281.
- (388) Müller, I. M.; Spillmann, S.; Franck, H.; Pietschnig, R. *Chem.—Eur. J.* **2004**, *10*, 2207.
- (389) Li, J.-R.; Timmons, D. J.; Zhou, H.-C. *J. Am. Chem. Soc.* **2009**, *131*, 6368.
- (390) Olenyuk, B.; Levin, M. D.; Whiteford, J. A.; Shield, J. E.; Stang, P. J. *J. Am. Chem. Soc.* **1999**, *121*, 10434.
- (391) Levin, M. D.; Stang, P. J. *J. Am. Chem. Soc.* **2000**, *122*, 7428.
- (392) Paquette, L. A.; Balogh, D. W.; Usha, R.; Kountz, D.; Christoph, G. G. *Science* **1981**, *211*, 575.
- (393) Melder, J.-P.; Pinkos, R.; Fritz, H.; Prinzbach, H. *Angew. Chem., Int. Ed. Engl.* **1989**, *28*, 305.
- (394) Olenyuk, B.; Whiteford, J. A.; Fechtenkötter, A.; Stang, P. J. *Nature* **1999**, *398*, 796.
- (395) Argent, S. P.; Adams, H.; Riis-Johannessen, T.; Jeffery, J. C.; Harding, L. P.; Ward, M. D. *J. Am. Chem. Soc.* **2006**, *128*, 72.
- (396) Al-Rasbi, N. K.; Tidmarsh, I. S.; Argent, S. P.; Adams, H.; Harding, L. P.; Ward, M. D. *J. Am. Chem. Soc.* **2008**, *130*, 11641.
- (397) Fujita, M.; Nagao, S.; Ogura, K. *J. Am. Chem. Soc.* **1995**, *117*, 1649.
- (398) Radhakrishnan, U.; Schweiger, M.; Stang, P. J. *Org. Lett.* **2001**, *3*, 3141.
- (399) Mukherjee, P. S.; Das, N.; Stang, P. J. *J. Org. Chem.* **2004**, *69*, 3526.
- (400) Ghosh, S.; Mukherjee, P. S. *Tetrahedron Lett.* **2006**, *47*, 9297.
- (401) Fujita, M.; Yu, S.-Y.; Kusukawa, T.; Funaki, H.; Ogura, K.; Yamaguchi, K. *Angew. Chem., Int. Ed.* **1998**, *37*, 2082.
- (402) Ghosh, S.; Batten, S. R.; Turner, D. R.; Mukherjee, P. S. *Organometallics* **2007**, *26*, 3252.
- (403) Wang, M.; Vajpayee, V.; Shanmugaraju, S.; Zheng, Y.-R.; Zhao, Z.; Kim, H.; Mukherjee, P. S.; Chi, K.-W.; Stang, P. J. *Inorg. Chem.* **2011**, *50*, 1506.
- (404) Bar, A. K.; Chakrabarty, R.; Mukherjee, P. S. *Inorg. Chem.* **2009**, *48*, 10880.
- (405) Garrison, J. C.; Panzner, M. J.; Custer, P. D.; Reddy, D. V.; Rinaldi, P. L.; Tessier, C. A.; Youngs, W. J. *Chem. Commun. (Cambridge, U. K.)* **2006**, 4644.
- (406) Schweiger, M.; Seidel, S. R.; Schmitz, M.; Stang, P. J. *Org. Lett.* **2000**, *2*, 1255.
- (407) Zheng, Y.-R.; Ghosh, K.; Yang, H.-B.; Stang, P. J. *Inorg. Chem.* **2010**, *49*, 4747.
- (408) Cui, Y.; Ngo, H. L.; Lin, W. *Inorg. Chem.* **2002**, *41*, 5940.
- (409) Kumazawa, K.; Biradha, K.; Kusukawa, T.; Okano, T.; Fujita, M. *Angew. Chem., Int. Ed.* **2003**, *42*, 3909.
- (410) Yoshizawa, M.; Nakagawa, J.; Kumazawa, K.; Nagao, M.; Kawano, M.; Ozeki, T.; Fujita, M. *Angew. Chem., Int. Ed.* **2005**, *44*, 1810.
- (411) Ono, K.; Yoshizawa, M.; Kato, T.; Watanabe, K.; Fujita, M. *Angew. Chem., Int. Ed.* **2007**, *46*, 1803.
- (412) Yoshizawa, M.; Ono, K.; Kumazawa, K.; Kato, T.; Fujita, M. *J. Am. Chem. Soc.* **2005**, *127*, 10800.
- (413) Kuehl, C. J.; Yamamoto, T.; Seidel, S. R.; Stang, P. J. *Org. Lett.* **2002**, *4*, 913.
- (414) For examples see: (a) Hiraoka, S.; Kubota, Y.; Fujita, M. *Chem. Commun. (Cambridge, U. K.)* **2000**, 1509. (b) Ikeda, A.; Udzu, H.; Zhong, Z.; Shinkai, S.; Sakamoto, S.; Yamaguchi, K. *J. Am. Chem. Soc.* **2001**, *123*, 3872. (c) Ikeda, A.; Yoshimura, M.; Udzu, H.; Fukuhara, C.; Shinkai, S. *J. Am. Chem. Soc.* **1999**, *121*, 4296. (d) Liu, H.-K.; Sun, W.-Y.; Ma, D.-J.; Yu, K.-B.; Tang, W.-X. *Chem. Commun. (Cambridge, U. K.)* **2000**, 591.
- (415) Ghosh, S.; Mukherjee, P. S. *Organometallics* **2008**, *27*, 316.
- (416) Ghosh, S.; Gole, B.; Bar, A. K.; Mukherjee, P. S. *Organometallics* **2009**, *28*, 4288.
- (417) Kuehl, C. J.; Kryschenko, Y. K.; Radhakrishnan, U.; Seidel, S. R.; Huang, S. D.; Stang, P. J. *Proc. Natl. Acad. Sci. U. S. A.* **2002**, *99*, 4932.
- (418) Kryschenko, Y. K.; Seidel, S. R.; Muddiman, D. C.; Nepomuceno, A. I.; Stang, P. J. *J. Am. Chem. Soc.* **2003**, *125*, 9647.



- (419) Crowley, J. D.; Goshe, A. J.; Bosnich, B. *Chem. Commun. (Cambridge, U. K.)* **2003**, 2824.
- (420) Sun, S.-S.; Lees, A. J. *Chem. Commun. (Cambridge, U. K.)* **2001**, 103.
- (421) Dinolfo, P. H.; Coropceanu, V.; Brédas, J.-L.; Hupp, J. T. *J. Am. Chem. Soc.* **2006**, 128, 12592.
- (422) Manimaran, B.; Rajendran, T.; Lu, Y.-L.; Lee, G.-H.; Peng, S.-M.; Lu, K.-L. *Eur. J. Inorg. Chem.* **2001**, 633.
- (423) Wu, J.-Y.; Chang, C.-H.; Thanasekaran, P.; Tsai, C.-C.; Tseng, T.-W.; Lee, G.-H.; Peng, S.-M.; Lu, K.-L. *Dalton Trans.* **2008**, 6110.
- (424) Govindaswamy, P.; Süß-Fink, G.; Therrien, B. *Organometallics* **2007**, 26, 915.
- (425) Govindaswamy, P.; Süß-Fink, G.; Therrien, B. *Inorg. Chem. Commun.* **2007**, 10, 1489.
- (426) Govindaswamy, P.; Linder, D.; Lacour, J.; Süß-Fink, G.; Therrien, B. *Chem. Commun. (Cambridge, U. K.)* **2006**, 4691.
- (427) Fan, Y.-F.; Lin, Y.-J.; Jia, W.-G.; Weng, L.-H.; Jin, G.-X. *Organometallics* **2007**, 26, 5848.
- (428) Mattsson, J.; Govindaswamy, P.; Furrer, J.; Sei, Y.; Yamaguchi, K.; Süß-Fink, G.; Therrien, B. *Organometallics* **2008**, 27, 4346.
- (429) Freudenreich, J.; Barry, N. P. E.; Süß-Fink, G.; Therrien, B. *Eur. J. Inorg. Chem.* **2010**, 2400.
- (430) Freudenreich, J.; Furrer, J.; Süß-Fink, G.; Therrien, B. *Organometallics* **2011**, 30, 942.
- (431) Therrien, B.; Süß-Fink, G.; Govindaswamy, P.; Renfrew, A. K.; Dyson, P. J. *Angew. Chem., Int. Ed.* **2008**, 47, 3773.
- (432) Shanmugaraju, S.; Bar, A. K.; Mukherjee, P. S. *Inorg. Chem.* **2010**, 49, 10235.
- (433) Mirtschin, S.; Slabon-Turski, A.; Scopelliti, R.; Velders, A. H.; Severin, K. J. *Am. Chem. Soc.* **2010**, 132, 14004.
- (434) Lee, S. J.; Mulfort, K. L.; O'Donnell, J. L.; Zuo, X.; Goshe, A. J.; Wesson, P. J.; Nguyen, S. T.; Hupp, J. T.; Tiede, D. M. *Chem. Commun. (Cambridge, U. K.)* **2006**, 4581.
- (435) Kelley, R. F.; Lee, S. J.; Wilson, T. M.; Nakamura, Y.; Tiede, D. M.; Osuka, A.; Hupp, J. T.; Wasielewski, M. R. *J. Am. Chem. Soc.* **2008**, 130, 4277.
- (436) Youm, K.-T.; Nguyen, S. T.; Hupp, J. T. *Chem. Commun. (Cambridge, U. K.)* **2008**, 3375.
- (437) Oliva, A. L.; Ventura, B.; Würthner, F.; Camara-Campos, A.; Hunter, C. A.; Ballester, P.; Flamigni, L. *Dalton Trans.* **2009**, 4023.
- (438) Indelli, M. T.; Chiorboli, C.; Scandola, F.; Iengo, E.; Osswald, P.; Würthner, F. *J. Phys. Chem. B* **2010**, 114, 14495.
- (439) Zheng, Y.-R.; Zhao, Z.; Wang, M.; Ghosh, K.; Pollock, J. B.; Cook, T. R.; Stang, P. J. *J. Am. Chem. Soc.* **2010**, 132, 16873.
- (440) Zhao, L.; Northrop, B. H.; Stang, P. J. *J. Am. Chem. Soc.* **2008**, 130, 11886.
- (441) Stephenson, A.; Argent, S. P.; Riis-Johannessen, T.; Tidmarsh, I. S.; Ward, M. D. *J. Am. Chem. Soc.* **2011**, 133, 858.
- (442) Campbell, V. E.; de Hatten, X.; Delsuc, N.; Kauffmann, B.; Huc, I.; Nitschke, J. R. *Nat. Chem.* **2010**, 2, 684.
- (443) Yamanaka, M.; Yamada, Y.; Sei, Y.; Yamaguchi, K.; Kobayashi, K. *J. Am. Chem. Soc.* **2006**, 128, 1531.
- (444) Bar, A. K.; Mostafa, G.; Mukherjee, P. S. *Inorg. Chem.* **2010**, 49, 7647.
- (445) Schmittel, M.; He, B.; Mal, P. *Org. Lett.* **2008**, 10, 2513.
- (446) Schmittel, M.; He, B. *Chem. Commun. (Cambridge, U. K.)* **2008**, 4723.
- (447) Barbour, L. J.; Orr, G. W.; Atwood, J. L. *Nature* **1998**, 393, 671.
- (448) Su, C.-Y.; Cai, Y.-P.; Chen, C.-L.; Zhang, H.-X.; Kang, B.-S. *J. Chem. Soc., Dalton Trans.* **2001**, 359.
- (449) Su, C.-Y.; Cai, Y.-P.; Chen, C.-L.; Smith, M. D.; Kaim, W.; zur Loye, H.-C. *J. Am. Chem. Soc.* **2003**, 125, 8595.
- (450) Liu, Z.-M.; Liu, Y.; Zheng, S.-R.; Yu, Z.-Q.; Pan, M.; Su, C.-Y. *Inorg. Chem.* **2007**, 46, 5814.
- (451) Owens, T. D.; Hollander, F. J.; Oliver, A. G.; Ellman, J. A. *J. Am. Chem. Soc.* **2001**, 123, 1539.
- (452) Chand, D. K.; Biradha, K.; Fujita, M. *Chem. Commun. (Cambridge, U. K.)* **2001**, 1652.
- (453) McMoran, D. A.; Steel, P. J. *Angew. Chem., Int. Ed.* **1998**, 37, 3295.
- (454) Yue, N. L. S.; Eisler, D. J.; Jennings, M. C.; Puddephatt, R. J. *Inorg. Chem.* **2004**, 43, 7671.
- (455) Barry, N. P. E.; Govindaswamy, P.; Furrer, J.; Süß-Fink, G.; Therrien, B. *Inorg. Chem. Commun.* **2008**, 11, 1300.
- (456) Barry, N. P. E.; Abd Karim, N. H.; Vilar, R.; Therrien, B. *Dalton Trans.* **2009**, 10717.
- (457) Han, Y.-F.; Lin, Y.-J.; Weng, L.-H.; Berke, H.; Jin, G.-X. *Chem. Commun. (Cambridge, U. K.)* **2008**, 350.
- (458) Barry, N. P. E.; Austeri, M.; Lacour, J.; Therrien, B. *Organometallics* **2009**, 28, 4894.
- (459) Manimaran, B.; Thanasekaran, P.; Rajendran, T.; Liao, R.-T.; Liu, Y.-H.; Lee, G.-H.; Peng, S.-M.; Rajagopal, S.; Lu, K.-L. *Inorg. Chem.* **2003**, 42, 4795.
- (460) Wang, M.; Zheng, Y.-R.; Ghosh, K.; Stang, P. J. *J. Am. Chem. Soc.* **2010**, 132, 6282.
- (461) Zhao, Z.; Zheng, Y.-R.; Wang, M.; Pollock, J. B.; Stang, P. J. *Inorg. Chem.* **2010**, 49, 8653.
- (462) Wang, M.; Zheng, Y.-R.; Cook, T. R.; Stang, P. J. *Inorg. Chem.* **2011**, 50, 6107.
- (463) Caskey, D. C.; Yamamoto, T.; Addicott, C.; Shoemaker, R. K.; Vacek, J.; Hawkridge, A. M.; Muddiman, D. C.; Kottas, G. S.; Michl, J.; Stang, P. J. *J. Am. Chem. Soc.* **2008**, 130, 7620.
- (464) Vacek, J.; Caskey, D. C.; Horinek, D.; Shoemaker, R. K.; Stang, P. J.; Michl, J. *J. Am. Chem. Soc.* **2008**, 130, 7629.
- (465) Yamanoi, Y.; Sakamoto, Y.; Kusukawa, T.; Fujita, M.; Sakamoto, S.; Yamaguchi, K. *J. Am. Chem. Soc.* **2001**, 123, 980.
- (466) Suzuki, K.; Kawano, M.; Fujita, M. *Angew. Chem., Int. Ed.* **2007**, 46, 2819.
- (467) Liu, H.-K.; Tong, X. *Chem. Commun. (Cambridge, U. K.)* **2002**, 1316.
- (468) Chand, D. K.; Biradha, K.; Fujita, M.; Sakamoto, S.; Yamaguchi, K. *Chem. Commun. (Cambridge, U. K.)* **2002**, 2486.
- (469) Hong, M.; Zhao, Y.; Su, W.; Cao, R.; Fujita, M.; Zhou, Z.; Chan, A. S. C. *J. Am. Chem. Soc.* **2000**, 122, 4819.
- (470) Moon, D.; Kang, S.; Park, J.; Lee, K.; John, R. P.; Won, H.; Seong, G. H.; Kim, Y. S.; Kim, G. H.; Rhee, H.; Lah, M. S. *J. Am. Chem. Soc.* **2006**, 128, 3530.
- (471) Ghosh, S.; Mukherjee, P. S. *J. Org. Chem.* **2006**, 71, 8412.
- (472) Duriska, M. B.; Neville, S. M.; Moubaraki, B.; Cashion, J. D.; Halder, G. J.; Chapman, K. W.; Balde, C.; Létard, J.-F.; Murray, K. S.; Kepert, C. J.; Batten, S. R. *Angew. Chem., Int. Ed.* **2009**, 48, 2549.
- (473) Duriska, M. B.; Neville, S. M.; Lu, J.; Iremonger, S. S.; Boas, J. F.; Kepert, C. J.; Batten, S. R. *Angew. Chem., Int. Ed.* **2009**, 48, 8919.
- (474) (a) Tominaga, M.; Suzuki, K.; Kawano, M.; Kusukawa, T.; Ozeki, T.; Sakamoto, S.; Yamaguchi, K.; Fujita, M. *Angew. Chem., Int. Ed.* **2004**, 43, 5621. (b) Fujita, D.; Takahashi, A.; Sato, S.; Fujita, M. *J. Am. Chem. Soc.* **2011**, DOI: 10.1021/ja2059236.
- (475) Moulton, B.; Lu, J.; Mondal, A.; Zaworotko, M. J. *Chem. Commun. (Cambridge, U. K.)* **2001**, 863.
- (476) Sun, Q.-F.; Iwasa, J.; Ogawa, D.; Ishido, Y.; Sato, S.; Ozeki, T.; Sei, Y.; Yamaguchi, K.; Fujita, M. *Science* **2010**, 328, 1144.
- (477) Reviews: (a) Scarso, A.; Rebek, J., Jr. *Top. Curr. Chem.* **2006**, 265, 1. (b) Mateos-Timoneda, M. A.; Crego-Calama, M.; Reinhoudt, D. N. *Chem. Soc. Rev.* **2004**, 33, 363.
- (478) Reviews: (a) Seeber, G.; Tiedemann, B. E. F.; Raymond, K. N. *Top. Curr. Chem.* **2006**, 265, 147. (b) Hamilton, T. D.; MacGillivray, L. R. *Cryst. Growth Des.* **2004**, 4, 419.
- (479) Saalfrank, R. W.; Löw, N.; Demleitner, B.; Stalke, D.; Teichert, M. *Chem.—Eur. J.* **1998**, 4, 1305.
- (480) (a) Saalfrank, R. W.; Demleitner, B.; Glaser, H.; Maid, H.; Bathelt, D.; Hampel, F.; Bauer, W.; Teichert, M. *Chem.—Eur. J.* **2002**, 8, 2679. (b) Saalfrank, R. W.; Maid, H.; Scheurer, A.; Puchta, R.; Bauer, W. *Eur. J. Inorg. Chem.* **2010**, 2903.
- (481) Fiedler, D.; Pagliero, D.; Brumaghim, J. L.; Bergman, R. G.; Raymond, K. N. *Inorg. Chem.* **2004**, 43, 846.
- (482) Terpin, A. J.; Ziegler, M.; Johnson, D. W.; Raymond, K. N. *Angew. Chem., Int. Ed.* **2001**, 40, 157.

- (483) Davis, A. V.; Fiedler, D.; Ziegler, M.; Terpin, A.; Raymond, K. N. *J. Am. Chem. Soc.* **2007**, *129*, 15354.
- (484) Ziegler, M.; Davis, A. V.; Johnson, D. W.; Raymond, K. N. *Angew. Chem., Int. Ed.* **2003**, *42*, 665.
- (485) Frantz, R.; Grange, C. S.; Al-Rasbi, N. K.; Ward, M. D.; Lacour, J. *Chem. Commun. (Cambridge, U. K.)* **2007**, 1459.
- (486) Argent, S. P.; Riis-Johannessen, T.; Jeffery, J. C.; Harding, L. P.; Ward, M. D. *Chem. Commun. (Cambridge, U. K.)* **2005**, 4647.
- (487) Hamilton, T. D.; Bučar, D.-K.; MacGillivray, L. R. *Chem. Commun. (Cambridge, U. K.)* **2007**, 1603.
- (488) Hamilton, T. D.; Papaefstathiou, G. S.; MacGillivray, L. R. *J. Am. Chem. Soc.* **2002**, *124*, 11606.
- (489) Müller, I. M.; Robson, R.; Separovic, F. *Angew. Chem., Int. Ed.* **2001**, *40*, 4385.
- (490) Müller, I. M.; Möller, D.; Schalley, C. A. *Angew. Chem., Int. Ed.* **2005**, *44*, 480.
- (491) Müller, I. M.; Möller, D. *Angew. Chem., Int. Ed.* **2005**, *44*, 2969.
- (492) Childs, L. J.; Alcock, N. W.; Hannon, M. J. *Angew. Chem., Int. Ed.* **2002**, *41*, 4244.
- (493) Liu, T.; Liu, Y.; Xuan, W.; Cui, Y. *Angew. Chem., Int. Ed.* **2010**, *49*, 4121.
- (494) Jeong, K. S.; Kim, Y. S.; Kim, Y. J.; Lee, E.; Yoon, J. H.; Park, W. H.; Park, Y. W.; Jeon, S.-J.; Kim, Z. H.; Kim, J.; Jeong, N. *Angew. Chem., Int. Ed.* **2006**, *45*, 8134.
- (495) Ayabe, M.; Yamashita, K.; Sada, K.; Shinkai, S.; Ikeda, A.; Sakamoto, S.; Yamaguchi, K. *J. Org. Chem.* **2003**, *68*, 1059–1066.
- (496) Kubota, Y.; Biradha, K.; Fujita, M.; Sakamoto, S.; Yamaguchi, K. *Bull. Chem. Soc. Jpn.* **2002**, *75*, 559.
- (497) Hiraoka, S.; Fujita, M. *J. Am. Chem. Soc.* **1999**, *121*, 10239.
- (498) Kamiya, N.; Tominaga, M.; Sato, S.; Fujita, M. *J. Am. Chem. Soc.* **2007**, *129*, 3816.
- (499) Kikuchi, T.; Sato, S.; Fujita, M. *J. Am. Chem. Soc.* **2010**, *132*, 15930.
- (500) Ikemi, M.; Kikuchi, T.; Matsumura, S.; Shiba, K.; Sato, S.; Fujita, M. *Chem. Sci.* **2010**, *1*, 68.
- (501) Ghosh, K.; Hu, J.; White, H. S.; Stang, P. J. *J. Am. Chem. Soc.* **2009**, *131*, 6695.
- (502) Tominaga, M.; Suzuki, K.; Murase, T.; Fujita, M. *J. Am. Chem. Soc.* **2005**, *127*, 11950.
- (503) Sato, S.; Iida, J.; Suzuki, K.; Kawano, M.; Ozeki, T.; Fujita, M. *Science* **2006**, *313*, 1273.
- (504) Suzuki, K.; Takao, K.; Sato, S.; Fujita, M. *J. Am. Chem. Soc.* **2010**, *132*, 2544.
- (505) Murase, T.; Sato, S.; Fujita, M. *Angew. Chem., Int. Ed.* **2007**, *46*, 1083.
- (506) Kikuchi, T.; Murase, T.; Sato, S.; Fujita, M. *Supramol. Chem.* **2008**, *20*, 81.
- (507) Suzuki, K.; Kawano, M.; Sato, S.; Fujita, M. *J. Am. Chem. Soc.* **2007**, *129*, 10652.
- (508) Suzuki, K.; Sato, S.; Fujita, M. *Nat. Chem.* **2010**, *2*, 25.
- (509) Suzuki, K.; Takao, K.; Sato, S.; Fujita, M. *Angew. Chem., Int. Ed.* **2011**, *50*, 4858.
- (510) Murase, T.; Sato, S.; Fujita, M. *Angew. Chem., Int. Ed.* **2007**, *46*, 5133.
- (511) Suzuki, K.; Iida, J.; Sato, S.; Kawano, M.; Fujita, M. *Angew. Chem., Int. Ed.* **2008**, *47*, 5780.
- (512) Li, D.; Zhou, W.; Landskron, K.; Sato, S.; Kiely, C. J.; Fujita, M.; Liu, T. *Angew. Chem., Int. Ed.* **2011**, *50*, 5182.
- (513) Li, D.; Zhang, J.; Landskron, K.; Liu, T. *J. Am. Chem. Soc.* **2008**, *130*, 4226.
- (514) Ballester, P.; Oliva, A. I.; Costa, A.; Deyà, P. M.; Frontera, A.; Gomila, R. M.; Hunter, C. A. *J. Am. Chem. Soc.* **2006**, *128*, 5560.
- (515) Flamigni, L.; Ventura, B.; Oliva, A. I.; Ballester, P. *Chem.—Eur. J.* **2008**, *14*, 4214.
- (516) Slagt, V. F.; van Leeuwen, P. W. N. M.; Reek, J. N. H. *Angew. Chem., Int. Ed.* **2003**, *42*, 5619.
- (517) Lee, S. J.; Mulfort, K. L.; Zuo, X.; Goshe, A. J.; Wesson, P. J.; Nguyen, S. T.; Hupp, J. T.; Tiede, D. M. *J. Am. Chem. Soc.* **2008**, *130*, 836.
- (518) Aratani, N.; Kim, D.; Osuka, A. *Acc. Chem. Res.* **2009**, *42*, 1922.
- (519) Tsuda, A.; Nakamura, T.; Sakamoto, S.; Yamaguchi, K.; Osuka, A. *Angew. Chem., Int. Ed.* **2002**, *41*, 2817.
- (520) Hwang, I.-W.; Kamada, T.; Ahn, T. K.; Ko, D. M.; Nakamura, T.; Tsuda, A.; Osuka, A.; Kim, D. *J. Am. Chem. Soc.* **2004**, *126*, 16187.
- (521) Review: Cram, D. J. *Nature* **1992**, *356*, 29.
- (522) Reviews: (a) Purse, B. W.; Rebek, J., Jr. *Proc. Natl. Acad. Sci. U. S. A.* **2005**, *102*, 10777. (b) Warmuth, R.; Yoon, J. *Acc. Chem. Res.* **2001**, *34*, 95. (c) Jasat, A.; Sherman, J. C. *Chem. Rev.* **1999**, *99*, 931.
- (523) Jacopozi, P.; Dalcanele, E. *Angew. Chem., Int. Ed. Engl.* **1997**, *36*, 613.
- (524) Fochi, F.; Jacopozi, P.; Wegelius, E.; Rissanen, K.; Cozzini, P.; Marastoni, E.; Fiscaro, E.; Manini, P.; Fokkens, R.; Dalcanele, E. *J. Am. Chem. Soc.* **2001**, *123*, 7539.
- (525) Zuccaccia, D.; Pirondini, L.; Pinalli, R.; Dalcanele, E.; Macchioni, A. *J. Am. Chem. Soc.* **2005**, *127*, 7025.
- (526) Cuminetti, N.; Ebbing, M. H. K.; Prados, P.; de Mendoza, J.; Dalcanele, E. *Tetrahedron Lett.* **2001**, *42*, 527.
- (527) Gruppi, F.; Boccini, F.; Elviri, L.; Dalcanele, E. *Tetrahedron* **2009**, *65*, 7289.
- (528) Kobayashi, K.; Yamada, Y.; Yamanaka, M.; Sei, Y.; Yamaguchi, K. *J. Am. Chem. Soc.* **2004**, *126*, 13896.
- (529) Lim, C. W.; Hong, J.-I. *Tetrahedron Lett.* **2000**, *41*, 3113.
- (530) Park, S. J.; Hong, J.-I. *Chem. Commun. (Cambridge, U. K.)* **2001**, 1554.
- (531) Park, S. J.; Shin, D. M.; Sakamoto, S.; Yamaguchi, K.; Chung, Y. K.; Lah, M. S.; Hong, J.-I. *Chem. Commun. (Cambridge, U. K.)* **2003**, 998.
- (532) Park, S. J.; Shin, D. M.; Sakamoto, S.; Yamaguchi, K.; Chung, Y. K.; Lah, M. S.; Hong, J.-I. *Chem.—Eur. J.* **2005**, *11*, 235.
- (533) Haino, T.; Kobayashi, M.; Chikaraishi, M.; Fukazawa, Y. *Chem. Commun. (Cambridge, U. K.)* **2005**, 2321.
- (534) Haino, T.; Kobayashi, M.; Fukazawa, Y. *Chem.—Eur. J.* **2006**, *12*, 3310.
- (535) Fox, O. D.; Dalley, N. K.; Harrison, R. G. *J. Am. Chem. Soc.* **1998**, *120*, 7111.
- (536) Fox, O. D.; Dalley, N. K.; Harrison, R. G. *Inorg. Chem.* **1999**, *38*, 5860.
- (537) Fox, O. D.; Leung, J. F.-Y.; Hunter, J. M.; Dalley, N. K.; Harrison, R. G. *Inorg. Chem.* **2000**, *39*, 783.
- (538) Harrison, R. G.; Burrows, J. L.; Hansen, L. D. *Chem.—Eur. J.* **2005**, *11*, 5881.
- (539) Pirondini, L.; Bertolini, F.; Cantadori, B.; Ugozzoli, F.; Massera, C.; Dalcanele, E. *Proc. Natl. Acad. Sci. U. S. A.* **2002**, *99*, 4911.
- (540) Pirondini, L.; Bonifazi, D.; Cantadori, B.; Braiuca, P.; Campagnolo, M.; Zorzi, R. D.; Geremia, S.; Diederich, F.; Dalcanele, E. *Tetrahedron* **2006**, *62*, 2008.
- (541) Pinalli, R.; Cristini, V.; Sottili, V.; Geremia, S.; Campagnolo, M.; Caneschi, A.; Dalcanele, E. *J. Am. Chem. Soc.* **2004**, *126*, 6516.
- (542) Ikeda, A.; Shinkai, S. *Chem. Rev.* **1997**, *97*, 1713.
- (543) Baldini, L.; Ballester, P.; Casnati, A.; Gomila, R. M.; Hunter, C. A.; Sansone, F.; Ungaro, R. *J. Am. Chem. Soc.* **2003**, *125*, 14181.
- (544) Cotton, F. A.; Lei, P.; Lin, C.; Murillo, C. A.; Wang, X.; Yu, S.-Y.; Zhang, Z.-X. *J. Am. Chem. Soc.* **2004**, *126*, 1518.
- (545) Fox, O. D.; Drew, M. G. B.; Beer, P. D. *Angew. Chem., Int. Ed.* **2000**, *39*, 136.
- (546) Fox, O. D.; Cookson, J.; Wilkinson, E. J. S.; Drew, M. G. B.; MacLean, E. J.; Teat, S. J.; Beer, P. D. *J. Am. Chem. Soc.* **2006**, *128*, 6990.
- (547) Fox, O. D.; Drew, M. G. B.; Wilkinson, E. J. S.; Beer, P. D. *Chem. Commun. (Cambridge, U. K.)* **2000**, 391.
- (548) Schröder, T.; Brodbeck, R.; Letzel, M. C.; Mix, A.; Schnatwinkel, B.; Tonigold, M.; Volkmer, D.; Mattay, J. *Tetrahedron Lett.* **2008**, *49*, 5939.
- (549) Reviews: (a) Rebek, J., Jr. *Acc. Chem. Res.* **2009**, *42*, 1660. (b) Ajami, D.; Rebek, J., Jr. *Supramol. Chem.* **2009**, *21*, 103. (c) Rebek, J., Jr. *Angew. Chem., Int. Ed.* **2005**, *44*, 2068. (d) Palmer, L. C.; Rebek, J., Jr. *Org. Biomol. Chem.* **2004**, *2*, 3051.
- (550) Pluth, M. D.; Raymond, K. N. *Chem. Soc. Rev.* **2007**, *36*, 161.



- (551) Pluth, M. D.; Johnson, D. W.; Szigethy, G.; Davis, A. V.; Teat, S. J.; Oliver, A. G.; Bergman, R. G.; Raymond, K. N. *Inorg. Chem.* **2009**, *48*, 111.
- (552) Leung, D. H.; Bergman, R. G.; Raymond, K. N. *J. Am. Chem. Soc.* **2008**, *130*, 2798.
- (553) Sgarlata, C.; Mugridge, J. S.; Pluth, M. D.; Tiedemann, B. E. F.; Zito, V.; Arena, G.; Raymond, K. N. *J. Am. Chem. Soc.* **2010**, *132*, 1005.
- (554) Pluth, M. D.; Tiedemann, B. E. F.; van Halbeek, H.; Nunlist, R.; Raymond, K. N. *Inorg. Chem.* **2008**, *47*, 1411.
- (555) Davis, A. V.; Raymond, K. N. *J. Am. Chem. Soc.* **2005**, *127*, 7912.
- (556) Davis, A. V.; Fiedler, D.; Seeber, G.; Zahl, A.; van Eldik, R.; Raymond, K. N. *J. Am. Chem. Soc.* **2006**, *128*, 1324.
- (557) Riddell, I. A.; Smulders, M. M. J.; Clegg, J. K.; Nitschke, J. R. *Chem. Commun. (Cambridge, U. K.)* **2011**, *47*, 457.
- (558) Biro, S. M.; Bergman, R. G.; Raymond, K. N. *J. Am. Chem. Soc.* **2007**, *129*, 12094.
- (559) Hastings, C. J.; Pluth, M. D.; Biro, S. M.; Bergman, R. G.; Raymond, K. N. *Tetrahedron* **2008**, *64*, 8362.
- (560) Glasson, C. R. K.; Clegg, J. K.; McMurtrie, J. C.; Meehan, G. V.; Lindoy, L. F.; Motti, C. A.; Moubaraki, B.; Murray, K. S.; Cashion, J. D. *Chem. Sci.* **2011**, *2*, 540.
- (561) Review: Klosterman, J. K.; Yamauchi, Y.; Fujita, M. *Chem. Soc. Rev.* **2009**, *38*, 1714.
- (562) Murase, T.; Otsuka, K.; Fujita, M. *J. Am. Chem. Soc.* **2010**, *132*, 7864.
- (563) Ono, K.; Yoshizawa, M.; Kato, T.; Fujita, M. *Chem. Commun. (Cambridge, U. K.)* **2008**, 2328.
- (564) Ono, K.; Klosterman, J. K.; Yoshizawa, M.; Sekiguchi, K.; Tahara, T.; Fujita, M. *J. Am. Chem. Soc.* **2009**, *131*, 12526.
- (565) Yamauchi, Y.; Yoshizawa, M.; Fujita, M. *J. Am. Chem. Soc.* **2008**, *130*, 5832.
- (566) Sato, S.; Morohara, O.; Fujita, D.; Yamaguchi, Y.; Kato, K.; Fujita, M. *J. Am. Chem. Soc.* **2010**, *132*, 3670.
- (567) Yamauchi, Y.; Hanaoka, Y.; Yoshizawa, M.; Akita, M.; Ichikawa, T.; Yoshio, M.; Kato, T.; Fujita, M. *J. Am. Chem. Soc.* **2010**, *132*, 9555.
- (568) Yamauchi, Y.; Yoshizawa, M.; Akita, M.; Fujita, M. *Proc. Natl. Acad. Sci. U. S. A.* **2009**, *106*, 10435.
- (569) Yamauchi, Y.; Yoshizawa, M.; Akita, M.; Fujita, M. *J. Am. Chem. Soc.* **2010**, *132*, 960.
- (570) Osuga, T.; Murase, T.; Ono, K.; Yamauchi, Y.; Fujita, M. *J. Am. Chem. Soc.* **2010**, *132*, 15553.
- (571) Ono, K.; Yoshizawa, M.; Akita, M.; Kato, T.; Tsunobuchi, Y.; Ohkoshi, S.; Fujita, M. *J. Am. Chem. Soc.* **2009**, *131*, 2782.
- (572) Ozaki, Y.; Kawano, M.; Fujita, M. *Chem. Commun. (Cambridge, U. K.)* **2009**, 4245.
- (573) Nakabayashi, K.; Ozaki, Y.; Kawano, M.; Fujita, M. *Angew. Chem., Int. Ed.* **2008**, *47*, 2046.
- (574) Nakabayashi, K.; Kawano, M.; Yoshizawa, M.; Ohkoshi, S.; Fujita, M. *J. Am. Chem. Soc.* **2004**, *126*, 16694.
- (575) Nakabayashi, K.; Kawano, M.; Kato, T.; Furukawa, K.; Ohkoshi, S.; Hozumi, T.; Fujita, M. *Chem. Asian J.* **2007**, *2*, 164.
- (576) Nakabayashi, K.; Kawano, M.; Fujita, M. *Angew. Chem., Int. Ed.* **2005**, *44*, 5322.
- (577) Fiedler, D.; Leung, D. H.; Bergman, R. G.; Raymond, K. N. *J. Am. Chem. Soc.* **2004**, *126*, 3674.
- (578) Yoshizawa, M.; Tamura, M.; Fujita, M. *Angew. Chem., Int. Ed.* **2007**, *46*, 3874.
- (579) Cram, D. J.; Tanner, M. E.; Thomas, R. *Angew. Chem., Int. Ed. Engl.* **1991**, *30*, 1024.
- (580) Ziegler, M.; Brumagim, J. L.; Raymond, K. N. *Angew. Chem., Int. Ed.* **2000**, *39*, 4119.
- (581) Brumagim, J. L.; Michels, M.; Raymond, K. N. *Eur. J. Org. Chem.* **2004**, 4552.
- (582) Brumagim, J. L.; Michels, M.; Pagliero, D.; Raymond, K. N. *Eur. J. Org. Chem.* **2004**, 5115.
- (583) Dong, V. M.; Fiedler, D.; Carl, B.; Bergman, R. G.; Raymond, K. N. *J. Am. Chem. Soc.* **2006**, *128*, 14464.
- (584) Fiedler, D.; Bergman, R. G.; Raymond, K. N. *Angew. Chem., Int. Ed.* **2006**, *45*, 745.
- (585) Pluth, M. D.; Fiedler, D.; Mugridge, J. S.; Bergman, R. G.; Raymond, K. N. *Proc. Natl. Acad. Sci. U. S. A.* **2009**, *106*, 10438.
- (586) (a) Kawano, M.; Kobayashi, Y.; Ozeki, T.; Fujita, M. *J. Am. Chem. Soc.* **2006**, *128*, 6558. (b) Horiuchi, S.; Murase, T.; Fujita, M. *J. Am. Chem. Soc.* **2011**, DOI: 10.1021/ja205450a.
- (587) Yoshizawa, M.; Kusukawa, T.; Fujita, M.; Yamaguchi, K. *J. Am. Chem. Soc.* **2000**, *122*, 6311.
- (588) Yoshizawa, M.; Kusukawa, T.; Fujita, M.; Sakamoto, S.; Yamaguchi, K. *J. Am. Chem. Soc.* **2001**, *123*, 10454.
- (589) Sawada, T.; Yoshizawa, M.; Sato, S.; Fujita, M. *Nat. Chem.* **2009**, *1*, 53.
- (590) Sawada, T.; Fujita, M. *J. Am. Chem. Soc.* **2010**, *132*, 7194.
- (591) Mal, P.; Breiner, B.; Rissanen, K.; Nitschke, J. R. *Science* **2009**, *324*, 1697.
- (592) Yoshizawa, M.; Tamura, M.; Fujita, M. *Science* **2006**, *312*, 251.
- (593) Nishioka, Y.; Yamaguchi, T.; Yoshizawa, M.; Fujita, M. *J. Am. Chem. Soc.* **2007**, *129*, 7000.
- (594) Murase, T.; Horiuchi, S.; Fujita, M. *J. Am. Chem. Soc.* **2010**, *132*, 2866.
- (595) Horiuchi, S.; Nishioka, Y.; Murase, T.; Fujita, M. *Chem. Commun. (Cambridge, U. K.)* **2010**, *46*, 3460.
- (596) Yoshizawa, M.; Takeyama, M.; Kusukawa, T.; Fujita, M. *Angew. Chem., Int. Ed.* **2002**, *41*, 1347.
- (597) Karthikeyan, S.; Ramamurthy, V. *Tetrahedron Lett.* **2005**, *46*, 4495.
- (598) Takaoka, K.; Kawano, M.; Ozeki, T.; Fujita, M. *Chem. Commun. (Cambridge, U. K.)* **2006**, 1625.
- (599) Karthikeyan, S.; Ramamurthy, V. *J. Org. Chem.* **2007**, *72*, 452.
- (600) Karthikeyan, S.; Ramamurthy, V. *J. Org. Chem.* **2006**, *71*, 6409.
- (601) Yoshizawa, M.; Takeyama, Y.; Okano, T.; Fujita, M. *J. Am. Chem. Soc.* **2003**, *125*, 3243.
- (602) Nishioka, Y.; Yamaguchi, T.; Kawano, M.; Fujita, M. *J. Am. Chem. Soc.* **2008**, *130*, 8160.
- (603) Furusawa, T.; Kawano, M.; Fujita, M. *Angew. Chem., Int. Ed.* **2007**, *46*, 5717.
- (604) Yamaguchi, T.; Fujita, M. *Angew. Chem., Int. Ed.* **2008**, *47*, 2067.
- (605) Yoshizawa, M.; Miyagi, S.; Kawano, M.; Ishiguro, K.; Fujita, M. *J. Am. Chem. Soc.* **2004**, *126*, 9172.
- (606) Furutani, Y.; Kandori, H.; Kawano, M.; Nakabayashi, K.; Yoshizawa, M.; Fujita, M. *J. Am. Chem. Soc.* **2009**, *131*, 4764.
- (607) Leung, D. H.; Fiedler, D.; Bergman, R. G.; Raymond, K. N. *Angew. Chem., Int. Ed.* **2004**, *43*, 963.
- (608) Leung, D. H.; Bergman, R. G.; Raymond, K. N. *J. Am. Chem. Soc.* **2006**, *128*, 9781.
- (609) Fiedler, D.; Bergman, R. G.; Raymond, K. N. *Angew. Chem., Int. Ed.* **2004**, *43*, 6748.
- (610) Brown, C. J.; Bergman, R. G.; Raymond, K. N. *J. Am. Chem. Soc.* **2009**, *131*, 17530.
- (611) Fiedler, D.; van Halbeek, H.; Bergman, R. G.; Raymond, K. N. *J. Am. Chem. Soc.* **2006**, *128*, 10240.
- (612) Hastings, C. J.; Fiedler, D.; Bergman, R. G.; Raymond, K. N. *J. Am. Chem. Soc.* **2008**, *130*, 10977.
- (613) Hastings, C. J.; Pluth, M. D.; Bergman, R. G.; Raymond, K. N. *J. Am. Chem. Soc.* **2010**, *132*, 6938.
- (614) Pluth, M. D.; Bergman, R. G.; Raymond, K. N. *Science* **2007**, *316*, 85.
- (615) Pluth, M. D.; Bergman, R. G.; Raymond, K. N. *J. Am. Chem. Soc.* **2008**, *130*, 11423.
- (616) Pluth, M. D.; Bergman, R. G.; Raymond, K. N. *Angew. Chem., Int. Ed.* **2007**, *46*, 8587.
- (617) Pluth, M. D.; Bergman, R. G.; Raymond, K. N. *J. Org. Chem.* **2009**, *74*, 58.
- (618) Leung, D. H.; Bergman, R. G.; Raymond, K. N. *J. Am. Chem. Soc.* **2007**, *129*, 2746.
- (619) Wang, Z. J.; Brown, C. J.; Bergman, R. G.; Raymond, K. N.; Toste, F. D. *J. Am. Chem. Soc.* **2011**, *133*, 7358.

- (620) Ito, H.; Kusakawa, T.; Fujita, M. *Chem. Lett.* **2000**, 598.
- (621) Yoshizawa, M.; Sato, N.; Fujita, M. *Chem. Lett.* **2005**, 34, 1392.
- (622) Lee, S. J.; Cho, S.-H.; Mulfort, K. L.; Tiede, D. M.; Hupp, J. T.; Nguyen, S. T. *J. Am. Chem. Soc.* **2008**, 130, 16828.
- (623) Noh, T. H.; Heo, E.; Park, K. H.; Jung, O.-S. *J. Am. Chem. Soc.* **2011**, 133, 1236.
- (624) Review: Hannon, M. J. *Chem. Soc. Rev.* **2007**, 36, 280.
- (625) Hannon, M. J.; Painting, C. L.; Jackson, A.; Hamblin, J.; Errington, W. *Chem. Commun. (Cambridge, U. K.)* **1997**, 1807.
- (626) Hannon, M. J.; Moreno, V.; Prieto, M. J.; Moldrheim, E.; Sletten, E.; Meistermann, I.; Isaac, C. J.; Sanders, K. J.; Rodger, A. *Angew. Chem., Int. Ed.* **2001**, 40, 879.
- (627) Khalid, S.; Hannon, M. J.; Rodger, A.; Rodger, P. M. *Chem.—Eur. J.* **2006**, 12, 3493.
- (628) Meistermann, I.; Moreno, V.; Prieto, M. J.; Moldrheim, E.; Sletten, E.; Khalid, S.; Rodger, P. M.; Peberdy, J. C.; Isaac, C. J.; Rodger, A.; Hannon, M. J. *Proc. Natl. Acad. Sci. U. S. A.* **2002**, 99, 5069.
- (629) Uerpmann, C.; Malina, J.; Pascu, M.; Clarkson, G. J.; Moreno, V.; Rodger, A.; Grandas, A.; Hannon, M. J. *Chem.—Eur. J.* **2005**, 11, 1750.
- (630) Childs, L. J.; Malina, J.; Rolfsnes, B. E.; Pascu, M.; Prieto, M. J.; Broome, M. J.; Rodger, P. M.; Sletten, E.; Moreno, V.; Rodger, A.; Hannon, M. J. *Chem.—Eur. J.* **2006**, 12, 4919.
- (631) Oleski, A.; Blanco, A. G.; Boer, R.; Usón, I.; Aymami, J.; Rodger, A.; Hannon, M. J.; Coll, M. *Angew. Chem., Int. Ed.* **2006**, 45, 1227.
- (632) Tashiro, S.; Tominaga, M.; Kawano, M.; Therrien, B.; Ozeki, T.; Fujita, M. *J. Am. Chem. Soc.* **2005**, 127, 4546.
- (633) Tashiro, S.; Tominaga, M.; Yamaguchi, Y.; Kato, K.; Fujita, M. *Angew. Chem., Int. Ed.* **2006**, 45, 241.
- (634) Tashiro, S.; Tominaga, M.; Yamaguchi, Y.; Kato, K.; Fujita, M. *Chem.—Eur. J.* **2006**, 12, 3211.
- (635) Dolain, C.; Hatakeyama, Y.; Sawada, T.; Tashiro, S.; Fujita, M. *J. Am. Chem. Soc.* **2010**, 132, 5564.
- (636) Tashiro, S.; Kobayashi, M.; Fujita, M. *J. Am. Chem. Soc.* **2006**, 128, 9280.
- (637) Hatakeyama, Y.; Sawada, T.; Kawano, M.; Fujita, M. *Angew. Chem., Int. Ed.* **2009**, 48, 8695.
- (638) Mattsson, J.; Zava, O.; Renfrew, A. K.; Sei, Y.; Yamaguchi, K.; Dyson, P. J.; Therrien, B. *Dalton Trans.* **2010**, 39, 8248.
- (639) Barry, N. P. E.; Zava, O.; Furrer, J.; Dyson, P. J.; Therrien, B. *Dalton Trans.* **2010**, 39, 5272.
- (640) Zava, O.; Mattsson, J.; Therrien, B.; Dyson, P. J. *Chem.—Eur. J.* **2010**, 16, 1428.
- (641) Pitto-Barry, A.; Barry, N. P. E.; Zava, O.; Deschenaux, R.; Dyson, P. J.; Therrien, B. *Chem.—Eur. J.* **2011**, 17, 1966.
- (642) Vajpayee, V.; Yang, Y. J.; Kang, S. C.; Kim, H.; Kim, I. S.; Wang, M.; Stang, P. J.; Chi, K.-W. *Chem. Commun. (Cambridge, U. K.)* **2011**, 47, 5184.
- (643) Reviews: (a) Lehn, J.-M. *Chem. Soc. Rev.* **2007**, 36, 151. (b) Lehn, J.-M. *Science* **2002**, 295, 2400. (c) Lehn, J.-M. *Proc. Natl. Acad. Sci. U. S. A.* **2002**, 99, 4763.
- (644) Ziegler, M.; Miranda, J. J.; Anderson, U. N.; Johnson, D. W.; Leary, J. A.; Raymond, K. N. *Angew. Chem., Int. Ed.* **2001**, 40, 733.
- (645) Reviews: (a) Albrecht, M. *Top. Curr. Chem.* **2004**, 248, 105. (b) Albrecht, M.; Janser, I.; Fröhlich, R. *Chem. Commun. (Cambridge, U. K.)* **2005**, 157.
- (646) Northrop, B. H.; Zheng, Y.-R.; Chi, K.-W.; Stang, P. J. *Acc. Chem. Res.* **2009**, 42, 1554.
- (647) Severin, K. *Chem. Commun. (Cambridge, U. K.)* **2006**, 3859.
- (648) Krämer, R.; Lehn, J.-M.; Marquis-Rigault, A. *Proc. Natl. Acad. Sci. U. S. A.* **1993**, 90, 5394.
- (649) Caulder, D. L.; Raymond, K. N. *Angew. Chem., Int. Ed. Engl.* **1997**, 36, 1440.
- (650) Albrecht, M.; Schneider, M.; Röttele, H. *Angew. Chem., Int. Ed.* **1999**, 38, 557.
- (651) Albrecht, M.; Schneider, M. *Eur. J. Inorg. Chem.* **2002**, 1301.
- (652) Albrecht, M.; Liu, Y.; Zhu, S. S.; Schalley, C. A.; Fröhlich, R. *Chem. Commun. (Cambridge, U. K.)* **2009**, 1195.
- (653) Addicott, C.; Das, N.; Stang, P. J. *Inorg. Chem.* **2004**, 43, 5335.
- (654) Zheng, Y.-R.; Yang, H.-B.; Northrop, B. H.; Ghosh, K.; Stang, P. J. *Inorg. Chem.* **2008**, 47, 4706.
- (655) Zheng, Y.-R.; Yang, H.-B.; Ghosh, K.; Zhao, L.; Stang, P. J. *Chem.—Eur. J.* **2009**, 15, 7203.
- (656) Yang, H.-B.; Ghosh, K.; Northrop, B. H.; Stang, P. J. *Org. Lett.* **2007**, 9, 1561.
- (657) Zheng, Y.-R.; Stang, P. J. *J. Am. Chem. Soc.* **2009**, 131, 3487.
- (658) Northrop, B. H.; Yang, H.-B.; Stang, P. J. *Inorg. Chem.* **2008**, 47, 11257.
- (659) Chi, K.-W.; Addicott, C.; Arif, A. M.; Stang, P. J. *J. Am. Chem. Soc.* **2004**, 126, 16569.
- (660) Zhao, L.; Northrop, B. H.; Zheng, Y.-R.; Yang, H.-B.; Lee, H. J.; Lee, Y. M.; Park, J. Y.; Chi, K.-W.; Stang, P. J. *J. Org. Chem.* **2008**, 73, 6580.
- (661) Mahata, K.; Schmittel, M. *J. Am. Chem. Soc.* **2009**, 131, 16544.
- (662) Schmittel, M.; Mahata, K. *Chem. Commun. (Cambridge, U. K.)* **2010**, 46, 4163.
- (663) Schmittel, M.; Kalsani, V.; Kishore, R. S. K.; Cölfen, H.; Bats, J. W. *J. Am. Chem. Soc.* **2005**, 127, 11544.
- (664) Mahata, K.; Saha, M. L.; Schmittel, M. *J. Am. Chem. Soc.* **2010**, 132, 15933.
- (665) Jiang, W.; Winkler, H. D. F.; Schalley, C. A. *J. Am. Chem. Soc.* **2008**, 130, 13852.
- (666) Jiang, W.; Schalley, C. A. *Proc. Natl. Acad. Sci. U. S. A.* **2009**, 106, 10425.
- (667) (a) Brusilowskij, B.; Dzyuba, E. V.; Troff, R. W.; Schalley, C. A. *Chem. Commun.* **2011**, 47, 1830. (b) Brusilowskij, B.; Dzyuba, E. V.; Troff, R. W.; Schalley, C. A. *Dalton. Trans.* **2011**, DOI: 10.1039/c1dt10621j.
- (668) Kamada, T.; Aratani, N.; Ikeda, T.; Shibata, N.; Higuchi, Y.; Wakamiya, A.; Yamaguchi, S.; Kim, K. S.; Yoon, Z. S.; Kim, D.; Osuka, A. *J. Am. Chem. Soc.* **2006**, 128, 7670.
- (669) Maeda, C.; Shinokubo, H.; Osuka, A. *Org. Lett.* **2009**, 11, 5322.
- (670) Grote, Z.; Scopelliti, R.; Severin, K. *Angew. Chem., Int. Ed.* **2003**, 42, 3821.
- (671) Saur, I.; Scopelliti, R.; Severin, K. *Chem.—Eur. J.* **2006**, 12, 1058.
- (672) Schultz, D.; Nitschke, J. R. *Proc. Natl. Acad. Sci. U. S. A.* **2005**, 102, 11191.
- (673) Hutin, M.; Frantz, R.; Nitschke, J. R. *Chem.—Eur. J.* **2006**, 12, 4077.
- (674) Schultz, D.; Nitschke, J. R. *Angew. Chem., Int. Ed.* **2006**, 45, 2453.
- (675) Schultz, D.; Nitschke, J. R. *J. Am. Chem. Soc.* **2006**, 128, 9887.
- (676) Bélanger, S.; Hupp, J. T.; Stern, C. L.; Slone, R. V.; Watson, D. F.; Carrell, T. G. *J. Am. Chem. Soc.* **1999**, 121, 557.
- (677) Bélanger, S.; Hupp, J. T. *Angew. Chem., Int. Ed.* **1999**, 38, 2222.
- (678) Keefe, M. H.; O'Donnell, J. L.; Bailey, R. C.; Nguyen, S. T.; Hupp, J. T. *Adv. Mater.* **2003**, 15, 1936.
- (679) Massari, A. M.; Gurney, R. W.; Schwartz, C. P.; Nguyen, S. T.; Hupp, J. T. *Langmuir* **2004**, 20, 4422.
- (680) Libera, J. A.; Gurney, R. W.; Schwartz, C.; Jin, H.; Lee, T.-L.; Nguyen, S. T.; Hupp, J. T.; Bedzyk, M. J. *J. Phys. Chem. B* **2005**, 109, 1441.
- (681) Williams, M. E.; Benkstein, K. D.; Abel, C.; Dinolfo, P. H.; Hupp, J. T. *Proc. Natl. Acad. Sci. U. S. A.* **2002**, 99, 5171.
- (682) Yuan, Q.-H.; Wan, L.-J.; Jude, H.; Stang, P. J. *J. Am. Chem. Soc.* **2005**, 127, 16279.
- (683) Semenov, A.; Spatz, J. P.; Möller, M.; Lehn, J.-M.; Sell, B.; Schubert, D.; Weidl, C. H.; Schubert, U. S. *Angew. Chem., Int. Ed.* **1999**, 38, 2547.
- (684) Ziener, U.; Lehn, J.-M.; Mourran, A.; Möller, M. *Chem.—Eur. J.* **2002**, 8, 951.
- (685) Safarowsky, C.; Merz, L.; Rang, A.; Broekmann, P.; Hermann, B. A.; Schalley, C. A. *Angew. Chem., Int. Ed.* **2004**, 43, 1291.
- (686) Yuan, Q.-H.; Yan, C.-J.; Yan, H.-J.; Wan, L.-J.; Northrop, B. H.; Jude, H.; Stang, P. J. *J. Am. Chem. Soc.* **2008**, 130, 8878.



- (687) Gong, J.-R.; Wan, L.-J.; Yuan, Q.-H.; Bai, C.-L.; Jude, H.; Stang, P. J. *Proc. Natl. Acad. Sci. U. S. A.* **2005**, *102*, 971.
- (688) Li, S.-S.; Yan, H.-J.; Wan, L.-J.; Yang, H.-B.; Northrop, B. H.; Stang, P. J. *J. Am. Chem. Soc.* **2007**, *129*, 9268.
- (689) Chen, T.; Pan, G.-B.; Wettach, H.; Fritzsche, M.; Höger, S.; Wan, L.-J.; Yang, H.-B.; Northrop, B. H.; Stang, P. J. *J. Am. Chem. Soc.* **2010**, *132*, 1328.
- (690) Levi, S. A.; Guatterri, P.; van Veggel, F. C. J. M.; Vancso, G. J.; Dalcanele, E.; Reinhoudt, D. N. *Angew. Chem., Int. Ed.* **2001**, *40*, 1892.
- (691) Menozzi, E.; Pinalli, R.; Speets, E. A.; Ravoo, B. J.; Dalcanele, E.; Reinhoudt, D. N. *Chem.—Eur. J.* **2004**, *10*, 2199.
- (692) Kogej, M.; Schalley, C. A. In *Analytical Methods in Supramolecular Chemistry*; Schalley, C. A., Ed.; Wiley-VCH: Weinheim, Germany, 2007; p 104.
- (693) Reviews:(a) Baytekin, B.; Baytekin, H. T.; Schalley, C. A. *Org. Biomol. Chem.* **2006**, *4*, 2825. (b) Schalley, C. A. *Mass Spectrom. Rev.* **2001**, *20*, 253. (c) Schalley, C. A. *Int. J. Mass Spectrom.* **2000**, *194*, 11.
- (694) Reviews:(a) Fenn, J. B. *Angew. Chem., Int. Ed.* **2003**, *42*, 3871. (b) Fenn, J. B.; Mann, M.; Meng, C. K.; Wong, S. F.; Whitehouse, C. M. *Mass Spectrom. Rev.* **1990**, *9*, 37.
- (695) Schalley, C. A.; Springer, A. *Mass Spectrometry and Gas-Phase Chemistry of Non-Covalent Complexes*; Wiley: Hoboken, NJ, 2009.
- (696) Reviews:(a) Sakamoto, S.; Fujita, M.; Kim, K.; Yamaguchi, K. *Tetrahedron* **2000**, *56*, 955. (b) Yamaguchi, K. *J. Mass Spectrom.* **2003**, *38*, 473.
- (697) Xia, Y.; Liang, X.; McLuckey, S. A. *Anal. Chem.* **2005**, *77*, 3683.
- (698) Hirabayashi, A.; Sakairi, M.; Koizumi, H. *Anal. Chem.* **1994**, *66*, 4557.
- (699) Gardner, J. S.; Harrison, R. G.; Lamb, J. D.; Dearden, D. V. *New J. Chem.* **2006**, *30*, 1276.
- (700) Schalley, C. A.; Müller, T.; Linnartz, P.; Witt, M.; Schäfer, M.; Lützen, A. *Chem.—Eur. J.* **2002**, *8*, 3538.
- (701) Engeser, M.; Rang, A.; Ferrer, M.; Gutiérrez, A.; Baytekin, H. T.; Schalley, C. A. *Int. J. Mass Spectrom.* **2006**, *255–256*, 185.
- (702) Kanu, A. B.; Dwivedi, P.; Tam, M.; Matz, L.; Hill, H. H., Jr. *J. Mass Spectrom.* **2008**, *43*, 1.
- (703) Reviews:(a) Bohrer, B. C.; Merenbloom, S. I.; Koeniger, S. L.; Hilderbrand, A. E.; Clemmer, D. E. *Annu. Rev. Anal. Chem.* **2008**, *1*, 293. (b) Ruotolo, B. T.; Benesch, J. L. P.; Sandercock, A. M.; Hyung, S.-J.; Robinson, C. V. *Nat. Protoc.* **2008**, *3*, 1139.
- (704) Chan, Y.-T.; Li, X.; Soler, M.; Wang, J.-L.; Wesdemiotis, C.; Newkome, G. R. *J. Am. Chem. Soc.* **2009**, *131*, 16395.
- (705) (a) Li, X.; Chan, Y.-T.; Newkome, G. R.; Wesdemiotis, C. *Anal. Chem.* **2011**, *83*, 1284. (b) Chan, Y.-T.; Li, X.; Yu, J.; Carri, G. A.; Moorefield, C. N.; Newcome, G. R.; Wesdemiotis, C. *J. Am. Chem. Soc.* **2011**, DOI: 10.1021/ja107307u. (c) Wang, J.-L.; Li, X.; Lu, X.; Hsieh, I.-F.; Cao, Y.; Moorefield, C. N.; Wesdemiotis, C.; Cheng, S. Z. D.; Newkome, G. R. *J. Am. Chem. Soc.* **2011**, DOI: 10.1021/ja203645m.
- (706) Pringle, S. D.; Giles, K.; Wildgoose, J. L.; Williams, J. P.; Slade, S. E.; Thalassinou, K.; Bateman, R. H.; Bowers, M. T.; Scrivens, J. H. *Int. J. Mass Spectrom.* **2007**, *261*, 1.
- (707) Brouck, E. R.; Anderson, S. E.; Northrop, B. H.; Stang, P. J.; Bowers, M. T. *J. Am. Chem. Soc.* **2010**, *132*, 13486.
- (708) For recent reviews see:(a) Mertens, H. D. T.; Svergun, D. I. *J. Struct. Biol.* **2010**, *172*, 128. (b) Makowski, L. *J. Struct. Funct. Genomics* **2010**, *11*, 9. (c) Putnam, C. D.; Hammel, M.; Hura, G. L.; Tainer, J. A. *Q. Rev. Biophys.* **2007**, *40*, 191. (d) Koch, M. H. J.; Vachette, P.; Svergun, D. I. *Q. Rev. Biophys.* **2003**, *36*, 147.
- (709) Megyes, T.; Jude, H.; Grósz, T.; Bakó, I.; Radnai, T.; Tárkányi, G.; Pálkás, G.; Stang, P. J. *J. Am. Chem. Soc.* **2005**, *127*, 10731.
- (710) O'Donnell, J. L.; Zuo, X.; Goshe, A. J.; Sarkisov, L.; Snurr, R. Q.; Hupp, J. T.; Tiede, D. M. *J. Am. Chem. Soc.* **2007**, *129*, 1578.
- (711) Slone, R. V.; Hupp, J. T.; Stern, C. L.; Albrecht-Schmitt, T. E. *Inorg. Chem.* **1996**, *35*, 4096.
- (712) Tiede, D. M.; Zhang, R.; Chen, L. X.; Yu, L.; Lindsey, J. S. *J. Am. Chem. Soc.* **2004**, *126*, 14054.
- (713) Mardis, K. L.; Sutton, H. M.; Zuo, X.; Lindsey, J. S.; Tiede, D. M. *J. Phys. Chem. A* **2009**, *113*, 2516.
- (714) Balzani, V.; Credi, A.; Venturi, M. *Molecular Devices and Machines: Concepts and Perspectives for the Nanoworld*, 2nd ed.; Wiley-VCH: Weinheim, Germany, 2008.
- (715) Reviews:(a) Wasielewski, M. R. *Acc. Chem. Res.* **2009**, *42*, 1910. (b) Fukuzumi, S. *Phys. Chem. Chem. Phys.* **2008**, *10*, 2283. (c) Nakamura, Y.; Aratani, N.; Osuka, A. *Chem. Soc. Rev.* **2007**, *36*, 831. (d) Choi, M.-S.; Yamazaki, T.; Yamazaki, I.; Aida, T. *Angew. Chem., Int. Ed.* **2004**, *43*, 150. (e) Imahori, H. *Org. Biomol. Chem.* **2004**, *2*, 1425.
- (716) Iengo, E.; Gatti, T.; Zangrando, E.; Indelli, M. T.; Scandola, F.; Alessio, E. *Chem. Commun. (Cambridge, U. K.)* **2011**, *47*, 1616.
- (717) Yatskou, M. M.; Koehorst, R. B. M.; Donker, H.; Schaafsma, T. J. *J. Phys. Chem. A* **2001**, *105*, 11425.
- (718) Yatskou, M. M.; Koehorst, R. B. M.; van Hoek, A.; Donker, H.; Schaafsma, T. J.; Gobets, B.; van Stokkum, I.; van Grondelle, R. *J. Phys. Chem. A* **2001**, *105*, 11432.
- (719) Kelley, R. F.; Goldsmith, R. H.; Wasielewski, M. R. *J. Am. Chem. Soc.* **2007**, *129*, 6384.
- (720) Kelley, R. F.; Lee, S. J.; Wilson, T. M.; Nakamura, Y.; Tiede, D. M.; Osuka, A.; Hupp, J. T.; Wasielewski, M. R. *J. Am. Chem. Soc.* **2008**, *130*, 4277.
- (721) Flynn, D. C.; Ramakrishna, G.; Yang, H.-B.; Northrop, B. H.; Stang, P. J.; Goodson, T., III. *J. Am. Chem. Soc.* **2010**, *132*, 1348.
- (722) Zhao, G.-J.; Northrop, B. H.; Stang, P. J.; Han, K.-L. *J. Phys. Chem. A* **2010**, *114*, 3418.